Master's thesis

NTNU
Norwegian University of Science and Technology
Faculty of Natural Sciences
Department of Chemistry

Susanne Hansen Troøyen

Synthesis of enantiopure β-blockers (*S*)-betaxolol and (*S*)-esmolol, and limonene valorization using biocatalysis

Master's thesis in Organic Chemistry
Supervisor: Elisabeth Egholm Jacobsen
May 2022

NTNU
Kunnskap for en bedre verden

Susanne Hansen Troøyen

Synthesis of enantiopure β-blockers (*S*)-betaxolol and (*S*)-esmolol, and limonene valorization using biocatalysis

Master's thesis in Organic Chemistry
Supervisor: Elisabeth Egholm Jacobsen
May 2022

Norwegian University of Science and Technology
Faculty of Natural Sciences
Department of Chemistry

NTNU
Kunnskap for en bedre verden

Preface

This thesis has been written in 2021-2022, as a part of of the Master's Degree Programme in Chemistry (MSCHEM) at the Department of Chemistry at the Norwegian University of Science and Technology (NTNU). The work has been performed under the supervision of Associate Professor Elisabeth Egholm Jacobsen.

I would like to thank Elisabeth for being an inspiring leader and role model, encouraging me to be creative and curious in the lab. She has also provided social group meetings every week, making it easy to stay motivated, and let us participate in lectures and publications, which has prepared us for the real world of science. I am truly thankful for that. I would also like to thank master student Lucas Bocquin for being an absolute joy to work with in the lab, and for countless scientific (and not-so-scientific) discussions. I am also happy that I got help from Mughilan Selvarajah on one of my syntheses. Thanks for being interested and asking questions.

I would also like to express my gratitude to the previous master candidates Anna Lifen Tennfjord, Raymond Trohjell, Snorre Bergmo Næss and Eirik Berg for starting the work I have been working on in this thesis. They have also been good company in the research group, together with previous master candidates Mari Rødseth and Kristoffer Klungseth, and the synthesis project students Maja Blakstad Christensen and Fredrik Bjørnes. We have also been fortunate to have visits and help in the lab from Andreea Ftodiev and Mara Badea from Romania, which was very fun.

My thesis would never have been completed without the help of the technical staff. Many thanks to chief engineer Roger Aarvik for always bringing new chemicals and supplies to the lab, and being good company. I am also grateful for all the help I have gotten from chief engineer Julie Asmussen with GC and HPLC analyses and troubleshooting, and from senior engineer Susana Villa Gonzales with GC-MS and LC-MS analyses. Thanks to chief engineer Torun Margareta Melø for assistance with the NMR analyses.

Finally, I want to thank my family and friends, with special thanks to my sister Lillian, for drawing oranges and pines - and for always being there for me. I also want to give special thanks to my boyfriend, Gunnar, for being the most patient person on the planet, cooking me dinners, and cheering me up when I have been low.

Abstract

The main objective in this thesis was to synthesize the two β-blockers (*S*)-betaxolol ((*S*)-**10**) and (*S*)-esmolol ((*S*)-**15**) using *Candida antarctica* lipase B (CALB) as an enantioselective biocatalyst. As a secondary goal, biocatalytic oxidation of limonene (**16**) was investigated in an attempt to produce more valuable compounds in a sustainable way.

Several routes to (*S*)-betaxolol ((*S*)-**10**) from the commercially available precursor 4-(2-hydroxyethyl)phenol (**1**) were tested, as shown in Scheme 0.1. Two successful routes (a and b) to the halohydrins 1-chloro-3-(4-(2-(cyclopropylmethoxy)ethyl)phenoxy)propan-2-ol (**8a**) and 1-bromo-3-(4-(2-(cyclopropylmethoxy)ethyl)phenoxy)propan-2-ol (**8b**) were performed, giving **8a** in a total yield of 26% and **8b** in a total yield of 25%. A route to the intermediate 4-(2-(cyclopropylmethoxy)ethyl)phenol (**2**) through protection of **1** with a tetrafluoropyridyl (TFP) group was also attempted, but it was not successful. Kinetic resolutions of **8a** and **8b** using CALB were performed to afford (*R*)-**8a** in 38% yield and 99% ee, and (*R*)-**8b** in 27% yield and 58% ee. The chlorohydrin (**8a**) was determined to be the best substrate for CALB. (*R*)-**8a** was converted to (*S*)-betaxolol ((*S*)-**10**) in 95% yield and 99% ee. The total yield of (*S*)-**10** was 9%.

A four-step synthesis to (*S*)-esmolol ((*S*)-**15**) was performed, as shown in Scheme 0.2. The commercially available precursor methyl 3-(4-hydroxyphenyl)propanoate (**11**) was converted to methyl 3-(4-(oxiran-2-ylmethoxy)phenyl)propanoate (**12**) in 68% yield. Epoxide **12** was converted to methyl 3-(4-(3-chloro-2-hydroxypropoxy)phenyl)propanoate (**13**) in 96% yield. Kinetic resolution of **13** using CALB was carried out to give (*R*)-**13** in 43% yield and 97% ee. (*R*)-**13** was converted to (*S*)-esmolol ((*S*)-**15**) in 92% yield and 97% ee. The overall yield of (*S*)-**15** was 26%.

Perillyl acetate (**18**) was synthesized in 62% yield from perillyl alcohol (**17**). A GC method for analysis of **18** and several standard limonene oxidation products was developed. Limonene (**16**) was oxidized using selenium dioxide, which produced 1-methyl-4-(prop-1-en-2-yl)benzene (**16b**) as the main product. Cytochrome P450-catalyzed oxidation of (*R*)- and (*S*)-limonene ((*R*)/(*S*)-**16**) was attempted using CypExpress™ 2C19, 2C9 and 2D6. The oxidations were not successful, as no oxidation products could be identified. It was discovered that the CypExpress™ 2C19 enzyme underwent denaturation at high enzyme concentrations or after 2 week long reaction times. (*S*)-Perillyl alcohol ((*S*)-**17**) was produced in 37% yield through KRED 228 catalyzed reduction of (*S*)-perillaldehyde ((*S*)-**20**). These reactions are summarized in Scheme 0.3.

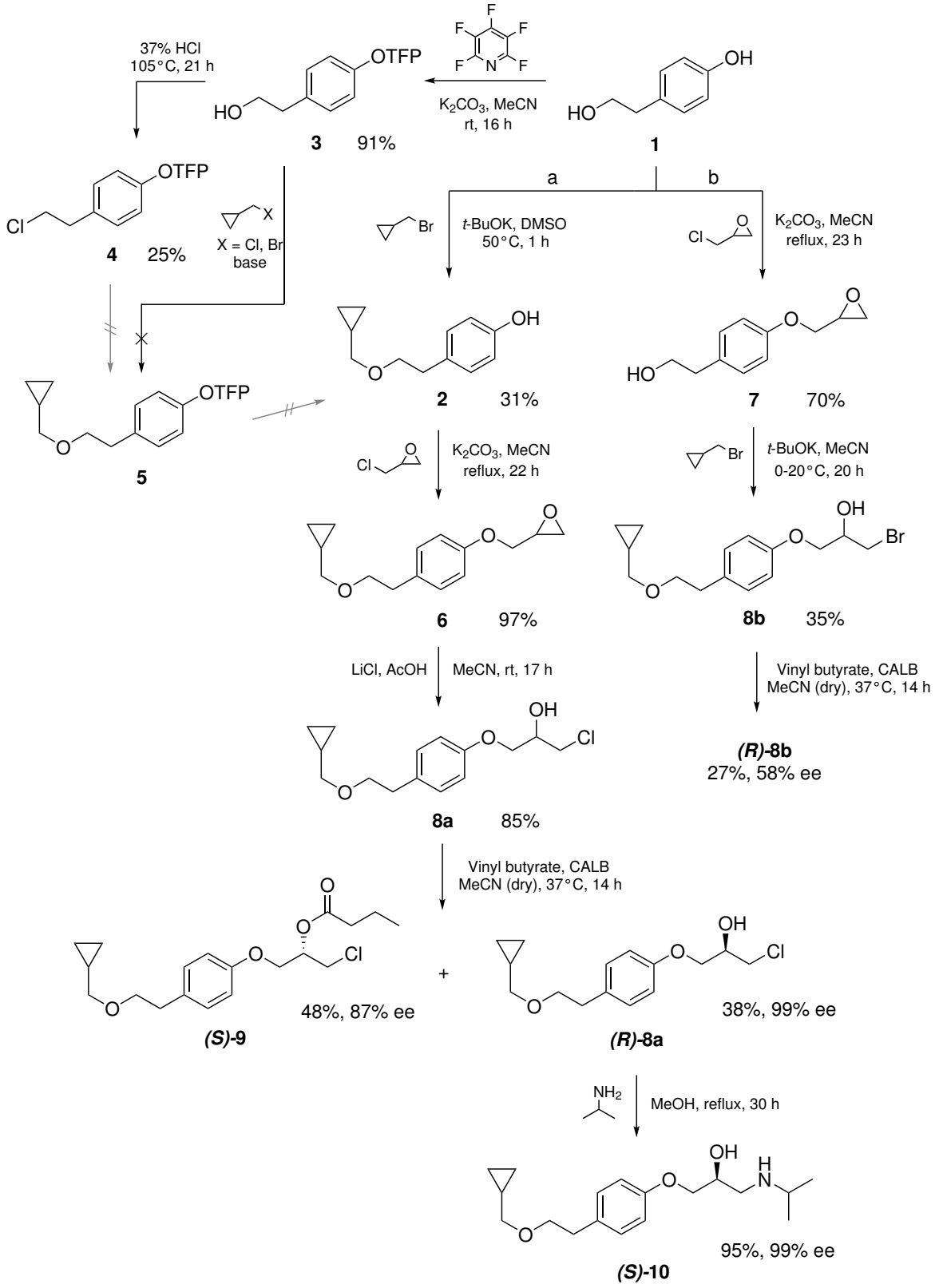

Scheme 0.1 Attempted routes to the target compound (S)-betaxolol ((S)-**10**) from 4-(2-hydroxyethyl)phenol (**1**), with yields for each step. Crossed arrows indicate unsuccessful reactions. Hashed arrows indicate reactions that have not been tested.

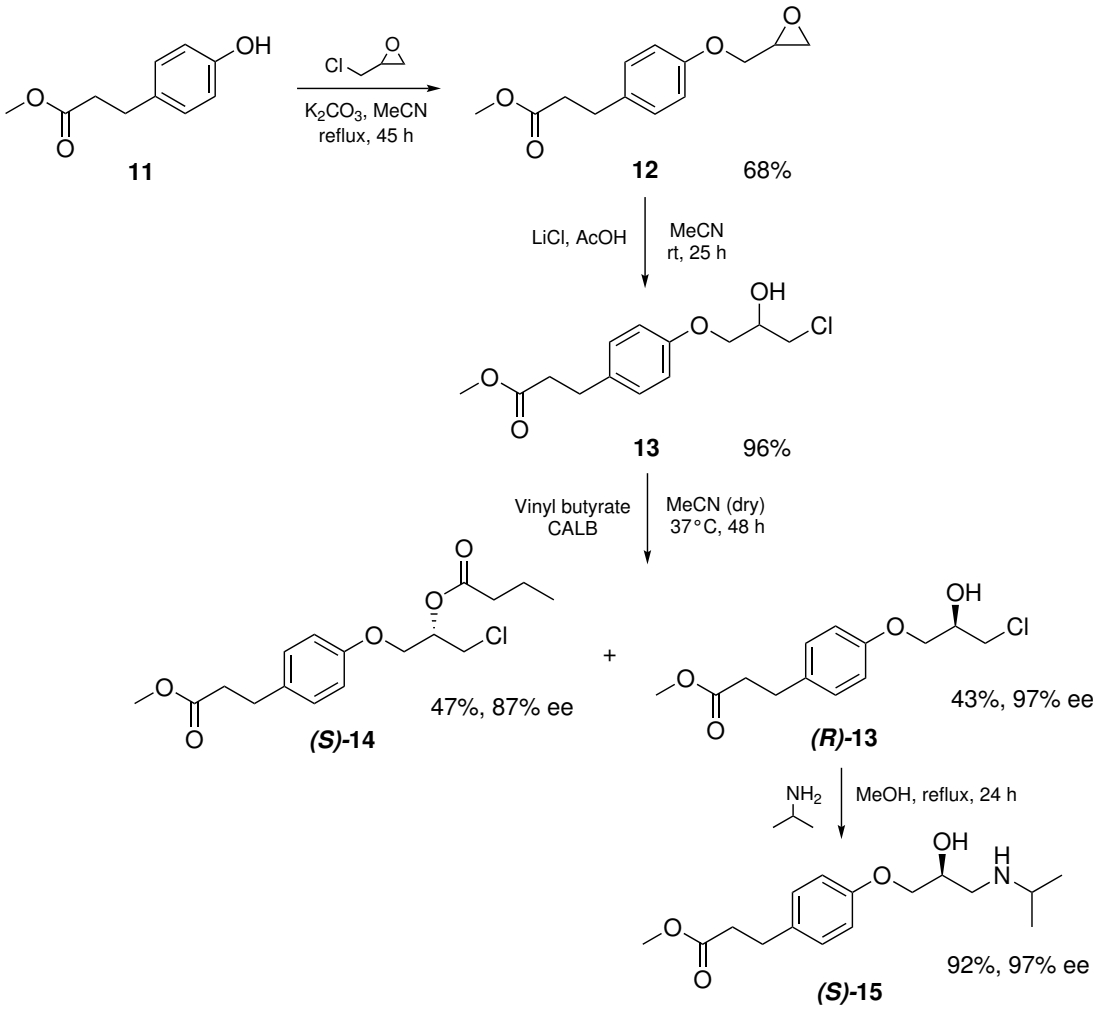

Scheme 0.2 Synthesis of the target compound (S)-esmolol ((S)-**15**) from methyl 3-(4-hydroxyphenyl)propanoate (**11**), with yields for each step.

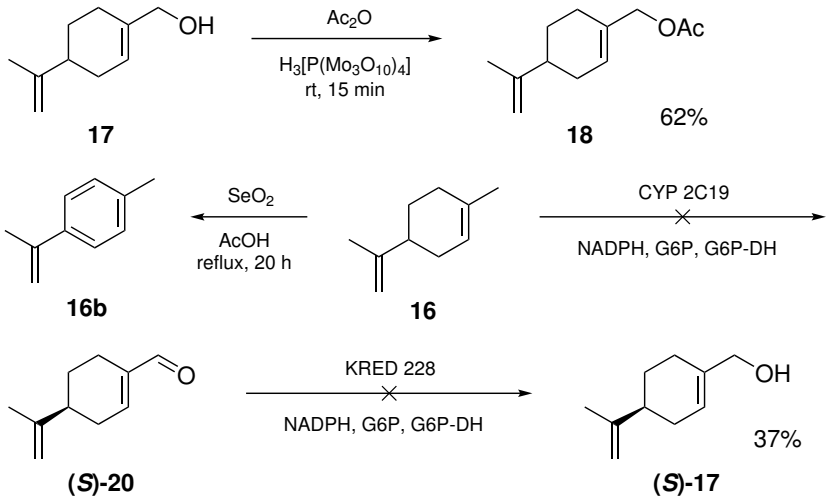

Scheme 0.3 Synthesis of perillyl acetate (**18**) (top). Attempted oxidation of limonene (**16**) using SeO_2 and CYP2C19 (middle). Reduction of (S)-perillaldehyde ((S)-**20**) using KRED 228 gave (S)-perillyl alcohol ((S)-**17**) (bottom).

Sammendrag

Hovedmålet i denne masteroppgaven var å syntetisere (*S*)-betaxolol ((*S*)-**10**) og (*S*)-esmolol ((*S*)-**15**) ved å bruke *Candida antarctica* lipase B (CALB) som en enantioselektiv biokatalysator. Et annet mål i oppgaven var å teste ut biokatalytisk oksidasjon av limonen (**16**) for bærekraftig produksjon av mer verdifulle stoffer.

Flere synteseveier til (*S*)-betaxolol ((*S*)-**10**) fra utgangstoffet 4-(2-hydroksyetyl)fenol (**1**) ble prøvd ut, som vist i Skjema 0.4. 1-Klor-3-(4-(2-(syklopropylmetoksy)etyl)fenoksy)propan-2-ol (**8a**) og 1-brom-3-(4-(2-(syklopropylmetoksy)etyl)fenoksy)propan-2-ol (**8b**) ble syntetisert i hhv. 26% og 25% utbytte via to forskjellige ruter. Det ble også forsøkt å beskytte fenolen **1** med en tetrafluoropyridylgruppe (TFP), men alkyleringen som fulgte var ikke vellykket. CALB ble brukt til kinetisk oppløsning av **8a** og **8b**. Dette ga (*R*)-**8a** i 38% utbytte og 99% enantiomert overskudd (ee), og (*R*)-**8b** i 27% utbytte og 58% ee. Dermed ble det bestemt at klorhydrinen **8a** var det beste substratet for CALB. (*R*)-**8a** ble omdannet til (*S*)-betaxolol ((*S*)-**10**) i 95% utbytte og 99% ee. Totalt utbytte for (*S*)-**10** var 9%.

(*S*)-Esmolol ((*S*)-**15**) ble syntetisert gjennom fire steg, som vist i Skjema 0.5. Utgangstoffet metyl-3-(4-hydroksyfenyl)propanoat (**11**) ble omdannet til metyl-3-(4-(oksiran-2-ylmetoksy)fenyl)propanoat (**12**) i 68% utbytte. Epoksid **12** ble omdannet til metyl-3-(4-(3-klor-2-hydroksypropoksy)fenyl)propanoat (**13**) i 96% utbytte. CALB ble brukt til kinetisk oppløsning av **13**. Dette ga (*R*)-**13** i 43% utbytte og 97% ee. (*R*)-**13** ble omdannet til (*S*)-esmolol ((*S*)-**15**) i 92% utbytte of 97% ee. Totalt utbytte for ((*S*)-**15**) var 26%.

Perillylacetat (**18**) ble syntetisert i 62% utbytte fra perillylalkohol (**17**). Det ble utviklet en metode for GC-analyse av limonen oksidasjonsprodukter. Limonen (**16**) ble oksidert ved hjelp av selendioksid, som ga 1-metyl-4-(prop-1-en-2-yl)bensen (**16b**) som hovedprodukt. Det ble forsøkt å oksidere (*R*)- og (*S*)-limonen (**16**) ved hjelp av cytokrom P450, av typen CypExpress™ 2C19, 2C9 and 2D6. Disse oksidasjonene var ikke velykkede, og ingen oksidasjonsprodukter ble observert. Det ble observert at enzymet denaturerte ved høye enzymkonsentrasjoner eller ved reaksjonstider på 2 uker. (*S*)-perillylalkohol ((*S*)-**17**) ble syntetisert i 37% utbytte etter KRED 228-katalysert reduksjon av (*S*)-perillaldehyd ((*S*)-**20**). Disse reaksjonene er vist i Skjema 0.6.

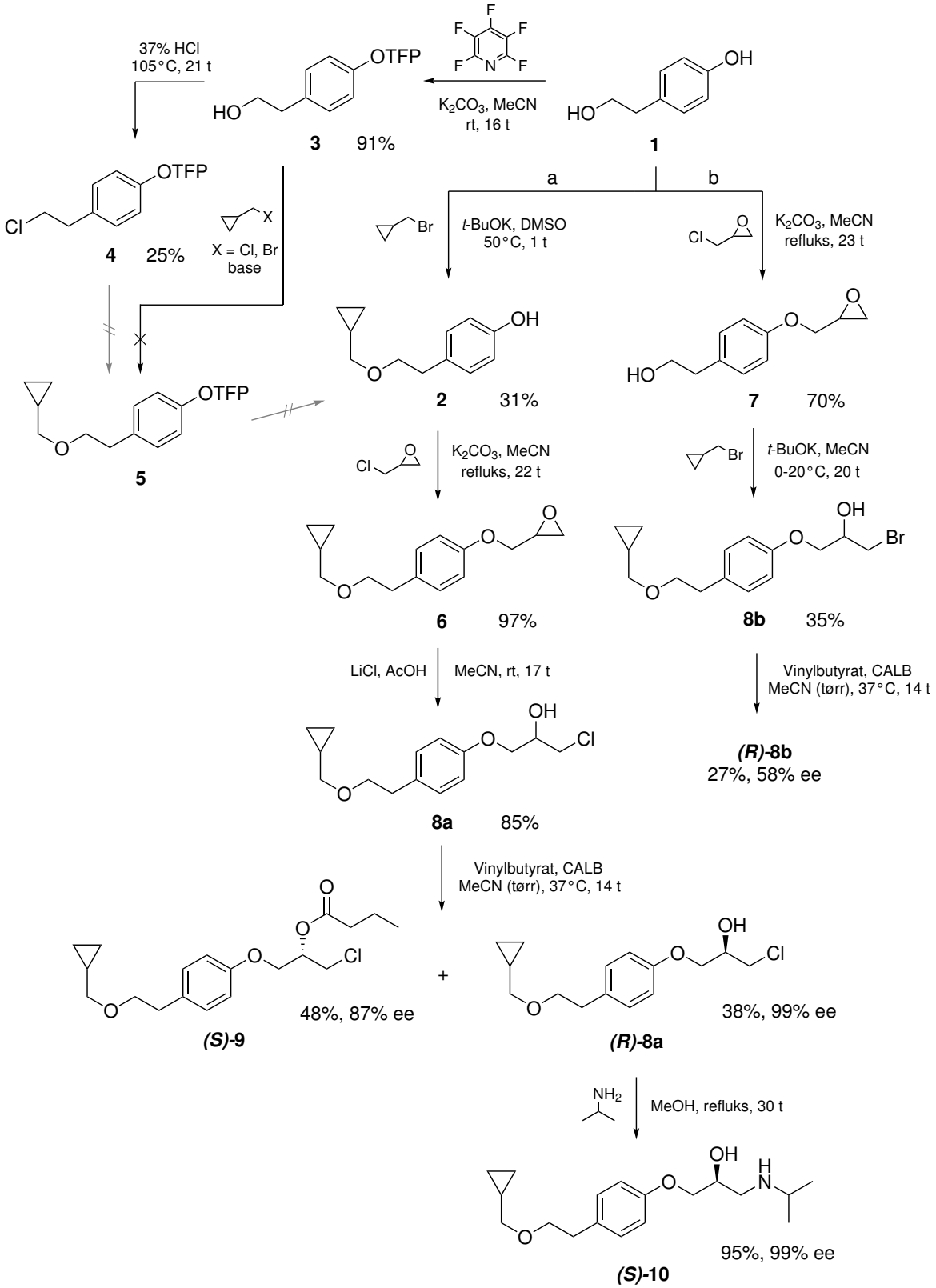

Scheme 0.4 Forsøkte synteseveier til (*S*)-betaxolol ((*S*)-**10**) fra 4-(2-hydroksyetyl)fenol (**1**), med utbytte for hvert steg. Kryssede piler viser mislykkede reaksjoner. Dobbeltkrysset pil viser reaksjoner som ikke har blitt utført.

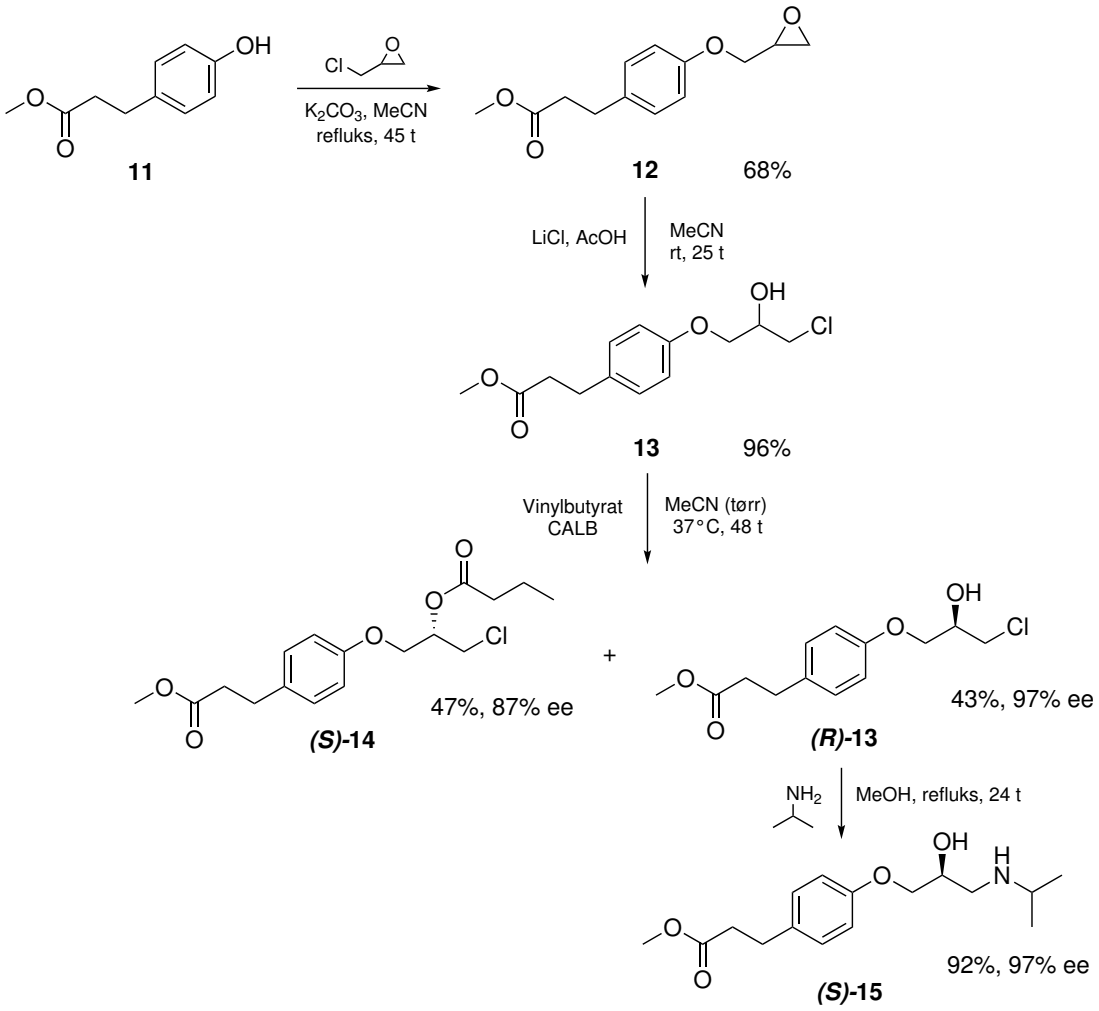

Scheme 0.5 Syntese av (S)-esmolol ((S)-**15**) fra metyl-3-(4-hydroksyfenyl)propanoat (**11**), med utbytte for hvert steg.

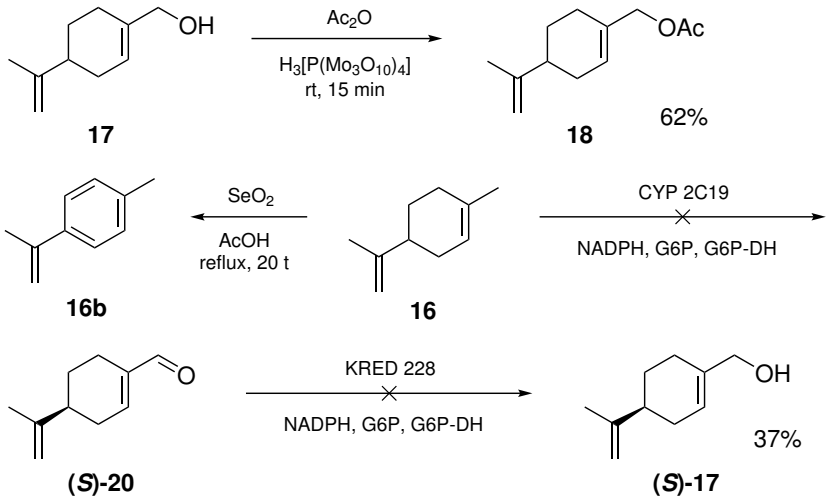

Scheme 0.6 Syntese av perillylacetat (**18**) (over). Forsøkt oksidasjon av limonen (**16**) med SeO_2 og CYP2C19 (i midten). Reduksjon av (S)-perillaldehyd ((S)-**20**) ved hjelp av KRED 228 ga (S)-perillylalkohol ((S)-**17**) (under).

List of compounds

Synthesized compounds

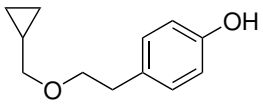

2

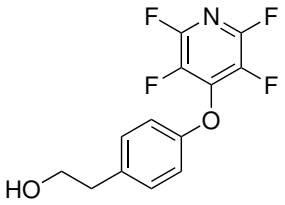

3

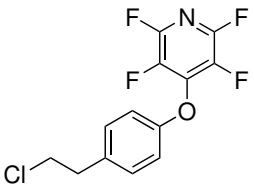

4

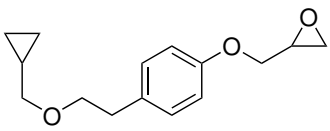

6

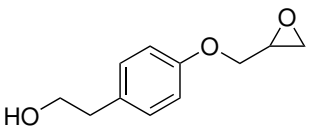

7

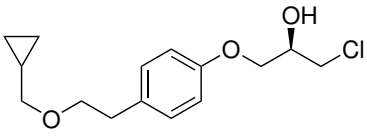

(***R***)-**8a***

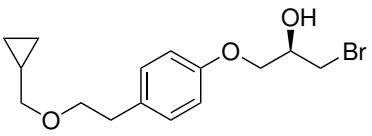

(***R***)-**8b***

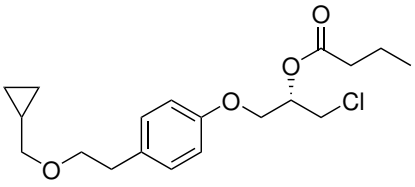

(***S***)-**9***

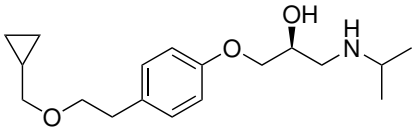

(***S***)-**10***

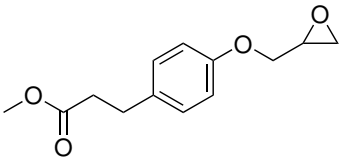

12

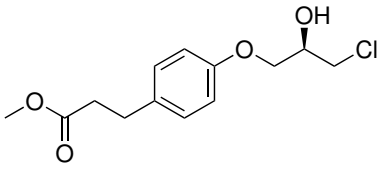

(***R***)-**13***

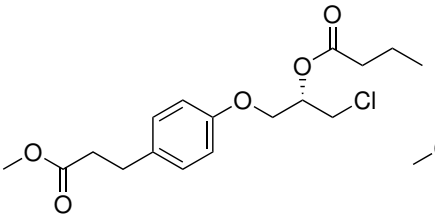

(***S***)-**14**

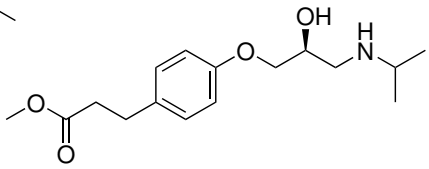

(***S***)-**15***

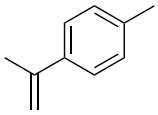

16b

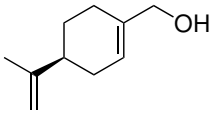

(***S***)-**17**

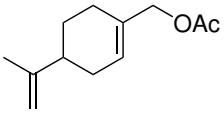

18

*Racemic mixture also synthesized.

By-products

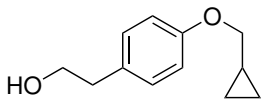

2b

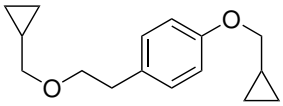

2c

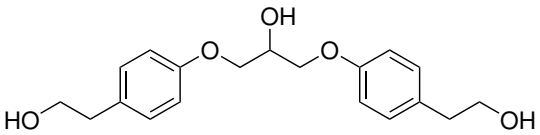

7b

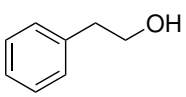

X

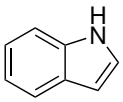

Y

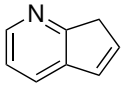

Yb

Starting materials

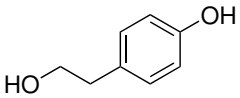

1

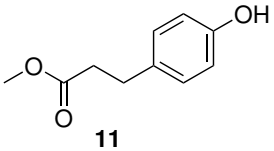

11

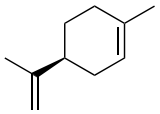

(*S*)-16

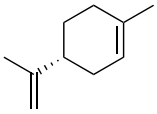

(*R*)-16

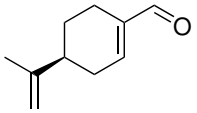

(*S*)-20

Other compounds

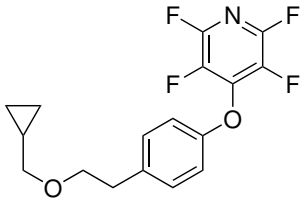

5

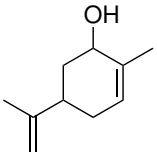

19

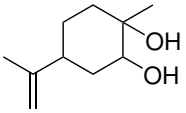

21

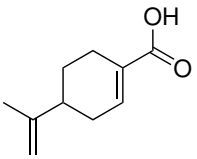

22

Symbols and abbreviations

$[\alpha]_D$	Specific rotation at λ= 589 nm
δ	Chemical shift
λ	Wavelength
br s	Broad singlet
CALB	*Candida arctica lipase B*
COSY	Correlation spectroscopy
CYP	Cytochrome P450
d	Doublet
dd	Doublet of doublets
ee	Enantiomeric excess
E	Enantiomeric ratio
EC	Enzyme Commission
eq	Equivalents
FDA	Food and Drug Administration
G6P-DH	Glucose-6-phosphate dehydrogenase
GC	Gas chromatography
GC-MS	Gas chromatography-mass spectrometry
HMBC	Heteronuclear multiple bond correlation
HPLC	High-performance liquid chromatography
HSQC	Heteronuclear single quantum coherence
I	Integral
IUBMB	International Union of Biochemistry and Molecular Biology
J	Coupling constant
k	Rate constant
KRED	Ketoreductase
m	Multiplicity, multiplet
NADH	Nicotinamide adenine dinucleotide
NADPH	Nicotinamide adenine dinucleotide phosphate
NIST	National Institute of Standards and Technology
NMR	Nuclear magnetic resonance
ppm	Parts per million
$\boldsymbol{pK_a}$	Acid dissociation constant
q	Quartet
quint	Quintet
$\mathbf{R_f}$	Retention factor
rpm	Revolutions per minute
$\boldsymbol{R_s}$	Resolution
rt	Room temperature
s	Singlet
sx	Sextet
$\mathbf{S_N2}$	Nucleophilic substitution (bimolecular)
$\mathbf{S_NAr}$	Nucleophilic aromatic substitution
TFP	Tetrafluoropyridyl
TLC	Thin-layer chromatography
t_R	Retention time
t	Triplet

Contents

1 Introduction

In this section, the theoretical background of the thesis is presented. The introduction starts with the motivation behind the performed experiments. This is followed by an introduction of the drugs that are relevant for the thesis, and an explanation of the use of biocatalysis in organic chemistry. The section closes with a description of organic synthesis theory and a review of relevant literature.

1.1 Motivation for the thesis

The aim of this thesis is to develop a total synthesis of the two β-blockers (*S*)-betaxolol and (*S*)-esmolol, with the use of enzymatic kinetic resolution to attain enantiopurity. A focus on green chemistry is emphasized because there is an increasing desire to develop environmentally friendly and safe chemical processes in the industry today. A second goal of the thesis is to attempt to apply biocatalysis for valorization of limonene sourced from citrus and paper industry waste.

1.1.1 The principles of green chemistry

The chemical industry is not regarded as a very environmentally friendly industry. While it brings many good things to the world, like medicine, materials and power, it also contributes to pollution and health risks. In the 90's, Paul T. Anastas and John C. Warner developed 12 principles of green chemistry, which would motivate the chemical industry to increase sustainability and still achieve profit [1]. The principles are listed below.

1. **Prevent waste:** It is better to produce less waste than to clean up waste.
2. **Atom economy:** Incorporate as much as possible of the materials used in a synthesis into the final product.
3. **Less hazardous chemical synthesis:** Aim to use and generate substances with low health and environmental toxicity.
4. **Safer chemicals:** Design chemical products that are less toxic while still preserving function and efficacy.
5. **Safer solvents and auxiliaries:** The use of auxiliary substances should be limited to the minimum, and when used, they should be innocuous.
6. **Energy efficiency:** The environmental and economic impact of the energy requirements of a chemical process should be recognized. Aim to design syntheses at ambient temperature and pressure.
7. **Renewable feedstocks:** Raw materials and feedstocks should be renewable and not depleting whenever possible.
8. **Reduce derivatives:** Avoid unnecessary derivatization (protecting groups, etc.) because they require additional reagents and generate waste.
9. **Catalysis:** Selective catalytic reagents are superior to stoichiometric reagents.

10. **Design for degradation:** Chemical products should be designed to break down to innocuous substances at the end of their function.

11. **Real-time analysis:** Develop analytical methods that allow for in-process monitoring and control to avoid pollution.

12. **Minimize potential for accidents:** Substances used in a chemical process should be chosen to minimize the potential for accidents such as explosions, fires and releases to the environment.

In this thesis, the principles of green chemistry are considered in the development of the synthesis paths to (*S*)-betaxolol and (*S*)-esmolol. Special focus is given to item 9, catalysis, as biocatalysis is applied. The use of enzymes for synthesis of enantiopure drugs is beneficial in many ways. First, enzymes are non-toxic catalysts, which is especially important in drug synthesis. Enzymes are also higly regio- and stereoselective which allows for efficient generation of enantiopurity. The advantages of biocatalysis is further discussed in Section 1.3. Item 5 encourages chemists to choose non-toxic solvents. Acetonitrile has lower toxicity and environmetal impacts than typical alternatives like dimethylformamide, toluene and chlorinated solvents [2]. Alcohols like methanol, propanol and butanol are preferred solvents.

1.1.2 Limonene valorization

The second part of this thesis is focused on limonene valorization. Limonene is a widely abundant monoterpene with two enantiomers, shown in Figure 1.1. The (*R*)-isomer is dextrorotatory, which means it rotates plane-polarized light in a clockwise manner [3]. Thus, it is often called d-limonene or (+)-limonene. It is the main component in the essential oils of citrus peel, and has a sweet orange scent. The (*S*)-isomer is levorotatory, represented by (-)- or l- prefixes [3]. This isomer originates from trees such as pine and oak, and can be obtained by isomerization of α-pinene, which is a main component of the natural solvent turpentine.

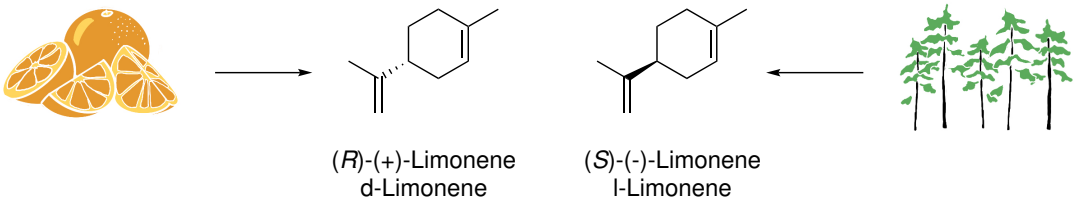

Figure 1.1 The two enantiomers of limonene. (*R*)-limonene is found in citrus peel, and (*S*)-limonene can be obtained from α-pinene from turpentine of pine and oak.

The use of limonene as a starting material for synthesis of more valuable compounds has been studied for decades, because natural (*R*)- or (*S*)-limonene are cheap sources to enantiopure compounds [4]. Both isomers can be sourced from industry waste; (*S*)-limonene from turpentine of the pulp and paper industry, and (*R*)-limonene from the orange juice industry [5]. Valorization of waste products such as limonene is in alignment with the principles of green chemistry. It may be considered as a special case of item 1, waste prevention, because the waste from one industry is used to generate value in another.

1.2 Chiral compounds in medicine

Chiral drugs make up about half of the drugs on the market today [6]. The two enantiomers of a chiral drug may have very different biological activities. A classic example of this is the thalidomide tragedy in the 60's, where one of the enantiomers of the drug thalidomide caused birth defects in children of women who had taken this drug for nausea during their pregnancy [7]. The different biological activity of two enantiomers can be explained by the fact that nature itself is chiral - the proteins and enzymes found in nature consist only of L-amino acids [8]. Thus, it is no surprise that drug interactions are stereospecific. An increased awareness of the different pharmacological activity of enantiomers developed in the decades following the thalidomide tragedy. In 1992, the US Food and Drug Administration (FDA) announced a policy demanding drug manufacturers to test the pharmacokinetic activity of both enantiomers of a drug separately, in order to avoid negative side effects caused by one enantiomer [9]. This has led to a high level of interest towards the development of economical methods for production and analysis of enantiopure drugs, and in many cases a "chiral switch" from racemic to enantiopure drugs [10]. An enantiomeric excess of >96% is required for a drug to be considered enantiopure [11].

1.2.1 β-Blockers against hypertension and arrhythmia

It is estimated that about 26 million people live with heart failure worldwide [12]. In 2020, over 9 000 people died from cardiovascular diseases in Norway [13]. β-blockers are a class of anti-hypertensive drugs that act as β-adrenergic receptor antagonists [14]. This means that they bind to the β-receptors and prevent the agonists epinephrine and norepinephrine from accessing the receptors, thus lowering the physiological effects of these hormones in the body. Typically, this results in lowered heart rate and blood pressure. There are several types of β-receptors in the human body, and they are located in different parts of the nervous system. Different β-blockers may selectively target different types of β-receptors, and this way they each treat different diseases [14]. The higher the selectivity of a β-blocker towards a specific type of receptor, the less side effects are typically observed. Traditionally, these popular drugs have been produced as racemates. In later years, efforts have been made to synthesize enantiopure β-blockers to limit side effects [15]. Figure 1.2 shows the (*S*)-enantiomer of the two β-blockers discussed in this thesis.

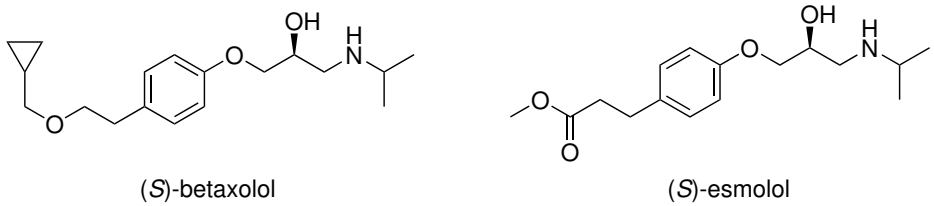

Figure 1.2 β_1-Receptor antagonists (*S*)-betaxolol and (*S*)-betaxolol.

Esmolol (brand name Brevivloc) is a popular β_1-blocker, which targets the β_1-receptors that are found primarily in the heart, and thus acts to treat arrhythmia and hypertension with a very rapid onset of action [16]. Betaxolol (brand names Kerlone and Optipres-S) is also a selective β_1-receptor antagonist, which may be used to treat hypertension. However, it is more commonly used topically as an anti-glaucoma agent [17]. Glaucoma is a dysfunction or damage affecting the optic nerve, leading to gradual loss of eye-sight.

It is often caused by high intraocular pressure [18]. It is the leading cause of irreversible blindness in the world, and it has been estimated that over 70 million people live with glaucoma worldwide, a portion of them being completely blind [19]. For both esmolol and betaxolol, the most effective enantiomer is the (*S*)-enantiomer [15].

1.2.2 Perillyl alcohol as an anti-cancer drug

Perillyl alcohol (Figure 1.3) is a monoterpene that is found in many natural essential oils, produced naturally from limonene through the mevalonate pathway, as described in Section 1.7.1. In the recent decades perillyl alcohol has been shown to have high antitumor activity, and shows great promise as a chemotherapeutic agent against many types of cancer, including leukemia, pancreatic, lung and breast cancer [20–23]. Cancer is one of the largest challenges in modern medicine, and close to 11 000 people died of cancer in Norway in 2020 [13].

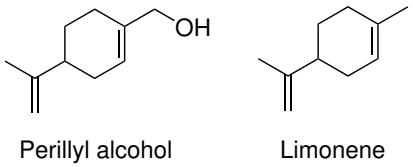

Figure 1.3 Anti-cancer agent perillyl alcohol and its natural precursor limonene.

The first pre-clinical trials of perillyl alcohol as an anti-cancer drug were disappointing, as the drug induced moderately severe side-effects, mainly gastrointestinal symptoms such as nausea and vomiting [24]. Lately, other methods for administration of the drug have been developed, such as intranasal administration, which showed very low toxicity when the method was used to treat a type of brain cancer [25]. A method employing microcapsules for gradual delivery of perillyl alcohol has also limited these unwanted side-effects significantly [26]. With these new methods, the use of perillyl alcohol in chemotherapy is still a promising possibility. Production of perillyl alcohol from limonene from waste would therefore be a very appealing concept.

1.3 Biocatalysis in organic chemistry

Biocatalysis is the use of enzymes or microorganisms to promote a chemical reaction. Nature continuously uses biocatalysis in the production of the large amount of natural compounds that exist on earth. Organic chemists have long been fascinated by nature's ability to produce complex natural products in a highly stereo- and regioselective manner, and in recent years the field of biocatalysis has grown to become a respectable competitor against traditional methods such as metal catalysis in organic synthesis [27]. With the expanding market for enantiopure drugs, biocatalysis is especially attractive in the field of pharmaceutical chemistry [10]. The use of biocatalysis is also considered as green chemistry, as mentioned in the motivation. Enzymes are ton-toxic catalysts, and can often be reused which is reflected in principles 3, 5, 7 and 9 as listed in Section 1.1.1. Enzymes are also typically used at ambient temperatures and pressures, and non-toxic solvents (often water) are preferred. These reaction conditions align with principles 5 and 6.

1.3.1 Availability of biocatalysts

A somewhat limited range of purified enzymes and lyophilized whole cells are now commercially available from many chemical vendors [28, 29]. Traditionally, biocatalysts have been sourced from natural sources, such as animal livers, bacteria, plants or fungi. This method is still used today, but due to recent advances in biotechnology, other methods are becoming increasingly popular. Now, the use of recombinant DNA allows for target enzymes to be over-expressed in host microorganisms that can be grown to produce the enzymes in larger quantities [29, 30]. It can often be difficult to find the correct enzyme to use for a specific biotransformation. Fortunately, there exists metagenomic libraries that can be screened for enzymes that may be suitable for the wanted purpose. Additionally, any enzyme may be produced synthetically if its amino acid sequence is known [28]. For the synthetic chemist, this is an option for obtaining enzymes that are not commercially available, although it is more expensive. The field of bioengineering is rapidly developing. Frances Arnold was awarded the 2018 Nobel Prize in Chemistry for her work on directed evolution of enzymes [31]. Directed evolution makes it possible to produce tailor-made enzymes with improved catalytic activity, substrate specificity and stability. While this technology is only just beginning to develop, it highlights the massive potential to apply biocatalysis for synthetic chemistry in the future, and thus the importance of conducting high-quality research in this field.

1.3.2 Enzyme preparations

There are several ways to use enzymes in organic reactions. Isolated, purified enzymes are typically less stable, but they are often more effective as they can tolerate higher substrate concentrations [30]. Whole cell systems are often cheaper as there is no need for enzyme purification, but as the cells usually contain several enzymes there can be more side reactions and often lower productivity [32]. Additionally, whole cells are often more sensitive to organic solvents and high substrate concentrations. In many cases the enzymes or cells are immobilized on a support material to make it easier to handle the catalysts and to recover and reuse them after a reaction [30].

1.3.3 Enzyme selectivity and activity

In nature, enzymes work in complex environments to perform very specific tasks. They are extremely chemo-, regio- and stereoselective catalysts. The selectivity comes from the three-dimensional structure of the enzymes, - the way that the polypeptide chains of the protein are arranged in space [30]. The active site of the enzyme is often located towards its core, and the amino acids surrounding the active site control its substrate selectivity through electrostatic interactions, covalent bonding, entropy effects and more [29].

Enantioselectivity is explained by the fact that there are several points of attachment or interactions between the substrate and the enzyme, which favours binding of one enantiomer (A) over the other (B) to the active site, as illustrated in Figure 1.4 [30]. Enzymatic kinetic resolution (discussed in Section 1.3.4) is based on this principle. In the case of prochiral substrates, the same idea can be applied. Here, the preferred orientation of the substrate in the active site of the enzyme determines which side of the substrate is most likely to react, - which in turn favours formation of one enantiomer of the product.

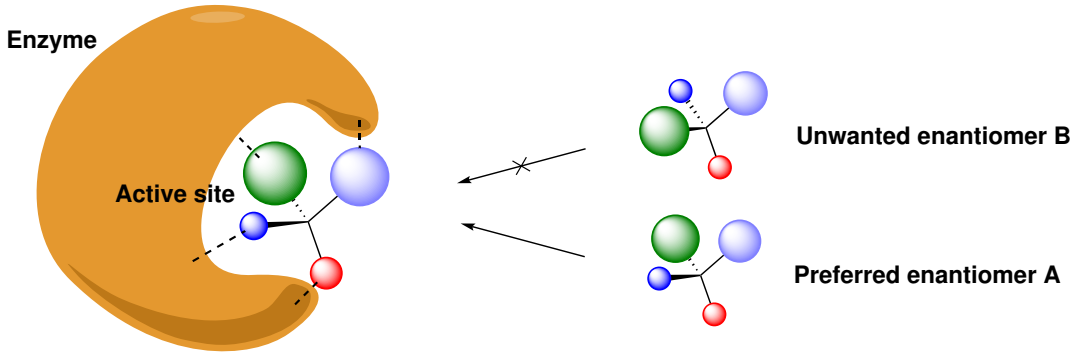

Figure 1.4 The three-dimensional active site of the enzyme selectively binds to one of the enantiomers of a chiral compound.

Any factor that affects the spatial structure of an enzyme can influence its catalytic activity and selectivity. If the enzyme is subjected to intolerable temperature, pH or mechanical stress, the enzyme can undergo denaturation and irreversibly lose its structure and activity [30]. Similarly, organic solvents may influence the activity of an enzyme. Water is the natural solvents of enzymes, and the use of organic solvents often leads to lower activity [33]. Nevertheless, organic co-solvents are often used to increase substrate solubility, and in cases where water cannot be present, the enzymatic reaction may be performed entirely in organic solvent [30]. It has been shown that water content of the solvent affects the selectivity of CALB in kinetic resolutions [34].

1.3.4 Kinetic resolution

Enantiomers may be differentiated from each other in a process called kinetic resolution. This process is based on the preference of the enzyme towards one of the enantiomers, as previously illustrated in Figure 1.4, so that it converts one of the enantiomers faster than the other into its respective product [35]. Increased rate of the transformation is a result of higher stabilization of the enzyme-substrate transition state, as shown graphically in Figure 1.5. Here, substrates A and B are two enantiomers in a racemic mixture, that are enzymatically converted to their products P_A and P_B with rate constants k_A and k_B.

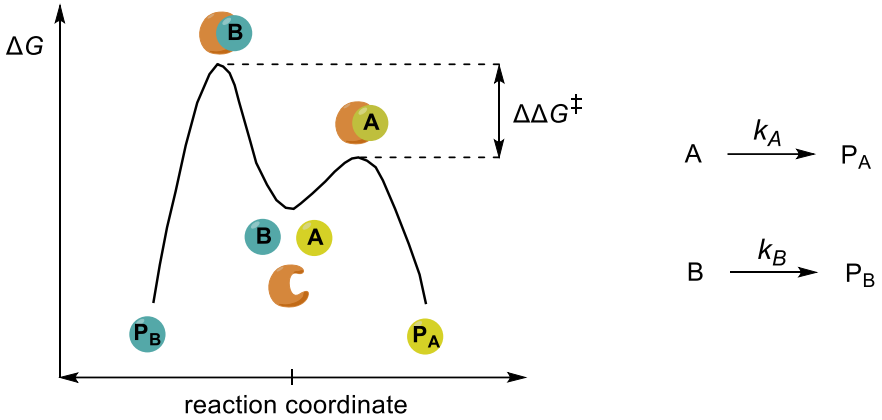

Figure 1.5 Kinetic resolution of the enantiomers A and B occurs because there is an energetic difference $\Delta\Delta G^{\ddagger}$ between the enzyme-substrate transition states. In this case, transformation of enantiomer A to P_A occurs faster, meaning $k_A > k_B$.

The activation energy for the conversion of A is much lower than for B ($k_A > k_B$), which results in excess amounts of product P_A and substrate B after the resolution. The difference in free energy ΔG between the transition states is denoted $\Delta\Delta G^{\ddagger}$, and it directly describes the selectivity of the reaction [30].

It is important to note that the maximum yield of an enantiomerically pure product from a kinetic resolution is 50%, because the racemic mixture only contains 50% of the wanted enantiomer.

1.3.5 Enantiomeric excess

The enantiomeric excess *ee* of a mixture describes the extent of which one enantiomer is in excess in the mixture [35]. It is typically given as a percentage,

$$\%ee = \frac{B - A}{A + B} \times 100\%, \tag{1}$$

where B is the amount of the enantiomer in excess and A is the amount of the other enantiomer. A and B are typically determined by HPLC.

1.3.6 Enantiomeric ratio

The enantioselectivity of an enzymatic reaction is often described by the enantiomeric ratio E. This ratio is specific for any substrate-enzyme reaction, and is independent of the conversion. It is related to the difference $\Delta\Delta G^{\ddagger}$ in activation energies through the equation

$$\Delta\Delta G^{\ddagger} = -RT \ln E, \tag{2}$$

where R is the universal gas constant, and T is the temperature [30]. E can also be expressed as the ratio of the specificity constants $\nu = k/K_m$ of the two competing reactions as shown in Equation 3 [36].

$$E = \frac{\nu_A}{\nu_B} = \frac{k_A/K_m^A}{k_B/K_m^B} \tag{3}$$

Here, K_m is the Michaelis-Menten constant of the reactions. E can also be determined from the enantiomeric excess of the substrate ee_S and product ee_P at any conversion using the equation

$$E = \frac{\ln\left[ee_P(1 - ee_S)/(ee_P + ee_S)\right]}{\ln\left[ee_P(1 + ee_S)/(ee_P + ee_S)\right]}. \tag{4}$$

The enantiomeric ratio E can also be determined accurately based on data from several degrees of conversion using the computer program "E&K calculator" developed by Anthonsen *et al.* [37]. A value of $E > 50$ is considered as excellent selectivity, which will give high enantiomeric excess of the products [30, 38].

1.3.7 Types of enzymes

The International Union of Biochemistry and Molecular Biology (IUBMB) keeps an enzyme repository that classifies all characterized enzymes [39]. The known enzymes are

classified by seven main classes: oxidoreductases, transferases, hydrolases, lyases, isomerases, ligases and translocases. These classes describe the main type of reaction that the enzymes catalyze, as summarized in Table 1.1. Each enzyme has a unique EC (Enzyme Commission) number EC A.B.C.D, where A is the main class number, B describes the substrate class, C describes the co-substrates and D is the final identification number [30]. The repository currently holds just above 6 600 classified enzymes, and is continuously expanding [39].

Table 1.1 The seven main classes of enzymes according to the IUBMB [39].

Number	Class	Reaction type
1	Oxidoreductases	Redox reactions
2	Transferases	Group transfers
3	Hydrolases	Hydrolysis reactions
4	Lyases	Addition-elimination on double bonds
5	Isomerases	Isomerizations
6	Ligases	Formation-cleavage of C-C, C-O, C-N and C-S bonds
7	Translocases	Translocation of molecules across membranes

Lipases

Lipases (EC 3.1.1.3) are a subclass of hydrolases that catalyze hydrolysis and synthesis of triglyceride esters in nature [38]. They are very popular enzymes for industrial purposes because they do not require any co-factors in addition to being very stable in organic solvents [40]. Today they are commonly used in the food industry (for cheese, oil and fat processing), the cosmetics industry and in production of detergents [41]. Lipases are also highly enantioselective, which makes them suited for production of enantiopure compounds. Typically, they are sourced from fungi or bacteria. *Candida antarctica* lipase B (CALB), shown in Figure 1.6, is a serine lipase produced by the fungus *Candida antarctica*.

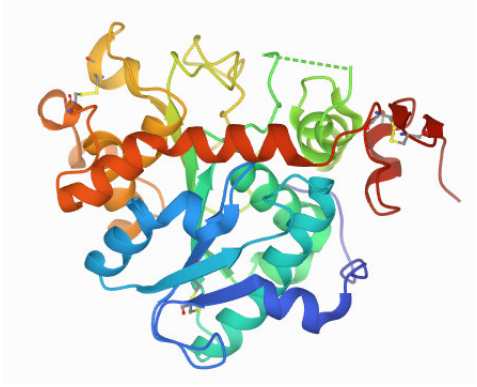

Figure 1.6 Structure of *Candida antarctica* lipase B (CALB). PBD ID: 4K6G [42].

CALB may be used in the kinetic resolution of alcohols in anhydrous environments in the presence of an acyl donor. The active site of CALB (and other lipases) contains a catalytic triad consisting of a histidine-aspartate-serine (His-Asp-Ser) amino acid sequence that is

key to its catalytic activity, as shown in Scheme 1.1. The reaction mechanism involves an enzyme-substrate transition state where the Ser residue (made nucleophilic by the catalytic triad through hydrogen bonding) forms a covalent bond to the substrate [30, 38]. Then, a nucleophile replaces the serine and the product is released from the enzyme. In nature, this nucleophile is usually water and the ester is hydrolyzed. In kinetic resolution of chiral alcohols, the alcohol is the nucleophile.

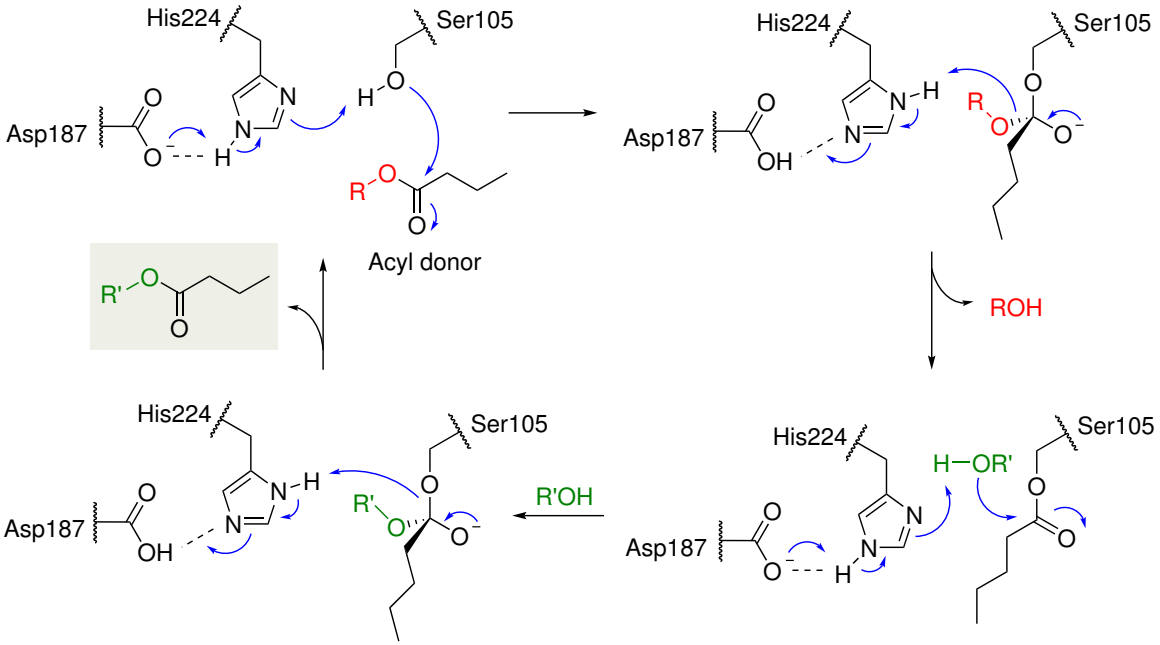

Scheme 1.1 Mechanism of lipase-catalyzed transesterification [38, 43]. A highly nucleophilic serine residue forms a covalent bond to the acyl donor. After release of the OR group of the ester, the preferred enantiomer of the alcohol is esterified.

Enantiomer differentiation of the chiral alcohol occurs because one of the enantiomers can be positioned in a way that favours a reaction inside the active site of the enzyme [43]. CALB has been shown to have a stereospecificity pocket containting a tryptophan residue (Trp104) that limits the size of the group contained in it [44]. For a chiral secondary alcohol with one small group (R_1) and one large group (-OR_2), the enzyme will prefer to keep the small group inside this pocket, as shown in Figure 1.7. This means that the (*S*)-enantiomer of the alcohol is preferred. The enantiomeric ratio of CALB towards secondary alcohols has been found to decrease when the size of the small group R_1 increases [44].

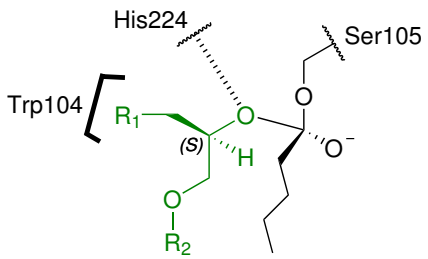

Figure 1.7 Illustration of the preffered enantiomer of CALB. The stereospecificity pocket (containing Trp104) prefers to house the smallest group (R_1) of the secondary alcohol substrate [44].

The cytochrome P450 family

Cytochrome P450s (CYPs, EC 1.4.-.-) are a large subclass of heme-containing oxygenases that catalyze various oxidation reactions in nature [45]. They are present in most types of organisms. In animals, CYPs are the main enzymes involved in the metabolism of drugs and other xenobiotics [46, 47]. In plants, they are the typical catalyst for terpenoid synthesis [48]. The classification and nomenclature of such a large group of enzymes has been a challenge, and they are now named CYP XYZ, where X denotes the main family, Y denotes the subfamily, and Z is the final "member" number [49]. CYP 2C19, shown in Figure 1.8, is the 19th enzyme of CYP family 2, subfamily C.

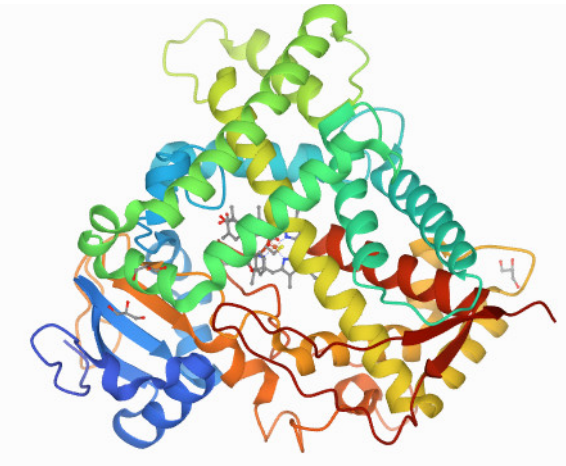

Figure 1.8 Structure of human cytochrome P450 (CYP) 2C19. PBD ID: 4GQS [50].

All CYPs contain a heme (usually iron protoporphyrin IX, shown in Scheme 1.2) prosthetic group which is involved in the binding of oxygen during the oxidation reaction [46]. A simplified scheme of the accepted mechanism of substrate hydroxylation by CYP monooxygenases is shown in Scheme 1.2.

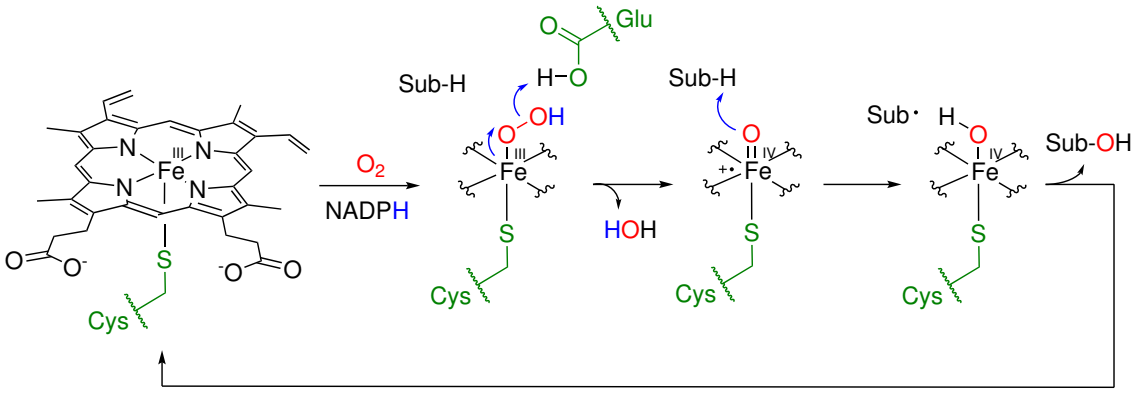

Scheme 1.2 Hydroxylation mechanism of cytochrome P450. The cysteine-bound heme prosthetic group is central in NADPH-aided binding of O_2 and transfer of an oxygen to the substrate Sub-H [47].

The ferric iron of the heme group binds to molecular oxygen as the substrate enters the active site of the enzyme [47]. The oxygen is then reduced to a hydroperoxide ligand by the cofactor nicotinamide adenine dinucleotide phosphate (NADPH). The peroxide O-O bond is then cleaved by accepting a proton from a glutamate residue. This is accompanied

by generation of a Fe=O radical which is highly reactive and induces homolytic cleavage of the substrate C-H bond (in the position of hydroxylation). A substrate radical is then formed, and the substrate proton is attached to the oxygen of the heme group. Finally, the substrate radical accepts the hydroxyl group, releasing the hydroxylated product from the active site. The ferric iron is restored.

Ketoreductases
Ketoreductases (KREDs, EC 1.1.1.-), also known as aldo-keto-reductases are a subclass of oxidoreductases that catalyze aldehyde or ketone reductions [51]. Like the CYPs, they are present in most organisms, and are involved in metabolism and detoxification. Figure 1.9 shows an example of a KRED enzyme structure. The KREDs are dependent on NADPH (or NADH) as a cofactor.

Figure 1.9 Structure of a ketoreductase (KRED1-Pglu) from *Ogataea glucozyma*. BD ID: 6YC8 [52].

1.3.8 Regeneration of cofactors

Oxidoreductases like CYPs and KREDs are cofactor-dependent enzymes, which means that they need a redox partner, like NADPH, to perform their function. These cofactors are typically expensive. In biocatalytic synthesis, cofactors are typically added in catalytic amounts, and a system for *in situ* regeneration of the cofactor is added. A common way to do this is to add an additional enzyme and a cheap stoichiometric auxiliary substrate that regenerates the spent cofactor, but does not interfere with the main enzyme-substrate reaction [30]. This is illustrated in Scheme 1.3, which shows a CYP catalyzed oxidation where glucose-6-phosphate dehydrogenase (G6P-DH) is used to regenerate the cofactor NADPH by catalyzing oxidation of the cheap auxiliary substrate glucose-6-phosphate.

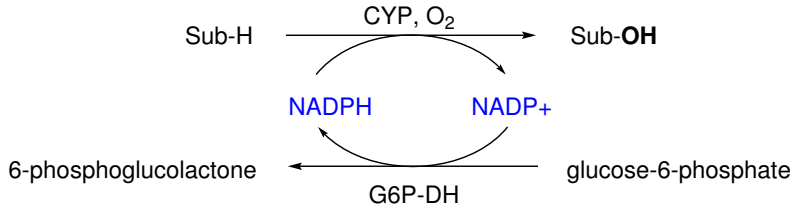

Scheme 1.3 CYP catalyzed hydroxylation of the main substrate Sub-H, with regeneration of NADPH through oxidation of glucose-6-phosphate using glucose-6-phosphate dehydrogenase (G6P-DH).

1.4 Organic synthesis theory

A brief introduction of the synthetic theory applied in this thesis is given in the following sections.

1.4.1 Nucleophilic substitution

Nucleophilic substitution is a common method for functional group interconversion in organic synthesis. In such a reaction, a leaving group (X) on the molecule is replaced by a nucleophile (Nu) [35]. If addition of the nucleophile and leaving group departure occurs simultaneously, the reaction is bimolecular and the mechanism is referred to as an S_N2 mechanism. This scenario is shown in Scheme 1.4. In cases where a stable carbocation can be formed, the substitution may proceed with leaving group departure before nucleophilic addition, forming a carbocation intermediate. The substitution is then unimolecular and the mechanism is called an S_N1 mechanism.

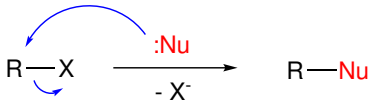

Scheme 1.4 S_N2 mechanism. A leaving group (X) is replaced by a nucleophile (Nu), a Lewis base, in a bimolecular reaction [35].

A special case of nucleophilic substitution is the Williamson ether synthesis. This is an S_N2 reaction between a deprotonated alcohol and and alkyl halide [35]. It is a convenient method for the synthesis of ethers.

1.4.2 Protection of phenols

It is sometimes desired to insert protecting groups that hinder reaction of a phenol group in a subsequent synthesis step. Common phenol protecting groups are alkyl ethers, trimethylsilyl ethers and benzyl ethers [53]. Benzyl ethers can be formed through a Williamson ether synthesis using benzyl bromide in basic conditions [53]. The benzyl group can be removed by Pd-catalyzed hydrogenolysis [54].

Brittain and Cobb have recently described a simple method for protecting phenols by introducing a tetrafluoropyridyl (TFP) protecting group, as shown in Scheme 1.5 [55]. The TFP-ether could be cleaved in excellent yields (up to 99%) by fluoride ions from KF in the presence of 18-crown-6 ether (18-C-6) and methyl thioglycolate.

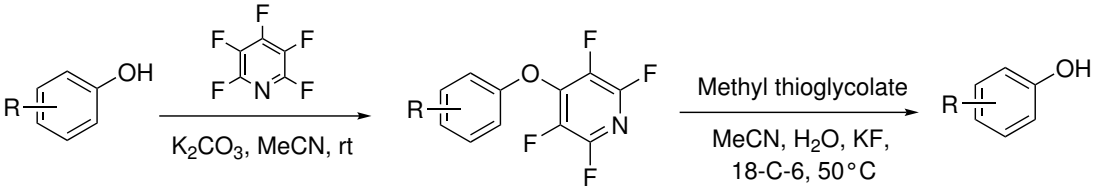

Scheme 1.5 Protection of a phenol with a TFP group, followed by deprotection under mild conditions [55].

The protection occurs through a nucleophilic aromatic substitution (S_NAr) mechanism, shown in Scheme 1.6. Pentafluoropyridine is a highly electron-deficient aromatic compound due to the electron-withdrawing fluorine substituents. It is able to form a resonance-stabilized anionic intermediate after nucleophilic addition of the phenol, before a fluoride ion leaves and aromaticity is re-established [54].

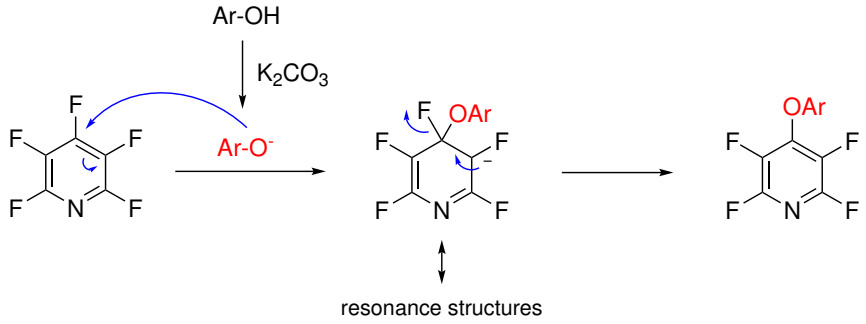

Scheme 1.6 S_NAr mechanism with a nucleophilic phenol on pentafluoropyridine through a resonance stabilized anionic intermediate [54, 55].

1.4.3 Nucleophilic addition to epoxides

Epoxides will go through ring-opening upon addition of nucleophiles [35]. The site of nucleophile addition depends on whether the reaction proceeds in acidic or basic conditions. In basic or neutral conditions, the reaction goes through an S_N2 mechanism. The nucleophile adds to the least hindered carbon of the epoxide, and the C-O bond on that carbon goes through heterolytic cleavage. This is shown in Scheme 1.7. In acidic conditions, the epoxide will be protonated to a certain extent before addition. This means that the reaction may proceed through an S_N1-like mechanism, where the nucleophile adds to the most substituted carbon as it can form the most stable carbocation [35].

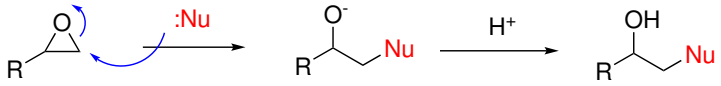

Scheme 1.7 Mechanism of nucleophilic addition to an epoxide under basic or neutral conditions [35].

1.4.4 Nucleophilic addition to epichlorohydrin

Epichlorohydrin is a popular reagent for introduction of a three-carbon segment into a compound [54]. A nucleophile can add to epichlorohydrin in several ways [11]. One possibility is nucleophilic subsitution of the chlorine atom, which was introduced in Section 1.4.1. Another is nucleophilic addition to the epoxide, as explained in Section 1.4.3.

1.4.5 Acylation of alcohols

Alcohols can be converted to esters by allowing them to react with an acyl chloride or acid anhydride [35]. The mechanism is shown in Scheme 1.8. Nucleophilic addition of the alcohol to the carbonyl of an acid anhydride gives a tetrahedral intermediate. The carbonyl is restored as the leaving group (here a carboxylic acid) departs. Often, pyridine is added as a catalyst, which generates an acyl pyridinium ion as a reactive intermediate,

as shown in path b of Scheme 1.8 [54]. The acyl pyridinium ion is more susceptible to nucleophilic attack by the alcohol than the acid anhydride or acyl chloride, leading to increased reaction rate.

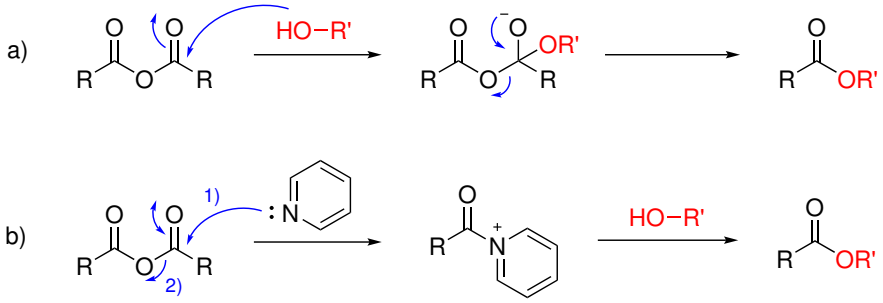

Scheme 1.8 Mechanism of (a) general acylation of alcohols using acid anhydrides and (b) pyridine-catalyzed acylation of alcohols [35, 54].

1.4.6 Allylic oxidation of alkenes using selenium dioxide

Selenium dioxide (SeO_2) is a trusted agent for allylic oxidation of alkenes [56]. The oxidation products can be allylic alcohols, enones or esters, and the oxidation is typically regioselective to favor insertion of oxygen in an allylic position at the most substituted end of the double bond [54]. The first step of the reaction proceeds through an electrophilic "ene" mechanism, where SeO_2 accepts an allylic proton from the alkene and forms a bond to the alkene accompanied by migration of the double bond, as shown in Scheme 1.9. The next step is a concerted [2,3]-sigmatropic rearrangement, where another double bond migration gives a selenium ester. The selenium ester is then hydrolyzed in a final step. If the reaction is carried out in the presence of water, the product will be an allylic alcohol. However, the allylic alcohol is prone to over-oxidation to form an allyllic enone. If the reaction is carried out in acetic acid, the oxidation will stop at the allylic ester, which easily can be hydrolyzed to the alcohol if that is the desired product. This mechanism was introduced by Sharpless in 1972 [57].

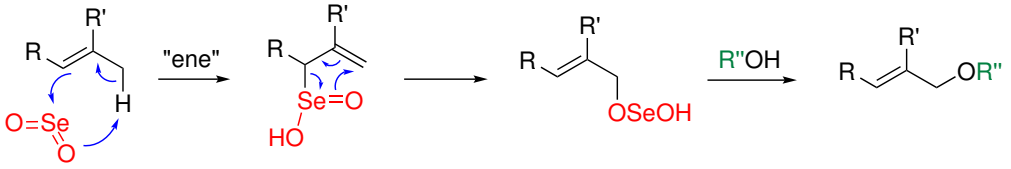

Scheme 1.9 Mechanism of SeO_2 catalyzed allylic oxidation of an alkene [54, 57]. The last step may be hydrolysis which forms an allylic alcohol, or solvolysis with a carboxylic acid which forms an allylic ester.

1.5 Methods for synthesis of (*S*)-betaxolol

An early study that reported the synthesis of enantiopure (*S*)-betaxolol in addition to a screening of its β-receptor blocking activity was performed by Manoury *et al.* in 1987 [58]. A screening of several para-substituted phenoxypropanolamines was performed, and it was discovered that (*S*)-betaxolol had great potential as a β-blocker, with potency exceeding the established drugs metoprolol and propranolol. (*S*)-betaxolol was

synthesized from 4-(2-(cyclopropylmethoxy)ethyl)phenol using (*S*)-2-phenyl-3-isopropyl-5-(hydroxylmethyl)oxazolidinyl tosylate, which is a chiral reagent that already possesses the desired stereocenter. It is not commercially available, and this method is not in use today.

A pathway to racemic betaxolol was patented by Wang *et al.* in 1998 [59]. The precursor 4-(2-(cyclopropylmethoxy)ethyl)phenol was synthesized in 51% yield through a seemingly selective alkylation of 4-(2-hydroxyethyl)phenol. After addition to epichlorohydrin in the presence of K_2CO_3 and addition of isopropylamine, racemic betaxolol was obtained in a total yield of 24%. They did not report resolution of the enantiomers. As kinetic resolution may only be performed in 50% yield, the theoretical maximum yield of (*S*)-betaxolol would be 12% applying this method.

Joshi *et al.* developed a pathway to enantiopure (*S*)-betaxolol in 2005, that involved a hydrolytic kinetic resolution of 2-((4-(2-(cyclopropylmethoxy)ethyl)phenoxy)methyl)oxirane using Jacobsen's catalyst (R,R-salen Co(III)), an asymmetric organometallic catalyst [60]. The epoxide was synthesized from 4-(2-hydroxyethyl)phenol in six steps, including phenol protection with a benzyl group, a Simmons-Smith cyclopropanation and deprotection by hydrogenation over Raney Nickel. The overall yield from the starting material to (*S*)-betaxolol in 99% ee was 17%.

A different approach was published by Datta *et al.* in 2006 [61]. A Pd-catalyzed Heck arylation of ((vinyloxy)methyl)cyclopropane with 1-chloro-4-nitrobenzene was performed. After some modifications, 4-(2-(cyclopropylmethoxy)ethyl)phenol was formed, and addition of the chiral epoxide (*R*)-3-isopro-pylamino-1,2-epoxypropane gave (*S*)-betaxolol in an overall yield of 16%. This approach relies heavily on the use of transition metal catalysts, which is not desired in green chemistry. Also, the enantiomeric purity comes from addition of an enantiomerically pure reagent, which is expensive.

In 2007, Muthukrishnan *et al.* prepared enantiopure (*S*)-betaxolol from 4-(2-hydroxyethyl)-phenol in four steps [62]. The first step was addition of epichlorohydrin, and then a kinetic resolution of the resulting epoxide 2-(4-(oxiran-2-ylmethoxy)phenyl)ethan-1-ol using Jacobsen's catalyst was carried our. The epoxide was then alkylated and aminated to give (*S*)-betaxolol in 33% overall yield and 99% ee. This method is perhaps the most attractive chemical method yet reported for synthesis of (*S*)-betaxolol, although it is desired to limit the use of transition metal catalysts.

Another synthesis of (*S*)-betaxolol in 5 steps from 4-(2-hydroxyethyl)phenol in 42% overall yield, was reported by Zhang *et al.* in 2009 [63]. This method involved kinetic resolution with a higher carbon sugar. The sugar can be synthesized in quite high yield (80%) from 1,4:3,6-dianhydro-D-fructose, which is an expensive sugar of limited availability [64]. The advantage of this method is the use of a non-metallic resolving agent, but the availability of the sugar limits the practical use of this method.

1.5.1 Chemo-enzymatic routes to (*S*)-betaxolol

Two chemo-enzymatic syntheses of (*S*)-betaxolol have been reported. Di Bono *et al.* synthesized enantiopure (*S*)-betaxolol by applying a lipase-catalyzed kinetic resolution

method in 1995 [65]. A kinetic resolution using lipase AK from *Pseudomonas sp.* on 1-chloro-3-(4-(2-(cyclopropylmethoxy)ethyl)phenoxy)pro-pan-2-ol was performed, and the (*R*)-enantiomer of this compound was isolated in 91% ee. After amination, (*S*)-betaxolol was obtained in 91% ee. They observed a lowering of enantiomeric excess to 82% ee upon crystallization of the hydrochloride salt. These results indicate that lipase AK from *Pseudomonas sp.* does not have high enough selectivity for this chlorohydrin to form (*S*)-betaxolol in high enough enantiopurity to be accepted as an enantiopure drug.

In 2011, Li *et al.* reported a synthesis of (*S*)-betaxolol in 95% ee [66]. Their method was based on a kinetic resolution of 4-(2-acetoxy-3-(*N*-isopropylacetamido)propoxy)phenethyl acetate using the bacterial strain *Rhodotorula mucilaginosa* DQ832198, which was screened from soil. Even though they discovered that the selectivity of the lipases from the bacteria was not ideal, giving a maximum of 95% ee, they reported an increase in enantiomeric excess to 99% ee after recrystallization of the hydrochloride salt (*S*)-betaxolol hydrochloride. The advantage of this method compared to that reported by Di Bono *et al.* [65], is that using microbial systems as the biocatalyst is cheaper than using pure enzymes. However, the substrate concentration tolerance was lower, and only 3 g/L substrate could be used. Another benefit is that their reaction is the hydrolysis of an ester, meaning they can perform the reaction in water.

1.6 Methods for synthesis of (*S*)-esmolol

Two articles on the synthesis of (*S*)-esmolol have been published. Narsaiah and Kumar published a synthetic pathway to (*S*)-esmolol in 2011 [67]. They started with 4-hydroxybenzaldehyde, which was converted to methyl 3-(4-hydroxyphenyl)propanoate in 87% yield through a Wittig reaction and a Pd-catalyzed hydrogenation. After conversion to the epoxide methyl 3-(4-(oxiran-2-ylmethoxy)phenyl)propanoate by reaction with epichlorohydrin, a kinetic resolution with Jacobsen's catalyst (R,R-salen Co(III)) was performed to give the (*S*)-epoxide in 94% ee. Amination gave (*S*)-esmolol, however the authors do not report any value for the enantiomeric excess of this product. The overall yield of (*S*)-esmolol from methyl 3-(4-hydroxyphenyl)propanoate was 30%.

Banoth and Banerjee developed a chemical and a chemo-enzymatic route to (*S*)-esmolol from methyl 3-(4-hydroxyphenyl)propanoate in 2014 [68]. The chemical route was based on treatment of the starting material with (*R*)-epichlorohydrin, which gave (*S*)-methyl 3-(4-(oxiran-2-ylmethoxy)phenyl)propanoate in 95% ee. The (*S*)-epoxide was converted to (*R*)-3-(4-(3-chloro-2-hydroxypropoxy)phenyl)propanoate, which was aminated to give (*S*)-esmolol in 93% ee. This requires enantiopure (*R*)-epichlorohydrin as a reagent, which is expensive. They also provided a method for kinetic resolution of the chlorohydrin using a commercially available lipase from *Pseudomonas cepacia*. After the resolution, the (*R*)-chlorohydrin was obtained in 98% ee. (*S*)-esmolol was then obtained in 98% ee. The overall yield of (*S*)-esmolol from methyl 3-(4-(oxiran-2-ylmethoxy)phenyl)propanoate was 34%.

1.7 Limonene synthesis and oxidation pathways

This section includes an introduction to limonene oxidation pathways found in nature, as well as oxidation pathways reported by synthetic chemists in the past.

1.7.1 Oxidation of limonene in plants - terpenoid biosynthesis

Terpenoids are oxygen-containing derivatives of terpenes (like limonene) [69]. Terpenoid formation in plants is typically catalyzed by various oxidoreductases (like CYPs), transferases and isomerases [70]. Scheme 1.10 shows the biosynthesis of some monoterpenoids from limonene by plants in the Lamiaceae (mint) family, including perillyl alcohol, isopiperitenol and carveol and their carbonyl derivatives. In nature, they are typically synthesized from the (*S*)-isomer of limonene.

All of these plants contain specific CYPs, that selectively hydroxylate certain positions on limonene. For example, *Mentha spicata* contains a (-)-limonene-6-hydroxylase (CYP 71D1), that selectively produces (-)-*trans*-carveol by hydroxylation in position 6 of (*S*)-limonene. Similarly, hydroxylation of position 3 is performed by (-)-limonene-3-hydroxylases (CYP 71D13, CYP 71D15), which are present in *Mentha* × *piperita* [71]. (-)-Limonene-7-hydroxylase, the enzyme that is responsible for hydroxylation of limonene to perillyl alcohol and further oxidation to perillaldehyde, is less known and does not have a CYP family name. However it has been isolated by Mau *et al.* [72], and further characterized and cloned by Fujiwara and Ito in 2017 [73].

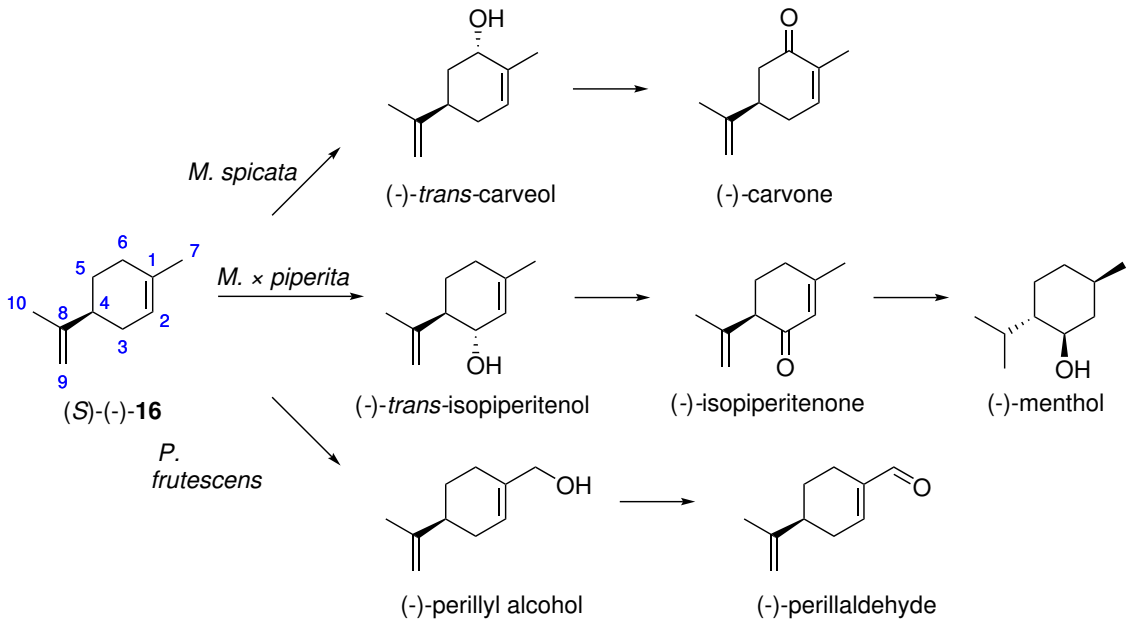

Scheme 1.10 Biosynthesis of selected monoterpenoids by the plants *Mentha spicata* (spearmint), *Mentha* × *piperita* (peppermint) and *Perilla frutescens* (perilla) [72, 74].

1.7.2 Oxidation of limonene with inorganic catalysts

As limonene is a uniform hydrocarbon with few functional groups, it is difficult to perform regioselective oxidations. Early studies on SeO_2-assisted oxidations of limonene were performed by Sharpless and other scientists [57, 75–77]. In recent years, many researchers have tested metal catalysts based on Mn [78], Fe [79], and V [80], and other inorganic catalysts such as activated carbon [81] for oxidation of limonene to more valuable terpenoids. They report complex product mixtures due to limitations in regioselectivity. Gawarecka and Wroblewska used titanium–silicate catalysts to oxidize limonene, and they obtained the allylic oxidation products perillyl alcohol and carveol in 58% and 28% yield [82].

Zítová *et al* studied zeolite catalyzed hydrations of limonene and β-pinene oxide. They achieved only 36% conversion of limonene, but the selectivity towards α-terpineol (for limonene) and perillyl alcohol (for β-pinene) was high (up to 80%) [83].

Figure 1.10 shows limonene with labelled carbons. Oxidation of limonene with selenium dioxide has been done in the past, and hydroxylation and overoxidation to ketones and aldehydes has been observed at positions 4, 6, 7 and 10, with carveol being the most reported main product [57, 75–77]. In the presence of H_2O_2, dihydroxylation and epoxidation of the double bond at position 1 was reported [77]. Thomas *et al.* performed SeO_2 catalyzed oxidation of limonene (**16**) in acetic anhydride [84]. They found the main products to be carveyl acetate (40%), mentha-1,8-dien-10-yl acetate (30%) and trans-mentha1(7)8-dien-2-yl acetate (20%).

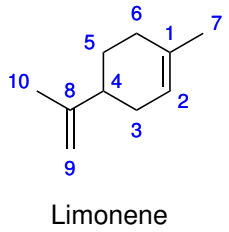

Figure 1.10 Limonene with labelled carbons.

1.7.3 Biocatalytic oxidation of limonene

Using biocatalysts to oxidize limonene can not only be safer and more environmentally friendly, but it may also lead to higher regio- and stereoselectivity compared to metal catalysis. However, biotransformations of limonene are not always easy to perform. The CYPs used for these oxidations are generally poorly compatible with organic solvents, but at the same time, limonene and similar substrates are poorly soluble in water [85]. Terpenes are often antimicrobial, and both substrate and solvent toxicity can limit the efficiency of the catalyst when whole microorganisms are used for the biotransformations [86–88].

Considering that the CYP superfamily is so large, it can be useful to distinguish between plant enzymes - enzymes that synthesize terpenoids, and mammalian or bacterial enzymes - enzymes that degrade xenobiotics such as limonene. The plant enzymes, introduced in Section 1.7.1, have not been studied extensively as biocatalysts for limonene valorization, due to limits in technology for expression and mass production of the plant enzymes in microbial systems [89]. Thus, the majority of biocatalytic oxidations of limonene that have been reported have used microbial systems as the biocatalyst [85]. The terpenoids carveol, carvone, perillyl alcohol, perillaldehyde, perillic acid, α-terpineol, limonene-1,2-epoxide, limonene-1,2-diol, iso-piperitenol, iso-piperitenone and limonene-8,9-epoxide have been reported as products from limonene-degrading microbes [87, 89–92]. Typically, the microbial transformations lead to a mixture of several of these oxidation products. When using genetically modified organisms, a smaller range of products have been reported [93, 94]. Miyazawa *et al.* used human liver microsomes, containing CYP 2C9 and 2C19, for limonene oxidation. In their study, these enzymes were found to oxidize limonene in position 6 and 7 (see Figure 1.10). The largest challenge of microbial and microsomal

biotransformations is substrate toxicity, low conversion, and that the substrate concentration has to be very low to be tolerable for the cell.

The CypExpress™ biocatalytic system
The CYP system used in this thesis was the commercial CypExpress™ system provided by Sigma Aldrich in collaboration with Oxford Biomedical Research [95]. This system is designed to be a robust biocatalyst that contains recombinant human CYPs expressed in *Pichia pastoris* yeast cells. The cells are inactivated, permeabilized and dried to give a stable powder. The cofactor regeneration system, consisting of G6P-DH, NADP+ and glucose-6-phosphate, is also present in the system, but the supplier recommends to add the cofactor and glucose-6-phosphate to increase activity [95]. The supplier claims that this affordable system provides higher yields, less byproducts, and greater longevity than traditional systems such as recombinant enzymes expressed in microbial systems or microsome preparations. They also refer to higher organic solvent tolerance and reusability [96, 97]. No articles have been published on using this system for oxidation of limonene.

1.8 Chromatography (HPLC and GC)

Chromatography is a method for physical separation of the components of a mixture, based on their difference in affinity to two different phases. One of the phases, the stationary phase, is contained inside a column. The other, the mobile phase, moves through the column, leading to migration of the components of the mixture at different speeds depending on their distribution between the phases [98].

In high performance liquid chromatography (HPLC), the mobile phase is a liquid and the stationary phase is a solid. HPLC is a versatile analysis technique which can be applied to many types of compounds. In normal phase HPLC, the mixture to be separated is passed through a column of with a polar stationary phase, by using a non-polar eluent as the mobile phase. Thus, polar compounds with high affinity to the stationary phase will be retained in the column for a longer time, and have a longer retention time t_R. In reverse phase HPLC, the stationary phase is non-polar and the eluent is polar. The enantiomers of a chiral compound may be separated by using a chiral HPLC column, where the stationary phase consists of a chiral material, like cellulose. These types of materials will distinguish between the enantiomers and they will have different retention times. The resolution R_s between the peaks of a chiral chromatogram is given by the equation,

$$R_s = 1.177\frac{t_{R2} - t_{R1}}{w_1 + w_2}, \tag{5}$$

where t_R is the retention time, w is the peak width at half height and the subscripts 1 and 2 denotes the first and second eluted entantiomer [99]. The value of R_s should be higher than 1.5, which means baseline separation has been achieved [98]. The composition of the mobile phase can be optimized to give good separation with as short analysis time as possible.

In gas chromatography (GC), the mobile phase is a gas, normally helium, and the stationary phase is normally a liquid coated on a solid support material inside a long capillary column. GC is used to analyze more volatile compounds than HPLC, and the compo-

nents are separated based on volatility and affinity to the stationary phase. During a GC experiment, the column temperature is increased according to a temperature-program, which allows for elution of compounds with a large range of boiling points.

2 Results and discussion

This section is divided into three parts: the synthesis paths to (*S*)-betaxolol, the synthesis path to (*S*)-esmolol and the experiments related to limonene oxidation. The purity of the synthesized compounds has been determined by ^{1}H NMR, unless otherwise specified. The absolute configuration of enantiopure compounds was determined by comparing the optical rotation to previous reports, and by the enantioselectivity of CALB, which has been reported previously [44]. In the HPLC analyses, some ghost peaks were observed. They were a result of some impurity in the injection system, which was more soluble in polar solvents. That meant that the ghost peak was much larger in the analyses where isopropyl alcohol was used as the sample solvent, and where the eluent was more polar. Thus, the size of the ghost peak varies in the chromatograms shown in this thesis. Efforts were made to remove the impurity, but the problem was not resolved completely. Blanks were run with all the analyses, and the peaks that were also seen in the blanks are labelled b in the chromatograms.

2.1 Pathway to (*S*)-betaxolol

This section reports the results obtained in the total synthesis of (*S*)-betaxolol ((*S*)-**10**). Previous master student Raymond Trohjell worked on a synthesis of the betaxolol precursor 4-(2-(cyclopropylmethoxy)ethyl)phenol (**2**) in his thesis [100]. The present study builds on his work in an attempt to improve the synthesis of **2** and develop a total synthesis of enantiopure (*S*)-betaxolol ((*S*)-**10**) from the starting material 4-(2-hydroxyethyl)phenol (**1**). The overall scheme for the synthesis is shown in Scheme 2.1.

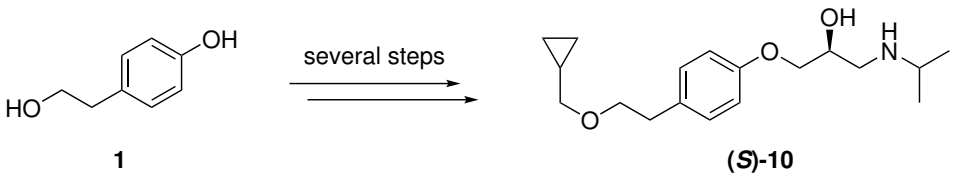

Scheme 2.1 (*S*)-Betaxolol ((*S*)-**10**) was synthesized from the commercially available starting material 4-(2-hydroxyethyl)phenol (**1**).

Halohydrins 1-chloro-3-(4-(2-(cyclopropylmethoxy)ethyl)phenoxy)propan-2-ol (**8a**) and 1-bromo-3-(4-(2-(cyclopropylmethoxy)ethyl)phenoxy)propan-2-ol (**8b**) are central precursors to betaxolol (**10**). In this project, two main pathways from the wanted starting material **1** to halohydrins **8a** and **8b** were tested; one with the intermediates 4-(2-(cyclopropylmethoxy)ethyl)phenol (**2**) and 2-((4-(2-(cyclopropylmethoxy)ethyl)phenoxy)-methyl)oxirane (**6**) (path a, discussed in Sections 2.1.1 to 2.1.4), and the other with the intermediate 2-(4-(oxiran-2-ylmethoxy)phenyl)ethan-1-ol (**7**) (path b, discussed in Sections 2.1.5 and 2.1.6), as illustrated in Scheme 2.2.

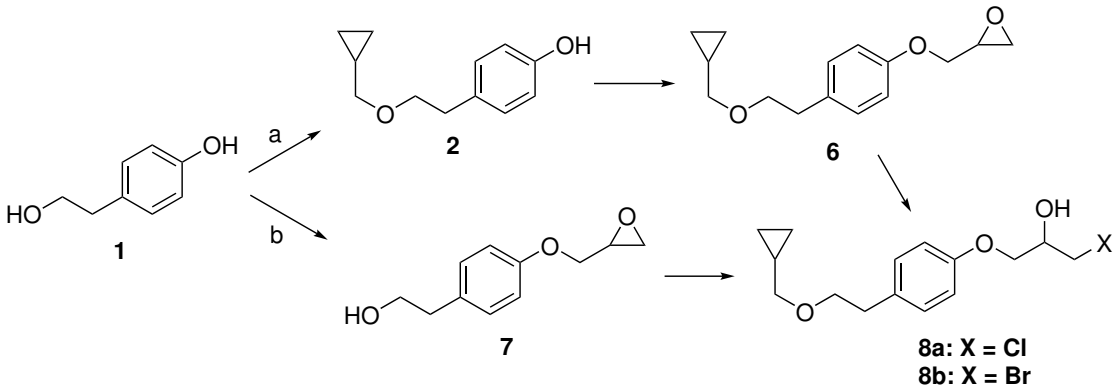

Scheme 2.2 The two pathways a and b to betaxolol precursors **8a** and **8b** from the desired starting material **1**.

2.1.1 Synthesis of 4-(2-(cyclopropylmethoxy)ethyl)phenol (2) by direct alkylation of 1

Path a in Scheme 2.2 starts with the synthesis of phenol **2**. Phenol **2** was attempted synthesized in two ways. One was through direct alkylation of **1** as first performed by Wang *et al.* [59]. The reaction is shown in Scheme 2.3. The selective alkylation of **1** was performed in DMSO at 50°C in the presence of potassium *tert*-butoxide, using (bromomethyl)cyclopropane as the alkylating agent.

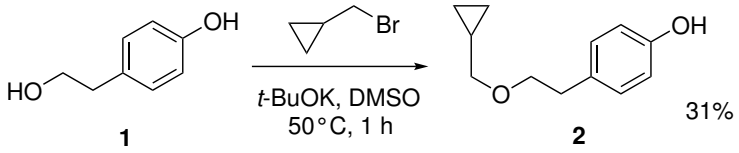

Scheme 2.3 Synthesis of phenol **2** in 31% yield by a direct selective alkylation of **1**.

After 1 hour, TLC confirmed full conversion of the starting material, and purification by flash chromatography (1:11 $MeCN/CH_2Cl_2$) gave phenol **2** in 31% yield and 95% purity.

Mechanism of formation of phenol 2

When the starting material **1** is subjected to a strong enough base, it forms a dianion, as shown in Scheme 2.4. In the synthesis of **2**, this dianion goes through selective alkylation in the presence of a (halomethyl)cyclopropane [59].

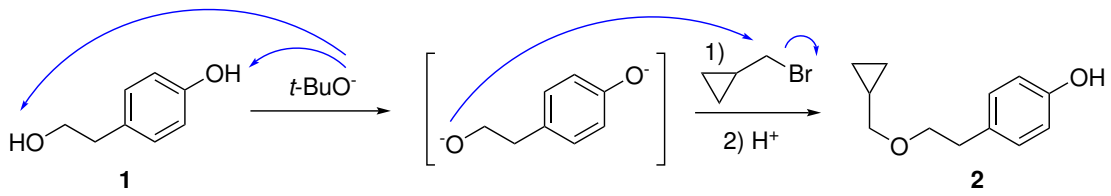

Scheme 2.4 Mechanism of selective alkylation of **1** via a dianion intermediate [59].

Phenols generally have lower pK_a values than aliphatic alcohols, due to resonance stabilization of their conjugate base, so they are more easily deprotonated [101]. It is thought that, because the primary alcohol is more difficult to deprotonate than the phenol of

1, the deprotonated primary alcohol will be less stable and thus a stronger nucleophile, which more easily attacks the alkyl halide, as seen in the mechanism in Scheme 2.4. The mechanism is a simple S_N2 reaction.

Structural characterization of phenol 2

The structure of phenol **2** was confirmed by ^{1}H, ^{13}C, COSY, HSQC and HMBC NMR. The NMR spectra are given in Appendix A.1. The labelled structure of **2** is shown in Figure 2.1, and the corresponding ^{1}H and ^{13}C NMR shifts as well as COSY and HMBC correlations are listed in Table 2.1. The shifts correspond to those reported by Joshi *et al.* [60].

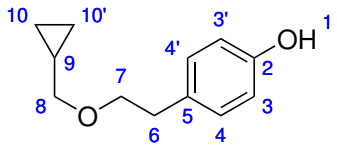

2

Figure 2.1 4-(2-(Cyclopropylmethoxy)ethyl)phenol (**2**) with labelled protons and carbons that correspond to NMR shifts in Table 2.1.

Table 2.1 NMR shifts and correlations observed for phenol **2** with labels shown in Figure 2.1. m = multiplicity, I = integrals, J = coupling constant.

Label	δ ^{1}H (ppm)	m	I	J (Hz)	COSY	δ ^{13}C (ppm)	HMBC
1	5.37	s	1H	-	-	-	-
2	-	-	-	-	-	154.3	3, 4
3	6.73-6.75	m	2H	-	4	115.4	3, 4
4	7.06-7.09	m	2H	-	3	130.0	4, 6
5	-	-	-	-	-	130.8	3, 6, 7
6	2.84	t	2H	7.43	7	35.5	4, 7
7	3.65	t	2H	7.43	6	72.0	6, 8
8	3.30	d	2H	7.00	9	75.8	7, 10
9	1.03-1.10	m	1H	-	10	10.7	8, 10
10	0.51-0.55	m	2H	-	9, 10	3.2	8, 10
	0.19-0.22	m	2H	-	9, 10	”	8, 10

Identification of by-products 2b and 2c

As the phenol group in **1** was not protected, the reaction shown in Scheme 2.3 was expected to have some by-products. Even though the reaction is supposed to be selective, it is not expected to be entirely specific. TLC analysis (1:11 $MeCN/CH_2Cl_2$) showed two by-products with R_f (**2b**) = 0.29 and R_f (**2c**) = 0.70. The by-products were identified as 2-(4-(cyclopropylmethoxy)phenyl)ethan-1-ol (**2b**) and 1-(cyclopropylmethoxy)-4-(2-(cyclopropylmethoxy)ethyl)benzene (**2c**) by NMR. As expected, these by-products

are the result of alkylation of the deprotonated phenol group as shown in Scheme 2.5. For **2c**, both the phenol and the primary alcohol reacted.

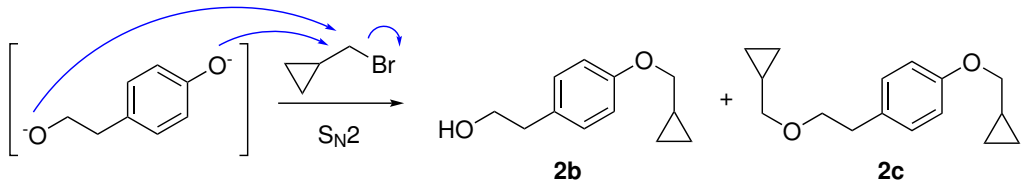

Scheme 2.5 Formation of by-products **2b** and **2c** from the dianion shown in Scheme 2.4.

The ^{1}H NMR spectra of **2b** and **2c** are shown in Figures A.46 and A.47, respectively. **2b** is easily distinguished from **2** on the ^{1}H NMR spectrum, by noting the multiplicity of the -CH_2-O- protons labeled 7 in Figure 2.1. In the spectrum of **2**, this peak is a triplet at 3.65 ppm, which indicates coupling to two other protons. These are the -CH_2- protons labelled 6 in Figure 2.1. The -OH peak is a singlet at 5.37 ppm, as seen in Table 2.1. For **2b**, the C**H**$_2$-OH peak is a doublet of triplets, which appears as a quartet due to the coupling constants being very similar. This means that there is an additional proton, the -OH proton, that couples to these protons. The coupling is also reflected in the -OH signal, which now shows up as a triplet. **2c** is also easily distinguishable, as it has two cyclopropylmethyl groups which have two different groups of signals in the ^{1}H NMR spectrum.

2.1.2 Attempted synthesis of 4-(2-(cyclopropylmethoxy)ethyl)phenol (2) via TFP-protected phenol 3

As discussed in the previous section, direct alkylation of **1** gave **2** in only 31% yield. Thus, another route was tested, which involved protection of the phenol group of **1** using pentafluoropyridine (see Section 1.4.2). The protection method was adapted from Brittain *et al.* [55]. Scheme 2.6 shows the planned synthesis paths.

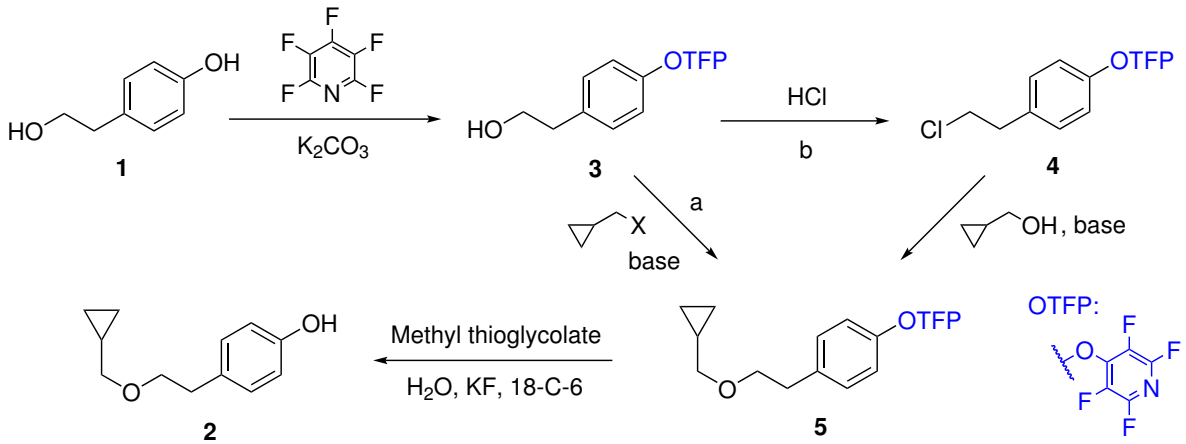

Scheme 2.6 Planned pathways from **1** to **2** via TFP-protected phenol **3**. Path a is alkylation of **3**. Path b is a conversion of **3** to the chloro derivative **4** before alkylation to form **5**. The last step is deprotection to the desired phenol **2**.

Two alternatives, path a and path b, were considered. The first step is the addition of pentafluoropyridine to **1** to form 2-(4-((perfluoropyridin-4-yl)oxy)phenyl)-ethan-1-ol (**3**).

Through path a, **3** was thought to be alkylated to form 4-(4-(2-(cyclopropylmethoxy)ethyl)phenoxy)-2,3,5,6-tetrafluoropyridine (**5**), before deprotection using KF and methyl thioglycolate. In path b, the roles of nucleophile and electrophile are reversed by converting **3** to the chloro derivative 4-(4-(2-chloroethyl)phenoxy)-2,3,5,6-tetrafluoropyridine (**4**) before the alkylation step. The attempted synthesis of **5** was not successful in this work. This meant that the last deprotection step was not attempted.

The choice of protecting group was based on earlier attempts. Previous master student Trohjell has attempted to protect the phenol using a benzyl group, but the following alkylation was not successful [100]. Joshi *et al.* used a benzyl group in their protection step [60]. The benzyl group was removed by hydrogenation with hydrogen gas over Raney Nickel, which is a common method. However, it cannot be categorized as green chemistry, due to the toxicity of the catalyst and the safety issues associated with the method. It also requires a water-free environment and use of H_2 gas, which is time-consuming. The use of the TFP protecting group requires no harmful reactants, and it can be performed quickly at room temperature.

Synthesis of 2-(4-((perfluoropyridin-4-yl)oxy)phenyl)ethan-1-ol (3)
TFP-protected phenol **3** was synthesized according to Scheme 2.7, by addition of pentafluoropyridine in the presence of the weak base potassium carbonate. The reaction mechanism was described in Scheme 1.6.

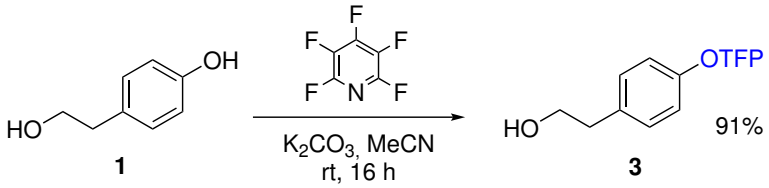

Scheme 2.7 Synthesis of TFP-protected phenol **3** in 91% yield from **1** by addition of pentafluoropyridine in the presence of base.

After 16 hours stirring at room temperature, **3** was obtained in 91% yield and 99% purity.

Structural characterization of protected phenol **3**
The ^{1}H, ^{13}C, COSY, HSQC and HMBC NMR spectra of **3** are given in Appendix A.2. The protected phenol (**3**) is quite similar in structure as the starting material (**1**). Figure A.11 shows both ^{1}H NMR spectra stacked for easier comparison. As the TFP-group does not contain any protons, it is important to confirm that the group has indeed been attached. By looking at Figure A.11, it can be confirmed. First, the phenol -OH peak is not present in the spectrum of **3**, which indicates that another group has replaced the proton. Secondly, the aromatic peaks have shifted downfield compared to the starting material (**1**), which indicates attachment of a highly electron-withdrawing group that deshields the protons of the aromatic ring. The TFP group is highly electron-withdrawing due to all the electronegative fluorine substituents. The COSY and HMBC spectra confirm that the OH peak at 1.45 ppm belongs to the aliphatic -OH group, and not the phenol.

In the ^{13}C NMR spectrum of **3**, the presence of the TFP-group is confirmed by the characteristic C-F splitting observed for the carbons of the TFP ring. The NMR pulse is designed to give C-H decoupling so that coupling between carbons and protons cannot

be seen, but it does not include C-F decoupling [102]. The HMBC correlations were used to determine the exact assignment of ^{1}H and ^{13}C signals, which is illustrated in Figure 2.2. The symmetrical splitting pattern for the ^{13}C peaks of the TFP ring suggests that the oxygen is attached *para* to the nitrogen.

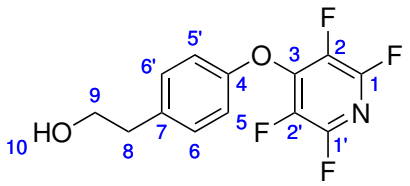

3

Figure 2.2 2-(4-((Perfluoropyridin-4-yl)oxy)phenyl)ethan-1-ol (**3**) with labelled protons and carbons with reference to NMR shifts in Table 2.2.

Table 2.2 NMR shifts and correlations observed for TFP-protected phenol **3** with atom labels shown in Figure 2.2.

Label	δ ^{1}H (ppm)	m	I	*J* (Hz)	COSY	δ ^{13}C (ppm)	HMBC
1	-	-	-	-	-	143.4-145.2 (m)	-
2	-	-	-	-	-	135.3-137.3 (m)	-
3	-	-	-	-	-	144.6-144.8 (m)	-
4	-	-	-	-	-	154.6	5, 6
5	7.00-7.02	m	2H	-	6	116.9	6
6	7.23-7.25	m	2H	-	5	130.6	5, 8
7	-	-	-	-	-	135.8	5, 8, 9
8	2.87	t	2H	6.55	9	38.4	6, 8, 10
9	3.86	q	2H	6.12	8, 10	63.6	8, 10
10	1.45	t	1H	5.32	9	-	8, 9

Synthesis of 4-(4-(2-chloroethyl)phenoxy)-2,3,5,6-tetrafluoropyridine (4)
Following path b in Scheme 2.6, the TFP-protected phenol **3** was converted to its chloro derivative **4** by heating it in concentrated hydrochloric acid, as outlined in Scheme 2.8. The mechanism for this reaction is an S_N2 mechanism (see Scheme 1.4) where the hydroxyl group is first converted to a good leaving group by protonation and then substituted by the chloride ion. The method was adapted from Prosenko *et al.* [103].

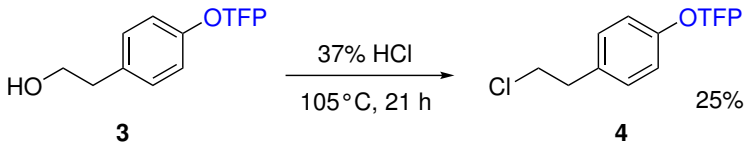

3 **4**

Scheme 2.8 Synthesis of chloro derivative **4** in 25% yield from **3** in concentrated hydrochloric acid.

After 4 hours reaction time at 105°C, NMR analysis showed only 12% conversion of **3** to **4**. After 21 h, TLC analysis still showed some starting material, but the reaction was stopped. After purification by flash chromatography (1:11 MecN/CH_2Cl_2), **4** was obtained in 25% yield and 99% purity. No by-products were detected by TLC or NMR.

If HCl (g) has escaped during the reaction, this could have led to low conversion of **3**. Prosenko *et al.* used a sealed, thermostable tube for the reaction [103]. For the synthesis in Scheme 2.8, a semi-closed environment was opted for in the absence of a pressure-tolerant closed tube. The reaction flask was connected to a condenser and a gas bubbler which could let out pressure if it became too high. This means that even though the environment was not open to air, the pressure build could have led to evaporation of the acid.

The planned route after this step was to perform the alkylation of **4** using cyclopropylmethanol in the presence of base, as seen in Scheme 2.6. However, due to the low yield obtained in this step and time restrictions, this was not attempted. Only **3** was attempted alkylated, as discussed in the next subsection.

NMR analysis of chloro derivative **4**
The ^{1}H NMR spectrum of **4** is shown in Appendix A.3. The spectrum is very similar to that of **3**, except some of the peaks have shifted slighly and it lacks the OH signal. Additionally, the -C**H**$_2$-OH signal is now a triplet instead of a quartet, due to lack of coupling to the OH proton. This confirms substitution of the hydroxyl group with the chlorine atom.

Attempted synthesis of 4-(4-(2-(cyclopropylmethoxy)ethyl)phenoxy)-2,3,5,6-tetrafluoropyridine (5)

The alkylation of TFP-protected phenol **3** following path a in Scheme 2.6 was attempted in several ways. Scheme 2.9 shows the general reaction that was attempted.

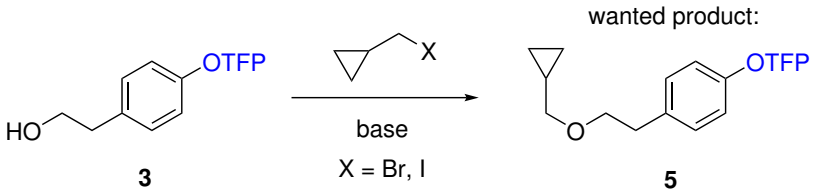

Scheme 2.9 Attempted synthesis of **5** through a Williamson ether synthesis between **3** and a halomethylcyclopropane. Several reaction conditions were tested, as listed in Table 2.3.

A Williamson ether synthesis using a TFP-protected substrate has not been reported before. Therefore, a trial-and-error approach, supplemented with information of the stability of the TFP group given by Brittain *et al.*, was used in the current work [55]. The tested reaction conditions are given in Table 2.3. The products were determined by NMR analysis.

In the presence of the strong base triethylamine in acetonitrile, the starting material **3** remained unchanged after 24 hours at reflux. The NMR analysis of the crude mixture after evaporation of the solvent showed the by-product *N*-(cyclopropylmethyl)-*N,N*-diethylethanaminium iodide (**5a**) and unreacted **3** in a 40:60 molar ratio. This is shown in Scheme 2.10. The ^{1}H NMR spectrum of the crude mixture is shown in Figure A.13.

Table 2.3 Reaction conditions tested for the alkylation of TFP-protected phenol **3**. None of the reactions were successful. The product mixtures were analyzed by NMR.

	X	Base	Solvent	T (°C)	Time (h)	Product mixture
1	I	Triethylamine, 2 eq	MeCN	80	24 h	**3** and **5a**
2	I	K_2CO_3, 4 eq	MeCN	80	20 h	Mainly **3**
3	I	NaOH, 4 eq	MeCN	rt	24 h	Unknown, no **3**
4	I	*t*-BuOK, 2 eq	DMSO	50	3 h	Unknown, no **3**
5	Br	NaOH (*aq*)*, 2 eq	CH_2Cl_2	rt	5 h	White, insoluble solid
6	Br	*t*-BuOK, 1.5 eq	CH_2Cl_2	rt	3 h	White, insoluble solid

*phase transfer catalyzed

Remaining triethylamine and (iodomethyl)cyclopropane had been removed under reduced pressure. After washing the crude mixture with dilute hydrochloric acid and water, the NMR analysis showed the pure starting material (**3**), as the salt (**5a**) was transferred to the aqueous phase. This shows that triethylamine is not suited as a base in these conditions, as it instead acted as a nucleophile. The TFP protecting group was stable in these conditions, which was also reported by Brittain *et al.* [55].

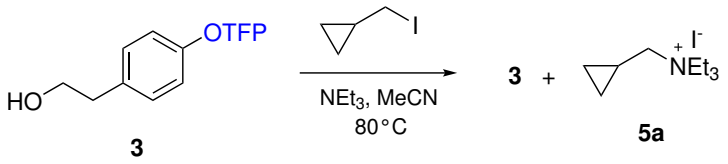

Scheme 2.10 Attempted alkylation of **3** with (iodomethyl)cyclopropane in the presence of triethylamine.

The alkylation was also tested with the weaker base potassium carbonate. No attachment of the alkyl group was observed. This base is not strong enough to deprotonate the primary alcohol of **3**. The crude NMR (see Figure A.14) showed mainly **3**, but also an unidentified aromatic compound. It was not analyzed further as the alkyl group was not observed.

In the presence of the strong base sodium hydroxide in acetonitrile, the TFP group seemed to be unstable. This was indicated by NMR (see Figure A.15) where the aromatic region showed multiple peaks that did not correspond to the aromatic peaks of the starting material **3**. However, the new aromatic peaks did not correspond to the unprotected phenol **1** either, which indicates that the TFP-group had not been cleaved. One possible explanation is that the hydroxide ions may have substituted the fluorine atoms on the TFP ring via an S_NAr mechanism, which could have given a mixture of several products depending on the site and degree of substitution. The NMR analysis did not show attachment of the alkyl group, which means that the experiment was not successful.

Using dimethyl sulfoxide as a solvent and the strong base potassium *tert*-butoxide resulted in three different spots detected by TLC (1:9 EtOAc/*n*-pentane) after work-up.

The crude reaction mixture was purified by flash chromatography. ^{1}H NMR analysis did not show the wanted product **5** in any of the fractions (see Figure A.16). However, this attempt was the most promising one, as the cyclopropyl group was visible on the NMR. The true structures of the products were not elucidated due to time limitations.

The reports of Brittain *et al.* suggested some instability of the TFP group in polar aprotic solvents when using strong bases [55]. Their study indicated that the stability was very high in chlorinated solvents. Thus, this reaction was tested with dichloromethane as the solvent. There are some immediate limitations to using this solvent. One is that dichloromethane is known to produce chlorocarbene in the presence of strong bases, which could lead to many side reactions. However, it was still tested to see if it would be more successful than using acetonitrile and dimethyl sulfoxide. The reaction was tested with both potassium hydroxide in the presence of a phase-transfer catalyst, and potassium *tert*-butoxide. In both cases, a white solid precipitated during the reaction. The solid was not soluble in dichloromethane, chloroform, toluene, *n*-hexane, acetone, dimethyl sulfoxide, acetonitrile, methanol or water. The poor solubility made it hard to analyze by NMR, which was tested unsuccesfully with deuterated chloroform, dimethyl-sulfoxide, methanol and water. It was proposed that a large molecule or polymer could have been formed, possibly through a nucleophilic attack of the deprotonated primary alcohol on the fluorine atoms of the TFP group. This could have created a polymer-like structure. The products were not analyzed further as it was not prioritized in this work.

These results show that the TFP protecting group is not suited for the ether synthesis that was desired here. However, only a limited range of reaction conditions were tested and it could be possible to find a method that works by using a more suitable solvent or base to perform the alkylation.

2.1.3 Synthesis of 2-((4-(2-(cyclopropylmethoxy)ethyl)phenoxy)methyl)oxirane (6)

As the attempts to protect the phenol of **1** were not successful, the phenol **2** from direct alkylation of **1** was used as a starting material for production of epoxide **6**. The method was adapted from Wang *et al.* and Banoth and Banerjee, and is shown in Scheme 2.11 [59, 68]. Phenol **2** was stirred with epichlorohydrin and potassium carbonate under reflux for 22 hours. Epoxide **6** was obtained in 97% yield and 98% purity as a light yellow liquid without the need for purification.

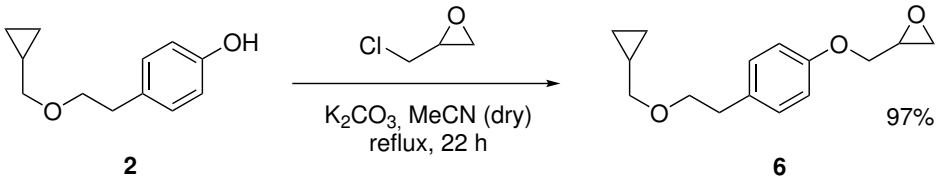

Scheme 2.11 Synthesis of epoxide **6** in 97% yield from **2** and epichlorohydrin in MeCN in the presence of base.

Mechanism of nucleophilic attack on epichlorohydrin

In the presence of base, phenol **2** will be deprotonated, and acts as a nucleophile to attack epichlorohydrin in two possible sites. This is shown in Scheme 2.12. Two main products

may be formed in this reaction; **6** through a direct S_N2 substitution of the Cl atom on epichlorohydrin, and **8a** through nucleophilic attack on the least hindered carbon of the epoxide. For the present experiment, only epoxide **6** was formed. Internal cyclization of anionic **8a** that may have been formed during the reaction could have produced epoxide **6**, as seen in pathway c of Scheme 2.12.

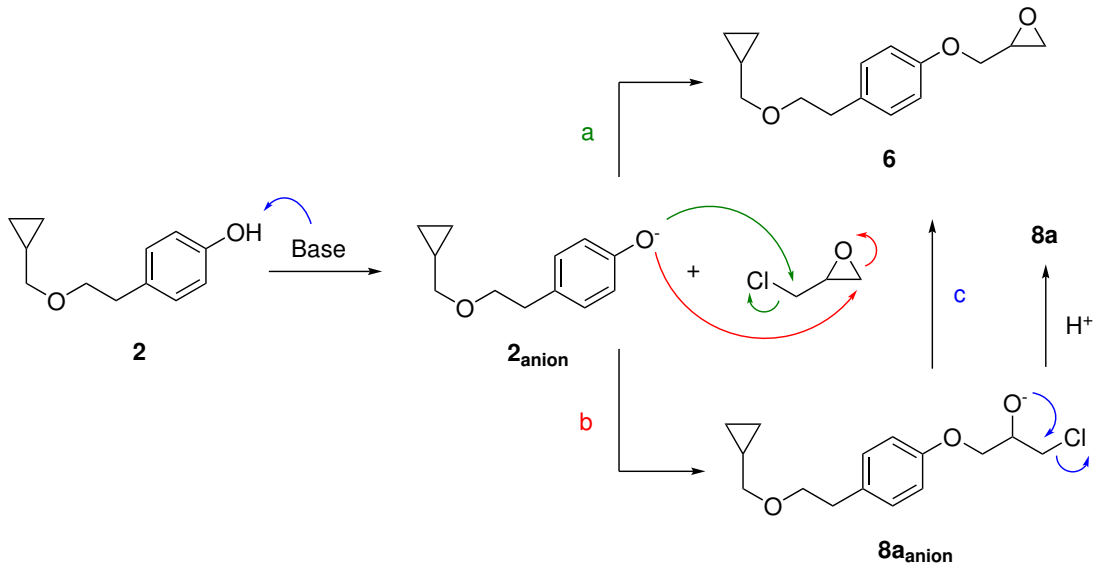

Scheme 2.12 Mechanism of nucleophilic attack of deprotonated **2** on epichlorohydrin. Path a is an S_N2 substitution of the Cl atom, forming **6**. Path b is nucleophilic epoxide ring opening on the least hindered carbon, forming anionic chlorohydrin **8a**. The negatively charged oxygen may reform an epoxide by a substitution of the Cl atom, shown as path c, or be protonated to give **8a** [11].

HPLC analysis of epoxide 6

Epoxide **6** was analyzed by HPLC. Two peaks were observed, with retention times $t_R((R)/(S)\text{-}\mathbf{6}) = 7.1$ min and $t_R((R)/(S)\text{-}\mathbf{6}) = 8.4$ min, and resolution $R_s = 3.9$. Each peak corresponds to one enantiomer of **6**, but it is not possible to tell which is which solely from the chromatogram. The chromatogram is shown in Figure 2.3.

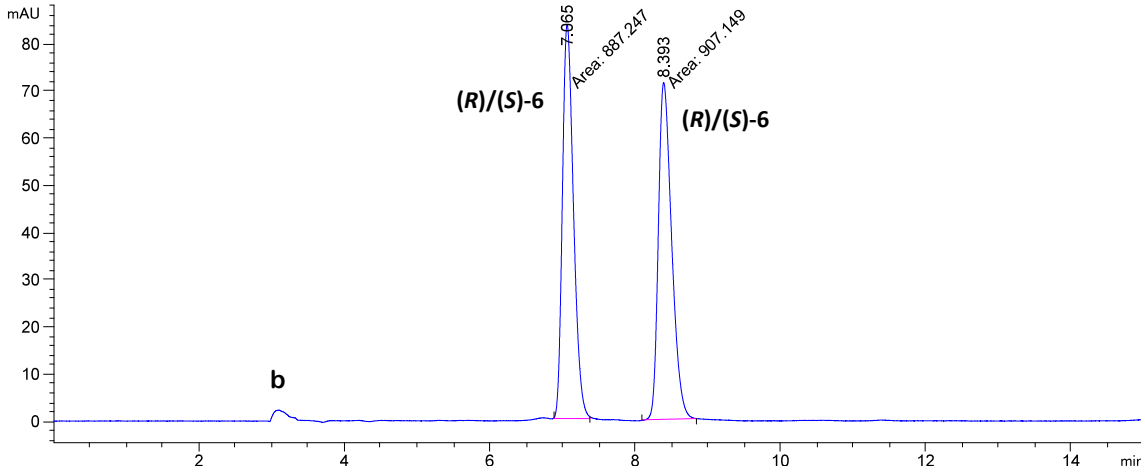

Figure 2.3 HPLC chromatogram of epoxide **6**, $t_R((R)/(S)\text{-}\mathbf{6}) = 7.1$ min and $t_R((R)/(S)\text{-}\mathbf{6}) = 8.4$ min, resolved on a Chiralcel OD-H column with mobile phase composition *n*-hexane:*i*-PrOH (90:10), and flow 1 mL min^{-1}. b = in the blank.

Structural characterization of epoxide 6

Figure 2.4 shows epoxide **6** with labelled carbon atoms. The corresponding ^{1}H, ^{13}C, COSY, HSQC and HMBC NMR spectra are shown in Appendix A.5. Together, they allow for complete characterization of **6**. Table 2.4 lists the NMR shifts assigned to protons and carbons. The NMR data is consistent with literature [60].

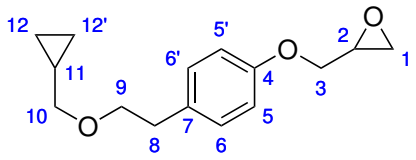

6

Figure 2.4 2-((4-(2-(Cyclopropylmethoxy)ethyl)phenoxy)methyl)oxirane (**6**) with labelled carbons with reference to NMR shifts in Table 2.4.

Table 2.4 NMR shifts and correlations observed for epoxide **6** with carbon labels shown in Figure 2.4.

Label	δ ^{1}H (ppm)	m	I	*J* (Hz)	COSY	δ ^{13}C (ppm)	HMBC
1	2.89	t	1H	4.76	1	44.8	1, 3
	2.74	dd	1H	4.76, 2.70	1, 2	”	1, 3
2	3.32-3.35	m	-	-	1, 3	50.3	1, 3
3	4.18	dd	1H	11.13, 3.35	3	68.9	-
	3.93	dd	1H	11.13, 5.40	2, 3	”	-
4	-	-	-	-	-	157.1	3, 5, 6
5	6.83-6.86	m	2H	-	6	114.7	5, 6
6	7.13-7.15	m	2H	-	5	129.9	6, 8
7	-	-	-	-	-	131.8	5, 8, 9
8	2.84	t	2H	7.60	9	35.6	6, 9
9	3.61	t	2H	7.60	8	71.9	8, 10
10	3.27	d	2H	6.71	11	75.7	9, 12
11	1.02-1.08	m	1H	-	10, 12	10.7	10, 12
12	0.51-0.54	m	2H	-	11, 12	1.3	10, 12
	0.18-0.21	m	2H	-	11, 12	”	10, 12

2.1.4 Synthesis of 1-chloro-3-(4-(2-(cyclopropylmethoxy)ethyl)phenoxy)propan-2-ol (8a)

Ring-opening of epoxide **6** was performed using a method adapted from previous master candidate Anna Tennfjord [104], who developed the method for synthesis of (*S*)-esmolol based on earlier work of the biocatalysis group [11, 105, 106]. The reaction, shown in

Scheme 2.13, was performed in acetonitrile at room temperature, using lithium chloride and acetic acid to open the epoxide (**6**).

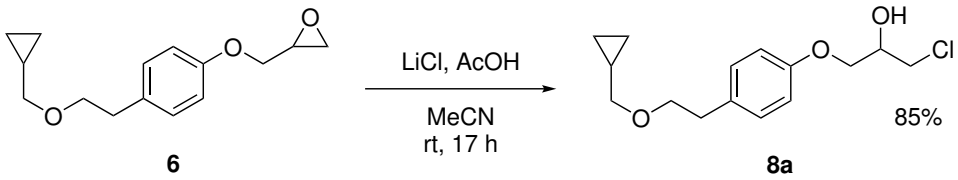

Scheme 2.13 Synthesis of chlorohydrin **8a** in 85% yield by ring-opening of epoxide **6** by LiCl and AcOH in MeCN at room temperature.

Chlorohydrin **8a** was obtained in 85% yield and 97% purity. This confirms that the method is suitable for synthesis of **8a**. The only other reported method for synthesis of **8a** was published by DiBono *et al.* who obtained **8a** in 80% yield from **6** using concentrated hydrochloric acid in $CHCl_3$ [65].

HPLC analysis of chlorohydrin 8a

The two enantiomers of **8a** were separated by chiral HPLC. The retention times were $t_R((S)\text{-}\mathbf{8a}) = 10.8$ min and $t_R((R)\text{-}\mathbf{8a}) = 12.8$ min, with a resolution $R_s = 3.1$, as shown in Figure 2.5. The absolute configurations were determined based on the enantioselectivity of CALB, and comparison of the optical rotation of the final product (*S*)-betaxolol ((*S*)-**10**) with literature. The epoxide **6** was also detected as an impurity at $t_R(\mathbf{6}) = 7.5$ min and $t_R(\mathbf{6}) = 8.9$ min, making up 3% of the total peak area. This confirms the purity of 97% determined by NMR.

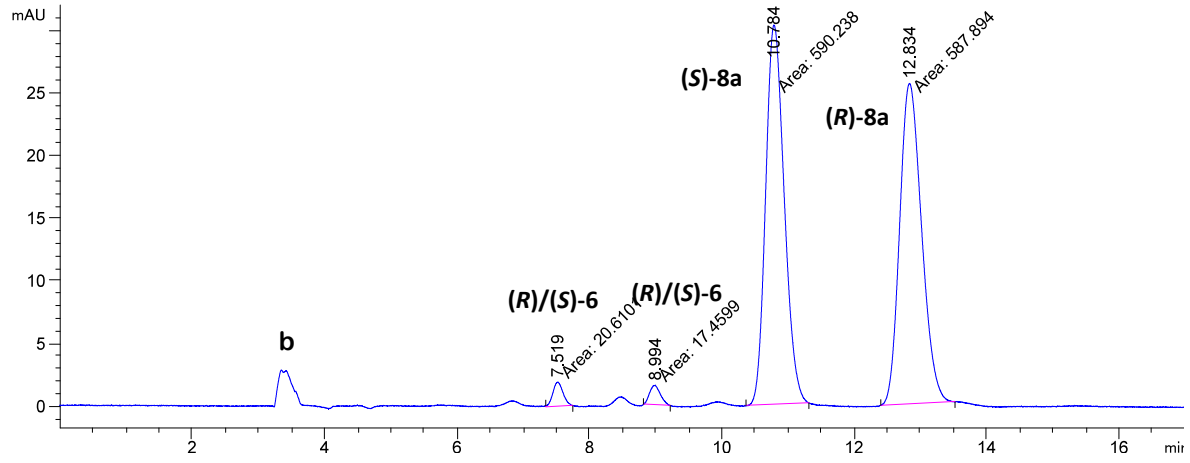

Figure 2.5 HPLC chromatogram of chlorohydrin **8a**, $t_R((S)\text{-}\mathbf{8a}) = 10.8$ min and $t_R((R)\text{-}\mathbf{8a}) = 12.8$ min, resolved on a Chiralcel OD-H column with mobile phase composition *n*-hexane:*i*-PrOH (90:10), and flow 1 mL min^{-1}. b = in the blank.

Structural characterization of chlorohydrin 8a

The structure of chlorohydrin **8a** was fully characterized using ^{1}H, ^{13}C, COSY, HSQC and HMBC NMR, according to Table 2.5. Corresponding atom labels are shown in Figure 2.6. The NMR spectra are shown in Appendix A.7, and the data is consistent with literature data [65].

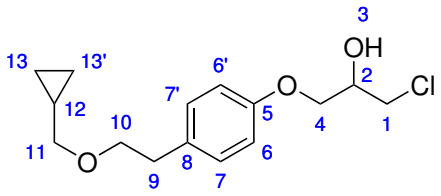

8a

Figure 2.6 1-Chloro-3-(4-(2-(cyclopropylmethoxy)ethyl)phenoxy)propan-2-ol (**8a**) with labelled atoms that correspond to assigned NMR shifts in Table 2.5.

Table 2.5 NMR shifts and correlations observed for chlorohydrin **8a** with carbon labels shown in Figure 2.6.

Label	δ ^{1}H (ppm)	m	I	*J* (Hz)	COSY	δ ^{13}C (ppm)	HMBC
1	3.70-3.79	m	2H	-	2	46.1	3,4
2	4.20	sx	1H	5.40	1, 3, 4	70.0	4
3	2.62-2.66	m	1H	-	2	-	1, 4
4	4.04-4.09	m	2H	-	2	68.9	1, 2, 5
5	-	-	-	-	-	156.8	4, 6, 7
6	6.83-6.86	m	2H	-	7	114.6	5, 8
7	7.14-7.16	m	2H	-	6	130.1	5, 9
8	-	-	-	-	-	132.1	6, 9, 10
9	2.85	t	2H	7.27	10	35.6	7, 10
10	3.62	t	2H	7.27	9	71.8	9, 11
11	3.28	d	2H	6.79	12	75.8	10, 13
12	1.02-1.09	m	1H	-	11, 13	10.7	11, 13
13	0.51-0.54	m	2H	-	12, 13	3.1	11, 13
	0.18-0.21	m	2H	-	12, 13	”	11, 13

2.1.5 Synthesis of 2-(4-(oxiran-2-ylmethoxy)phenyl)ethan-1-ol (7)

The other method that was explored for arriving at halohydrin **8a**/**8b** was through the intermediate epoxide **7**, following path b in Scheme 2.2. In this method, the starting material **1** is reacted with epichlorohydrin *before* alkylation of the primary alcohol group. It was presumed that performing the steps in the opposite order could help eliminate the issues related to protection of the phenol group: if the phenol is allowed to react in the first step, the phenol will not be able to react in the alkylation step. However, it was not clear whether the reactive epoxide group could introduce other difficulties in the subsequent alkylation step.

The reaction for synthesis of **7** is shown in Scheme 2.14. By using the weak base potassium carbonate, only the phenol of **1** is deprotonated. Thus, epichlorohydrin is attacked by the

anion of **1** in a similar manner as seen previously in Scheme 2.12. The reaction performed here was adapted from Muthukrishnan *et al.* and Banoth and Banerjee [62, 68].

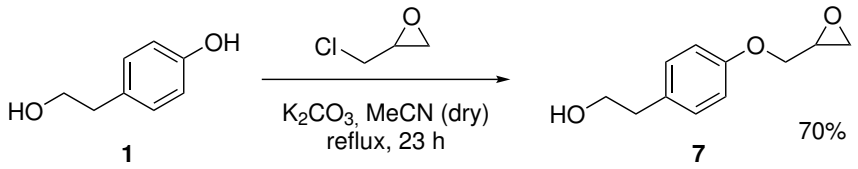

Scheme 2.14 Synthesis of intermediate epoxide **7** in 70% yield from **1** and epichlorohydrin in the presence of base.

After 16 hours reaction time, TLC confirmed that all the starting material had been consumed. After purification by flash chromatography (1:10 MeOH/CH_2Cl_2), the intermediate epoxide **7** was isolated in 70% yield and 99% purity.

Structural characterization of intermediate epoxide 7

Intermediate epoxide **7** was characterized by ^{1}H, ^{13}C, COSY, HSQC and HMBC NMR. Figure 2.7 shows the labelled structure of **7**, and the assigned shifts are shown in Table 2.6. The NMR spectra are given in Appendix A.6. The shifts are consistent with those reported previously, except the reported study did not report the -OH proton triplet at 1.52 ppm [62]. They also reported a triplet instead of a quartet at 3.80 ppm, which is logical as their spectrum lacks the coupling to the -OH proton.

In Table 2.6, the quartet at 3.80 ppm is actually a doublet of triplets, but because the coupling constants (5.70 Hz and 6.29 Hz) are so similar, it appears like a quartet with coupling constant 6.00 Hz.

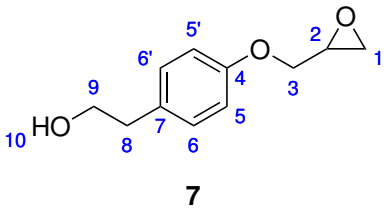

Figure 2.7 2-(4-(Oxiran-2-ylmethoxy)phenyl)ethan-1-ol (**7**) with labelled protons and carbons corresponding to NMR shifts in Table 2.6.

Table 2.6 NMR shifts and correlations observed for intermediate epoxide **7** with atom labels shown in Figure 2.7.

Label	δ ^{1}H (ppm)	m	I	*J* (Hz)	COSY	δ ^{13}C (ppm)	HMBC
1	2.90	t	1H	4.70	1, 2	44.8	3
	2.75	dd	1H	4.70, 2.58	1, 2	”	3
2	3.33-3.35	m	-	-	1, 3	50.3	1, 3
3	4.19	dd	1H	11.16, 3.12	2, 3	68.9	1
	3.94	dd	1H	11.16, 5.58	2, 3	”	1
4	-	-	-	-	-	157.3	3, 5, 6
5	6.86-6.888	m	2H	-	6	114.9	5, 6
6	7.13-7.15	m	2H	-	5	130.1	6, 8
7	-	-	-	-	-	131.2	5, 8, 9
8	2.80	t	2H	6.29	9	38.4	6, 8
9	3.80	q	2H	6.00	8, 10	63.9	8, 10
10	1.52	t	1H	5.70	9	-	8, 9

Identification of by-product 7b

During purification of **7**, a by-product was isolated. It was detected by TLC (1:10 MeOH/CH_2Cl_2); R_f (**7b**) = 0.28. It was determined by NMR that this by-product was the dimer 2,2'-(((2-hydroxypropane-1,3-diyl)bis(oxy))bis(4,1-phenylene))bis(ethan-1-ol) (**7b**). The ^{1}H NMR spectrum of dimer **7b** is shown in Figure A.45. The aromatic and CH_2 peaks integrate to 4H each, indicating dimer formation. The sextet at 4.36 ppm integrates to 1H. This sextet belongs to the proton attached to the tertiary carbon, which couples to five other protons with approximately the same coupling constant. The dimer **7b** is an expected by-product, as the product epoxide **7** is prone to nucleophilic attack by the deprotonated phenol **1** on the least hindered carbon, as shown in Scheme 2.15.

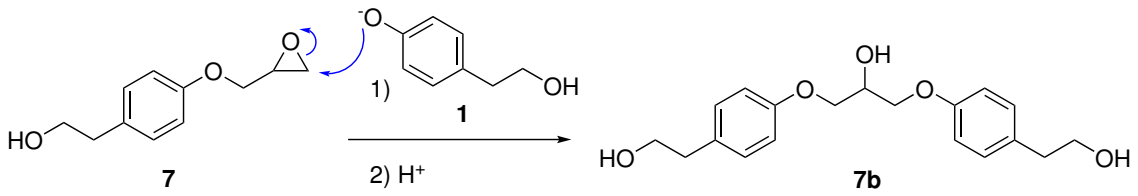

Scheme 2.15 Proposed mechanism for formation of dimer **7b** by nucleophilic attack of **1** on epoxide **7**.

Effect of epichlorohydrin equivalents on the reaction

In a preliminary run of the reaction shown in Scheme 2.14, 1.1 equivalents of epichlorohydrin was used. Only 41% yield was obtained. The dimer **7b** was isolated in 25% yield, which means that about 50% of the starting material was consumed in the formation of this by-product. Thus, it was thought that increasing the amount of epichlorohydrin could help to lower the amount of by-product **7b** that was formed. It was presumed

that having more epichlorohydrin in the reaction mixture would increase the probability of nucleophilic attack of **1** on epichlorohydrin instead of the product epoxide **7**. Indeed, increasing the epichlorohydrin equivalents to 3 gave a yield of 70% of the wanted product **7**. These results are summarized in Table 2.7.

Table 2.7 Effect of epichlorohydrin equivalents (eq) on the yields of **7** and **7b**.

Epichlorohydrin eq	Yield of 7	Yield of 7b
1.1	41%	25%
3.0	70%	7%

2.1.6 Synthesis of 1-bromo-3-(4-(2-(cyclopropylmethoxy)ethyl)phenoxy)propan-2-ol (8b)

Alkylation of the intermediate epoxide **7** with (bromomethyl)cyclopropane was believed to produce epoxide **6**, as this has been reported previously by Muthukrisnan *et al.* [62]. However, after careful analysis, the main product obtained in the present experiment was identified as bromohydrin **8b**. The reaction is shown in Scheme 2.16. The intermediate epoxide **7** was stirred with (bromomethyl)cyclopropane in acetonitrile. The solution was cooled in an ice bath upon slow addition of the base. After 5 hours, the ice bath was removed and the reaction was left to stir at room temperature overnight.

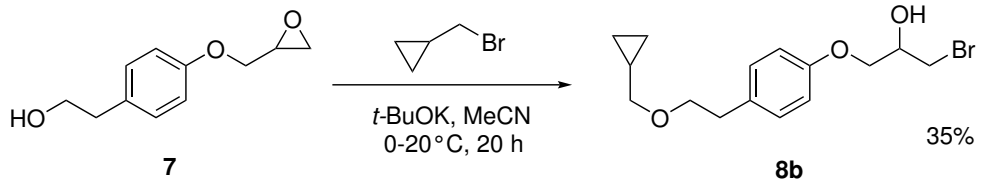

Scheme 2.16 Synthesis of bromohydrin **8b** in 35% yield from by alkylation of intermediate epoxide **7** with (bromomethyl)cyclopropane.

The reaction mixture was purified by flash chromatography (1:10 $MeOH/CH_2Cl_2$) to give bromohydrin **8b** in 35% yield and 84% purity. TLC analysis (1:10 $MeOH/CH_2Cl_2$) showed two spots; R_f (**8b**) = 0.72 and an unidentified compound with R_f = 0.33. The TLC showed full conversion of the starting material (**7**), and the expected product (**6**) was not observed on NMR in any of the two fractions collected after flash chromatography. The spot at R_f = 0.33 was not identified, but the NMR analysis indicated dimer formation. This was also seen on GC-MS, which showed molecular masses of m/z = 600 to 850. The structure of the by-products was not analyzed further.

Proposed mechanism of formation of bromohydrin 8b

Scheme 2.17 shows a possible mechanism for formation of bromohydrin **8b**. After deprotonation of the primary alcohol function of **7**, the anion acts as a nucleophile that attacks the (bromomethyl)cyclopropane in an S_N2 reaction, forming **6**. Subsequently, it is possible that the bromide ion that now exists in the solution attacks the epoxide on the least substituted carbon, giving anionic **8b** which is converted to the bromohydrin (**8b**) during acidic work-up.

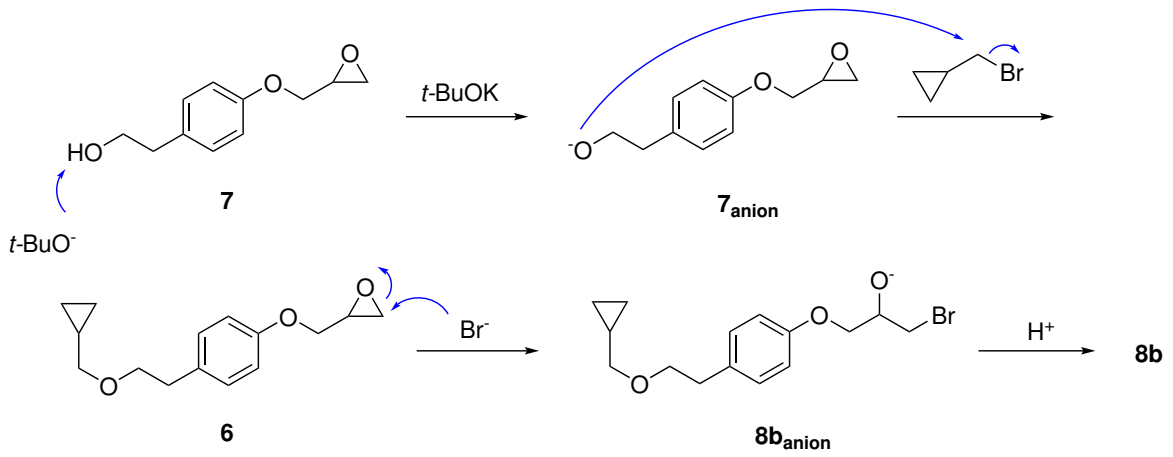

Scheme 2.17 Suggested mechanism for formation of bromohydrin **8b** from **7**. Nucleophilic attack on (bromomethyl)cyclopropane by deprotonated **7** may be followed by nucleophilic addition of the released bromide to epoxide **6**.

HPLC analysis of bromohydrin 8b

Chiral HPLC was used to separate the enantiomers of **8b**. The chromatogram in Figure 2.8 shows two main peaks at t_R((*S*)-**8b** = 11.3 min and t_R((*R*)-**8b** = 13.7 min, with a resolution R_s = 4.1. Two unknown impurities were also detected, at t_R = 5.0 min and t_R = 7.0 min. The retention times of bromohydrin **8b** are very similar to those observed for chlorohydrin **8a**, which is expected as they are similar in structure.

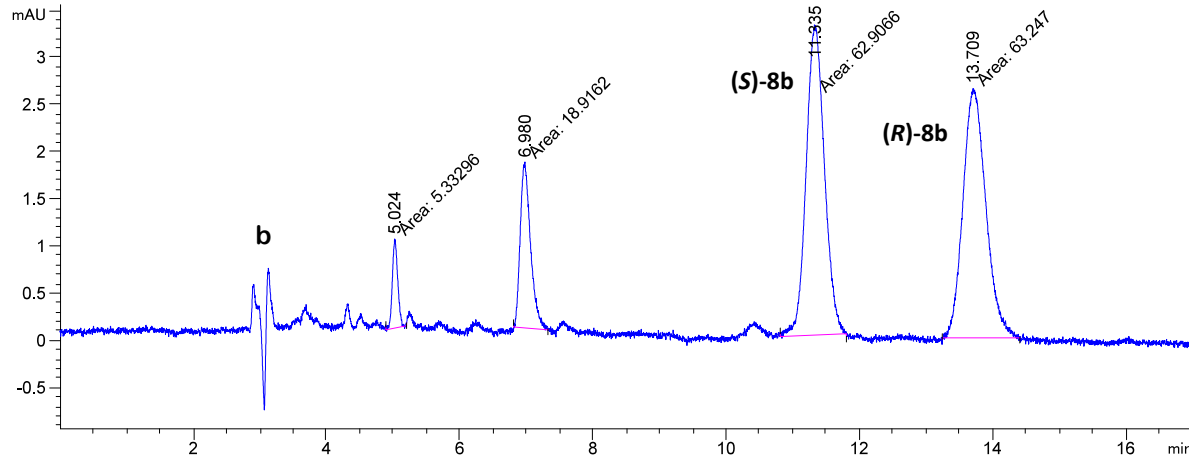

Figure 2.8 HPLC chromatogram of bromohydrin **8b**, t_R((*S*)-**8b**) = 11.3 min and t_R((*R*)-**8b**) = 13.7 min, resolved on a Chiralcel OD-H column with mobile phase composition *n*-hexane:*i*-PrOH (90:10), and flow 1 mL min^{-1}. b = in the blank.

LC-MS validation of bromohydrin 8b

The product of the reaction was confirmed to be bromohydrin **8b** by LC-MS. As shown in Figure 2.9, the bromohydrin eluted at t_R(**8b**) = 6.9 min. Several peaks are observed at later retention times in this chromatogram. Some of them could correspond to the impurities observed in the chiral HPLC chromatogram in Figure 2.8. The LC-MS analysis was performed on a reverse phase column, which is why the peaks appear in the opposite order as in the normal-phase chiral HPLC analysis. Most of the impurities have higher molecular masses and could correspond to dimers or other more complicated structures.

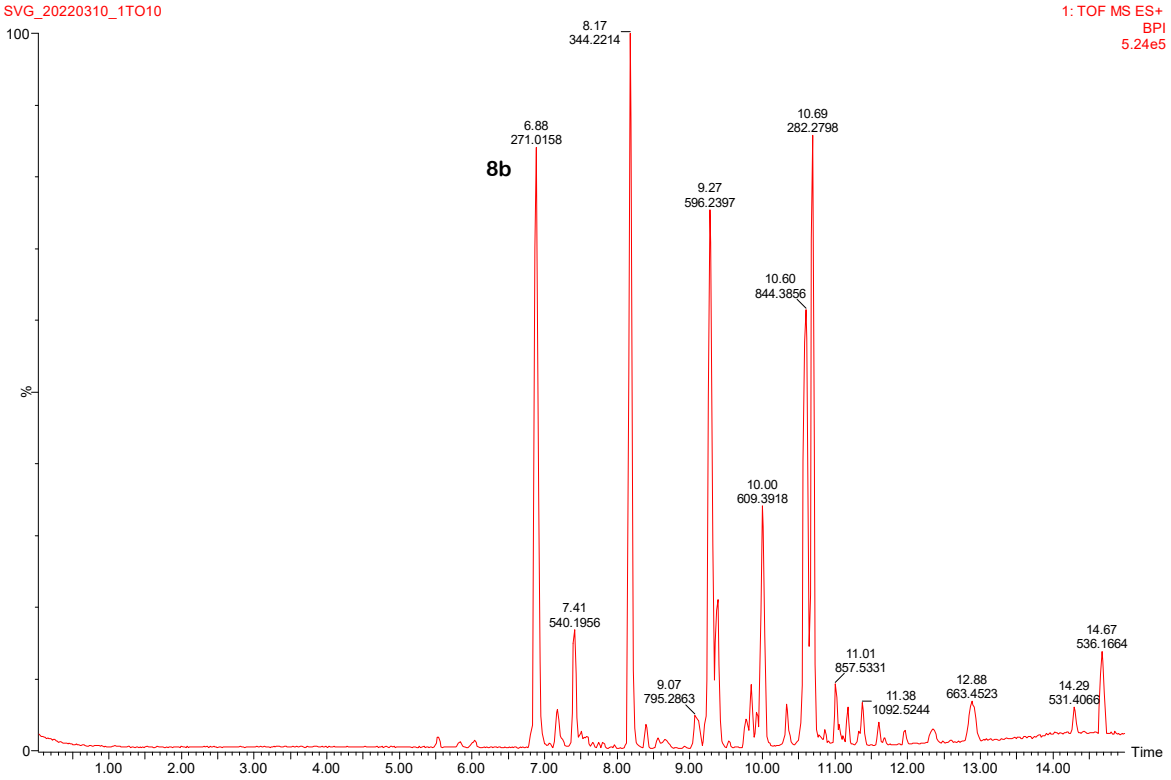

Figure 2.9 LC-MS chromatogram of bromohydrin **8b**, t_R(**8b**) = 6.9 min, eluted on an ACQUITY UPLC HSS T3 Column.

The MS spectrum of the peak observed at t_R(**8b**) = 6.9 min is shown in Figure 2.10. The molecular ion peak $[M+Na]^+$ was observed at $m/z = 351.0572$, which corresponds to the chemical formula $C_{15}H_{21}BrNaO_3$. Thus, bromohydrin **8b** was confirmed as the main product of this reaction.

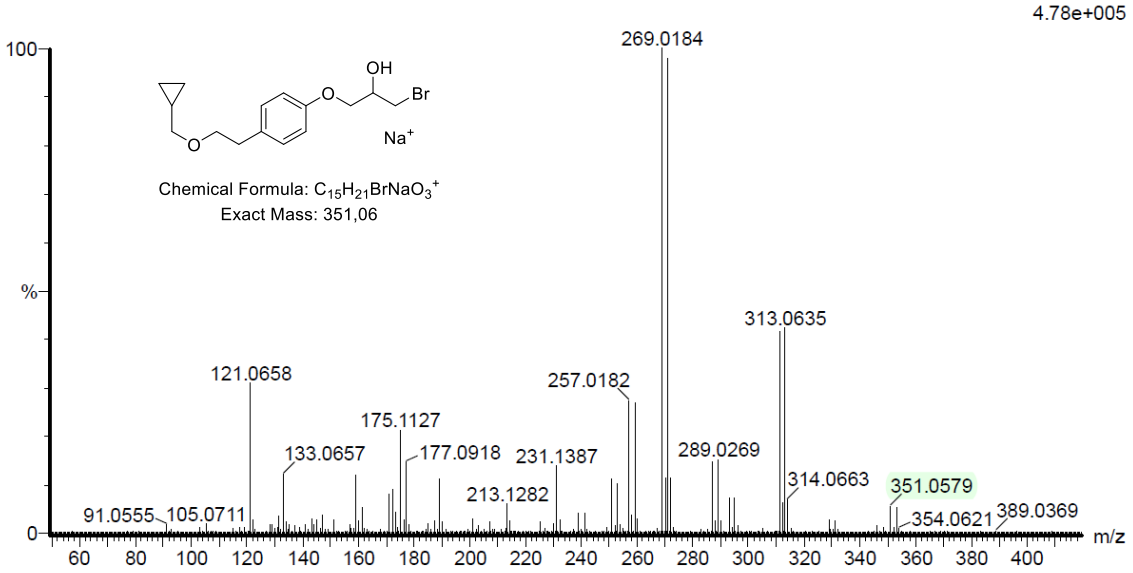

Figure 2.10 TOF MS ES+ spectrum of **8b** with $m/z = 351.0572$ $[M+Na]^+$.

Structural characterization of bromohydrin 8b

The structure of bromohydrin **8b** was confirmed with ^{1}H and ^{13}C NMR. The spectra are shown in Appendix A.8. The NMR spectra were almost identical to that of chlorohydrin **8a**, except that some peaks between 2.5 and 4.2 ppm were observed at different shifts, as shown in Figure 2.11. The most apparent change is an upfield shift for the -CH_2-Br protons, which is a result of increased shielding due to lower electronegativity of the bromine substituent compared to chlorine.

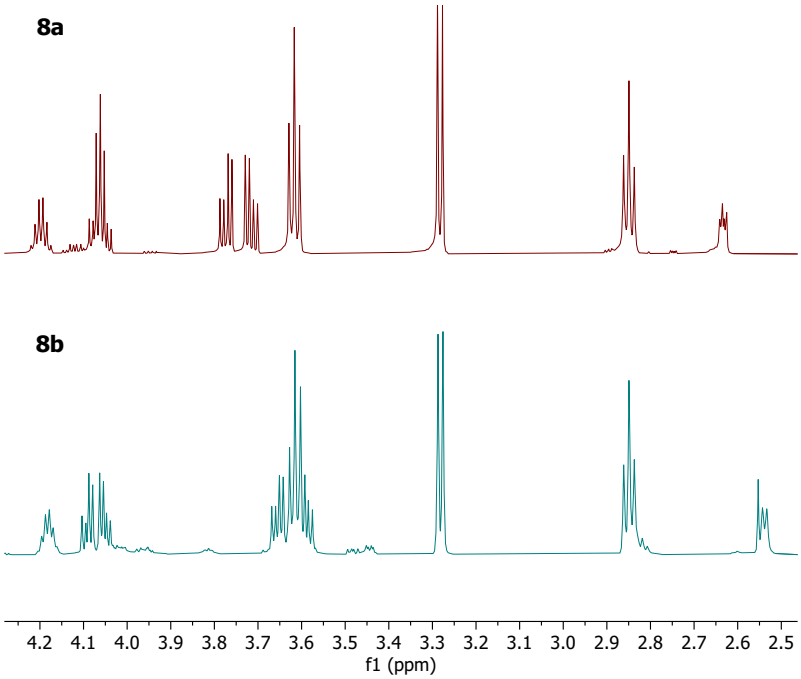

Figure 2.11 Comparison of ^{1}H NMR shifts of chlorohydrin **8a** (top) and bromohydrin **8b** (bottom) in the 2.5-4.2 ppm range.

The NMR spectra of **8b** showed some impurities, which may correspond to the impurities seen in the HPLC and LC-MS chromatograms.

Discussion of reaction conditions in the synthesis of bromohydrin 8b

The reaction conditions of the current experiment (see Scheme 2.18, path A) were based on the work of Muthukrisnan *et al.* [62]. They synthesized epoxide **6** in 96% yield by mixing **7** with (bromomethyl)cyclopropane in N,N-dimethylacetamide. They cooled the mixture to -5°C before adding the base slowly, and let the reaction proceed for 3 h at 0°C, before it was quenched with aqueous hydrochloric acid and extracted with diethyl ether. This is outlined in Scheme 2.18, path B.

The present experiment was very similar to that reported by Muthukrisnan *et al.*, except for three factors: solvent, temperature and reaction time. In the previously reported experiment, N,N-dimethylacetamide was used as the solvent, whereas in the present experiment it was substituted with acetonitrile because it was already available in the lab and is easier to remove under reduced pressure. They are both polar aprotic solvents with similar properties, so it was not apparent that this solvent switch would affect the reaction to a large extent [107].

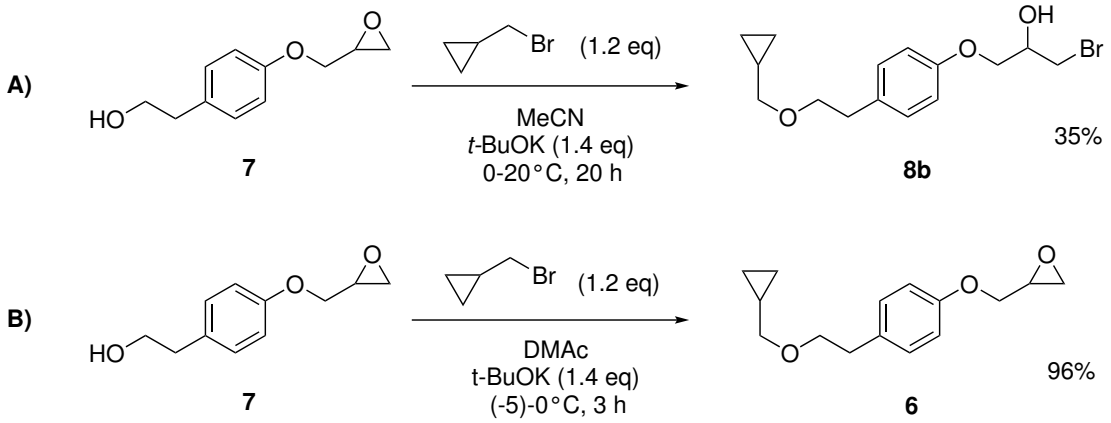

Scheme 2.18 A) Current reaction conditions for alkylation of **7** gave **8b**. B) Reaction conditions reported by Muthukrisnan *et al.* gave **6** [62].

The temperature difference between path A and B in Scheme 2.18 is small in the beginning of the experiments, but is likely that keeping the reaction going at room temperature overnight may have allowed extra time for addition of the bromide ion to the epoxide, which led to formation of **8b**, as explained in Scheme 2.17. The reaction was allowed to react overnight because TLC did not show full conversion after 3 or 5 h. It is possible that Mutukrishnan *et al.* tuned the reaction conditions (time, temperature and solvent) specifically to prevent formation of **8b**, as their target was epoxide **6**. In this project, bromohydrin **8b** is actually preferred over the epoxide, as it may be used directly in the CALB kinetic resolution.

Discussion of work-up conditions in the synthesis of bromohydrin 8b

It was discovered that the acid used in the work-up of this reaction was important for the reaction outcome. The first time this reaction was performed for this thesis, aqueous hydrochloric acid was used to quench the reaction. The product was analyzed by HPLC and LC-MS (see Appendix A.9). LC-MS analysis of the purified reaction mixture revealed that a mixture of chlorohydrin **8a** and bromohydrin **8b** had been formed. Chiral HPLC analysis showed that the main product was the chlorohydrin, and the relationship between the chloro and bromo derivatives was approximately 80:20.

It was suggested that traces of epichlorohydrin in the starting material (**7**) could have been a source of chloride in the reaction. However, the starting material had been purified by flash chromatography, and NMR analysis showed complete absence of epichlorohydrin. Thus, it was presumed that quenching with hydrochloric acid could somehow lead to an exchange of the two halogens, possibly through a fast subsitution reaction. The chloride ion is known to be a stronger nucleophile than bromide in polar aprotic solvents such as acetonitrile [35]. It appears that the presence of water (a protic solvent) did not counteract this effect. The reaction was then performed in the same way as before, on the same batch of starting material, but this time the aqueous hydrochloric acid was substituted with aqueous sulfuric acid. This time, LC-MS did not show presence of the chlorohydrin. Thus, it was concluded that aqueous hydrochloric acid most likely led to exchange of bromine with chloride in the reaction mixture.

2.1.7 Summary and discussion of the two tested synthesis paths to halohydrins 8a and 8b

The intermediates **8a** and **8b** were synthesized in overall yields of 26% and 25%, respectively, from the desired starting material **1** (see Scheme 2.19). Thus, the choice of path should depend on the number of steps and simplicity of each path. Path a consists of three steps, with reaction times 1 h, 22 h and 17 h. Only the first step required purification by flash chromatography, and the purification was easy to perform. Path b required only two steps, with reaction times 23 h and 20 h, but flash chromatography was needed for both, which makes it a slightly more complicated synthesis path. It also required larger quantities of organic solvents during purification, which from a green chemistry perspective is unwanted.

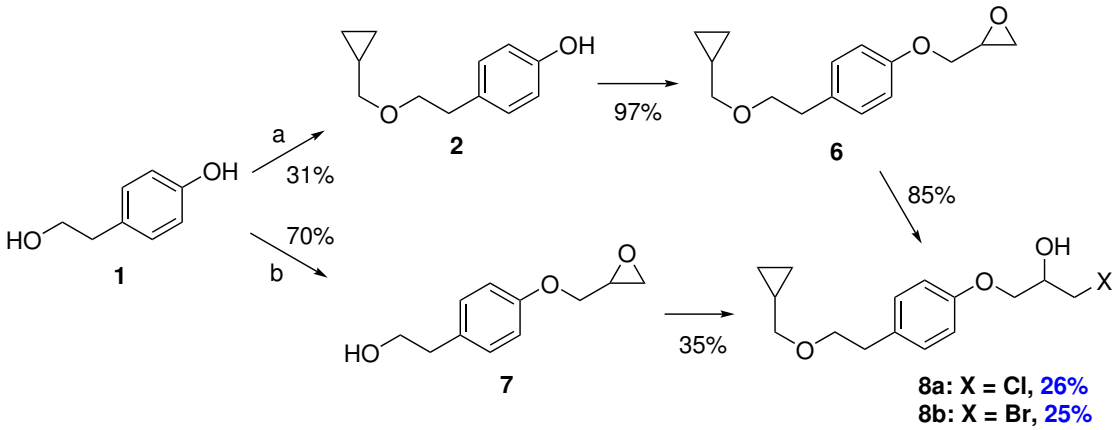

Scheme 2.19 The two pathways a and b gave overall yields of 26% and 25% of the betaxolol intermediates **8a** and **8b** from the starting material **1**.

Optimization of these reactions has only been done to a certain extent in this project. Thus, it would be interesting to see how each step in the pathways could be optimized. For example, Wang *et al* performed step 1 in path a with a yield of 51%, using the same conditions as here [59]. This means that path a in theory could produce **8a** in 42% overall yield, or higher if the last step also can be improved. However, it is unlikely that the yield could be much higher than this, because the phenol has not been protected. Protection of the phenol was not performed successfully in this thesis, but it has been reported before with the use of a benzyl protecting group [60]. The use of protection groups in this case poses a dilemma; the overall yield may be increased, but does it make up for the time, reagents, solvents, safety precautions and "black" catalysts needed? All of these factors would need to be considered with regards to the principles of green chemistry (see Section 1.1.1). Using a more convenient protecting group may be the solution, which is why the TFP protecting group was tested previously in this thesis, although the results were unsatisfactory.

For path b, it was discussed previously that increasing the amount of epichlorohydrin improved the yield of **7** (see Table 2.7). Even though it is not desired to use very large quantities of highly toxic epichlorohydrin, the yield could be improved for this reaction, too. For the last step in path b, there is also high potential for increasing the yield. This makes path b especially appealing, because it most likely can be optimized without introducing additional steps. If the chlorohydrin **8a** is the desired product, it should

be possible to use (chloromethyl)cyclopropane in the alkylation step of path b, or use hydrochloric acid in the work-up, as discussed previously.

This means that both path a and b could be used to produce chlorohydrin **8a**, and path b has greater potential for optimization as it does not require protection. This is a good example of following principle 8 of Section 1.1.1, where derivatization has been avoided by changing the order of the synthesis steps.

2.1.8 Synthesis of racemic 1-chloro-3-(4-(2-(cyclopropylmethoxy)ethyl)phenoxy)propan-2-yl butyrate (9)

With the aim of developing an HPLC method for separation of the enantiomers of the ester product 1-chloro-3-(4-(2-(cyclopropylmethoxy)ethyl)phen-oxy)propan-2-yl butyrate (**9**) from the CALB kinetic resolution of **8a** (discussed in Section 2.1.10), an acylation of **8a** with butyric anhydride was carried out. Pyridine was added as a catalyst. The reaction is shown in Scheme 2.20. The product was not isolated, as the only intention of this reaction was to find a suitable HPLC method for analysis of **9**.

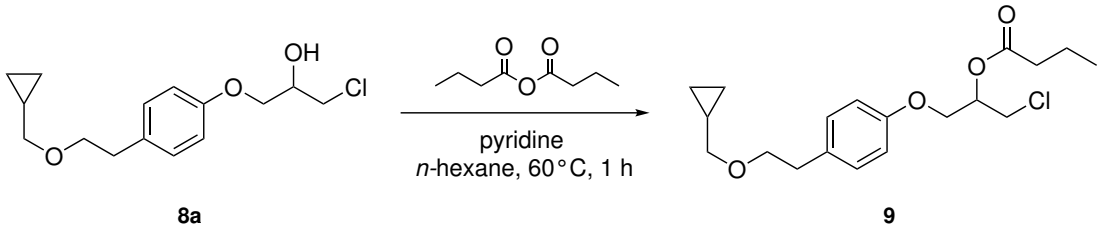

Scheme 2.20 Synthesis of ester **9** by acylation of chlorohydrin **8a** with butyric anhydride in the presence of pyridine.

HPLC analysis of ester 9

A single suitable HPLC method for separation of the enantiomers of ester **9** and chlorohydrin **8a** was not found. The ester required a much weaker eluent. Table 2.8 lists the HPLC mobile phase compositions that were tested for **9**, and the achieved resolution R_s. Sufficient resolution ($R_s > 1.5$) was only obtained with a mobile phase composition *n*-hexane:*i*-PrOH (99:1), and flow 1 mL min^{-1}. With this method, the recorded retention times were t_R((*S*)-**9**) = 14.4 min and t_R((*R*)-**9**) = 15.7 min. This method was not suited for analysis of chlorohydrin **8a**, because it led to too wide peaks and long elution times. The chromatogram obtained with the method is shown in Figure 2.12. After the analysis, the column was flushed with a stronger eluent to elute the remaining chlorohydrin.

Table 2.8 Tested HPLC methods for separation of **9** on a Chiralcel OD-H column.

***n*-hexane:*i*-PrOH**	**Flow (mL min^{-1})**	R_s
95:5	1	0.63
97:3	1	1.11
97:3	0.5	1.26
98:2	1	1.06
99:1	1	1.83

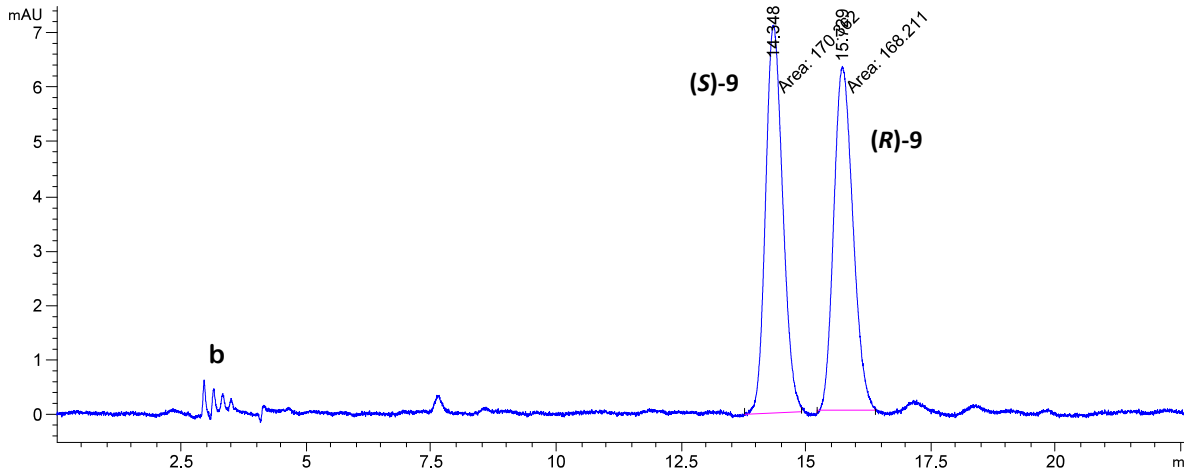

Figure 2.12 HPLC chromatogram of ester **9**, t_R((*S*)-**9**) = 14.4 min and t_R((*R*)-**9**) = 15.7 min, resolved on a Chiralcel OD-H column with mobile phase composition *n*-hexane:*i*-PrOH (99:1), and flow 1 mL min^{-1}. b = in the blank.

Structural characterization of ester 9

Ester **9** was characterized by ^{1}H, ^{13}C, COSY, HSQC and HMBC NMR. Figure 2.13 shows the labelled structure of **9**, and the assigned shifts are shown in Table 2.9. The NMR spectra of **9** are shown in Appendix A.10. The NMR sample was taken from the isolated **9** of the CALB reaction presented in Section 2.1.10.

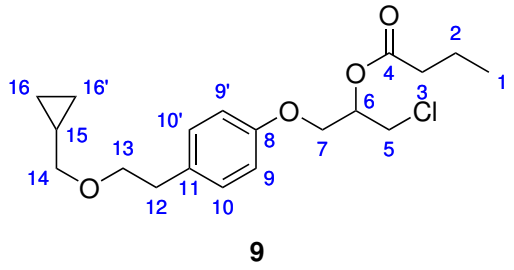

9

Figure 2.13 1-Chloro-3-(4-(2-(cyclopropylmethoxy)ethyl)phen-oxy)propan-2-yl butyrate (**9**) with labelled carbons corresponding to NMR shifts in Table 2.9.

Table 2.9 NMR shifts and correlations observed for ester **9** with carbon labels shown in Figure 2.13.

Label	δ ^{1}H (ppm)	m	I	*J* (Hz)	COSY	δ ^{13}C (ppm)	HMBC
1	0.93-0-99	m	3H	-	2	13.7	2, 3
2	1.65-1.70	m	2H	-	1, 3	18.6	1, 3
3	2.32-2.37	m	2H	-	2	36.2	1, 2, 3
4	-	-	-	-	-	172.9	2, 3, 6
5	3.76-3.86	m	2H	-	6	42.8	6, 7
6	5.33	quint	1H	5.11	5, 7	71.0	4, 5, 7
7	4.12-4.22	m	2H	-	6	66.3	5, 6, 8

Table 2.9 (cont.) NMR shifts and correlations observed for ester **9** with carbon labels shown in Figure 2.13.

Label	δ ^{1}H (ppm)	m	I	*J* (Hz)	COSY	δ ^{13}C (ppm)	HMBC
8	-	-	-	-	-	156.9	7, 9, 10
9	6.83-6.85	m	2H	-	10	114.7	8, 9, 11
10	7.13-7.16	m	2H	-	9	130.1	10, 12
11	-	-	-	-	-	132.1	9, 12, 13
12	2.83-2.86	m	2H	-	13	35.6	10, 11, 13
13	3.59-3.62	m	2H	-	12	71.9	12, 14
14	3.28	d	2H	7.16	15	75.8	13, 16
15	1.04-1.07	m	1H	-	14, 16	10.8	14, 16
16	0.51-0.54	m	2H	-	15, 16	3.1	14, 15, 16
	0.18-0.21	m	2H	-	15, 16	”	14, 15, 16

2.1.9 Synthesis of racemic betaxolol (10)

The method for synthesis of betaxolol (**10**) was adapted from Banoth and Banerjee [68]. Chlorohydrin **8a** was stirred under reflux with isopropylamine in methanol, as shown in Scheme 2.21. This reaction proceeds through an S_N2 mechanism, where the amine replaces the chlorine atom.

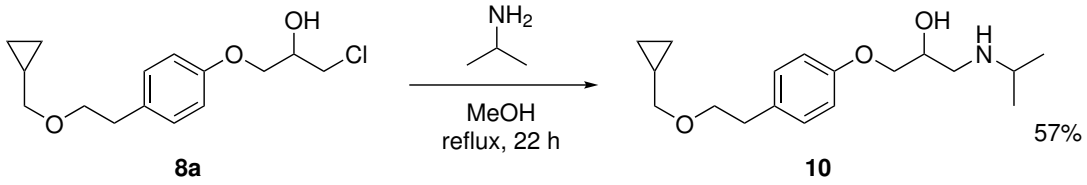

Scheme 2.21 Synthesis of racemic betaxolol (**10**) in 57% yield by amination of chlorohydrin **8a** with isopropylamine.

Betaxolol (**10**) was obtained in 57% yield and 95% purity. The yield was improved during the synthesis of enantiopure betaxolol (**10**), described in Section 2.1.12.

HPLC analysis of racemic betaxolol (10)

The racemic mixture of **10** was analyzed by HPLC to record the retention times of the two enantiomers. This gave t_R((*S*)-**10**) = 6.4 min and t_R((*S*)-**10**) = 12.4 min, as shown in Figure 2.14. The ghost peak (labelled b) was more apparent when using diethylamine in the eluent and using *i*-PrOH as the solvent for the HPLC sample, as done here. The blank also showed the ghost peak (see Figure A.48).

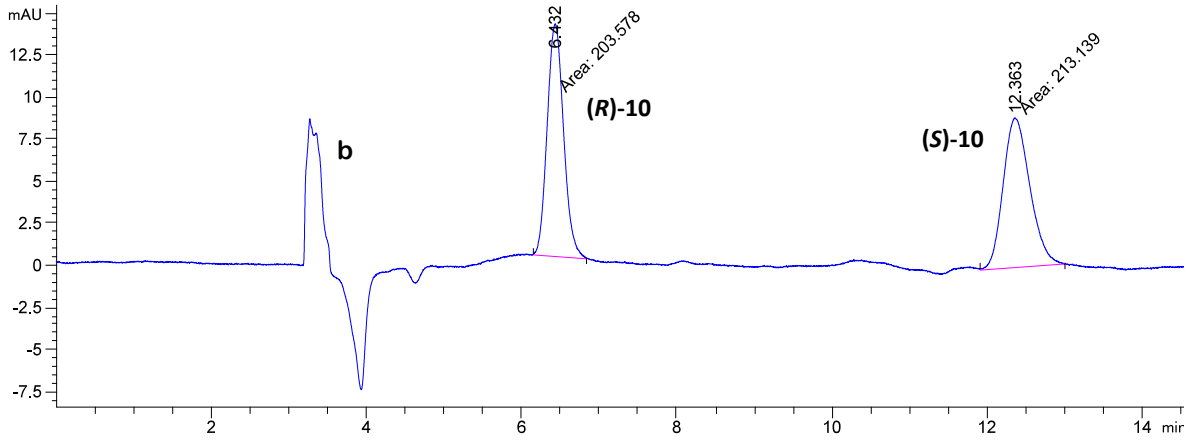

Figure 2.14 HPLC chromatogram of betaxolol (**10**), t_R((*R*)-**10**) = 6.4 min, t_R((*S*)-**10**) = 12.4 min, resolved on a Chiralcel OD-H column with mobile phase composition *n*-hexane:*i*-PrOH:diethylamine (90:9.8:0.2), and flow 1 mL min^{-1}. b = in the blank.

Structural characterization of betaxolol (10)

The ^{1}H, ^{13}C, COSY, HSQC and HMBC NMR spectra of betaxolol (**10**), from the synthesis in Section 2.1.12, are given in Appendix A.11. **10** was fully characterized by NMR, and the assignments of NMR shifts are given in Table 2.10, with the corresponding atom labels shown in Figure 2.15. The -OH and -NH protons gave a broad singlet at 3.81 ppm. This peak was confirmed to belong to these protons by adding a drop of deuterated water to the NMR sample, which made the signals disappear due to exchange of the protons with deuterium, which is invisible on ^{1}H NMR.

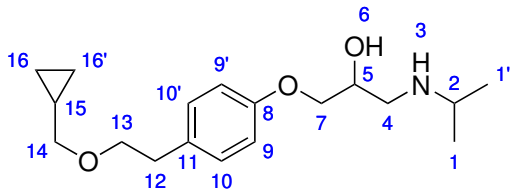

Figure 2.15 Betaxolol (**10**), with labelled atoms corresponding to NMR shifts in Table 2.10.

Table 2.10 NMR shifts and correlations observed for betaxolol (**10**) with atom labels shown in Figure 2.15.

Label	δ ^{1}H (ppm)	m	I	*J* (Hz)	COSY	δ ^{13}C (ppm)	HMBC
1	1.19	dd	6H	3.17, 6.34	2	22.2, 22.0	1, 2
2	2.98-3.01	m	1H	-	1	49.8	1, 4
3/6	3.81	bs	2H	-	-	-	-
4	2.98-3.01	m	1H	-	4, 5	49.2	2, 5, 7
	2.82-2-85	m	1H	-	4, 5	”	2, 5, 7
5	4.15-4.18	m	1H	-	4, 7	67.9	4, 7
7	3.93-4.00	m	2H	-	5	70.4	4, 5, 8
8	-	-	-	-	-	157.2	7, 9, 10

Table 2.10 (cont.) NMR shifts and correlations observed for betaxolol (**10**) with atom labels shown in Figure 2.15.

Label	δ ^{1}H (ppm)	m	I	*J* (Hz)	COSY	δ ^{13}C (ppm)	HMBC
9	6.82-6.84	m	2H	-	10	114.6	9
10	7.12-7.14	m	2H	-	9	130.0	10, 12
11	-	-	-	-	-	131.7	9, 12, 13
12	2.84	t	2H	7.38	13	35.6	10, 13
13	2.60	t	2H	7.38	12	71.9	12, 14
14	3.28	d	2H	6.85	15	75.8	13, 16
15	1.04-1.06	m	1H	-	14, 16	10.8	14, 16
16	0.51-0.54	m	2H	-	15, 16	3.1	14, 16
16	0.18-0.20	m	2H	-	15, 16	”	14, 16

Attempted synthesis of betaxolol (10) through alternative method

Another method for synthesis of **10** was also tested. This method has been successful for amination of similar chlorohydrin precursors performed previously by the biocatalysis group [11]. For this synthesis, shown in Scheme 2.22, isopropylamine was used as the solvent, and a few drops of water were added to dissolve the released HCl that would be formed during the reaction.

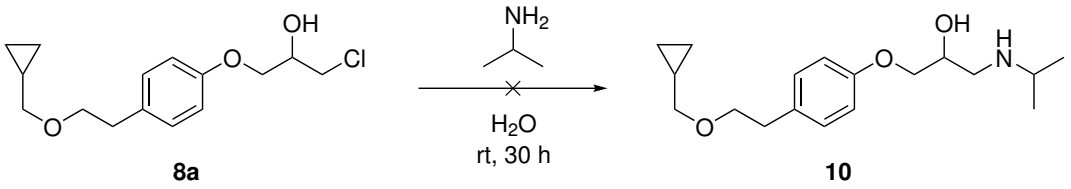

Scheme 2.22 Attempted synthesis of racemic betaxolol (**10**) by amination of chlorohydrin **8a** with isopropylamine as the solvent.

After 30 hours of reaction time, TLC showed mostly starting material. The crude mixture was analyzed by ^{1}H NMR, which showed 99% of chlorohydrin **8a**. This shows that the reaction was not successful with isopropylamine and water, and should be performed with methanol as the solvent.

2.1.10 CALB catalyzed kinetic resolution of 1-chloro-3-(4-(2-(cyclopropylmethoxy)ethyl)phenoxy)propan-2-ol (8a)

CALB was used as an enantioselective biocatalyst for the kinetic resolution of chlorohydrin **8a**. As shown in Scheme 2.23, the reaction was run in dry acetonitrile in a closed vial to prevent water from reacting as the nucleophile. Vinyl butyrate was used as the acyl donor. The product of the esterification was ester (*S*)-**9**, and chlorohydrin (*R*)-**8a** was the remaining unreacted substrate. CALB is selective towards the (*S*)-enantiomer of **8a** and similar chlorohydrins, and this type of kinetic resolution has been performed successfully with chlorohydrin precursors to other β-blockers [11, 105].

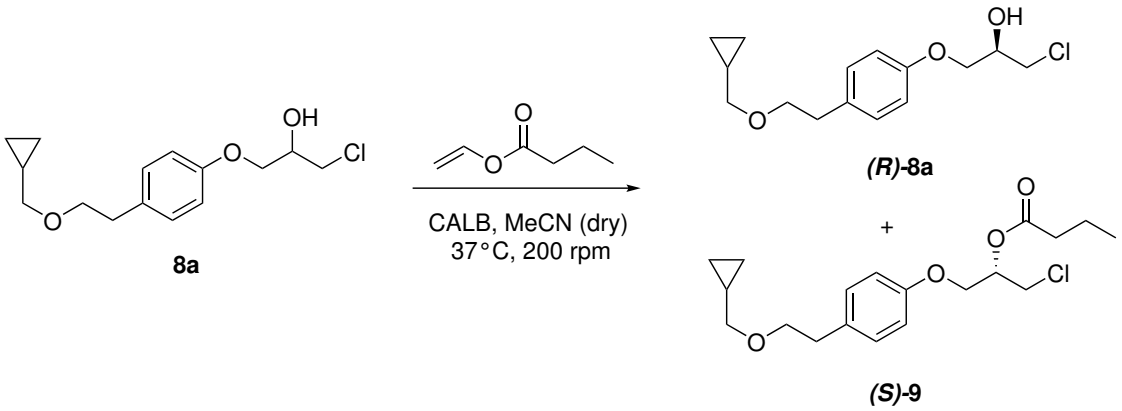

Scheme 2.23 General scheme for the kinetic resolution of chlorohydrin **8a**, catalyzed by CALB.

Reaction monitoring and determination of enantiomeric ratio *E*

The CALB-catalyzed kinetic resolution of **8a** was monitored over time to determine the time at which optimal yield and %ee would be obtained, and to calculate the enantiomeric ratio E of CALB in this specific reaction using the "E&K calculator" [37]. Samples of 100 µL were withdrawn from the reaction at regular time intervals over a total of 12 hours. The samples were analyzed by HPLC to determine the %ee of the ester product and chlorohydrin reactant. Figure 2.16 shows the %ee of the chlorohydrin (blue squares) and ester (red circles) as functions of the % conversion. Based on this, the enantiomeric ratio was determined to be $E = 67$. An entantiomeric excess of 99% was obtained at 53% conversion, which corresponded to a reaction time of 12 hours.

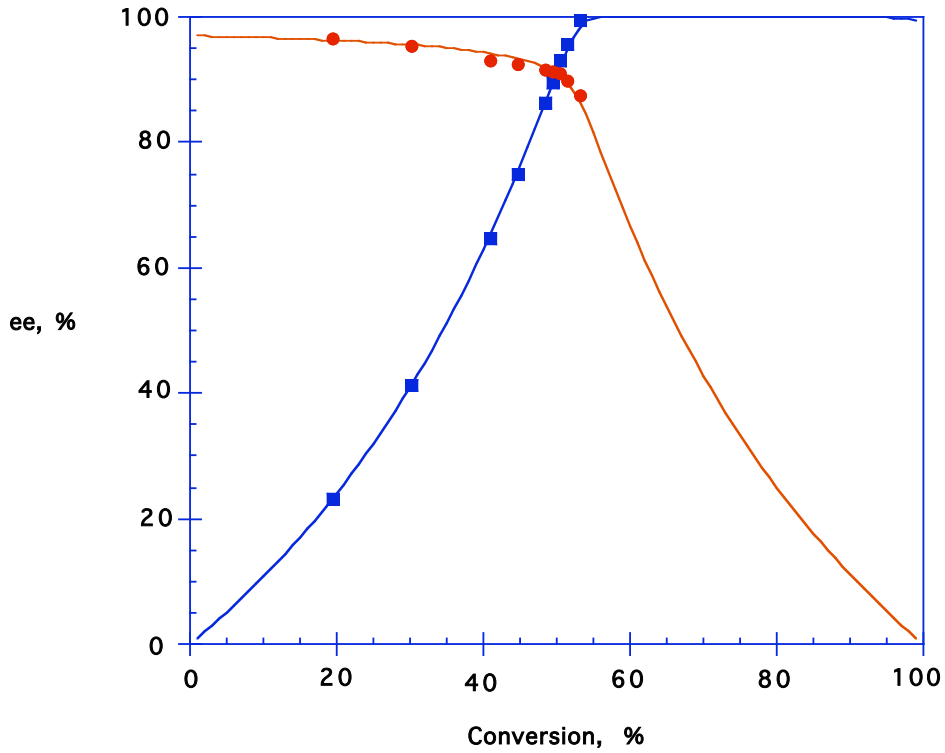

Figure 2.16 Enantiomeric excess (%ee) of the chlorohydrin substrate (blue squares, (*R*)-**8a**) and ester product (red circles, (*S*)-**9a**) as functions of % conversion during the CALB-catalyzed kinetic resolution of **8a** with $E = 67$.

Large scale kinetic resolution of chlorohydrin 8a

The kinetic resolution was also performed on a larger scale to isolate the enantiopure ester product ((*S*)-**9**) and left-over chlorohydrin reactant ((*R*)-**8a**). The reaction is shown in Scheme 2.24. When the reaction was stopped at 12 hours reaction time, the enantiomeric excess of (*R*)-**8a** was calculated to be 97%. Thus, the reaction was allowed to proceed for 14 hours, which increased the enantiomeric excess to 99%.

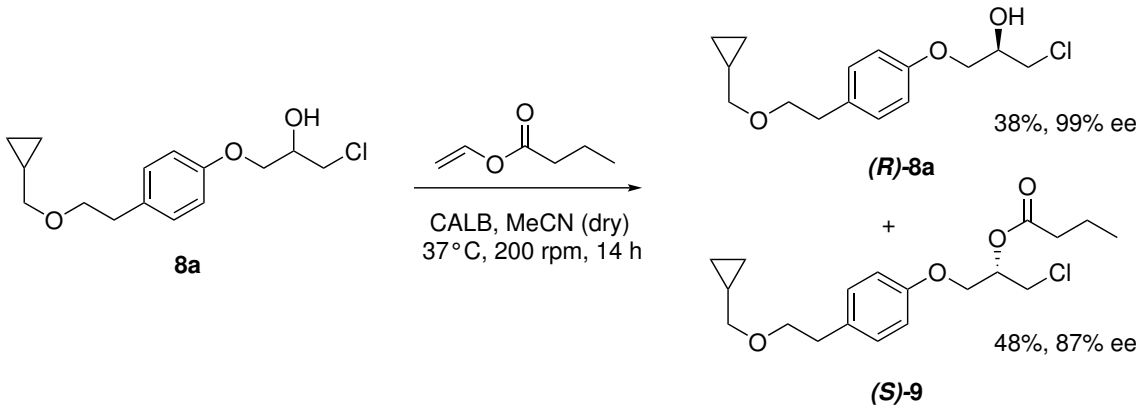

Scheme 2.24 Kinetic resolution of chlorohydrin **8a**, catalyzed by CALB. (*R*)-**8a** was obtained in 38% yield and 99% ee. (*S*)-**9** was obtained in 48% yield and 87% ee.

Flash chromatography (1:4 EtOAc/*n*-pentane) was used to separate the components of the crude mixture. This gave (*R*)-**8a** in 38% yield, 99% purity and 99% ee. The specific rotation of (*R*)-**8a** was measured to $[\alpha]_D^{20} = -1.92$ (*c* 1.04, $CHCl_3$). Ester (*S*)-**9** was obtained in 48% yield, 96% purity and 87% ee. The specific rotation of (*S*)-**9** was measured to $[\alpha]_D^{20} = +13.4$ (*c* 0.97, $CHCl_3$).

The high enantiomeric excess (99% ee) obtained in this experiment shows that CALB is a useful catalyst for the kinetic resolution of **8a**. The method could be optimized to give a higher yield of (*R*)-**8a**, even though it was not attempted in this thesis due to time limitations. The enzymatic kinetic resolution reported by Di Bono *et al.*, using *Pseudomonas sp.* lipase AK, gave (*S*)-betaxolol in 91% ee [65]. The CALB experiments in this thesis shows that CALB is a better suited biocatalyst for this transformation.

Discussion of specific rotation of ester (*S*)-9 and chlorohydrin (*R*)-8a

There is no previously reported data on the specific rotation of (*S*)-**9**. DiBono *et al.* reported the specific rotation of (*R*)-**8a** in 91% ee to be $[\alpha]_D^{20} = +16$ (*c* 1, $CHCl_3$) [65]. In the same publication, the optical rotation of (*S*)-1-chloro-3-(4-(2-(cyclopropylmethoxy)ethyl)-phenoxy)propan-2-yl acetate in 98% ee was reported as $[\alpha]_D^{20} = -1.6$ (*c* 1, $CHCl_3$). This ester is very similar to (*S*)-**9**, except it has an acetate group instead of the butyrate group. These previously reported optical rotation values are similar to the values measured in the current work, except they are assigned to opposite compounds. In the current thesis, the optical rotations were measured twice to ensure that the samples had not been switched by mistake. Below is a summary of observations that indicate that the previously reported optical rotations are incorrect.

The first evidence is the HPLC analyses. In the current thesis, a Chiralcel OD-H column was used for separation of the enantiomers. DiBono *et al.* used a Chiralcel OD column,

which contains the same stationary phase. The only difference between the columns is a larger particle size for the OD column. The same solvent system (*n*-hexane:*i*-PrOH) was used for both analyses. Thus, the enantioselectivity should be the same for both analyses. Indeed, the (*S*)-enantiomers were reported to elute before the (*R*)-enantiomers for both the chlorohydrin and the esters in both analyses. This indicates that the enantiopure (*R*)-chlorohydrin was obtained in both the current work, and the work reported by DiBono *et al.* Additionally, the following amination of (*R*)-**8a** gave (*S*)-betaxolol ((*S*)-**10**), with a negative optical rotation in both the current and previously reported work. This further supports that the same enantiomers have been obtained in both syntheses. Consequently, it is not reasonable that the optical rotations do not match, and one of them are probably incorrect.

It is likely that the optical rotation values of the chlorohydrin and ester have been mistakenly switched in the work of DiBono *et al.* If that is the case, the specific rotation of (*R*)-**8a** in 99% ee is $[\alpha]_D^{20} = -1.92$ (*c* 1.04, $CHCl_3$), as measured in the current work. The specific rotation of the same compound in 91% ee would then be $[\alpha]_D^{20} = -1.6$ (*c* 1, $CHCl_3$). This is a valid result, because the optical rotation is expected to increase with increased enantiomeric excess. If the measurement of the current thesis is instead wrong, (*R*)-**8a** would have a positive optical rotation value. Then, the more enantiomerically pure sample would have a lower optical rotation value (+13.4, compared to +16). This is not an expected result. The conclusion is that the value of $[\alpha]_D^{20} = -1.92$ (*c* 1.04, $CHCl_3$) reported in this thesis is correct.

HPLC analysis of chlorohydrin (*R*)-8a

The enantiomeric excess of the enantiopure chlorohydrin (*R*)-**8a** was determined to 99% ee based on the chromatogram in Figure 2.17. One peak can be observed at t_R((*R*)-**8a**) = 12.5 min, showing that the sample is enantiopure.

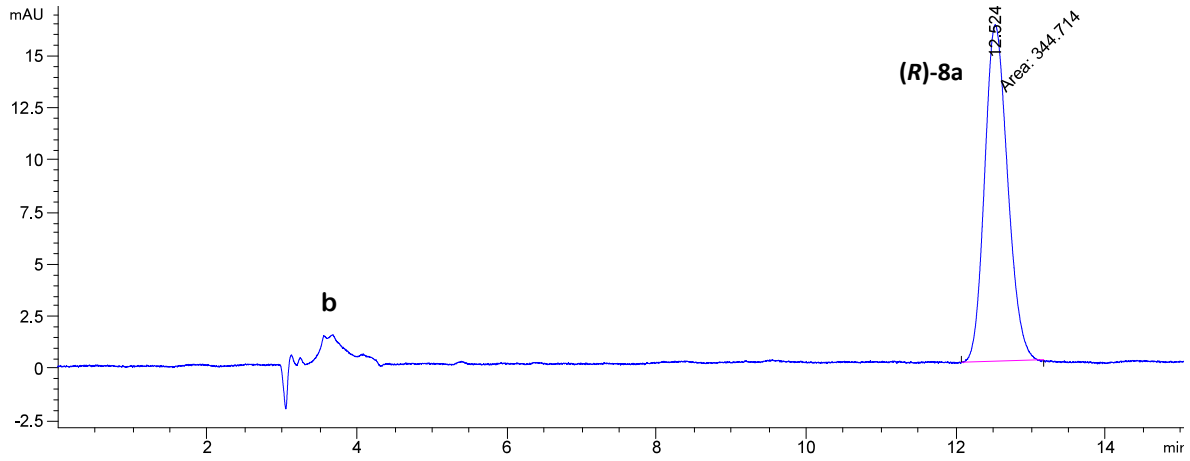

Figure 2.17 HPLC chromatogram of chlorohydrin (*R*)-**8a**. t_R((*R*)-**8a**) = 12.5 min, eluted on a Chiralcel OD-H column with mobile phase composition *n*-hexane:*i*-PrOH (90:10), and flow 1 mL min^{-1}. b = in the blank.

HPLC analysis of ester (*S*)-9

Ester (*S*)-**9** was analyzed by HPLC, producing the chromatogram shown in Figure 2.18. The ester gave peaks at t_R((*R*)-**9**) = 13.3 and t_R((*S*)-**9**) = 14.6 min. The peak of an unknown impurity is also seen at t_R = 15.8 min. The enantiomeric excess of (*S*)-**9** was

calculated to be 87% ee. Lower enantiomeric excess of the ester is expected, because the enzyme may also convert some of the (*R*)-enantiomer into the ester product. As long as the reaction is allowed to proceed long enough, it is expected that all the (*S*)-substrate should have reacted, leaving the remaining (*R*)-substrate in high enantiomeric purity. This can also be seen in Figure 2.16.

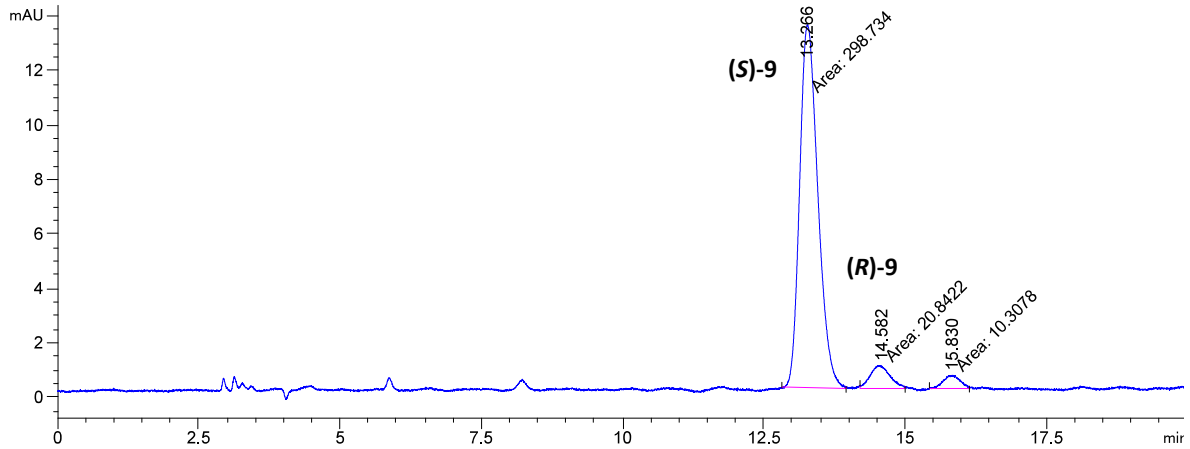

Figure 2.18 HPLC chromatogram of ester (*S*)-**9**. t_R((*R*)-**9**) = 13.3, t_R((*R*)-**9**) = 14.6 min, eluted on a Chiralcel OD-H column with mobile phase composition *n*-hexane:*i*-PrOH (99:1), and flow 1 mL min^{-1}.

2.1.11 CALB catalyzed kinetic resolution of 1-bromo-3-(4-(2-(cyclopropylmethoxy)ethyl)phenoxy)propan-2-ol (8b)

The CALB-catalyzed kinetic resolution was also performed on bromohydrin **8b**. The bromine substituent is larger than chlorine, which means CALB could have a different selectivity on bromohydrin **8b** compared to chlorohydrin **8a**. The reaction, shown in Scheme 2.25, was carried out under the same conditions as for the chlorohydrin.

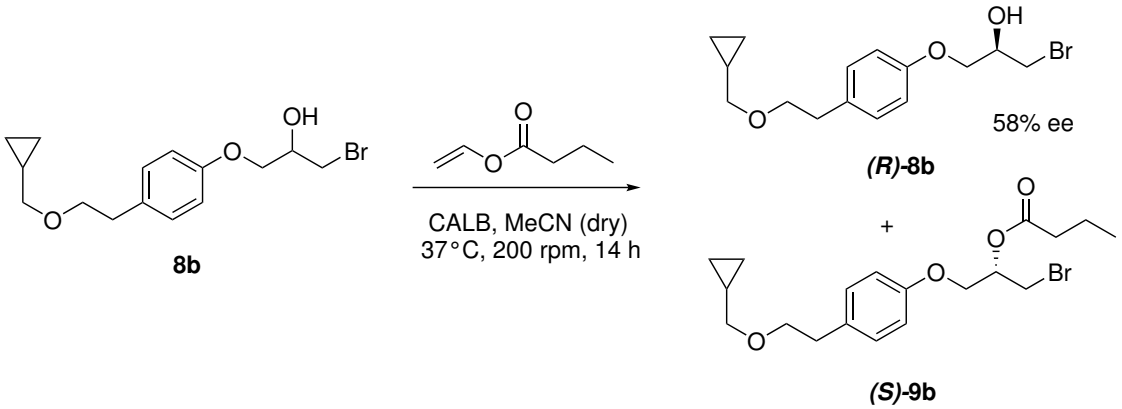

Scheme 2.25 Kinetic resolution of bromohydrin **8b**, catalyzed by CALB. (*R*)-**8b** was produced in 58% ee.

After 14 hours reaction time, bromohydrin **8b** was isolated in 27% yield and 58% ee. The reaction time was then increased to 3 days see if it could increase the enantiomeric excess. The crude sample now showed the chlorohydrin in 54% ee. This shows that CALB has poorer selectivity for **8b** than **8a**, and sufficient enantiomeric excess was not

achieved. The larger size of bromine compared to chlorine could be the reason. The selectivity of the enzyme is dependent on the presence of one large and one small group on the chlorohydrin, as shown in Figure 1.7. When the chlorine atom, the small group, is exchanged for a larger one, it is reasonable that the selectivity may decrease. A lower E-value for CALB with bromohydrins compared to chlorohydrins has been seen before [44]. The selectivity could be improved by using a different acyl donor, as demonstrated with other substrates previously [44]. This was not tested in this thesis due to time limitations.

HPLC analysis of bromohydrin (*R*)-8b

The enantiomeric excess of the enantiomerically enriched bromohydrin **8b** was determined to be 58% ee based on the chromatogram in Figure 2.19. The two enantiomers gave peaks at $t_R((S)\text{-}\mathbf{8b}) = 11.3$ min and $t_R((R)\text{-}\mathbf{8b}) = 13.6$ min.

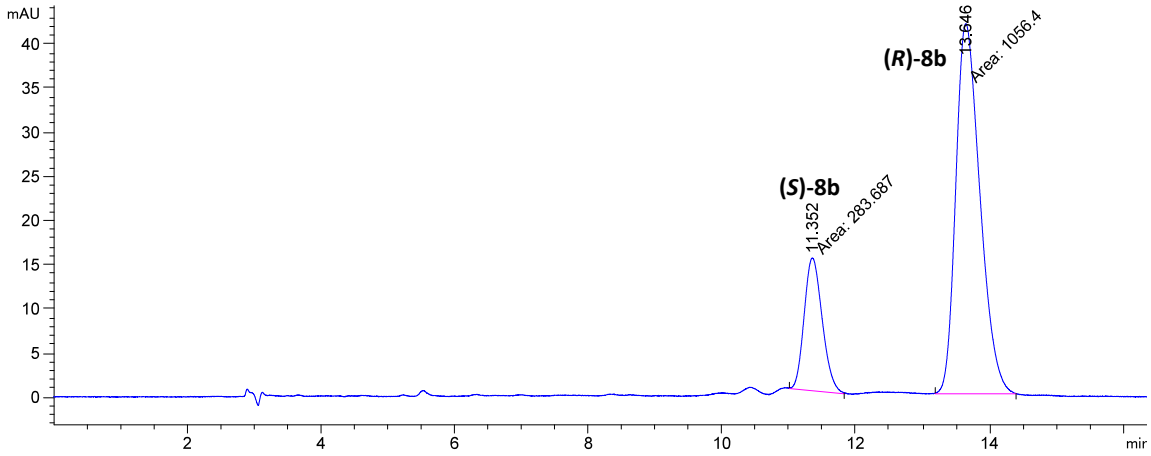

Figure 2.19 HPLC chromatogram of bromohydrin (*R*)-**8b**. $t_R((S)\text{-}\mathbf{8b}) = 11.3$ min, $t_R((R)\text{-}\mathbf{8b}) = 13.6$ min, eluted on a Chiralcel OD-H column with mobile phase composition *n*-hexane:*i*-PrOH (90:10), and flow 1 mL min^{-1}.

2.1.12 Synthesis of (*S*)-betaxolol ((*S*)-10)

Enantiopure chlorohydrin (*R*)-**8a** was converted to (*S*)-betaxolol ((*S*)-**10**) through an amination reaction with isopropylamine in methanol, as shown in Scheme 2.26.

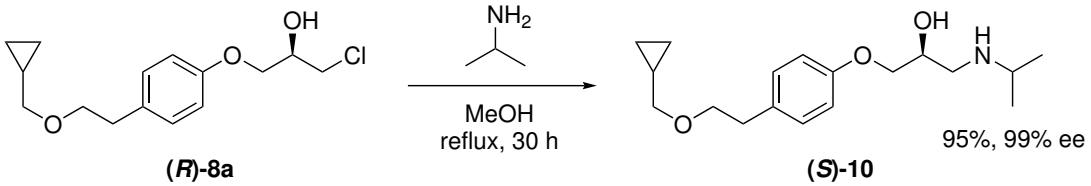

Scheme 2.26 Synthesis of (*S*)-betaxolol ((*S*)-**10**) in 95% yield and 99% ee by amination of chlorohydrin (*R*)-**8a** (99% ee) with isopropylamine in methanol.

After 30 hours, full conversion was detected by TLC (1:11 MeCN/CH_2Cl_2). (*S*)-Betaxolol ((*S*)-**10**) was obtained in 95% yield, 98% purity and 99% ee. The specific rotation was $[\alpha]_D^{20} = -7.21$ (*c* 0.97, $CHCl_3$). This value corresponds with the reported literature value, which is $[\alpha]_D = -7.13$ (*c* 1, $CHCl_3$) [60]. In the synthesis of racemic **10**, the yield was 57% (see section 2.1.9). In the synthesis of (*S*)-**10**, the yield was improved to 95% by

extracting with dichloromethane instead of ethyl acetate. It was discovered that the solubility of **10** in ethyl acetate was not ideal, as the product precipitated when ethyl acetate was added to the crude mixture.

HPLC analysis of enantiopure (*S*)-betaxolol ((*S*)-10)

The HPLC analysis of (*S*)-**10** gave t_R((*S*)-**10**) = 12.3 min, as shown in Figure 2.20. The blank (see Figure A.48) also showed the ghost peak, which is labelled b in the chromatogram. The enantiomeric excess of (*S*)-**10** was determined to be 99% ee.

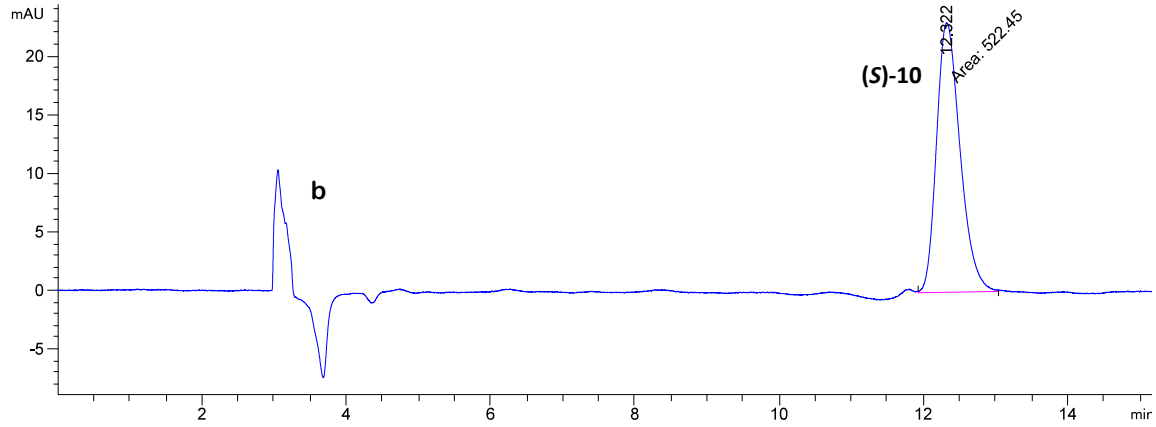

Figure 2.20 HPLC chromatogram of (*S*)-betaxolol ((*S*)-**10**), t_R((*S*)-**10**) = 12.4 min, eluted on a Chiralcel OD-H column with mobile phase composition *n*-hexane:*i*-PrOH:diethylamine (90:9.8:0.2), and flow 1 mL min^{-1}. b = in the blank.

Importance of removing the (*S*)-ester ((*S*)-9)

The synthesis of enantiopure (*S*)-**10** was attempted several times. Often, there was a loss of enantiomeric excess after the amination of the chlorohydrin (*R*)-**8a** to form (*S*)-**10**. It was discovered that this was a result of incomplete separation the ester and chlorohydrin during flash chromatography after the CALB catalyzed kinetic resolution. If traces of the (*S*)-ester could be observed on the NMR sample of the chlorohydrin ((*R*)-**8a**), the product ((*S*)-**10**) of the amination would have lower enantiopurity. This could be a result of aminolysis of the (*S*)-ester, followed by amination of the resulting (*S*)-chlorohydrin to give the unwanted (*R*)-betaxolol ((*R*)-**10**), as shown in Scheme 2.27. The problem was solved by using a longer flash chromatography column for the separation.

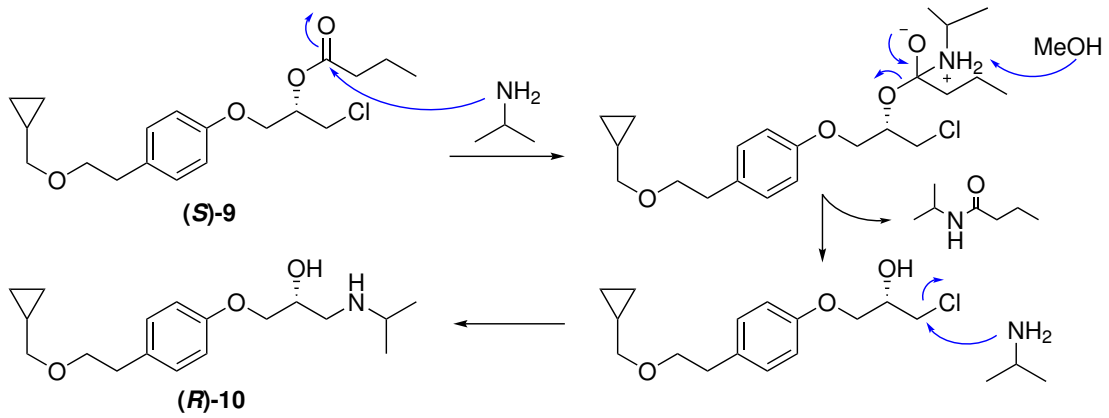

Scheme 2.27 Suggested mechanism for conversion of ester (*S*)-**9** to the unwanted enantiomer (*R*)-betaxolol ((*R*)-**10**).

2.2 Pathway to (*S*)-esmolol

This part of the results and discussion section reports the results obtained in the synthesis of (*S*)-esmolol (**15**) and precursors. The work performed in this thesis has been based on the work of previous master student Anna Lifen Tennfjord [104], who studied the mechanisms and by-products seen in the pathway to (*S*)-esmolol ((*S*)-**15**) in greater detail than what will be done here. The precursors to (*S*)-**15** have been fully characterized in her thesis, which is why only the ^{1}H NMR spectra are provided here.

The main goal of this part of the current thesis was to obtain high purity and enantiomeric excess of (*S*)-esmolol, as this was not achieved in the previous work [104].

2.2.1 Synthesis of methyl 3-(4-(oxiran-2-ylmethoxy)phenyl)propanoate (12)

The epoxide methyl 3-(4-(oxiran-2-ylmethoxy)phenyl)propanoate (**12**) was synthesized from the commercially available starting material methyl 3-(4-hydroxyphenyl)propanoate (**11**) as shown in Scheme 2.28, using a method adapted from Banoth and Banerjee [68]. Phenol **11** was stirred with epichlorohydrin and potassium carbonate under reflux.

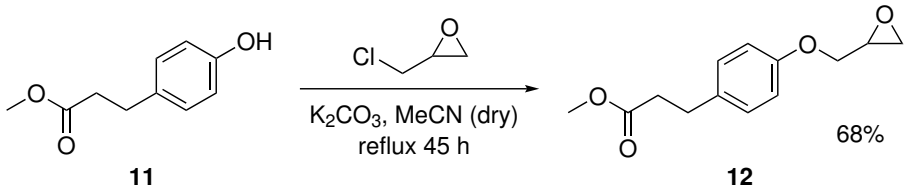

Scheme 2.28 Synthesis of epoxide **12** in 68% yield from **11** and epichlorohydrin in the presence of base.

TLC analysis showed full conversion of phenol **11** into epoxide **12** and an unidentified by-product after 2 days. The crude mixture was separated by flash chromatography (1:11 $MeCN/CH_2Cl_2$). Epoxide **12** was isolated in 68% yield and 99% purity. The ^{1}H NMR spectrum is given in Appendix B.1.

For this reaction, 2 equivalents of epichlorohydrin was used. Increasing the amount of epichlorohydrin could possibly increase the yield of **12**, as seen in the synthesis of **6** (see Table 2.7). The by-product detected by TLC is likely the dimer of **12** (equivalent to dimer **7b**), as this was confirmed as a by-product of this reaction previously by Tennfjord [104]. It was not analyzed in this work.

2.2.2 Synthesis of methyl 3-(4-(3-chloro-2-hydroxypropoxy)phenyl)propanoate (13)

The chlorohydrin methyl 3-(4-(3-chloro-2-hydroxypropoxy)phenyl)propanoate (**13**) was synthesized by epoxide ring-opening on **12** induced by lithium chloride and acetic acid, as shown in Scheme 2.29. This synthesis was first performed by previous master candidate Tennfjord [104].

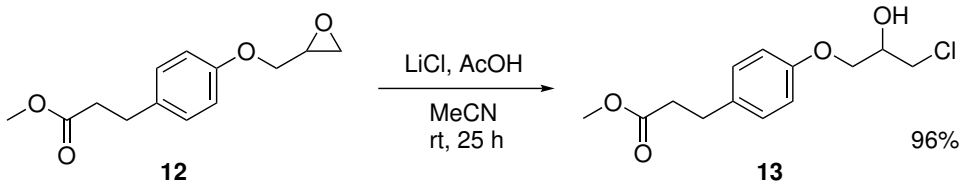

Scheme 2.29 Synthesis of chlorohydrin **13** in 96% yield by ring-opening of epoxide **12** by LiCl and AcOH in MeCN at room temperature.

Chlorohydrin **13** was obtained in 96% yield and 96% purity without purification. This was deemed pure enough to continue to the enzymatic kinetic resolution, as flash chromatography would be run after the resolution which would remove any impurities from this previous step. The ^{1}H NMR spectrum of **13** is given in Appendix B.2.

HPLC analysis of chlorohydrin 13

The HPLC chromatogram of racemic **13** is shown in Figure 2.21. It shows the two enantiomers of **13** at $t_R((S)\text{-}\mathbf{13}) = 9.4$ min and $t_R((R)\text{-}\mathbf{13}) = 10.3$ min, with a resolution of $R_s = 3.1$. The absolute configurations were determined based on the selectivity of CALB and the chromatogram of the enantiopure chlorohydrin (R)-**13**, shown in Figure 2.24. Two minor impurities are also observed at $t_R = 4.6$ and $t_R = 7.3$. According to Tennfjord, these should be residues of the dimer and epoxide **12** [104]. They were not analyzed further in this work.

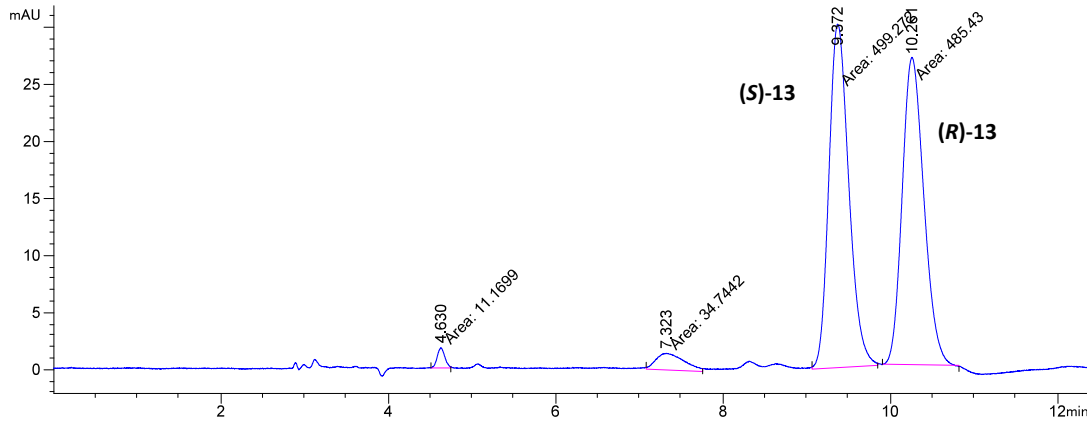

Figure 2.21 HPLC chromatogram of racemic chlorohydrin **13**. $t_R((S)\text{-}\mathbf{13}) = 9.4$ min, $t_R((R)\text{-}\mathbf{13}) = 10.3$ min, eluted on a Chiralcel OD-H column with mobile phase composition n-hexane:i-PrOH (80:20), and flow 1 mL min^{-1}.

2.2.3 Synthesis of racemic esmolol (15)

Racemic esmolol (**15**) was synthesized using a method adapted from Banoth and Banerjee [68]. Chlorohydrin **13** was stirred under reflux with isopropylamine in methanol, according to Scheme 2.30.

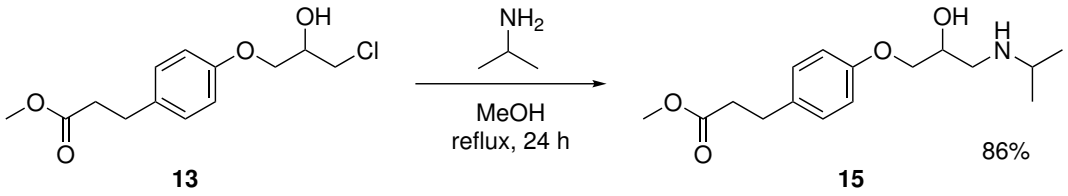

Scheme 2.30 Synthesis of racemic esmolol (**15**) in 86% yield by amination of chlorohydrin **13** with isopropylamine.

The resulting product **15** was obtained in 86% yield and 88% purity. Due to the presence of small amounts of **13**, isopropylamine and some solvent residues, this NMR spectrum was not used to characterize **15**. Instead, the characterization was performed on enantiopure (*S*)-**15**. It was not important that the racemic product was entirely pure, because the only reason for this synthesis was to measure the retention times of both enantiomers of **15**.

HPLC analysis of racemic esmolol (15)

HPLC analysis of racemic **15** was performed to measure the retention times of the enantiomers. They eluted at $t_R((R)\text{-}\mathbf{15}) = 6.1$ min and $t_R((S)\text{-}\mathbf{15}) = 9.5$ min, as shown in Figure 2.22. Baseline separation was achieved, with a resolution of $R_s = 11.5$. The chromatogram also shows two impurities, one of them being the chlorohydrin **13** at $t_R((R)\text{-}\mathbf{13}) = 10.2$ min.

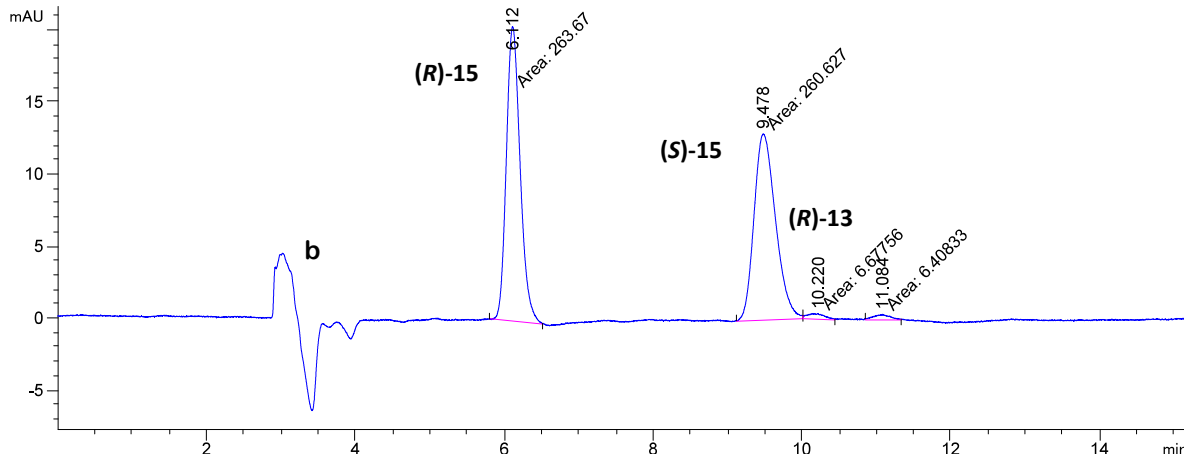

Figure 2.22 HPLC chromatogram of racemic esmolol (**15**). $t_R((R)\text{-}\mathbf{15}) = 6.1$ min, $t_R((S)\text{-}\mathbf{15}) = 9.5$ min, eluted on a Chiralcel OD-H column with mobile phase composition *n*-hexane:*i*-PrOH:diethylamine (80:19.6:0.4), and flow 1 mL min^{-1}. b = in the blank.

Strucutral characterization of esmolol (15)

The ^{1}H, ^{13}C, COSY, HSQC and HMBC NMR spectra of esmolol (**15**, from the synthesis in Section 2.2.5) are given in Appendix B.4. **15** was fully characterized by NMR. The assignment of NMR shifts are given in Table 2.11, with the corresponding atom labels shown in Figure 2.23. The -OH and -NH protons were not observed in the ^{1}H NMR spectrum.

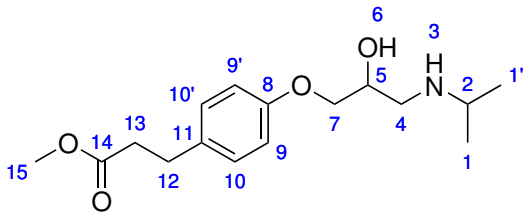

15

Figure 2.23 Esmolol (**15**), with labelled atoms corresponding to NMR shifts in Table 2.11.

Table 2.11 NMR shifts and correlations observed for esmolol (**15**) with atom labels shown in Figure 2.23.

Label	δ ^{1}H (ppm)	m	I	*J* (Hz)	COSY	δ ^{13}C (ppm)	HMBC
1	1.07	d	6H	6.30	2	23.1, 23.2	1, 4
2	2.81	quint	1H	6.30	1	49.0	1, 4
4	2.70	dd	1H	8.03, 12.14	4	49.5	2, 5, 7
	2.86	dd	1H	3.80, 12.14	4	”	2, 5, 7
5	3.98-4.00	m	1H	-	4, 7	68.6	4, 7
7	3.92-3.96	m	2H	-	5	70.7	4
8	-	-	-	-	-	157.3	7, 9, 10
9	6.82-6.84	m	2H	-	10	114.7	9
10	7.08-7.10	m	2H	-	9	129.3	10, 12
11	-	-	-	-	-	133.0	9, 12, 13
12	2.87	t	2H	7.60	13	30.2	10, 13
13	2.58	t	2H	7.60	12	36.0	12
14	-	-	-	-	-	173.5	12, 13, 15
15	3.65	s	3H	-	51.7	-	

2.2.4 CALB catalyzed kinetic resolution of methyl 3-(4-(3-chloro-2-hydroxypropoxy)phenyl)propanoate (13)

Enantiopure (*R*)-**13** was obtained through CALB-catalyzed kinetic resolution in an enantioselective esterification of **13** with vinyl butyrate, as shown in Scheme 2.31. The product of the esterification was (*S*)-1-chloro-3-(4-(3-methoxy-3-oxopropyl)phenoxy)propan-2-yl butyrate (*S*)-**14**, and chlorohydrin (*R*)-**13** was the remaining unreacted substrate. The enantiomeric ratio *E* of CALB with chlorohydrin **13** as the substrate has been calculated by Tennfjord to be $E = 157$ [104].

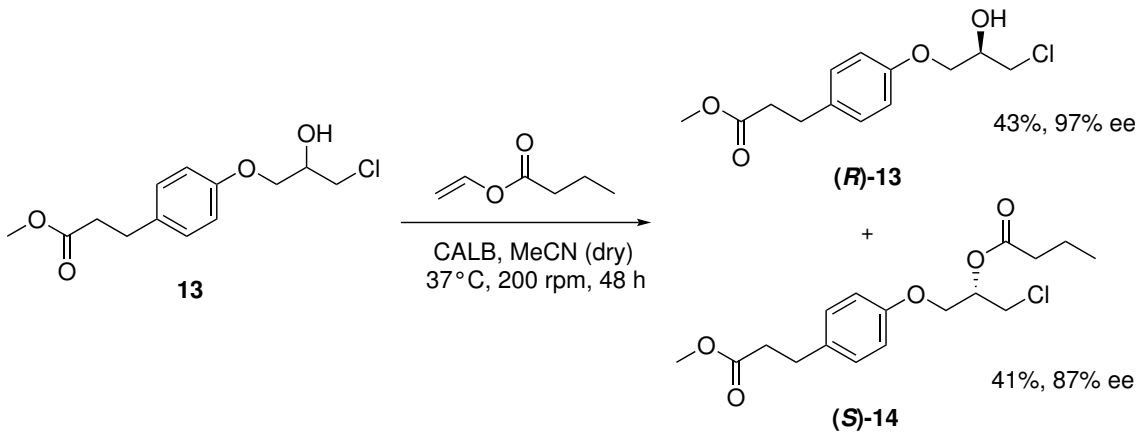

Scheme 2.31 Kinetic resolution of chlorohydrin **13**, catalyzed by CALB. (*R*)-**13** was obtained in 43% yield and 97% ee. (*S*)-**14** was obtained in 41% yield and 87% ee.

Chlorohydrin (*R*)-**13** and ester (*S*)-**14** were separated by flash chromatography (1:4 EtOAc/*n*-pentane) to give (*R*)-**13** in 43% yield, 99% purity and 97% ee. The specific rotation of (*R*)-**13** was measured to $[\alpha]_D^{20} = -5.33$ (*c* 1.6, *i*-PrOH). Ester (*S*)-**14** was isolated in 41% yield, 99% purity and 87% ee. The specific rotation of (*S*)-**14** was measured to $[\alpha]_D^{20} = +30.71$ (*c* 1.4, *i*-PrOH). No previous reports of the specific rotation of these two compounds exist. Absolute configurations were determined based on the enantioselectivity of CALB [44]. The ^{1}H NMR spectra of **13** and **14** are given in Appendices B.2 and B.3.

HPLC analysis of chlorohydrin (*R*)-13

The enantiomeric excess of the two products after kinetic resolution was determined by HPLC analysis. The chromatogram of enantiopure (*R*)-**13** is shown in Figure 2.24 with the retention times t_R((*S*)-**13**) = 9.2 min and t_R((*R*)-**13**) = 10.2 min. The chromatogram shows an unidentified impurity at t_R = 8.3 min. The enantiomeric excess of (*R*)-**13** was determined to be 97%.

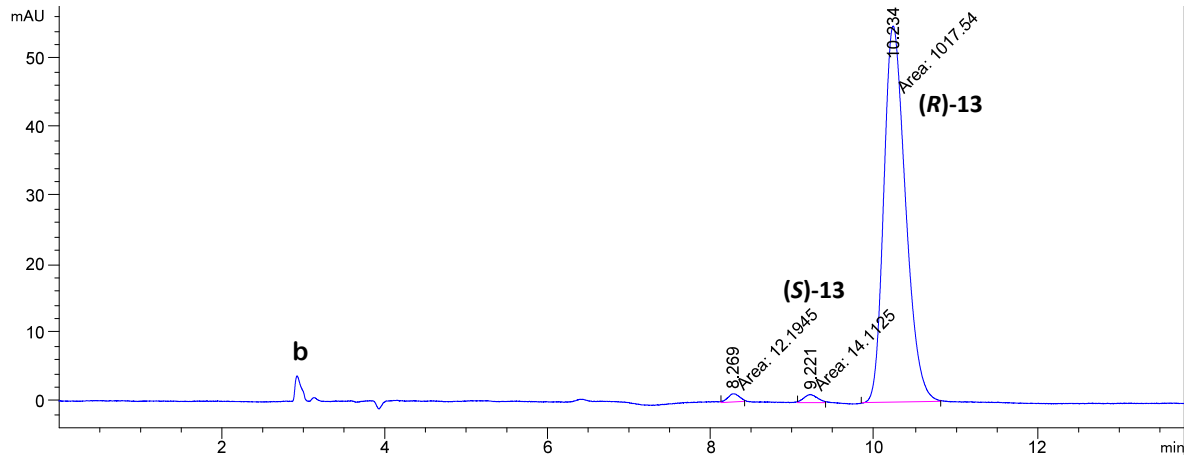

Figure 2.24 HPLC chromatogram of chlorohydrin (*R*)-**13**. t_R((*S*)-**13**) = 9.2 min, t_R((*R*)-**13**) = 10.2 min, eluted on a Chiralcel OD-H column with mobile phase composition *n*-hexane:*i*-PrOH (80:20), and flow 1 mL min^{-1}. b = in the blank.

HPLC analysis of ester (*S*)-14

Ester (*S*)-**14** was analyzed using a different mobile phase composition than chlorohydrin

(*R*)-**13**, which produced the chromatogram shown in Figure 2.25. The recorded retention times were t_R((*S*)-**14**) = 15.6 min and t_R((*R*)-**14**) = 17.3 min. By integration of the peaks, the chromatogram shows that ester (*S*)-**14** was synthesized in 87% ee. As seen previously with betaxolol (**10**), the enantiomeric excess of the ester is lower than the chlorohydrin, which is expected.

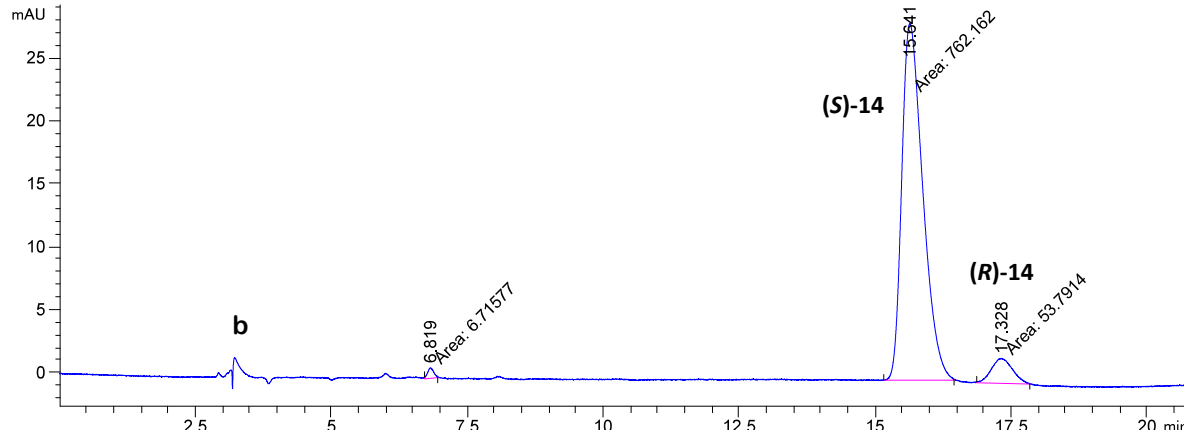

Figure 2.25 HPLC chromatogram of ester (*S*)-**14**. t_R((*S*)-**14**) = 15.6 min, t_R((*R*)-**14**) = 17.3 min, eluted on a Chiralcel OD-H column with mobile phase composition *n*-hexane:*i*-PrOH (97:3), and flow 1 mL min^{-1}. b = in the blank.

2.2.5 Synthesis of (*S*)-esmolol ((*S*)-15)

The enantiopure chlorohydrin (*R*)-**13** was converted to (*S*)-esmolol ((*S*)-**15**) by using the same method as for racemic esmolol (**15**). Tennfjord has used the same method in an attempt to synthesize enantiopure (*S*)-**15**, but she observed a loss of enantiomeric excess from 98% to 89% after this step [104]. This was also observed in the synthesis of (*S*)-betaxolol, as described in Section 2.1.12. This work has been focused on improving this last step of the synthesis of (*S*)-esmolol ((*S*)-**15**). The reaction is shown in Scheme 2.32.

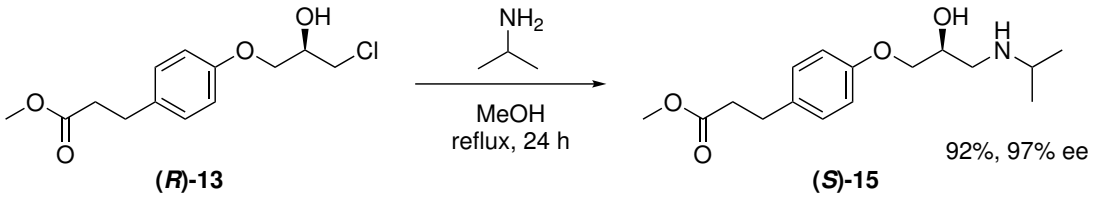

Scheme 2.32 Synthesis of (S)-esmolol ((*S*)-**15**) in 92% yield and 97% ee by amination of chlorohydrin (*R*)-**13** with isopropylamine in methanol.

After 24 hours, TLC analysis (1:11 MeCN/CH_2Cl_2) showed a weak spot for the starting material (*R*)-**13**) and traces of another impurity, which could also be seen on HPLC. The crude mixture was purified by preparative TLC (1:11 MeCN/CH_2Cl_2), to afford (*S*)-esmolol ((*S*)-**15**) in 92% yield, 99% purity and 97% ee. The specific rotation was $[\alpha]_D^{20} = -6.80$ (*c* 1.03, $CHCl_3$). The specific rotation of (*S*)-esmolol ((*S*)-**15**) has been reported as $[\alpha]_D^{20} = +4.5$ (*c* 1, $CHCl_3$) by Narsaiah and Kumar [67]. However, they did not report how the optical rotation was measured. Additionally, for their synthesis of (*S*)-**15**, they did not report the enantiomeric excess, and they did not mention the use

of chiral HPLC for analysis of their chiral compounds. Thus, their value for the specific rotation of (*S*)-**15** is unreliable. The only other report of the specific rotation of (*S*)-**15** gives a value of $[\alpha]_D^{20} = -19.6$ (*c* 1, MeOH), but this is for the hydrochloride salt of (*S*)-**15**, so it can not be directly compared to the free base [108]. They did not mention how the optical rotation or the enantiomeric excess was measured. Due to these sources not being reliable, the absolute configuration of the current product was determined through the known enantioselectivity of CALB, which has been reported previously [44].

The enantiomeric excess was retained in the amination, because the ester and chlorohydrin were completely separated after the previous step. The flash chromatography separation was optimized by using a more effective eluent. The previous method used 1:9 *i*-PrOH/*n*-hexane as the eluent [104]. This gave a difference in R_f vaues of $\Delta R_f = 0.16$. The optimized method (1:4 EtOAc/*n*-pentane) gave $\Delta R_f = 0.36$.

HPLC analysis of enantiopure (*S*)-esmolol ((*S*)-15)

The HPLC chromatogram of (S)-esmolol ((*S*)-**15**) is shown in Figure 2.26. The recorded retention times were t_R((*R*)-**15**) = 5.8 and t_R((*S*)-**15**) = 8.3. The enantiomeric excess was determined to be 97%.

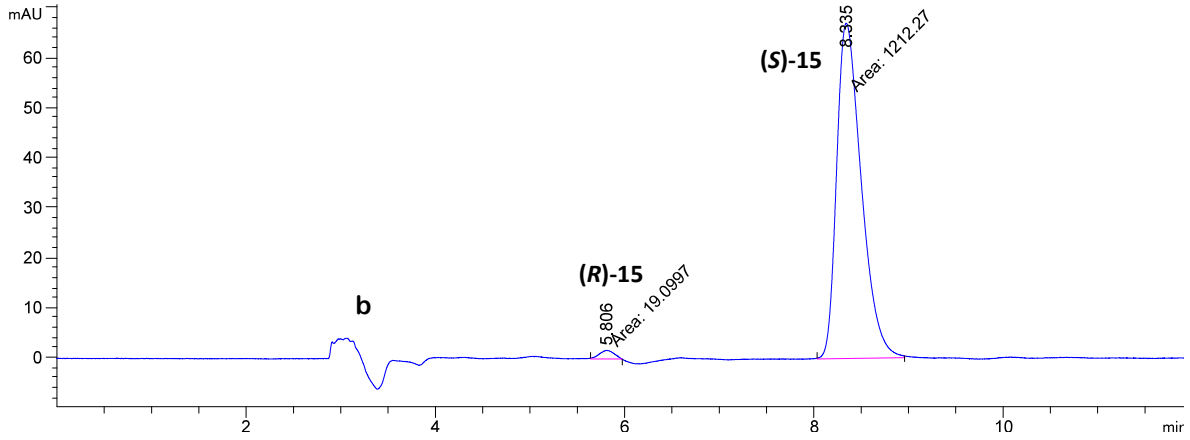

Figure 2.26 HPLC chromatogram of (*S*)-esmolol ((*S*)-**15**), t_R((*R*)-**15**) = 5.8 min and t_R((*S*)-**15**) = 8.3 min, eluted on a Chiralcel OD-H column with mobile phase composition *n*-hexane:*i*-PrOH:diethylamine (80:19.6:0.4), and flow 1 mL min^{-1}. b = in the blank.

2.3 Limonene oxidation and synthesis of perillyl alcohol

This section describes the results of the experiments involving limonene oxidation and related reactions. Previous master students Snorre Bergmo Næss [109] and Eirik Berg [110] have both discussed this topic in their master theses, but their experiments were almost completely limited by the covid-19 outbreak in the spring of 2020. Some of the experiments performed in this thesis are based on their work, which will be specified in the relevant sections.

The results presented here include a preliminary GC method optimization using standard limonene derivatives, a section on SeO_2-aided oxidation of limonene (**16**), the results from limonene (**16**) oxidation with various cytochrome P450s, and the results from reduction of perillaldehyde (**20**) with ketoreductases.

In this thesis, the results from the experiments with CYP catalyzed oxidation of limonene (**16**) were limited. Many obstacles were encountered, and the experiments were mostly unsuccessful. As the focus in this work was on synthesis of the β-blockers **10** and **15**, this part was not finished due to time limitations. However, a thorough literature review has been performed and suggestions on how to improve the experiments will be given.

2.3.1 Synthesis of perillyl acetate (18)

Perillyl acetate (**18**) was synthesized by phosphomolybdic acid catalyzed acylation of perillyl alcohol (**17**), as shown in Scheme 2.33. Kadam *et al.* have used this method for acylation of similar alcohols [111]. The synthesis was carried out to obtain a sample of **18** to be included in the GC analysis discussed in Section 2.3.2.

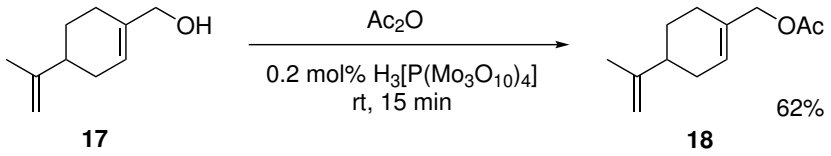

Scheme 2.33 Synthesis of perillyl acetate (**18**) in 62% yield by acylation of perillyl alcohol (**17**) using acetic anhydride.

After distillation under reduced pressure, pure perillyl acetate (**18**), bp 35°C (0.017 mmHg), was obtained in 62% yield. GC-MS and NMR analysis confirmed that the synthesis was successful.

GC-MS validation of perillyl acetate (18)
To confirm the identity of **18**, the purified product was analyzed by GC-MS (the method is described in Section 5.1.11), which gave a molecular ion peak $[M]^+$ at m/z = 194.1. Perillyl acetate (**18**) has the chemical formula $C_{12}H_{18}O_2$, and a calculated mass of m/z = 194.13. The MS spectrum of **18** was confirmed through a NIST MS 2.0 library search. The GC-MS chromatogram and MS spectrum are shown in Appendix C.1, together with the results from the NIST library search.

Structural characterization of perillyl acetate (18)
Perillyl acetate (**18**) was characterized by ^{1}H, ^{13}C, HSQC and HMBC NMR. The spectra are given in Appendix C.2. Table 2.12 shows the assignments of NMR shifts to the labelled atoms shown in Figure 2.27. Most of the ^{1}H NMR shifts are in the range 1.5-2.0 ppm, and are hard to distinguish. Position 10 and 3 in Figure 2.27 were used as anchor points to determine the correct assignment of the atoms of the cyclohexene ring of **18**, by looking at HMBC correlations. The singlet at 4.45 ppm unmistakably belongs to the equivalent protons at position 10, as it integrates to 2H. The ^{13}C shift of carbon 3 was assigned by looking at the HMBC correlations to the protons at positions 1 and 2. HSQC was used to confirm direct C-H correlations. The NMR shifts are in accordance with literature [112].

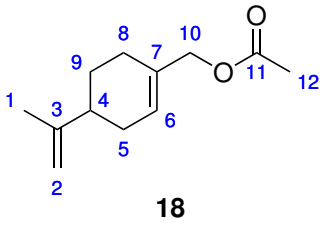

18

Figure 2.27 Perillyl acetate (**18**) with labelled atoms corresponding to NMR shifts in Table 2.12.

Table 2.12 NMR shifts and correlations observed for perillyl acetate (**18**) with carbon labels shown in Figure 2.27.

Label	δ ^{1}H (ppm)	m	I	δ ^{13}C (ppm)	HMBC
1	1.73	s	3H	20.8	2, 3, 4
2	4.72-7.73	br s	1H	108.9	1, 3, 4
	4.70-4.71	br s	1H	”	1, 3, 4
3	-	-	-	149.7	1, 2, 4, 5, 9
4	2.16-2.18	m	1H	40.9	2, 3, 5, 6, 9
5	2.13-2.15	m	1H	30.6	2, 4, 6, 9
	2.07-2.09	m	1H	”	2, 4, 6, 9
6	5.74-5.76	br s	1H	126.1	4, 5, 10
7	-	-	-	132.7	4, 5, 9, 10
8	1.96-2.00	m	1H	26.5	4, 9, 10
	2.07-2.09	m	1H	”	4, 9, 10
9	1.47-1.51	m	1H	27.4	4, 5, 7, 8
	1.83-1.87	m	1H	”	4, 5, 7, 8
10	4.45	s	2H	68.6	6, 7, 11, 12
11	-	-	-	171.6	10, 12
12	2.07	s	3H	21.3	11

2.3.2 GC analysis of limonene (16) and related compounds

Several monoterpenoid standards were analyzed by GC on an achiral RTX1701 column with the intent of developing a GC method for identification of products from the following reactions. This work was started by Næss [109], who developed a 40 min analysis which needed optimization to reduce the analysis time. The standards used were limonene (**16**), perillyl alcohol (**17**), perillyl acetate (**18**), a mixture of *cis*- and *trans*-carveol (**19**), perillaldehyde (**20**), limonene-1,2-diol (**21**) and perillic acid (**22**). DMSO was also analyzed using the same methods, as it would be used as a co-solvent in the enzymatic reactions. The goal of the GC optimization process was to achieve good separation of

the standards with as short analysis time as possible. In the end, two GC temperature programs were developed. They are described in Section 5.1.9 as GC method A and B. Method A had an analysis time of 17.3 min, and achieved good separation of all of the standards, but failed to separate limonene (**16**) and DMSO. Method B successfully separated limonene (**16**) and DMSO, with a longer analysis time of 29.3 min.

Table 2.13 lists the retention times t_R observed for each standard using GC methods A and B, and the literature values for the boiling points of each compound. The chromatograms recorded with method A are attached in Appendix C.3.

Table 2.13 Retention times t_R of limonene derivative standards recorded with GC methods A and B on an RTX1701 column, He flow 2 mL min^{-1}, and theoretical boiling points (bp).

Standard	bp (°C, 760 mmHg)	t_R (min), method A	t_R (min), method B
DMSO	192 [113]	1.7	9.2
16	178 [113]	1.7	9.6
19	228 [113]	5.2, 5.7	22.3, 22.6
20	237 [114]	6.7	23.3
17	244* [115]	7.4	23.8
18	258* [116]	9.8	25.2
21	242* [116]	10.3	25.4
22	284* [116]	13.0	-

*predicted values

As seen in Figure 2.28, method 2 just barely separated limonene (**16**) from DMSO, with a difference in retention times of only 0.4 min, and a resolution $R_s = 1.47$. To achieve this separation, the analysis had to be started at 50°C, which was held for 5 min, then a 2°C min^{-1} increase for 12.5 min. To make the rest of the analysis as short as possible, the rest of the compounds were eluted during a temperature ramp of 10°C min^{-1}, which led to poorer resolution between them.

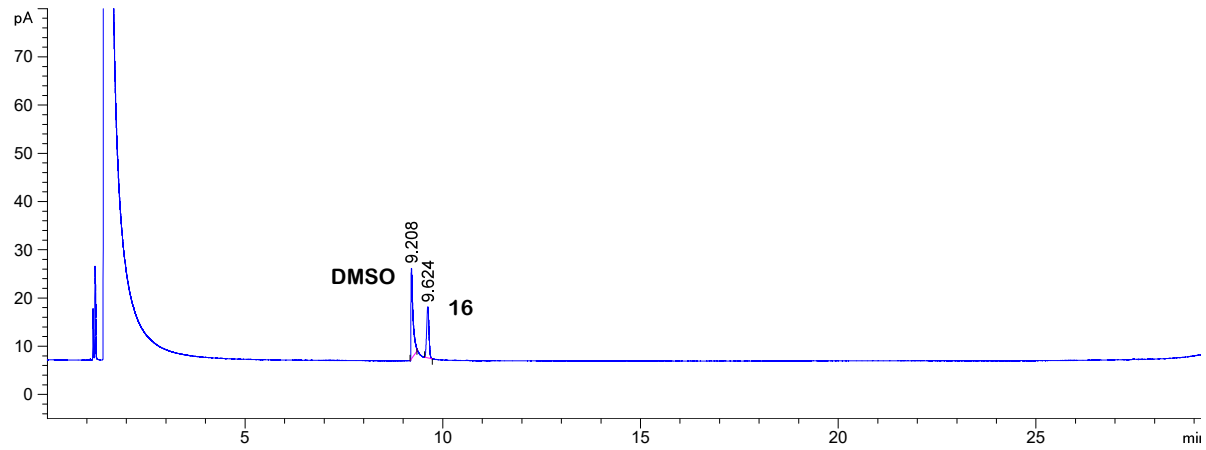

Figure 2.28 GC chromatogram for the separation of DMSO and limonene (**16**) using GC method B, on an RTX1701 column, He flow 2 mL min^{-1}.

In comparison, method A was started at 110°C. It was decided that method B was ideal for identification of oxidation products, whereas method A would be used to identify limonene in reactions where DMSO was used as a co-solvent, or to verify complete removal of DMSO.

2.3.3 Oxidation of limonene (16) using SeO_2

Oxidation of limonene was first attempted using SeO_2 as the oxidating agent. In Section 1.4.6, it was described that the SeO_2 oxidation of alkenes is regioselective, favouring hydroxylation at the most substituted end of the double bond. For limonene (**16**), this would mean at positions 4, 6, 7 and 10, as indicated in Figure 2.29.

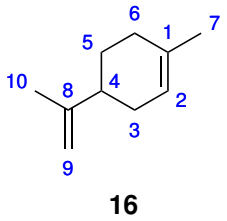

Figure 2.29 Limonene (**16**) with labelled atoms.

As introduced in Section 1.7.2, this reaction has been tested before. The reaction has not previously been performed in acetic acid, so it was tested in this work, as it could limit over-oxidation by forming an acetate. The previous reports indicate that the expected main product could be carveyl acetate, but as the reaction seems to have only moderate regioselectivity, several products were expected. The oxidation was carried out at reflux with AcOH as the solvent, as shown in Scheme 2.34.

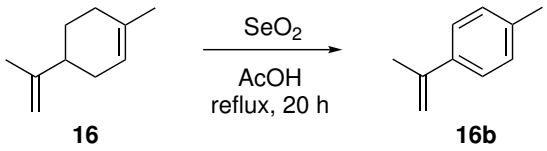

Scheme 2.34 Oxidation of limonene (**16**) using SeO_2 in AcOH.

During the oxidation, black selenium flakes precipitated, indicating reduction of SeO_2 to elemental Se. After 20 hours, the main product of the reaction turned out to be the aromatic compound 1-methyl-4-(prop-1-en-2-yl)benzene (**16b**). The mechanism of formation of this unexpected product will be discussed after presentation of the GC analysis.

It should be noted that SeO_2 is toxic and it is not desired to use Se-based catalysts. This experiment, and previous reports of SeO_2-based oxidations of **16**, show that the regioselectivity is not optimal to produce desired oxidation products in high yields, and it is desired to find better alternatives with respect to selectivity, safety and environmental considerations. The product obtained in this reaction (**16b**) is a co-monomer for polymers such as polystyrene, and it would be desired to find methods to produce this valuable compound from sustainable sources such as limonene waste [117, 118]. However, because SeO_2 is toxic, alternative methods would be preferred.

GC and GC-MS analysis of the crude reaction mixture from SeO_2 oxidation of limonene (16)

The crude reaction mixture was analyzed by GC, using GC method A. The chromatogram is shown in Figure 2.30. The largest peak is observed at $t_R = 2.31$ min, which does not coincide with any of the standards reported in Table 2.13. To identify this product, a GC-MS analysis was performed as described in Section 5.1.11. The chromatogram and mass spectrum are shown in Appendix C.4. The largest peak corresponds to $m/z = 132.1$ [M^+], and a NIST MS 2.0 library search confirmed that **16b** was the product. The calculated mass for **16b** is $m/z = 132.09$ ($C_{10}H_{12}$).

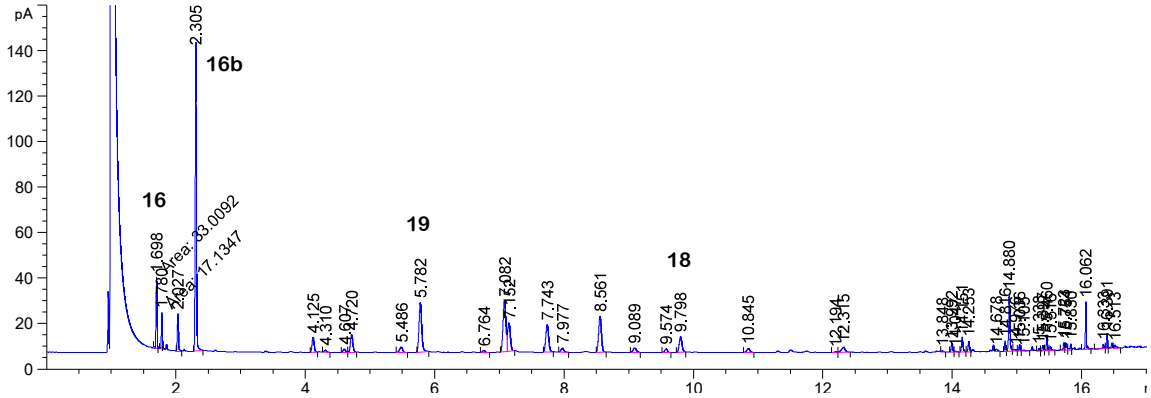

Figure 2.30 GC chromatogram of the crude reaction mixture from SeO_2-aided oxidation of limonene, using GC method A, on an RTX1701 column, He flow 2 mL min^{-1}.. The main product was **16b** at $t_R = 2.31$ min. $t_R = 5.78$ min and $t_R = 9.80$ min could represent carveol (**19**) and perillyl acetate (**18**), although it was not confirmed with MS.

The chromatogram in Figure 2.30 also shows several minor products. They were not identified by MS. However, by comparing the retention times to Table 2.13, the peaks at $t_R = 5.78$ min and $t_R = 9.80$ min could represent carveol (**19**) and perillyl acetate (**18**), which are both expected products. Remaining limonene (**16**) can also be seen at $t_R = 1.70$. The peak is small compared to the **16b** peak, which indicates that most of the starting material has been consumed in the reaction.

Proposed mechanism of formation of 16b

The aromatic compound **16b** is not an expected product of the performed reaction. However, it is possible that a series of allylic oxidation-dehydration steps may have occured due to the presence of acid, as illustrated in Scheme 2.35. Acid-catalyzed dehydration of alcohols to alkenes is known to occur during heating [35]. After formation of carveol (**19**), dehydration could occur. It is possible that **16b** is a favoured product under the current conditions due to the high stability of the aromatic ring. The same type of elimination could happen for carveyl acetate, the acetate derivative of carveol (**19**).

The long reaction time of 20 hours could explain why **16b** is the main product. The longer the reaction is left, the more time it has to go through dehydration. If the reaction had been stopped earlier, it may have given higher relative amounts of **19** and **18**, compared to **16b**. This was not tested in this work, as it was not a prioritized experiment. It could also be a result of the acidic environment.

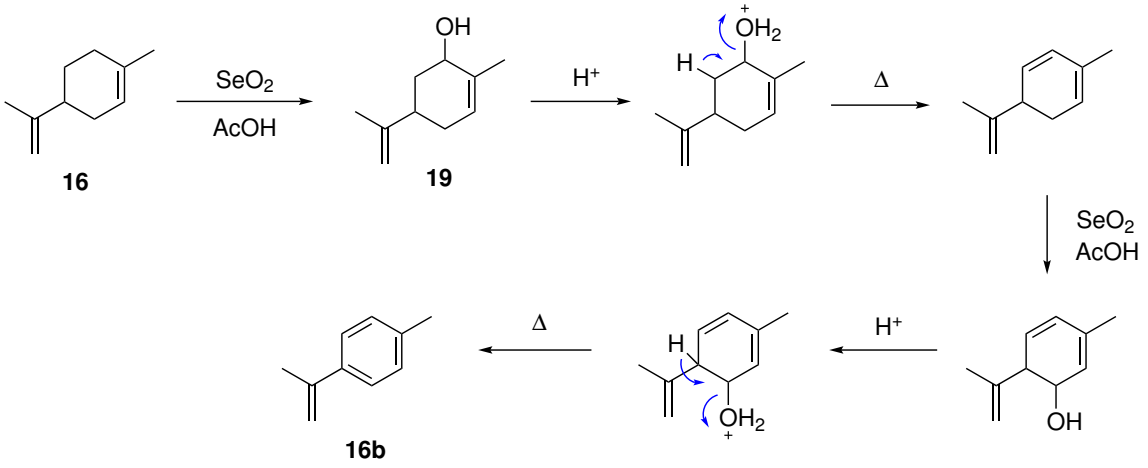

Scheme 2.35 Suggested mechanism for formation of **16b** during SeO_2-aided oxidation of limonene (**16**). Allylic hydroxylation may be followed by acid-catalyzed dehydration to produce a highly stable aromatic compound (**16b**).

2.3.4 Oxidation of limonene (16) using cytochrome P450

Both (*R*)- and (*S*)-limonene ((*R*)/(*S*)-**16**) were attempted oxidized using CYPs. The general scheme is shown in Scheme 2.36. The preferred product of the oxidation would be perillyl alcohol (**17**). Previous experiments by master students Næss [109] and Berg [110] were used as the basis for these experiments. A protocol established by the supplier of the enzymes (Sigma Aldrich), was also used [95].

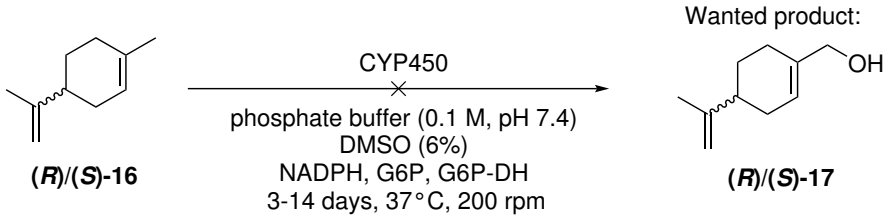

Scheme 2.36 General scheme for the CYP catalyzed oxidation of limonene (**16**).

An affordable and robust enzyme system, the CypExpress™ system, was used here, which would have many advantages over the previously reported microbial oxidations (see Section 1.7.3), if successful. In the current work, CypExpress™ 2C19, 2C9 and 2D6 were tested. The choice of enzyme was based on availability from the supplier, and previoulsy reported results that found human microsomal CYP 2C19 and 2C9 to be regioselective for limonene oxidation in positions 6 and 7 [119]. The oxidation attempts were not successful in this thesis, but the results that were obtained are still presented and possible improvements will be suggested.

Choice of initial reaction conditions for oxidation of limonene (16) using CYPs
As the CypExpress™ biocatalysts are quite new on the market, only one scientific paper using them has been published, where they studied the inhibitory effect of plant substances on the drug metabolism of CYP 2D6 in human liver [120]. Due to lack of other references, the supplier protocol was used to set the reaction conditions for the first reaction tests [95].

The reaction was run in a phosphate buffer solution (0.1 M, pH 7.4) containing glucose-6-phosphate (5 mM) and NADPH (2 mM), in a test tube with a glass wool plug. The CypExpress^{TM} powder (20 mg mL^{-1}) was added to the buffer, and stirred carefully with a glass rod to break up lumps. A solution of (*S*)- or (*R*)-limonene ((*S*)/(*R*)-**16**) in DMSO was added to the buffer mixture to give a final substrate concentration of 0.57 mM, and a DMSO concentration of 6%. The tube was placed in an incubator at 37°C and 200 rpm. To analyze the reaction mixture, the reaction was terminated by filtration, extraction with EtOAc and washing several times with water. The washing procedure was confirmed to remove DMSO from the mixture, by working up an unreacted batch of limonene in DMSO/buffer solution, and analyzing with GC method B, which only showed the limonene (**16**) peak (see Figure C.14). This sample was also used as a limonene (**16**) standard to have a reference of any impurities in the starting material, so they could not be assumed as products.

Results from the limonene oxidation assay

CypExpress^{TM} 2C19, 2C9 and 2D6 were used in preliminary oxidation tests. Only the CYP 2C19 gave other peaks than the starting material, so the others were not tested further. The CYP 2C19 reaction with (*S*)-**16** was analyzed by GC after 65 h reaction time, which gave two small peaks other than the starting material, as shown in Figure 2.31. The peaks were not present in the limonene (**16**) standard (see Figure C.15). The retention times correlate with that of *cis*/*trans*-carveol (**19**), but the identity was not confirmed with GC-MS. Næss also indicated conversion to **19** in his corresponding reaction, but with very low conversion [109]. In the present experiment, conversion of (*S*)-**16** was also very low, and the result shows that this method is not suited for biotransformation of (*S*)-**16**. However, it was not clear what caused the poor conversion, so other approaches were tested, as CYP 2C19 has been reported to oxidize (*S*)-limonene ((*S*)-**16**) previously [119].

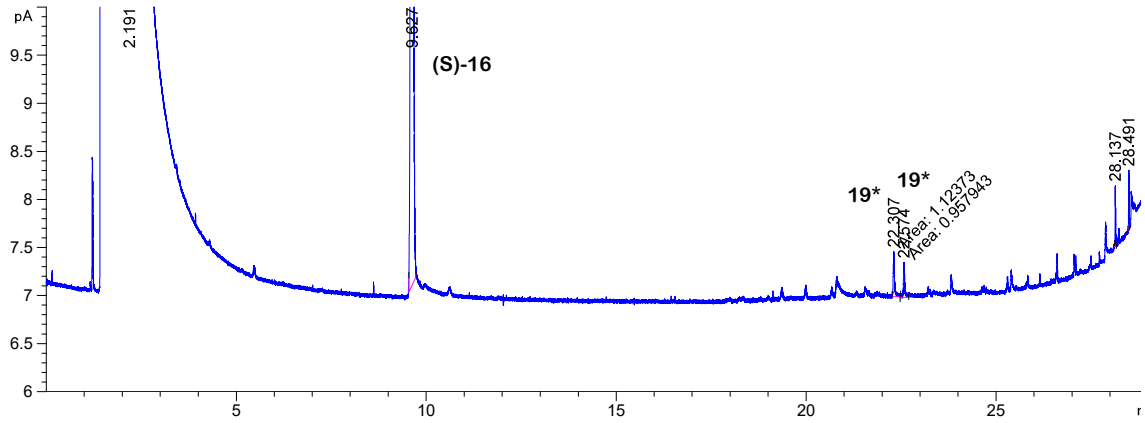

Figure 2.31 GC chromatogram from CYP 2C19 oxidation of (*S*)-limonene ((*S*)-**16**) after 65 h reaction time, using GC method B. (*S*)-**16** is shown at t_R = 9.63 min. t_R = 22.31 min and t_R = 22.57 min could represent traces of *cis*/*trans*-carveol (**19**).

Effect of increased reaction time

One possible explanation to the low conversion could be that the conversion is slow. The reaction time was increased to test this assumption. This time, the reaction was run in a larger, closed vial, to prevent evaporation of the substrate and buffer solution over the course of 14 days. The large vial was placed in a tilted position to increase surface area,

and thus increase O_2 supply [121].

The GC chromatogram from this reaction, showing two unknown compounds **X** and **Y** at t_R(**X**) = 20.80 min and t_R(**Y**) = 25.30 min, is shown in Figure 2.32. The two new peaks were similar in peak area as the limonene peak (t_R((*S*)-**16**) = 9.62 min), and they were thought to possibly represent products from the oxiation. The sample was also analyzed with GC method A, which gave t_R(**X**) = 3.75 min and t_R(**Y**) = 9.99 min. This chromatogram is shown in Figure C.18 of Appendix C.5.

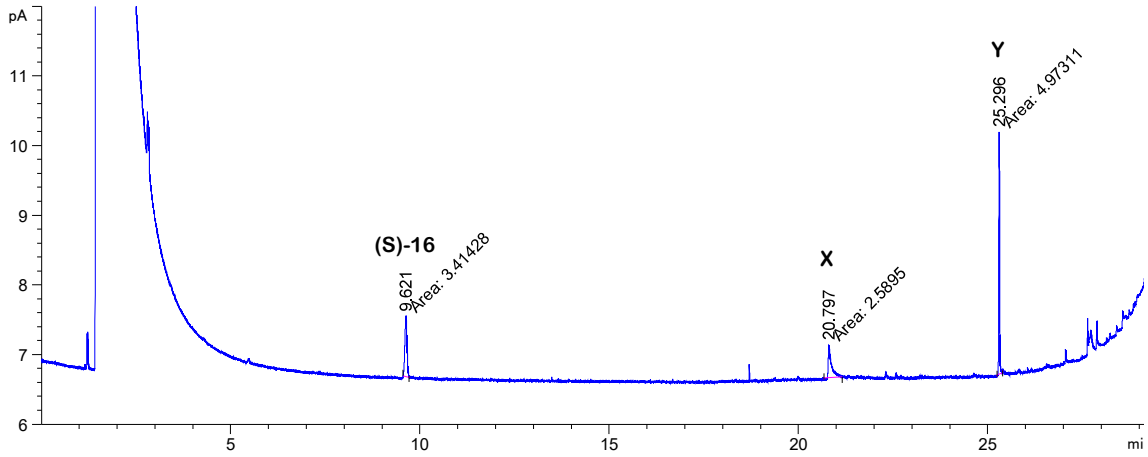

Figure 2.32 GC chromatogram from CYP 2C19 oxidation of (*S*)-limonene ((*S*)-**16**) after 14 days reaction time, using GC method B. The starting material is shown at t_R((*S*)-**16**) = 9.62 min. Two other peaks are shown at t_R(**X**) = 20.80 min and t_R(**Y**) = 25.30 min.

By comparison with Table 2.13, it could seem as if **Y** could have been perillyl acetate (**18**) with retention times that correlate for both GC methods. However, **18** is not an expected product from CYP 2C19 oxidation of **16**. The sample was therefore analyzed further by GC-MS. The GC-MS chromatogram and MS spectra are shown in Appendix C.5.

Compound **X** gave m/z = 122.1 [M^+], and by comparison to the NIST MS 2.0 library, a match was found for 2-phenylethanol (**X**). Compound **Y** gave m/z = 117.0 [M^+], which matched with either indole (**Y**) or 7H-cyclopenta[*b*]pyridine (**Yb**). The indole nucleus is a well-known structure, which is present in for example the amino acid L-tryptophan. As the MS results do not correlate to limonene oxidation pathways, it could be that **X** and **Y** are enzyme degradation products. Figure 2.37 illustrates the possible scenario. The amino acid L-phenylalanine could decompose to **X** after deamination, forming an α-keto acid, followed by decarboxylation and reduction [122]. Degradation of tryptophan could have released indole (**Y**). The amino acids could have been released from the enzyme during denaturation as a result of long reaction time, mechanical stress from shaking or too high content of DMSO.

This hypothesis was tested by running a batch of the enzyme in the same conditions as before, without adding limonene. After 16 days, the GC analysis (see Figure C.23) showed peaks at t_R = 15.3 min, 19.6 min, 25.2 min, 25.7 min and 28.7 min, using GC method B. This indicates that the protein goes through denaturation after long incubations.

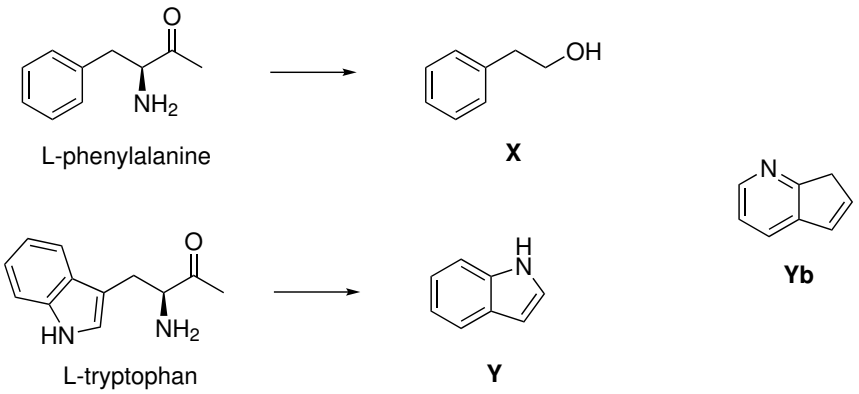

Scheme 2.37 Possible sources of the detected compounds **X** and **Y** could be the amino acids L-phenylalanine and L-tryptophan released during enzyme denaturation.

Test of stereoselectivity
Parallell reactions were tested with (*R*)-limonene ((*R*)-**16**) to see if the enzyme preferred the *R*-isomer of the substrate. No products were observed on the chromatogram after 3 days reaction time. After 2 weeks, enzyme degradation products were observed at t_R = 19.6, 25.3 min and 27.8 min (see Figure C.24). The results indicate that no observable preference for either enantiomer of **16** exists. However, there could be a preference which is masked by a flaw in the method that prevents any product from being made. For example, if the enzyme does not tolerate 6% DMSO despite the claims of the supplier, this could limit the activity of the enzyme so that no products can be obtained. Thus, there is no way to measure the stereoselectivity without removing this source of error.

Effect of increased enzyme concentration
In some cases, increasing the concentration of the enzyme in the mixture could increase the reaction rate (see Section 2.3.5). Effectively, this increases the enzyme-substrate ratio. This was tested for the CYP 2C19 catalyzed oxidation of (*R*)- and (*S*)-**16**. First a reaction was run with 20 mg mL^{-1} CypExpress^{TM} 2C19 powder, as in the previous attempts. After 9 days reaction time, no products or degradation products were observed. The enzyme concentration was then increased from 20 mg mL^{-1} to 40 mg mL^{-1}. The substrate concentration was kept at 0.57 mM. After 9 days, both the isomers showed the decomposition product **X** at t_R = 25.3 min. The (*R*)-isomer sample also showed minor peaks at t_R = 19.6 min and 28.7 min, which was also seen in the blank enzyme sample which was used to detect enzyme degradation products, as described earlier. The chromatograms are shown in Figures C.25 and C.26. This result shows that increasing the enzyme concentration led to more rapid degradation, but it did not significantly increase conversion of either enantiomer of **16**.

Improvements for future experiments with CYPs
The results obtained in these oxidation tests show that CypExpress^{TM} 2C19, 2C9 and 2D6 most likely are not suitable for oxidation of limonene (**16**) to obtain more valuable products. However, there are some factors that have not been evaluated in this thesis, due to time limitations. These factors include tests of DMSO concentration, substrate concentration, temperature and stirring rate, pH and buffer concentration, concentrations of cofactors, and more.

The most promising change would perhaps be to either change DMSO concentration or substitute DMSO for a different solvent, such as DMF. MeOH could also be tested, although the supplier of CypExpress^{TM} enzymes has warned that alcohols may significantly lower the activity of the catalyst [95, 96]. Previous master student Næss tested this reaction with a substrate concentration of 250 mM, but did not get satisfactory results [109]. In the present experiments, the substrate concentration was kept at 0.57 mM. Lowering the substrate concentration could solve problems with substrate solubility and toxicity, but a much lower concentration would make the analysis more challenging. The reaction environment could also be tuned with regards to temperature, stirring rate and pH. This was not attempted here, as the procedure was developed based on the supplier recommendations [95].

A commercially available biocatalyst, the CypExpress^{TM} system, was purchased for the current experiments. There are currently not many CYPs to choose from when using this system. As the CYP 2C19, 2C9 and 2D6 did not perform the desired transformation of limonene (**16**) to more valuable compounds such as perillyl alcohol (**17**) or carveol (**19**), other CYPs should be explored in the future. A very attractive option would be to use plant enzymes (see Section 1.7.1). Intuitively, it seems reasonable that the plant enzymes could be more selective than the limonene-degrading enzymes. Their job is to synthesize specific natural products that serve the plant in special ways, like provide smell, taste or toxic properties. Limonene-degrading enzymes, such as human liver CYPs, work by oxidizing the unwanted substance to increase solubility, so that it can be secreted more easily from the organism. Consequently, the site of oxidation is less important. Due to recent advances in biotechnology, it could be possible to produce recombinant limonene-7-hydroxylase, the enzyme responsible for perillyl alcohol production in *Perilla frutescens*, and use the isolated enzyme to carry out this biotransformation. The isolated enzyme could be supported on a carrier material to increase its mechanical stability and tolerance for organic solvents [30]. A more advanced option would be to use directed evolution, with limonene-7-hydroxylase as a starting point [31].

2.3.5 KRED 228 catalyzed reduction of (*S*)-perillaldehyde ((*S*)-20)

As mentioned in Section 1.7.1, limonene-7-hydroxylase is responsible for both hydroxylation of limonene (**16**) and further oxidation of perillyl alcohol (**17**) to perillaldehyde (**20**) [72]. If this enzyme is to be used as a biocatalyst for production of perillyl alcohol (**17**), it would be desired to re-oxidize the aldehyde (**20**) produced in the reaction. KRED 228 could be a useful enzyme for this purpose. Thus, the reduction of (*S*)-perillaldehyde ((*S*)-**20**) was tested with this enzyme, according to Scheme 2.38.

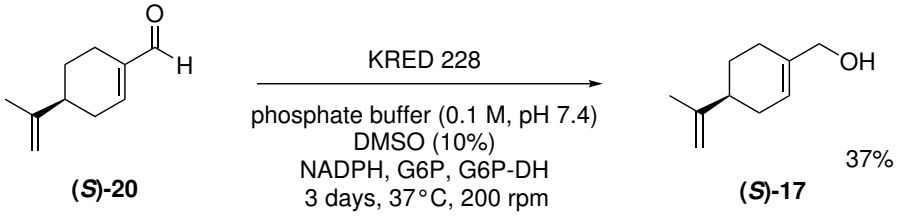

Scheme 2.38 KRED catalyzed reduction of (*S*)-perillaldehyde ((*S*)-**20**) gave (*S*)-perillyl alcohol ((*S*)-**17**) in 37% yield.

After 3 days reaction time and purification by flash chromatography (1:4 EtOAc/*n*-pentane), (*S*)-perillyl alcohol ((*S*)-**17**) was obtained in 37% yield and 95% purity (determined by GC, see Figure 2.33). The remaining substrate was also isolated as 20% of the initial amount. No additional products were observed. According to Figure 2.34, the maximum yield should be around 56%, as this was the maximum conversion that was achieved. Some of the product may have been lost during the purification. The synthesis was not optimized further in this work, as other syntheses were prioritized.

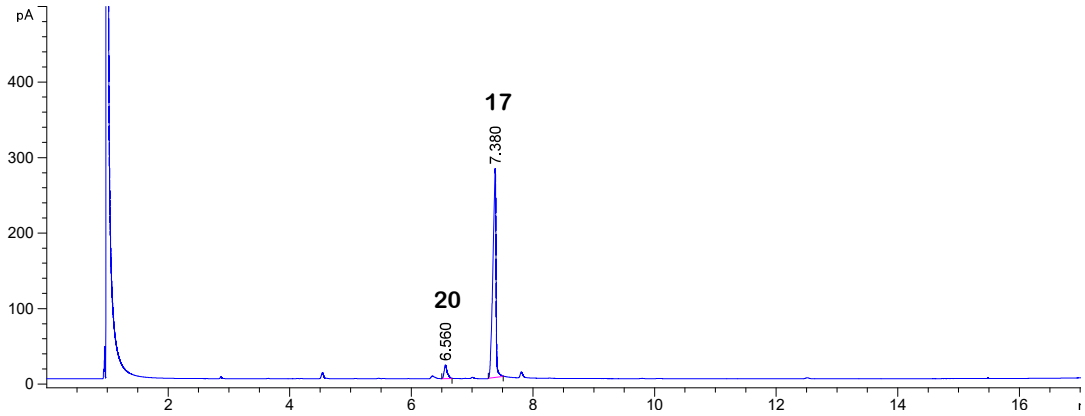

Figure 2.33 GC chromatogram of purified (*S*)-perillyl alcohol ((*S*)-**17**) from KRED 228 catalyzed reduction of (*S*)-perillaldehyde ((*S*)-**20**), recorded using GC method A.

Reaction monitoring and effect of substrate concentration on the conversion of (*S*)-perillaldehyde ((*S*)-20)

Before isolating the product, as described above, the reaction was monitored over time to discover how long the reaction time should be. The monitoring was carried out by taking out samples at regular time intervals and analyzing the conversion by GC, using GC method A. First, a reaction was run with a substrate concentration of 30 mg mL^{-1}, and it was monitored over 6 days. During this time, the total conversion of (*S*)-**20** to (*S*)-**17** was only 40%, as shown on the left in Figure 2.34. To increase the turnover, the concentration of the substrate was halved, which increased the overall conversion to 56%, as shown on the right in Figure 2.34.

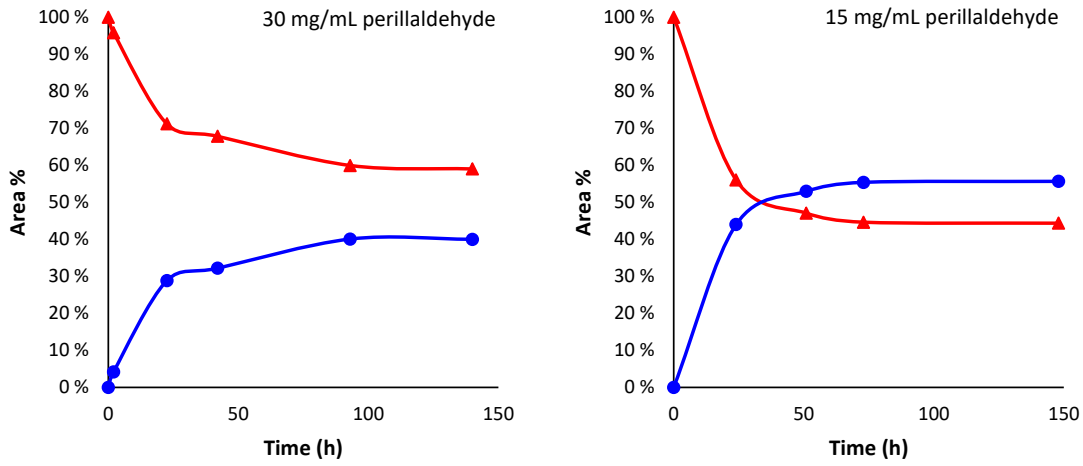

Figure 2.34 Relative amounts (based on area percentage on GC chromatograms) of perillaldehyde (red triangles, **20**) and perillyl alcohol (blue circles, **17**) at during monitoring of the KRED 228 catalyzed reduction of **20** at substrate concentrations 30 mg mL^{-1} and 15 mg mL^{-1}.

After about 60 h reaction time, no significant conversion was observed for both reactions shown in Figure 2.34. It is unclear why the turnover stops here. One explanation is that the ketoreductase may be losing its activity due to product inhibition or denaturation. It could be interesting to increase the amount of enzyme relative to the substrate further to see if it speeds up the process even more. This was not tested in this thesis, as it was not a priority.

3 Conclusion

A five-step synthesis of (*S*)-betaxolol ((*S*)-**10**) in 9% overall yield and 99% ee from the starting material **1** was developed, as summarized in Scheme 3.1, path a. In path a, a selective alkylation of **1** was performed, which produced phenol **2** in 31% yield. **2** was converted to chlorohydrin **8a** in two steps via epoxide **6**.

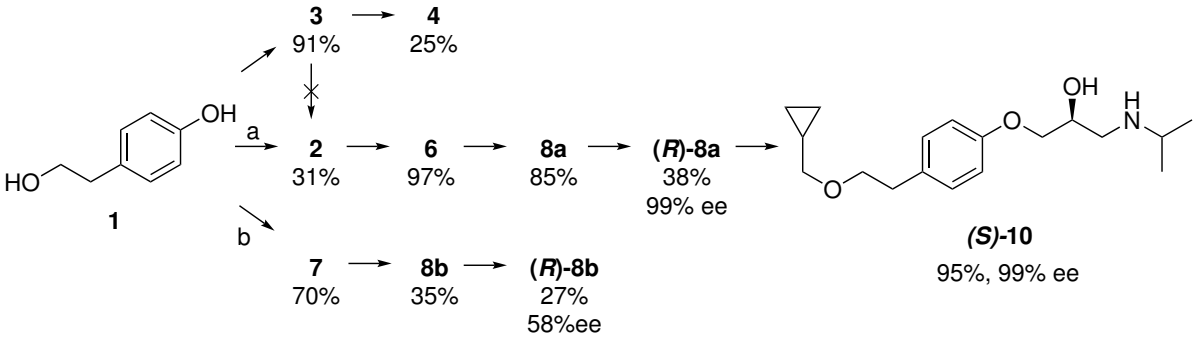

Scheme 3.1 Synthesis routes to (*S*)-betaxolol ((*S*)-**10**) from 4-(2-hydroxyethyl)phenol (**1**), with yields for each step.

The yield of phenol **2** was low because the phenol group of **1** was not protected, which led to alkylation of both -OH groups. An attempt to protect the phenol of **1** with a tetrafluoropyridyl (TFP) group was carried out, giving the TFP-protected substrates **3** and **4**. However, the alkylation of **3** was not successful.

To avoid the protecting step, an alternative route (path b in Scheme 3.1) was tested. This involved synthesis of the intermediate epoxide **7** before the alkylation step. The alkylation of **7** was expected to give epoxide **6**, but instead bromohydrin **8b** was formed. This was explained as a result of nucleophilic attack of the bromide ion released from the alkylating agent on the epoxide functional group. It was proposed that exchanging the alkylating agent with its chloro derivative could produce chlorohydrin **8a** instead. This observation indicated that paths a and b could both be good pathways to **8a**, as they both had equal overall yields of the halohydrin intermediates. Because low yield was obtained in the first step of path a, path b was considered the most promising route, with good potenial for optimization to give higher yields without adding reaction steps. This would be desired from a green chemistry and economical perspective, as a lower number of steps means less energy and material consumption.

The enantiopure chlorohydrin (*R*)-**8a** was produced in 38% yield and 99% ee, through a CALB catalyzed kinetic resolution of **8a**. A correction of the previously reported [65]

optical rotations of chlorohydrin (*R*)-**8a** and ester (*S*)-**9** was suggested. The specific rotation of (*R*)-**8a** (99% ee) was measured to $[\alpha]_D^{20} = -1.92$ (*c* 1.04, $CHCl_3$), and for (*S*)-**9** (87% ee) it was measured to $[\alpha]_D^{20} = +13.4$ (*c* 0.97, $CHCl_3$). The following amination gave (*S*)-betaxolol ((*S*)-**10**) in 95% yield and 99% ee. The synthesis was considered an environmentally friendly alternative to previously reported methods using transition metal catalysts. In drug synthesis, metal catalysis should be avoided.

A four-step synthesis of (*S*)-esmolol ((*S*)-**15**) in 26% overall yield and 97% ee was performed, as summarized in Scheme 3.2. The starting material **11** was converted to chlorohydrin **13** via epoxide **12**.

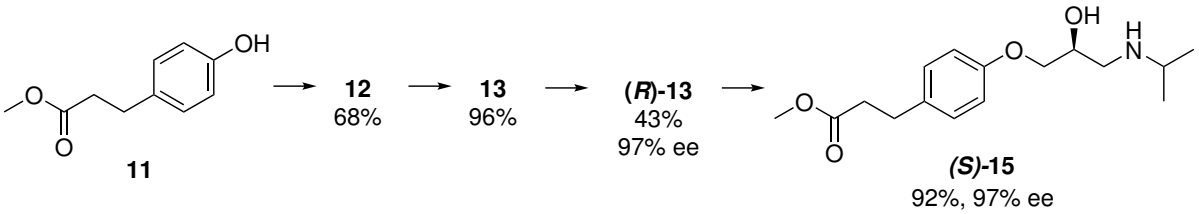

Scheme 3.2 Synthesis route to (*S*)-esmolol ((*S*)-**15**) from methyl 3-(4-hydroxyphenyl)-propanoate (**11**), with yields for each step.

A CALB catalyzed kinetic resolution of **13** was then carried out to obtain (*R*)-**13** in 43% yield and 97% ee. The enantiopure chlorohydrin was then converted to (*S*)-esmolol ((*S*)-**15**) in 92% yield and 97% ee. A correction of the previously reported [67] optical rotation of (*S*)-**15** was given. The correct specific rotation of (*S*)-**15** (97% ee) was $[\alpha]_D^{20} = -6.80$ (*c* 1.03, $CHCl_3$). The previously reported [104] loss of enantiomeric excess during the last amination step was avoided by ensuring that the chlorohydrin ((*R*)-**13**) was completely separated from the ester ((*S*)-**14**) after the CALB reaction.

Limonene (**16**) was oxidized using selenium dioxide as the oxidizing agent. The main product was 1-methyl-4-(prop-1-en-2-yl)benzene (**16b**), which was identified by GC-MS. A more environmentally friendly oxidation of (*R*)- and (*S*)-**16** was also attempted, where CYP 2C19, 2C9 and 2D6 were used as a biocatalyst. The CYP-catalyzed oxidations were not successful, and it was discovered that degradation of the enzyme occured during long reaction times or when large amounts of enzyme were used. (*S*)-perillyl alcohol ((*S*)-**17**) was produced in 37% yield through KRED 228 catalyzed reduction of (*S*)-perillaldehyde ((*S*)-**20**). It was suggested that this reduction could be performed in combination with the CYP catalyzed oxidation of limonene to prevent over-oxidation to perillaldehyde (**20**).

4 Future work

The possibility of using pentafluoropyridine to perform a protection of phenol **1** should be explored further, by using a better suited solvent and/or base for the alkylation step. This could be a greener alternative to protection with a benzyl group.

As an alternative to protection of the phenol **1**, path b in Scheme 2.19 should be performed using (chloromethyl)cyclopropane as the alkylating agent, as this would produce chlorohydrin **8a**, which is preferred over the bromohydrin **8b** in the kinetic resolution

step using CALB. The reactions should also be optimized to increase yield. If this can be done, path b is the most environmentally friendly and economical alternative for synthesis of chlorohydrin **8a**.

The synthesis of (*S*)-esmolol ((*S*)-**15**) was successful in this thesis, and much optimization has already been done. The first step of the synthesis path, addition of epichlorohydrin, should be optimized to give a higher yield than 68%. This could possibly be achieved by increasing the amount of epichlorohydrin equivalents in the reaction, as seen in the synthesis of **7** (see Table 2.7). Alternatively, using a different base or a different amount of base could influence the conversion without having to add more toxic epichlorohydrin.

A proper method for CYP catalyzed oxidation of limonene (**16**) should be developed, as it was not successful in this work. As discussed in Section 2.3.4, the enzyme limonene-7-hydroxylase was suggested as a promising alternative to the enzymes tested in this thesis. Since limonene-7-hydroxylase has a tendency to over-oxidize limonene (**16**) to perillaldehyde (**20**), a KRED could be incorporated in a one-pot biotransformation together with the hydroxylase for an efficient and green synthesis of perillyl alcohol (**17**). Both enzymes use NADPH as a cofactor, and the synthesis could be performed in water with DMSO as the co-solvent. The KRED reduction of **20** was achieved in this work, but it has not been tested together with the oxidation.

5 Experimental

This section is divided into four parts, describing general materials, the synthetic pathways to the two β-blockers (*S*)-betaxolol ((*S*)-**10**) and (*S*)-esmolol ((*S*)-**15**), and the experiments related to oxidation of limonene (**16**) that have been performed in this work.

5.1 General materials and methods

5.1.1 Chemicals

The chemicals and solvents used in this work were purchased from Sigma Aldrich (Oslo, Norway). Distilled water was obtained from an ELGA PURELAB flex purification system. Dry MeCN was obtained from an MBraun MB-SPS-800 solvent purifier, and stored over 4Å molecular sieves. Molecular sieves (4Å) were dried at 1000°C for 24 h, and stored in a dessicator.

5.1.2 Enzymes

Candida antarctica lipase B (CALB) expressed in *Pichia pastoris*, and immobilized on a hydrophobic polymer resin (> 10 000 PLU, lot# 20170315) was kindly gifted from SyncoZymes (Shanghai) Co., Ltd.

CypExpress™ 2C19, 2C9 and 2D6 expressed in *Pichia pastoris* was purchased from Sigma Aldrich (Oslo, Norway).

Glucose-6-phosphate dehydrogenase from *S. cerevisiae* (lyophilized powder, 200-400 U/mg, lot# SLBP6152V), and from *Leuconostoc mesenteroides* (lyophilized powder, 550-1100

U/mg, lot# 0000110704) were purchased from Sigma Aldich (Oslo, Norway).

Ketoreductase (KRED) 228 and 238 (pure enzymes) were kindly gifted from SyncoZymes (Shanghai) Co., Ltd.

5.1.3 Incubation

Enzymatic reactions were carried out in a New Brunswick G24 Environmental Incubator Shaker at 37°C and 200 rpm.

5.1.4 Optical rotation

Optical rotation was measured on an Anton Paar MCP 5100 polaritmeter, light source at $\lambda = 589$ nm, and a path length of 10 mm.

5.1.5 Absolute configuration

The absolute configuration of enantiopure compounds was determined by comparison to previously reported data, or by the enantioselectivity of CALB which has been described by Jacobsen *et al.* [44].

5.1.6 Nuclear magnetic resonance spectroscopy (NMR)

NMR spectra were obtained using a 600 MHz Bruker Avance III HD NMR spectrometer with a 5 mm CryoProbe or a 400 MHz Bruker Avance III HD NMR spectrometer with a 5 mm Smartprobe. Chemical shifts δ are given in ppm relative to TMS, and coupling constants J are given in Hz.

5.1.7 Flash chromatography and thin-layer chromatography (TLC)

Flash chromatography was performed with silica gel (pore size 60 Å, mesh particle size 230-400, particle size 40-63 µm) from Sigma Aldrich. The TLC plates used were Merck silica 60 F_{254} (0.2 mm) plates from Sigma Aldrich. TLC analyses were detected by UV at $\lambda = 254$ nm.

5.1.8 High-performance liquid chromatography (HPLC)

Chiral HPLC analyses were performed on an Agilent 1200 HPLC system equipped with an autosampler (10 µL injection volume) and a diode array detector (DAD). HPLC chromatograms presented in this thesis were recorded at $\lambda = 254$ nm. A Diacel Chiralcel OD-H column (cellulose tris (3,5-dimethylphenylcarbamate) on silica gel, 250 mm × 4.6 mm ID, 5 µm particle size) was used for all separations.

Separation of **6**, **8a** and **8b**: *n*-hexane:*i*-PrOH (90:10) flow rate: 1 mL min^{-1}.
t_R(**6**) = 7.1 min, t_R(**6**) = 8.4 min, t_R((*S*)-**8a**) = 10.8 min, t_R((*R*)-**8a**) = 12.8 min, t_R((*S*)-**8b**) = 11.3 min, t_R((*R*)-**8b**) = 13.7 min.

Separation of **9**: *n*-hexane:*i*-PrOH (99:1) flow rate: 1 mL min^{-1}.
t_R((*S*)-**9**) = 14.4 min, t_R((*R*)-**9**) = 15.7 min.

Separation of **10**: *n*-hexane:*i*-PrOH:diethylamine (90:9.8:0.2), flow rate: 1 mL min^{-1}. t_R((*R*)-**10**) = 6.4 min, t_R((*S*)-**10**) = 12.4 min.

Separation of **13**: *n*-hexane:*i*-PrOH (80:20), flow rate: 1 mL min^{-1}. t_R((*S*)-**13**) = 9.4 min, t_R((*R*)-**13**) = 10.3 min.

Separation of **14**: *n*-hexane:*i*-PrOH (97:3) flow rate: 1 mL min^{-1}. t_R((*S*)-**14**) = 15.6 min, t_R((*R*)-**14**) = 17.3 min.

Separation of **15**: *n*-hexane:*i*-PrOH:diethylamine (80:19.6:0.4), flow rate: 1 mL min^{-1}. t_R((*R*)-**15**) = 6.1 min, t_R((*S*)-**15**) = 9.5 min.

5.1.9 Gas chromatography (GC)

GC analyses were performed using an Agilent 7890A gas chromatograph with an RTX-1701 column (25 m × 320 µm ID, 0.25 µm film thickness), with 2 mL min^{-1} He (*g*) flow, split injection (injection volume 1 µL, split ratio 50:1, inlet temperature 250°C) and a flame ionization detector (FID) (280°C). The temperature programs used were as follows:

GC method A: Initial temperature 110°C for 5 min, 5°C min^{-1} increase for 8 min to 150°C, 30°C min^{-1} increase for 4.3 min to 280°C. Total time 17.3 min.

GC method B: Initial temperature 50°C for 5 min, 2°C min^{-1} increase for 12.5 min to 75°C, 10°C min^{-1} increase for 7.5 min to 150°C, 30°C min^{-1} increase for 4.3 min to 280°C. Total time 29.3 min.

5.1.10 Liquid chromatography-Mass spectroscopy (LC-MS)

LC-MS analyses were performed on an AQUITY UPLC system with an ACQUITY UPLC HSS T3 column (100 mm × 2.1 mm ID, 100 Å, 1.8 µm film thickness) with a mobile phase of A: water with 0.12% NH_4OH and B: MeCN, flow rate: 0.25 mL min^{-1}. The analysis was run with a gradient of 10-100% B for 12 min, hold for 2 min, then 100-10% B for 1 min. Total time 15.0 min. The mass analyzer was a SYNAPT-G2S quadrouple time of flight mass analyzer with a Waters ZSpray electron spray ion source.

5.1.11 Gas chromatography-Mass spectroscopy (GC-MS)

GC-MS analyses were performed on an Agilent 7890A gas chromatograph with a GC Pal autosampler and a Thermo Scientific™ TraceGOLD™ TG-5MS column (5% diphenyl/ 95% dimethyl polysiloxane, 30 m × 0.25 mm ID, 0.5 µm film thickness), with 1 mL min^{-1} He (*g*) flow, split injection, (injection volume 1 µL, split ratio 50:1, inlet temperature 280°C). Initial temperature 110°C for 5 min, 5°C min^{-1} increase for 8 min to 150°C, 30°C min^{-1} increase for 4.3 min to 280°C. Total time 17.3 min. The mass analyzer was an Agilent 5975 single quadrupole mass spectrometer with a temperature of 150°C.

5.2 Pathway to (*S*)-betaxolol ((*S*)-10)

5.2.1 Synthesis of 4-(2-(cyclopropylmethoxy)ethyl)phenol (2)

A solution of 4-(2-hydroxyethyl)phenol (**1**) (1.01 g, 7.24 mmol) and *t*-BuOK (2.44 g, 21.7 mmol) in DMSO (5 mL) was stirred at 50°C for 30 min under an N_2 atmosphere. A solution of (bromomethyl)cyclopropane (1.10 mL, 10.8 mmol) in DMSO (5 mL) was then added dropwise, and the reaction was stirred for 1 h under the same conditions. The reaction was cooled to rt and quenched with water (10 mL), and washed with toluene (2 × 5 mL) to remove impurities. The aqueous phase was added dilute HCl until neutral pH, and extracted with toluene (4 × 15 mL). The combined organic phase was washed with water (5 × 20 mL) to remove excess DMSO, and dried over $MgSO_4$. The solvent was removed under reduced pressure. The crude mixture (0.64 g) was purified by flash chromatography (1:11 MeCN/CH_2Cl_2) to afford 4-(2-(cyclopropylmethoxy)ethyl)phenol (**2**) as a transparent oil in 31% yield (0.42 g, 2.21 mmol) and 95% purity (^{1}H NMR). ^{1}H NMR (600 MHz, $CDCl_3$) δ: 7.06-7.09 (m, 2H, Ar-**H**), 6.73-6.75 (m, 2H, Ar-**H**), 5.37 (s, 1H, Ar-O**H**), 3.65 (t, 2H, ^3J=7.43 Hz, CH_2CH_2O), 3.30 (d, 2H, ^3J=7.00 Hz, CH_2O-CH), 2.84 (t, 2H, ^3J=7.43 Hz, Ar-CH_2), 1.03-1.10 (m, 1H, C**H**), 0.51-0.55 (m, 2H, CH_2), 0.19-0.22 (m, 2H, CH_2). ^{13}C NMR (150 MHz, $CDCl_3$) δ: 154.3, 130.8, 130.0, 115.4, 75.8, 72.0, 35.5, 10.7, 3.2. NMR spectra are given in Appendix A.1.

5.2.2 Synthesis of 2-(4-((perfluoropyridin-4-yl)oxy)phenyl)ethan-1-ol (3)

To a stirred solution of 4-(2-hydroxyethyl)phenol (**1**) (0.99 g, 7.19 mmol) and K_2CO_3 (1.05 g, 7.60 mmol) in MeCN (40 mL), pentafluoropyridine (835 µL, 7.60 mmol) was added. The solution was stirred for 16 h at rt. Full conversion was confirmed by TLC (1:11 MeCN/CH_2Cl_2); R_f (**1**) = 0.10, R_f (**3**) = 0.33. The mixture was filtrated and the solvent and excess pentafluoropyridine was removed under reduced pressure. Protected phenol **3** was obtained as a white solid in 91% yield (1.88 g, 6.54 mmol) and 99% purity (^{1}H NMR). ^{1}H NMR (600 MHz, $CDCl_3$) δ: 7.23-7.25 (m, 2H, Ar-**H**), 7.00-7.02 (m, 2H, Ar-**H**), 3.86 (m, 2H, CH_2-OH), 2.87 (t, 2H, ^3J=6.49Hz, CH_2-Ar), 1.45 (t, 1H, ^3J=5.40 Hz, -O**H**). ^{13}C NMR (150 MHz, $CDCl_3$) δ: 154.6, 144.6-144.8 (m), 143.4-145.2 (m), 135.8, 135.3-137.3 (m), 130.6, 116.9, 63.6, 38.4. NMR spectra are given in Appendix A.2.

5.2.3 Synthesis of 4-(4-(2-chloroethyl)phenoxy)-2,3,5,6-tetrafluoropyridine (4)

2-(4-((Perfluoropyridin-4-yl)oxy)phenyl)ethan-1-ol (**3**) (97.6 mg, 0.34 mmol) was added to concentrated HCl (37%, 5 mL). The solution was stirred and heated to 105°C for 21 h, connected to a condenser under N_2 atmosphere. Distilled water (15 mL) was added, and the mixture was extracted with CH_2Cl_2 (3 × 10 mL). The combined organic phase was washed with distilled water and dried over $MgSO_4$. The solvent was removed under reduced pressure. The crude mixture (86.5 mg) was purified by flash chromatography (1:11 MeCN/CH_2Cl_2) to give **4** as a transparent oil in 25% yield (25.2 mg, 0.08 mmol) and 99% purity (^{1}H NMR). ^{1}H NMR (600 MHz, $CDCl_3$) δ: 7.23-7.25 (m, 2H, Ar-**H**), 7.01-7.04 (m, 2H, Ar-**H**), 3.71 (t, 2H, ^3J=7.25, CH_2-Cl), 3.07 (t, 2H, ^3J=7.25, CH_2-Ar). The ^{1}H NMR spectrum is given in Appendix A.3.

5.2.4 Attempted synthesis of 4-(4-(2-(cyclopropylmethoxy)ethyl)phenoxy)-2,3,5,6-tetrafluoropyridine (5)

The listed methods correspond to the entries of Table 2.3. The reactions were monitored by TLC (1:11 MeCN/CH_2Cl_2); R_f (**3**) = 0.33.

Method 1: To a stirred solution of 2-(4-((perfluoropyridin-4-yl)oxy)phenyl)ethan-1-ol (**3**) (0.10 g, 0.35 mmol), triethylamine (146 µL, 1.04 mmol) and (iodomethyl)cyclopropane (40 µL, 0.42 mmol) was added and the mixture was stirred at reflux for 24 h. The solvent and base were removed under reduced pressure to give a mixture of **3** and **5a** as a yellow oil. The crude mixture was purified by dilution with CH_2Cl_2 (10 mL) and washing with dilute HCl (0.1 M, 10 mL) and water (10 mL). The organic phase was dried over $MgSO_4$ and the solvent removed under reduced pressure to give **3**.

Method 2: To a stirred solution of 2-(4-((perfluoropyridin-4-yl)oxy)phenyl)ethan-1-ol (**3**) (0.10 g, 0.35 mmol), K_2CO_3 (0.19 g, 1.39 mmol) and (iodomethyl)cyclopropane (40 µL, 0.42 mmol) was added and the mixture was stirred at reflux for 20 h. The reaction mixture was filtered and the solvent removed under reduced pressure, to give a yellow oil.

Method 3: To a stirred solution of 2-(4-((perfluoropyridin-4-yl)oxy)phenyl)ethan-1-ol (**3**) (0.10 g, 0.35 mmol), NaOH (55.7 mg, 1.39 mmol) and (iodomethyl)cyclopropane (40 µL, 0.42 mmol) was added and the mixture was stirred at rt for 24 h. The crude mixture was diluted with water (20 mL) and extracted with CH_2Cl_2 (3 × 10 mL). The combined organic phase was dried over $MgSO_4$ and the solvent removed under reduced pressure, to give a light yellow oil with white particles.

Method 4: To a stirred solution of 2-(4-((perfluoropyridin-4-yl)oxy)phenyl)ethan-1-ol (**3**) (0.20 g, 0.70 mmol), *t*-BuOK (0.16 g, 1.4 mmol) was added and the mixture was stirred under N_2 at 50°C for 30 min. A solution of (iodomethyl)cyclopropane (98 µL, 1.05 mmol) in DMSO (1 mL) was added dropwise and the solution was stirred for 3 h under the same conditions. The reaction was quenched with water (20 mL) and extracted with toluene (3 × 10 mL). The organic phase was washed with water (15 mL) and dried over $MgSO_4$. The combined water phase was extracted with CH_2Cl_2 (3 × 10 mL). The CH_2Cl_2 phase was washed with water (15 mL) and brine (10 mL), and dried over $MgSO_4$. The combined toluene and CH_2Cl_2 phases were concentrated under reduced pressure to give a brown liquid with yellow crystals.

Methods 5 and 6: To a stirred solution of 2-(4-((perfluoropyridin-4-yl)oxy)phenyl)ethan-1-ol (**3**) (0.10 g, 0.35 mmol) in CH_2Cl_2 (1 mL), NaOH (*aq*, 28 mg, 0.70 mmol) and Bu_4HNSO_4 (3.7 mg, 0.01 mmol), or *t*-BuOK (59.0 mg, 0.52 mmol), was added and the mixture was stirred under N_2 at rt for 30 min. A solution of (bromomethyl)cyclopropane (56 µL, 0.54 mmol) in CH_2Cl_2 (0.3 mL) was added dropwise and the solution was stirred for 5 h. The mixture was quenched with water (5 mL) and extracted with CH_2Cl_2 (2 × 10 mL) and EtOAc (2 × 10 mL). A white solid precipitated in the organic phase during the extraction. The organic phase was washed with water (2 × 5 mL) and brine (10 mL). The combined aqueous phase was extracted with toluene (2 × 10 mL). The combined organic phases were concentrated under reduced pressure to give a white solid.

5.2.5 Synthesis of 2-((4-(2-(cyclopropylmethoxy)ethyl)phenoxy)methyl)oxirane (6)

To a stirred solution of 4-(2-(cyclopropylmethoxy)ethyl)phenol (**2**) (0.20 g, 1.04 mmol) and K_2CO_3 (0.43 g, 3.12 mmol) in dry MeCN (15 mL), epichlorohydrin (0.33 mL, 4.16 mmol) was added. The mixture was heated under reflux for 22 h. Full conversion was confirmed by TLC (1:11 MeCN/CH_2Cl_2); R_f (**2**) = 0.48, R_f (**6**) = 0.61. The mixture was filtered and the filtrate was concentrated under reduced pressure. EtOAc (25 mL) was added, and the solution was washed with distilled water. The aqueous phase was extracted with EtOAc (3 × 15 mL), and the combined organic phase was washed with brine and dried over $MgSO_4$. Epoxide **6** was obtained as a light yellow liquid in 97% yield (0.25 g, 1.01 mmol) and 98% purity (^{1}H NMR). HPLC, eluent: *n*-hexane:*i*-PrOH (90:10), t_R(**6**) = 7.1 min, t_R(**6**) = 8.4 min. ^{1}H NMR (600 MHz, $CDCl_3$) δ: 7.13-7.15 (m, 2H, Ar-**H**), 6.83-6.86 (m, 2H, Ar-**H**), 4.18 (dd, 1H, ^3J=3.35 Hz, ^2J=11.13 Hz, O-C**H**$_2$CH-O), 3.93 (dd, 1H, ^3J=5.40 Hz, ^2J=11.13 Hz, O-C**H**$_2$CH-O), 3.61 (t, 2H, ^3J=7.60 Hz, O-C**H**$_2$CH$_2$), 3.32-3.35 (m, 1H, C**H**-O), 3.27 (d, 2H, ^3J=6.71 Hz, C**H**$_2$-O), 2.89 (t, 1H,^3J=4.76 Hz, ^2J=4.76 Hz, C**H**$_2$ (epoxide)), 2.84 (t, 2H, ^3J=7.60 Hz, C**H**$_2$-Ar), 2.74 (dd, 1H, ^2J=4.76 Hz, ^3J=2.70 Hz, C**H**$_2$ (epoxide)), 1.02-1.08 (m, 1H, C**H** (cyclopropyl)), 0.51-0.54 (m, 2H, C**H**$_2$ (cyclopropyl)), 0.18-0.21 (m, 2H, C**H**$_2$ (cyclopropyl)). ^{13}C NMR (150 MHz, $CDCl_3$) δ: 157.1, 131.8, 129.9, 114.7, 75.7, 71.9, 68.9, 50.3, 44.8, 35.6, 10.7, 1.3. NMR spectra are given in Appendix A.5.

5.2.6 Synthesis of 2-(4-(oxiran-2-ylmethoxy)phenyl)ethan-1-ol (7)

To a solution of 4-(2-hydroxyethyl)phenol (**1**) (1.10 g, 7.94 mmol) and K_2CO_3 (3.45 g, 25.0 mmol) in dry MeCN (20 mL), epichlorohydrin (1.70 mL, 21.6 mmol) was added. The mixture was stirred under reflux for 23 h. Full conversion was detected by TLC (1:10 MeOH/CH_2Cl_2); R_f (**7**) = 0.45. The mixture was filtrated and the solvent removed under reduced pressure. The crude mixture (1.31 g) was purified by flash chromatography (1:10 MeOH/CH_2Cl_2) to yield **7** as a white crystalline solid in 70% yield (1.06 g, 5.46 mmol) and 99% purity (^{1}H NMR). ^{1}H NMR (600 MHz, $CDCl_3$) δ: 7.13-7.15 (m, 2H, Ar-**H**), 6.86-6.88 (m, 2H, Ar-**H**), 4.19 (dd, 1H, ^3J=3.12 Hz, ^2J=11.16 Hz, O-C**H**$_2$CH-O), 3.94 (dd, 1H, ^3J=5.58 Hz, ^2J=11.16 Hz, O-C**H**$_2$CH-O), 3.80 (q, 2H, ^3J=6.60 Hz, C**H**$_2$-OH), 3.33-3.35 (m, 1H, C**H**), 2.90 (t, 1H, ^2J=^3J=4.70 Hz, C**H**$_2$ (epoxide)), 2.80 (t, 2H, ^3J=6.29 Hz, C**H**$_2$-Ar), 2.75 (dd, ^2J=4.70 Hz, ^3J=2.58 Hz, C**H**$_2$ (epoxide)), 1.52 (t, 1H, ^3J=5.70 Hz, O**H**). ^{13}C NMR (150 MHz, $CDCl_3$) δ: 157.3, 131.2, 114.9, 68.9, 63.9, 50.3, 44.8, 38.4. The NMR spectra are given in Appendix A.6.

5.2.7 Synthesis of 1-chloro-3-(4-(2-(cyclopropylmethoxy)ethyl)phenoxy)propan-2-ol (8a)

To a stirred solution of 2-((4-(2-(cyclopropylmethoxy)ethyl)phenoxy)methyl)oxirane (**6**) (0.22 g, 0.87 mmol) and LiCl (80.0 mg, 1.74 mmol) in MeCN (5 mL), glacial AcOH (250 µL, 4.35 mmol) was added. The solution was stirred at rt for 17 h, monitored by TLC (1:11 MeCN/CH_2Cl_2); R_f (**6**) = 0.61, R_f (**8a**) = 0.45. The reaction was then quenched with $NaHCO_3$ (aq), until neutral pH. The aqueous mixture was extracted with CH_2Cl_2 (3 × 20 mL). The combined organic phase was washed with brine and dried over $MgSO_4$. The solvent was removed under reduced pressure to give chlorohydrin (**8**a) as a pale yellow oil in 85% yield (0.23 g, 0.82 mmol) and 97% purity (^{1}H NMR). HPLC, eluent:

n-hexane:*i*-PrOH (90:10), t_R((*S*)-**8a**) = 10.8 min, t_R((*R*)-**8a**) = 12.8 min. ^{1}H NMR (600 MHz, $CDCl_3$) δ: 7.14-7.16 (m, 2H, Ar-**H**), 6.83-6.86 (m, 2H, Ar-**H**), 4.20 (sx, 1H, ^3J=5.40 Hz, C**H**-OH), 4.04-4.09 (m, 2H, O-C**H**$_2$-CHOH), 3.70-3.79 (m, 2H, C**H**$_2$-Cl), 3.62 (t, 2H, ^3J=7.27 Hz, CH_2-C**H**$_2$O), 3.28 (d, 2H, ^3J=6.79 Hz, C**H**$_2$-cyclopropyl)), 2.85 (t, 2H, ^3J=7.27 Hz, Ar-C**H**$_2$), 2.62-2.66 (m, 1H, O**H**), 1.02-1.09 (m, 1H, C**H** (cyclopropyl)), 0.51-0.54 (m, 2H, C**H**$_2$ (cyclopropyl)), 0.18-0.21 (m, 2H, C**H**$_2$ (cyclopropyl)). ^{13}C NMR (150 MHz, $CDCl_3$) δ: 156.8, 132.1, 130.1, 114.6, 75.8, 71.8, 70.0, 68.9, 46.1, 35.6, 10.7, 3.1. NMR spectra are given in Appendix A.7.

5.2.8 Synthesis of 1-bromo-3-(4-(2-(cyclopropylmethoxy)ethyl)phenoxy)propan-2-ol (8b)

A solution of 2-(4-(oxiran-2-ylmethoxy)phenyl)ethan-1-ol (**7**) (0.58 g, 2.98 mmol) (bromomethyl)cyclopropane (371 µL, 3.57 mmol) in MeCN (5 mL) was stirred under N_2 for 15 min. The solution was cooled to 0°C and *t*-BuOK (0.47 g, 4.17 mmol) was added slowly over a period of 10 min. The mixture was stirred under N_2 at 0°C for 5 h, then left at rt for 19 h. The reaction was monitored by TLC (1:10 MeOH/CH_2Cl_2); R_f (**7**) = 0.45, R_f (**8b**) = 0.72. The reaction was quenched with aqueous H_2SO_4 (4 M, 3 mL), and extracted with diethyl ether (3 × 15 mL). The combined organic phase was washed with water (2 × 10 mL) and brine (10 mL), and dried over $MgSO_4$. The solvent was removed under reduced pressure. The crude mixture (0.89 g) was purified by flash chromatography (1:10 MeOH/CH_2Cl_2) to yield bromohydrin **8b** as a pale yellow oil in 35% yield. HPLC, eluent: *n*-hexane:*i*-PrOH (90:10), t_R((*S*)-**8b**) = 11.3 min, t_R((*R*)-**8b**) = 13.7 min. ^{1}H NMR (600 MHz, $CDCl_3$) δ: 7.14-7.16 (m, 2H, Ar-**H**), 6.83-6.86 (m, 2H, Ar-**H**), 4.17-4.20 (m, 1H, C**H**-OH), 4.04-4.10 (m, 2H, O-C**H**$_2$-CHOH), 3.58-3.67 (m, 4H, C**H**$_2$-Cl, CH_2-C**H**$_2$O), 3.28 (d, 2H, ^3J=7.17 Hz, C**H**$_2$-cyclopropyl)), 2.85 (t, 2H, ^3J=7.20 Hz, Ar-C**H**$_2$), 2.53-2.55 (m, 1H, O**H**), 1.04-1.07 (m, 1H, C**H** (cyclopropyl)), 0.51-0.54 (m, 2H, C**H**$_2$ (cyclopropyl)), 0.18-0.21 (m, 2H, C**H**$_2$ (cyclopropyl)). ^{13}C NMR (150 MHz, $CDCl_3$) δ: 156.8, 132.2, 130.1, 114.6, 75.8, 71.9, 69.7, 69.4, 35.6, 35.2, 10.8, 3.1. NMR spectra are given in Appendix A.8. MS (TOF MS ES+): *m/z* = 351.0572 $[M+Na]^+$, (calc. mass $[M+Na]^+$ = 351.06, $C_{15}H_{21}BrNaO_3$).

5.2.9 Synthesis of 1-chloro-3-(4-(2-(cyclopropylmethoxy)ethyl)phenoxy)propan-2-yl butyrate (9)

A small vial was charged with 1-chloro-3-(4-(2-(cyclopropylmethoxy)ethyl)phenoxy)propan-2-ol (**8a**) (18.0 mg, 0.06 mmol), butyric acid (2 drops), pyridine (2 drops) and *n*-hexane (0.5 mL). The vial was placed in an air bath at 60°C for 1 h. The solution was washed with distilled water (5 × 1 mL) and dried over $MgSO_4$. Excess pyridine was removed by adding toluene (3 mL) and evaporating under reduced pressure. This process was repeated once before the sample was analyzed by HPLC. HPLC, eluent: *n*-hexane:*i*-PrOH (99:1), t_R((*S*)-**9**) = 14.4 min, t_R((*R*)-**9**) = 15.7 min.

5.2.10 Synthesis of racemic betaxolol (10)

Method 1: To a stirred solution of 1-chloro-3-(4-(2-(cyclopropylmethoxy)ethyl)phenoxy)-propan-2-ol (**8a**) (24.9 mg, 0.09 mmol) in MeOH (2 mL), isopropylamine (157 µL, 1.80 mmol) was added. The solution was stirred under reflux for 22 h. Full conversion was detected by TLC (1:11 MeCN/CH_2Cl_2); R_f (**8a**) = 0.45, R_f (**10**) = 0.05. The solution

was diluted with EtOAc (50 mL) and washed with $NaHCO_3$ (aq, 10 mL) and distilled water (2 × 20 mL). The combined organic phase was dried over $MgSO_4$ and concentrated under reduced pressure to yield betaxolol (**10**) in 57% yield (15.7 mg, 0.05 mmol) and 95% purity as a pale pink oil. HPLC, eluent: *n*-hexane:*i*-PrOH:diethylamine (90:9.8:0.2), t_R((*R*)-**10**) = 6.4 min, t_R((*S*)-**10**) = 12.4 min. ^{1}H NMR (600 MHz, $CDCl_3$) δ: 7.12-7.14 (m, 2H, Ar-**H**), 6.82-6.84 (m, 2H, Ar-**H**), 4.15-4.18 (m, 1H, C**H**-OH), 3.93-4.00 (m, 2H, C$\mathbf{H}_2$-Ar), 3.81 (bs, 2H, O**H**, N**H**), 3.60 (t, 2H, ^3J=7.38 Hz, O-C$\mathbf{H}_2$-CH_2-), 3.28 (d, 2H, ^3J=6.85 Hz, O-C$\mathbf{H}_2$-CH-), 2.98-3.01 (m, 2H, C$\mathbf{H}_2$-NH-, C**H**-NH-), 2.84 (t, 2H, ^3J=7.38 Hz, C$\mathbf{H}_2$-Ar), 2.82-2.85 (m, 1H, C$\mathbf{H}_2$-NH-), 1.19 (dd, 6H, ^3J=3.17, ^3J=6.34, C$\mathbf{H}_3$), 1.04-1.06 (m, 1H, C**H** (cyclopropyl)), 0.51-0.54 (m, 2H, C$\mathbf{H}_2$ (cyclopropyl)), 0.18-0.20 (m, 2H, C$\mathbf{H}_2$ (cyclopropyl)). ^{13}C NMR (150 MHz, $CDCl_3$) δ: 157.2, 131.7, 130.0, 114.6, 75.8, 71.9, 70.4, 67.9, 49.8, 49.2, 35.6, 22.2, 22.0, 10.8, 3.1. The NMR spectra are given in Appendix A.11.

Method 2: A solution of 1-chloro-3-(4-(2-(cyclopropylmethoxy)ethyl)phenoxy)propan-2-ol (**8a**) (49.7 mg, 0.17 mmol) and H_2O (2 drops) in isopropylamine (2.5 mL) was stirred at rt for 30 h. The solvent was removed under reduced pressure. Conversion was not detected by TLC (1:11 MeCN/CH_2Cl_2). NMR analysis gave only the starting material **8a**.

5.2.11 CALB catalyzed kinetic resolution of 1-chloro-3-(4-(2-(cyclopropylmethoxy)ethyl)phenoxy)propan-2-ol (8a)

To a solution of 1-chloro-3-(4-(2-(cyclopropylmethoxy)ethyl)phenoxy)propan-2-ol (**8a**) (0.17 g, 0.61 mmol) in dry MeCN (12 mL) containing activated 4Å molecular sieves, vinyl butanoate (319 µL, 2.52 mmol) and CALB (360 mg) was added. The reaction vial was capped and placed in an incubator at 37°C and 200 rpm for 14 h. The reaction mixture was filtered and the solvent was removed under reduced pressure before separation of (*R*)-1-chloro-3-(4-(2-(cyclopropylme-thoxy)ethyl)phenoxy)propan-2-ol ((*R*)-**8a**) and (*S*)-1-chloro-3-(4-(2-(cyclopropylmethoxy)ethyl)phenoxy)pro-pan-2-yl butyrate ((*S*)-**9**) by flash chromatography (1:4 EtOAc/*n*-pentane); R_f (**8a**) = 0.28, R_f (**9**) = 0.63. Separately, the two fractions were diluted with EtOAc (15 mL) and washed with distilled water (3 × 10 mL). The combined aqueous phase was extracted with EtOAc (10 mL). The combined organic phase was washed with brine (15 mL), dried over $MgSO_4$ and concentrated under reduced pressure. Chlorohydrin (*R*)-**8a** was isolated as a transparent oil in 38% yield (0.06 g, 0.23 mmol), 99% purity (^{1}H NMR) and 99% ee (HPLC), $[\alpha]_D^{20} = -1.92$ (*c* 1.04, $CHCl_3$). Ester (*S*)-**9** was isolated as a yellow oil in 48% yield (0.10 g, 0.29 mmol), 96% purity (^{1}H NMR) and 87% ee (HPLC), $[\alpha]_D^{20} = +13.4$ (*c* 0.97, $CHCl_3$). ^{1}H NMR (600 MHz, $CDCl_3$) of **9** δ: 7.13-7.16 (m, 2H, Ar-**H**), 6.83-6.85 (m, 2H, Ar-**H**), 5.33 (quint, 1H, ^3J=5.11 Hz, C**H**), 4.12-4.22 (m, 2H, C$\mathbf{H}_2$-OAr), 3.76-3.86 (m, 2H, CH_2-Cl), 3.59-3.62 (m, 2H, ^3J=7.46 Hz, C$\mathbf{H}_2$-O), 3.28 (d, 2H, ^3J=7.16 Hz, CH_2-cyclopropyl), 2.83-2.86 (m, 2H, ^3J=7.46 Hz, C$\mathbf{H}_2$-Ar), 2.32-2.37 (m, 2H, C$\mathbf{H}_2$-COOR), 1.65-1.70 (m, 2H, C$\mathbf{H}_2$$CH_3$), 1.04-1.07 (m, 1H, C**H** (cyclopropyl)), 0.93-0.99 (m, 3H, C$\mathbf{H}_3$), 0.51-0.54 (m, 2H, C$\mathbf{H}_2$ (cyclopropyl)), 0.18-0.21 (m, 2H, C$\mathbf{H}_2$ (cyclopropyl)). ^{13}C NMR (150 MHz, $CDCl_3$) of **9** δ: 172.9, 156.9, 132.1, 130.1, 114.7, 75.8, 71.9, 71.0, 66.3, 42.8, 36.2, 35.6, 18.6, 13.7, 10.7, 3.1. The NMR spectra of **9** are shown in Appendix A.10.

5.2.12 CALB catalyzed kinetic resolution of 1-bromo-3-(4-(2-(cyclopropylmethoxy)ethyl)phenoxy)propan-2-ol (8b)

To a solution of 1-bromo-3-(4-(2-(cyclopropylmethoxy)ethyl)phenoxy)propan-2-ol (**8b**) (0.11 g, 0.33 mmol) in dry MeCN (12 mL) containing activated 4Å molecular sieves, vinyl butanoate (166 µL, 1.32 mmol) and CALB (230 mg) was added. The reaction vial was capped and placed in an incubator at 37°C and 200 rpm for 14 h. The reaction mixture was filtered and the solvent was removed under reduced pressure before separation of (*R*)-1-bromo-3-(4-(2-(cyclopropylme-thoxy)ethyl)phenoxy)propan-2-ol ((*R*)-**8b**) and (*S*)-1-bromo-3-(4-(2-(cyclopropylmethoxy)ethyl)phenoxy)pro-pan-2-yl butyrate ((*S*)-**9b**) by flash chromatography (1:4 EtOAc/*n*-pentane); R_f (**8b**) = 0.29, R_f (**9b**) = 0.50. The fraction containing (*R*)-**8b** was diluted with EtOAc (15 mL) and washed with distilled water (15 mL) and brine (10 mL), dried over $MgSO_4$ and concentrated under reduced pressure. Bromohydrin (*R*)-**8b** was isolated as a light yellow oil in 27% yield (30.0 mg, 0.09 mmol) and 58% ee.

5.2.13 Synthesis of (*S*)-betaxolol ((*S*)-10)

Following the procedure described in Section 5.2.10, method 1, (*R*)-1-chloro-3-(4-(2-(cyclopropylmethoxy)ethyl)phenoxy)propan-2-ol (**8a**) (33.0 mg, 0.12 mmol, 99% ee) was converted to (*S*)-betaxolol ((*S*)-**10**) as a pale pink oil in 95% yield (33.8 mg, 0.11 mmol), 98% purity (^{1}H NMR) and 99% ee (HPLC), $[\alpha]_D^{20} = -7.21$ (*c* 0.97, $CHCl_3$).

5.3 Pathway to (*S*)-esmolol ((*S*)-15)

5.3.1 Synthesis of methyl 3-(4-(oxiran-2-ylmethoxy)phenyl)propanoate (12)

To a stirred solution of methyl 3-(4-hydroxyphenyl)propanoate (**11**) (0.25 g, 2.84 mmol) in dry MeCN (30 mL), K_2CO_3 (1.01 g, 7.40 mmol) and epichlorohydrin (0.44 mL, 5.68 mmol) was added. The mixture was heated under reflux for 45 h. Full conversion was detected by TLC (1:11 MeCN/CH_2Cl_2); R_f (**11**) = 0.39, R_f (**12**) = 0.66. The reaction mixture was filtered, and the filtrate was concentrated under reduced pressure. EtOAc (25 mL) was added, and the resulting solution was washed with distilled water. The water phase was extracted with EtOAc (3 × 15 mL). The organic phases were combined, washed with brine (20 mL) and dried over $MgSO_4$. The crude mixture (0.62 g) was purified by flash chromatography (1:11 MeCN/CH_2Cl_2) to afford **12** as a transparent liquid in 68% yield (0.45 g, 1.92 mmol) and 99% purity (^{1}H NMR). ^{1}H NMR (600 MHz, $CDCl_3$) δ: 7.10-7.12 (m, 2H, Ar-**H**), 6.83-6.86 (m, 2H, Ar-**H**), 4.19 (dd, 1H, ^2J=11.01 Hz, ^3J=3.20 Hz, C**H**$_2$-O), 3.94 (dd, 1H, ^2J=11.01 Hz, ^3J=5.65 Hz, C**H**$_2$-O), 3.66 (s, 3H, C**H**$_3$), 3.34 (ddt, 1H, ^3J=2.70 Hz, ^3J=3.20 Hz, ^3J=5.65 Hz, C**H**-O), 2.88-2.91 (m, 3H, Ar-C**H**$_2$/C**H**$_2$-O), 2.75 (dd, 1H, ^2J=4.94, ^3J=2.70, C**H**$_2$-O), 2.59 (t, 2H, C**H**$_2$COOR). The ^{1}H NMR spectrum is given in Appendix B.1.

5.3.2 Synthesis of methyl 3-(4-(3-chloro-2-hydroxypropoxy)phenyl)propanoate (13)

To a stirred solution of methyl 3-(4-(oxiran-2-ylmethoxy)phenyl)propanoate (**12**) (0.44 g, 1.86 mmol) and LiCl (0.16 g, 3.72 mmol) in MeCN (10 mL), glacial AcOH (350 µL, 9.30 mmol) was added. The solution was stirred at rt for 47 h. The reaction was monitored by TLC (1:11 MeCN/CH_2Cl_2); R_f (**12**) = 0.66, R_f (**13**) = 0.44. The reaction was quenched

with Na_2CO_3 (aq) and extracted with CH_2Cl_2 (3 × 20 mL). The organic phase was washed with brine and dried over $MgSO_4$ before the solvent was removed under reduced pressure. Chlorohydrin **13** was obtained as a light yellow oil in 96% yield (0.49 g, 1.79 mmol) and 96% purity (^{1}H NMR). HPLC, eluent: *n*-hexane:*i*-PrOH (80:20), t_R((*S*)-**13**) = 9.4 min, t_R((*R*)-**13**) = 10.3 min. ^{1}H NMR (600 MHz, $CDCl_3$) δ: 7.11-7.14 (m, 2H, Ar-**H**), 6.83-6.85 (m, 2H, Ar-**H**), 4.18-4.23 (m, 1H, C**H**-OH), 4.04-4.09 (m, 2H, C$\mathbf{H}_2$-O), 3.71-3.79 (m, 2H, C$\mathbf{H}_2$-Cl), 3.66 (s, 3H, C$\mathbf{H}_3$), 2.90 (t, 2H, ^3J=7.92 Hz, C$\mathbf{H}_2$-Ar), 2.60 (t, 2H, ^3J=7.92 Hz, C$\mathbf{H}_2$COOR), 2.49-2.52 (m, 1H, -O**H**). The ^{1}H NMR spectrum of **13** is given in Appendix B.2.

5.3.3 Synthesis of racemic esmolol (15)

Methyl 3-(4-(3-chloro-2-hydro-xypropoxy)phenyl)propanoate (**13**) (24.7 mg, 0.09 mmol) was dissolved in MeOH (3 mL) and isopropylamine (157 µL, 1.84 mmol) was added. The mixture was stirred under reflux for 24 h. The reaction was monitored by TLC (1:11 MeCN/CH_2Cl_2); R_f (**15**) = 0.16. The solvent was removed under reduced pressure, and the residue was diluted with EtOAc (50 mL) and washed with distilled water (2 × 20 mL). The organic phase was dried over $MgSO_4$ and the solvent was removed under reduced pressure to afford racemic esmolol (**15**) as a pale yellow solid in 86% yield (23.4 mg, 0.08 mmol), 88% purity (^{1}H NMR). HPLC, eluent: *n*-hexane:*i*-PrOH:diethylamine (80:19.6:0.4), t_R((*R*)-**15**) = 6.1 min, t_R((*S*)-**15**) = 9.5 min. ^{1}H NMR (600 MHz, $CDCl_3$) δ: 7.08-7.10 (m, 2H, Ar-**H**), 6.82-6.84 (m, 2H, Ar-**H**), 3.98-4.00 (m, 1H, C**H**-OH), 3.92-3.96 (m, 1H, C$\mathbf{H}_2$O), 3.65 (s, 3H, C$\mathbf{H}_3$), 2.85-2.89 (m, 3H, C$\mathbf{H}_2$-Ar, C**H**-NH), 2.81 (p, 1H, ^3J=6.30 Hz, C**H**Me$_2$), 2.70 (dd, 1H, ^3J=8.03 Hz, ^2J=12.14, C**H**-NH), 2.58 (t, 2H, ^3J=7.60, C$\mathbf{H}_2$COOR), 1.07 (d, 6H, ^3J=6.30 Hz, C$\mathbf{H}_3$). ^{13}C NMR (150 MHz, $CDCl_3$) δ: 173.5, 157.3, 133.0, 129.3, 114.7, 70.7, 68.6, 51.7, 49.5, 49.0, 36.0, 30.2, 23.2, 23.1. The NMR spectra of **15** are given in Appendix B.4.

5.3.4 CALB catalyzed kinetic resolution of methyl 3-(4-(3-chloro-2-hydroxy-propoxy)phenyl)propanoate (13)

To a solution of methyl 3-(4-(3-chloro-2-hydroxypropoxy)phenyl)propanoate (**13**) (0.13 g, 0.49 mmol) in dry MeCN (10 mL) containing activated 4Å molecular sieves, vinyl butanoate (249 µL, 1.96 mmol) and CALB (150 mg) was added. The reaction vial was capped and placed in an incubator at 37°C and 200 rpm for 48 h. The reaction mixture was filtered and the solvent was removed under reduced pressure before separation of (*R*)-methyl 3-(4-(3-chloro-2-hydroxypropoxy)phenyl)propanoate ((*R*)-**13**) and (*S*)-1-chloro-3-(4-(3-methoxy-3-oxopropyl)phenoxy)propan-2-yl butyrate ((*S*)-**14**) by flash chromatography (1:4 EtOAc/*n*-pentane); R_f (**13**) = 0.15, R_f (**14**) = 0.51. Chlorohydrin (*R*)-**13** was isolated as a transparent oil in 43% yield (57 mg, 0.21 mmol), 99% purity (^{1}H NMR) and 97% ee (HPLC), $[\alpha]_D^{20} = -5.33$ (*c* 1.6, *i*-PrOH). Ester (*S*)-**14** was isolated as a pale yellow oil in 41% yield (68 mg, 0.20 mmol), 99% purity (^{1}H NMR) and 87% ee, $[\alpha]_D^{20} = +30.71$ (*c* 1.4, *i*-PrOH). HPLC, eluent: *n*-hexane:*i*-PrOH (97:3), t_R((*S*)-**14**) = 15.6 min, t_R((*R*)-**14**) = 17.3 min. ^{1}H NMR (600 MHz, $CDCl_3$) of **14** δ: 7.10-7.13 (m, 2H, Ar-**H**), 6.82-6.85 (m, 2H, Ar-**H**), 5.33 (quint, 1H, ^3J=5.11 Hz, C**H**), 4.12-4.16 (m, 2H, C$\mathbf{H}_2$-O), 3.76-3.86 (m, 2H, C$\mathbf{H}_2$-Cl), 3.66 (s, 3H, C$\mathbf{H}_3$-O), 2.89 (t, 2H, ^3J=7.96 Hz, C$\mathbf{H}_2$-Ar), 2.59 (t, 2H, ^3J=7.96 Hz, C$\mathbf{H}_2$COOCH$_3$), 2.32-2.38 (m, 2H, C$\mathbf{H}_2$COOR), 1.68 (sx, 2H, ^3J=7.25 Hz, C$\mathbf{H}_2$CH$_3$), 0.96 (t, 3H, ^3J=7.25 Hz, CH$_2$C$\mathbf{H}_3$). The ^{1}H NMR spectrum of **14** is given in Appendix B.3.

5.3.5 Synthesis of (*S*)-esmolol ((*S*)-15)

Following the procedure described in Section 5.3.3, and purification by preparative TLC (1:11 MeCN/CH_2Cl_2), (*R*)-methyl 3-(4-(3-chloro-2-hydroxypropoxy)phenyl)propanoate ((*R*)-**13**) (38.0 mg, 0.14 mmol, 97% ee) was converted to (*S*)-esmolol ((*S*)-**15**) as a transparent liquid in 92% yield (37.9 mg, 0.13 mmol), 99% purity (^{1}H NMR) and 97% ee (HPLC), $[\alpha]_D^{20} = -6.80$ (*c* 1.03, $CHCl_3$).

5.4 Synthesis of compounds related to limonene (16)

5.4.1 Synthesis of perillyl acetate (18)

Perillyl alcohol (**17**) (2.00 g, 11.1 mmol) and acetic anhydride (1.34 g, 11.1 mmol) was stirred at rt. Phosphomolybdic acid (40 mg, 0.022 mmol) was added and the mixture was stirred for 15 min, when full conversion was detected by TLC (1:9 EtOAc/*n*-pentane). The reaction was quenched with $NaHCO_3$ (aq) and extracted with EtOAc (3 × 20 mL). The combined organic phase was washed with distilled water and dried over $MgSO_4$. The crude mixture (2.36 mg) was distilled under reduced pressure to afford perillyl acetate (**18**) as a transparent oil in 62% yield and 94% purity (GC). ^{1}H NMR (600 MHz, $CDCl_3$) δ: 5.74-5.76 (br s, 1H, C**H**=CH), 4.72-4.73 (br s, 1H, CH=C**H**$_2$), 4.70-4.71 (br s, 1H, CH=C**H**$_2$), 4.45 (s, 2H, C**H**$_2$O), 2.07-2.18 (m, 4H, C**H**, C**H**$_2$), 2.06 (s, 3H, C**H**$_3$-CO), 1.83-2.00 (m, 2H, C**H**$_2$), 1.73 (s, 3H, C**H**$_3$C=CH$_2$), 1.47-1.51 (m, 1H, C**H**$_2$). ^{13}C NMR (150 MHz, $CDCl_3$) δ: 171.2, 149.7, 132.7, 126.2, 108.9, 68.6, 40.9, 30.6, 27.4, 26.5, 21.1, 20.9. MS: *m/z* = 194.1 [M^+] (calc. mass [M^+] = 194.13, $C_{12}H_{18}O_2$). The GC-MS results and the NMR spectra are given in Appendices C.1 and C.2.

5.4.2 Oxidation of limonene (16) using SeO_2

To a stirred solution of limonene (**16**) (0.50 g, 3.67 mmol) in glacial AcOH (10 mL), SeO_2 (0.20 g, 1.80 mmol) was added slowly. The reaction mixture was stirred under reflux for 20 h, during which black selenium flakes developed in the mixture. The reaction mixture was cooled to rt and filtered before the solvent was removed under reduced pressure. The main component of the crude mixture was 1-methyl-4-(prop-1-en-2-yl)benzene (**16b**). MS: *m/z* = 132.1 [M^+] (calc. mass [M^+] = 132.09, $C_{10}H_{12}$). The GC-MS results are presented in Appendix C.4. The crude mixture was not purified.

5.4.3 General procedure for CYP catalyzed oxidation of limonene (16)

To a phosphate buffer solution (1-2 mL, 0.1 M, pH 7.4) containing glucose-6-phosphate (5 mM) and NADPH (2 mM), CypExpress^{TM} 2C19 powder (20-40 mg mL^{-1}) was added. The solution was stirred carefully with a glass rod to break up lumps. A solution of (*S*)- or (*R*)-limonene ((*S*)/(*R*)-**16**) in DMSO was added to the buffer mixture to give a final substrate concentration of 0.57 mM, and a DMSO concentration of 6%. The tube was placed in an incubator at 37°C and 200 rpm. The mixture was filtered and extracted with EtOAc (2 × 2 mL). The organic phase was washed with water (5 × 1 mL) and concentrated under a stream of N_2.

5.4.4 KRED228 catalyzed synthesis of (*S*)-perillyl alcohol ((*S*)-17) from (*S*)-perillaldehyde ((*S*)-20)

Reaction monitoring
KRED 228 (16.0 mg), NADPH (0.6 mg, 0.7 µmol), glucose-6-phosphate (160 mg) and glucose-6-phosphate dehydrogenase (0.2 mg, >550 U/mg) was added to a phosphate buffer solution (0.9-1.8 mL, 0.1 M, pH 7.4), and the mixture was stirred carefully with a glass rod to break up lumps. A solution of (*S*)-perillaldehyde (**20**) (15 mg) in DMSO (0.1-0.2 mL) was transferred to the aqueous mixture to give a total volume of 1-2 mL. The reaction was placed in an incubator at 37°C and 200 rpm for 6 days. The reaction was monitored by taking out 100 µL samples at regular intervals. The samples were extracted with EtOAc (3 × 1 mL), and the combined organic phase was washed with distilled water and dried over $MgSO_4$. The resulting solution was concentrated under a stream of N_2 gas, and analyzed by GC.

Large scale reaction
A sample was prepared as described above, scaled up ×3 (total volume: 6 mL, 53 mg (*S*)-perillaldehyde ((*S*)-**20**)). After 3 days, the reaction mixture was filtered and extracted with EtOAc (6 × 10 mL). The combined organic phase was washed with distilled water, dried over $MgSO_4$, and the solvent was removed under reduced pressure. The crude mixture (47.6 mg) was purified by flash chromatography (1:4 EtOAc/*n*-pentane) to yield (*S*)-perillyl alcohol ((*S*)-**17**) as a pale yellow oil in 37% yield and 95% purity (GC).

References

1. Anastas, P. M. & Warner, J. C. *Green chemistry: theory and practice* ISBN: 9780198 502340 (Oxford University Press, 1998).
2. Byrne, F. P. *et al.* Tools and techniques for solvent selection: green solvent selection guides. *Sustain Chem Process* **4,** 7 (2016).
3. Ciriminna, R., Lomeli-Rodriguez, M., Demma Carà, P., Lopez-Sanchez, J. A. & Pagliaro, M. Limonene: a versatile chemical of the bioeconomy. *Chem Comm* **50,** 15288–15296 (2014).
4. Thomas, A. F. & Bessière, Y. Limonene. *Nat Prod Rep* **6,** 291–309 (1989).
5. Negro, V., Mancini, G., Ruggeri, B. & Fino, D. Citrus waste as feedstock for bio-based products recovery: Review on limonene case study and energy valorization. *Bioresour Technol* **214,** 806–815 (2016).
6. Nguyen, L. A., He, H. & Pham-Huy, C. Chiral drugs: an overview. *Int J Biomed Sci* **2,** 85–100 (2006).
7. Kim, J. H. & Scialli, A. R. Thalidomide: The Tragedy of Birth Defects and the Effective Treatment of Disease. *Toxicol Sci* **122,** 1–6 (2011).
8. Nelson, D. L. & Cox, M. M. *Lehninger Principles of Biochemistry: 6th Edition* ISBN: 9781464109621 (Macmillan Learning, 2012).
9. FDA's policy statement for the development of new stereoisomeric drugs. *Chirality* **4,** 338–340 (1992).
10. Calcaterra, A. & D'Acquarica, I. The market of chiral drugs: Chiral switches versus de novo enantiomerically pure compounds. *J Pharm Biomed Anal* **147,** 323–340 (2018).
11. Gundersen, M. A. *et al.* Lipase Catalyzed Synthesis of Enantiopure Precursors and Derivatives for β-Blockers Practolol, Pindolol and Carteolol. *Catalysts* **11** (2021).
12. Ponikowski, P. *et al.* Heart failure: preventing disease and death worldwide. *ESC Heart Fail* **1,** 4–25 (2014).
13. *Causes of Death, Norway 2020* `http://statistikkbank.fhi.no/dar/`. Accessed: 14.01.22.
14. Gorre, F. & Vandekerckhove, H. Beta-blockers: focus on mechanism of action Which beta-blocker, when and why? *Acta Cardiol* **65,** 565–570 (2010).
15. Agustian, J., Kamaruddin, A. & Bhatia, S. Single enantiomeric β-blockers—The existing technologies. *Process Biochem* **45,** 1587–1604 (2010).
16. Wiest, D. B. & Haney, J. S. Clinical Pharmacokinetics and Therapeutic Efficacy of Esmolol. *Clin Pharmacokinet* **51,** 347–356 (2012).

17. Al-wadei, M. J., Bakheit, A. H., Abdel-Aziz, A. A. & Wani, T. A. *Chapter Three - Betaxolol: A comprehensive profile in Profiles of Drug Substances, Excipients and Related Methodology* 91–136. ISBN: 18715125 (Academic Press, 2021).

18. Weinreb, R. N. & Khaw, P. T. Primary open-angle glaucoma. *The Lancet* **363,** 1711–1720 (2004).

19. The number of people with glaucoma worldwide in 2010 and 2020. *Br J Ophthalmol* **90,** 262 LP –267 (2006).

20. Clark, S. S., Perman, S. M., Sahin, M. B., Jenkins, G. J. & Elegbede, J. A. Antileukemia activity of perillyl alcohol (POH): uncoupling apoptosis from G0/G1 arrest suggests that the primary effect of POH on Bcr/Abl-transformed cells is to induce growth arrest. *Leukemia* **16,** 213–222 (2002).

21. Matos, J. M. *et al.* A Pilot Study of Perillyl Alcohol in Pancreatic Cancer. *J Surg Res* **147,** 194–199 (2008).

22. Yeruva, L., Pierre, K. J., Elegbede, A., Wang, R. C. & Carper, S. W. Perillyl alcohol and perillic acid induced cell cycle arrest and apoptosis in non small cell lung cancer cells. *Cancer Lett* **257,** 216–226 (2007).

23. Yuri, T. *et al.* Perillyl Alcohol Inhibits Human Breast Cancer Cell Growth in vitro and in vivo. *Breast Cancer Res Treat* **84,** 251–260 (2004).

24. Chen, T. C., Fonseca, C. O. D. & Schönthal, A. H. Preclinical development and clinical use of perillyl alcohol for chemoprevention and cancer therapy. eng. *Am J Cancer Res* **5,** 1580–1593 (2015).

25. Da Fonseca, C. O. *et al.* Preliminary results from a phase I/II study of perillyl alcohol intranasal administration in adults with recurrent malignant gliomas. *Surg Neurol* **70,** 259–266 (2008).

26. Marson, B. M. *et al.* Effect of Different Tensoactives on the Morphology and Release Kinetics of PLA-b-PEG Microcapsules Loaded With the Natural Anticancer Compound Perillyl Alcohol. *J Pharm Sci* **108,** 860–869 (2019).

27. Pellis, A., Cantone, S., Ebert, C. & Gardossi, L. Evolving biocatalysis to meet bioeconomy challenges and opportunities. *N Biotechnol* **40,** 154–169 (2018).

28. Bell, E. L. *et al.* Biocatalysis. *Nat Rev Methods Primers* **1,** 46 (2021).

29. Sheldon, R. A., Brady, D. & Bode, M. L. The Hitchhiker's guide to biocatalysis: recent advances in the use of enzymes in organic synthesis. *Chem Sci* **11,** 2587–2605 (2020).

30. Faber, K. *Biotransformations in Organic Chemistry* ISBN: 9783642173929 (Springer-Verlag Berlin Heidelberg, 2011).

31. Arnold, F. H. Directed Evolution: Bringing New Chemistry to Life. *Angew Chem Int Ed* **57,** 4143–4148 (2018).

32. Garzón-Posse, F., Becerra-Figueroa, L., Hernández-Arias, J. & Gamba-Sánchez, D. Whole Cells as Biocatalysts in Organic Transformations. eng. *Molecules* **23,** 1265 (2018).

33. Humphrey, C. E., Ahmed, M., Ghanem, A. & Turner, N. J. *Application of Enzymes in Kinetic Resolutions, Dynamic Kinetic Resolutions and Deracemization Reactions* 2014.

34. Jacobsen, E. E. & Anthonsen, T. Water content influences the selectivity of CALB-catalyzed kinetic resolution of phenoxymethyl-substituted secondary alcohols. *Can J Chem* **80,** 577–581 (2002).

35. Solomons, T. W. G., Fryhle, C. B. & Snyder, S. A. *Organic Chemistry* ISBN: 9781119077251 (Wiley, 2016).

36. Straathof, A. J. J. & Jongejan, J. A. The enantiomeric ratio: origin, determination and prediction. *Enzyme Microb Technol* **21,** 559–571 (1997).

37. Anthonsen, H. W., Hoff, B. H. & Anthonsen, T. Calculation of enantiomer ratio and equilibrium constants in biocatalytic ping-pong bi-bi resolutions. *Tetrahedron: Asymmetry* **7,** 2633–2638 (1996).

38. Jacobsen, E. E. *Enantiopure Biologically Active Compounds by Lipase Catalysis* ISBN: 9783659281365 (Lap Lambert Academic Publishing GmbH KG, 2012).

39. Bairoch, A. The ENZYME database in 2000. *Nucleic Acids Research* **28,** 304–305 (2000).

40. Jaeger, K.-E. & Reetz, M. T. Microbial lipases form versatile tools for biotechnology. *Trends Biotechnol* **16,** 396–403 (1998).

41. Chandra, P., Enespa, Singh, R. & Arora, P. K. Microbial lipases and their industrial applications, a comprehensive review. *Microb Cell Fact* **19,** 169 (2020).

42. An, J, Xie, Y, Feng, Y & Wu, G. Crystal structure of CALB from Candida antarctica. `www.rcsb.org/structure/4K6G` (2014).

43. Muralidhar, R. V. *et al.* Understanding lipase stereoselectivity. *World J Microbiol Biotechnol* **18,** 81–97 (2002).

44. Jacobsen, E. E., Hoff, B. H. & Anthonsen, T. Enantiopure derivatives of 1,2-alkanediols: Substrate requirements of lipase B from Candida antarctica. *Chirality* **12,** 654–659 (2000).

45. Alexander. Cytochrome P450 (E.C. 1.14.-.-). *Br J Pharmacol* **158,** S215–S217 (2009).

46. Sono, M., Roach, M. P., Coulter, E. D. & Dawson, J. H. Heme-containing oxygenases. *Chem Rev* **96,** 2841–2887 (1996).

47. Groves, J. T. Cytochrome P450 enzymes: understanding the biochemical hieroglyphs. *F1000Research* **4** (2015).

48. Bathe, U. & Tissier, A. Cytochrome P450 enzymes: A driving force of plant diterpene diversity. *Phytochemistry* **161,** 149–162 (2019).

49. Nelson, D. R. The Cytochrome P450 Homepage. *Hum Genomics* **4,** 59 (2009).

50. Reynald, R. L., Sansen, S, Stout, C. D. & Johnson, E. F. Structure of Human Microsomal Cytochrome P450 (CYP) 2C19. `www.rcsb.org/structure/4gqs` (2012).

51. Barski, O. A., Tipparaju, S. M. & Bhatnagar, A. The aldo-keto reductase superfamily and its role in drug metabolism and detoxification. *Drug metab rev* **40,** 553–624 (2008).

52. Rabuffetti, M, Cannazza, P, Contente, L, Di Pisa, F & Molinari, F. Structural insights into the desymmetrization of bulky 1,2-dicarbonyls through enzymatic monoreduction. `https://www.rcsb.org/structure/6YC8` (2021).

53. Wuts, P. G. M. & Greene, W. T. *"Protection for Phenols and Catechols" in Greene's Protective Groups in Organic Synthesis,* 367–430. ISBN: 9780470053485 (Wiley, 2006).

54. Carey, F. A. & Sundberg, R. J. *Advanced Organic Chemistry: Part B: Reactions and Synthesis* ISBN: 9780387714813 (Springer US, 2007).

55. Brittain, W. D. G. & Cobb, S. L. Tetrafluoropyridyl (TFP): a general phenol protecting group readily cleaved under mild conditions. *Org Biomol Chem* **17,** 2110–2115 (2019).

56. Nakamura, A. & Nakada, M. Allylic Oxidations in Natural Product Synthesis. *Synthesis* **45,** 1421–1451 (2013).

57. Sharpless, K. B. & Lauer, R. F. Selenium dioxide oxidation of olefins. Evidence for the intermediacy of allylseleninic acids. *J Am Chem Soc* **94,** 7154–7155 (1972).

58. Manoury, P. M., Binet, J. L., Rousseau, J., Lefevre-Borg, F. M. & Cavero, I. G. Synthesis of a series of compounds related to betaxolol, a new beta1-adrenoceptor antagonist with a pharmacological and pharmacokinetic profile optimized for the treatment of chronic cardiovascular diseases. *J Med Chem* **30,** 1003–1011 (1987).

59. Wang, X. W., Bhatia, A. V., Chamberlin, S. A. & Luping, L. US Patent 5731463, 1872–1876 (1998).

60. Joshi, R. A., Garud, D. R., Muthukrishnan, M, Joshi, R. R. & Gurjar, M. K. A convenient synthesis of the enantiomerically pure β-blocker (S)-betaxolol using hydrolytic kinetic resolution. *Tetrahedron: Asymmetry* **16,** 3802–3806 (2005).

61. Datta, G. K., von Schenck, H., Hallberg, A. & Larhed, M. Selective Terminal Heck Arylation of Vinyl Ethers with Aryl Chlorides, A Combined Experimental Computational Approach Including Synthesis of Betaxolol. *J Org Chem* **71,** 3896–3903 (2006).

62. Muthukrishnan, M., Garud, D. R., Joshi, R. R. & Joshi, R. A. Concise synthesis of β-blockers (S)-metoprolol and (S)-betaxolol using hydrolytic kinetic resolution. *Tetrahedron* **63,** 1872–1876 (2007).

63. Zhang, J.-Y., Liu, H.-M., Wang, X.-J., Wang, P. & Zheng, J.-X. Application of kinetic resolution using HCS as chiral auxiliary, Novel synthesis of β-blockers (S)-betaxolol and (S)-metoprolol. *Chirality* **21,** 745–750 (2009).

64. Liu, H.-M., Liu, F.-W., Song, X.-P., Zhang, J.-Y. & Yan, L. A novel free C-12 higher carbon sugar: asymmetric synthesis and reactivity with nucleophiles. *Tetrahedron: Asymmetry* **17,** 3230–3236 (2006).

65. Di Bono, G. & Scilimati, A. A Chemoenzymatic Route to Both Enantiomers of Betaxolol. *Synthesis* **6,** 699–702 (1995).

66. Li, Y.-H., Huang, L.-H. & Liu, H.-M. Chemoenzymatic Route to S-Betaxolol. *Synth Comm* **41,** 2468–2474 (2011).

67. Narsaiah, A. V. & Kumar, J. K. Novel Asymmetric Synthesis of (S)-Esmolol Using Hydrolytic Kinetic Resolution. *Synth Comm* **41,** 1603–1608. ISSN: 0039-7911 (2011).

68. Banoth, L. & Banerjee, U. C. New chemical and chemo-enzymatic synthesis of (RS)-, (R)-, and (S)-esmolol. *Arab J Chem* **10,** S3603–S3613 (2017).

69. Torssell, K. B. G. *Natural Product Chemistry: A mechanistic, biosyntetic and ecological approach* ISBN: 9186274635 (Swedish Pharmaceutical Press, 1997).

70. Bohlmann, J. & Keeling, C. I. Terpenoid biomaterials. *Plant J* **54,** 656–669 (2008).

71. Lupien, S., Karp, F., Wildung, M. & Croteau, R. Regiospecific cytochrome P450 limonene hydroxylases from mint (Mentha) species. *Arch Biochem Biophys* **368,** 181–192 (1999).

72. Mau, C. J. D., Karp, F., Ito, M., Honda, G. & Croteau, R. B. A candidate cDNA clone for (-)-limonene-7-hydroxylase from Perilla frutescens. *Phytochemistry* **71,** 373–379 (2010).

73. Fujiwara, Y. & Ito, M. Molecular cloning and characterization of a Perilla frutescens cytochrome P450 enzyme that catalyzes the later steps of perillaldehyde biosynthesis. *Phytochemistry* **134,** 26–37 (2017).

74. Karp, F., Mihaliak, C. A., Harris, J. L. & Croteau, R. Monoterpene biosynthesis: Specificity of the hydroxylations of (-)-limonene by enzyme preparations from peppermint (Mentha piperita), spearmint (Mentha spicata), and perilla (Perilla frutescens) leaves. *Arch Biochem Biophys* **276,** 219–226 (1990).

75. Sakuda, Y. The Oxidation of Limonene with Selenium Dioxide. *Bull Chem Soc Jpn* **42,** 3348–3349 (1969).

76. Trachtenberg, E. N., Nelson, C. H. & Carver, J. R. Mechanism of selenium dioxide oxidation of olefins. *J Org Chem* **35,** 1653–1658 (1970).

77. Wilson, C. W. & Shaw, P. E. (+)-Limonene oxidation with selenium dioxide-hydrogen peroxide. *J Org Chem* **38,** 1684–1687 (1973).

78. Sobkowiak, A., Szczepanik, A., Narog, D. & Charczuk, M. Oxidation of limonene with dioxygen catalyzed by 2,2'-bipyridyl manganese(II) and iron(II) complexes supported on a bentonite carrier. *Przemysl Chemiczny* **94,** 2006–2009 (2015).

79. Młodzik, J., Wróblewska, A., Makuch, E., Wróbel, R. J. & Michalkiewicz, B. Fe/EuroPh catalysts for limonene oxidation to 1,2-epoxylimonene, its diol, carveol, carvone and perillyl alcohol. *Catal Today* **268,** 111–120 (2016).

80. Parmar, D. K. *et al.* Oxy-functionalization of olefins with neat and heterogenized binuclear V(IV)O and Fe(II) complexes: Effect of steric hindrance on product selectivity and output in homogeneous and heterogeneous phase. *Mol Cat* **474,** 110424 (2019).

81. Glonek, K. *et al.* Oxidation of limonene using activated carbon modified in dielectric barrier discharge plasma. *Appl Surf Sci* **420,** 873–881 (2017).

82. Gawarecka, A. & Wróblewska, A. Limonene oxidation over Ti-MCM-41 and Ti-MWW catalysts with t-butyl hydroperoxide as the oxidant. *React Kinet Mech Catal* **124** (2018).

83. Zítová, K., Vyskočilová, E. & Červený, L. Preparation of α-terpineol and perillyl alcohol using zeolites beta. *Res Chem Intermed* **47,** 4297–4310 (2021).

84. Thomas, A. & Bucher, W. Menthatrienes and the Oxidation of Limonene. *Helv Chim Acta* **53,** 770–775 (2004).

85. De Carvalho, C. C. C. R. & da Fonseca, M. M. R. Biotransformation of terpenes. *Biotechnol Adv* **24,** 134–142 (2006).

86. De Carvalho, C. C. C. R. & da Fonseca, M. M. R. Principal component analysis applied to bacterial cell behaviour in the presence of organic solvents. *Biocatal Biotransformation* **22,** 203–214. ISSN: 1024-2422 (2004).

87. Cornelissen, S., Liu, S., Deshmukh, A., Schmid, A. & Bühler, B. Cell physiology rather than enzyme kinetics can determine the efficiency of cytochrome P450-catalyzed C-H-oxyfunctionalization. *J ind microbiol biotechnol* **38,** 1359–1370 (2011).

88. Tai, Y.-N. *et al.* Optimisation of α-terpineol production by limonene biotransformation using Penicillium digitatum DSM 62840. *J Sci Food Agric* **96,** 954–961 (2016).

89. Duetz, W. A., Bouwmeester, H, van Beilen, J. B. & Witholt, B. Biotransformation of limonene by bacteria, fungi, yeasts, and plants. *Appl Microbiol Biotechnol* **61,** 269–277 (2003).

90. Van der Werf, M. J., Keijzer, P. M. & van der Schaft, P. H. Xanthobacter sp. C20 contains a novel bioconversion pathway for limonene. *J Biotechnol* **84,** 133–143 (2000).

91. Chatterjee, T & Bhattacharyya, D. Biotransformation of limonene by Pseudomonas putida. *Appl Microbiol Biotechnol* **55,** 541–546 (2001).

92. Menéndez, P., García-Carnelli, C., Rodríguez, P., Moyna, P. & Heinzen, H. Enzymatic systems involved in D-limonene biooxidation. *Braz Arch Biol Technol* **45** (2002).

93. Van Beilen, J. B. *et al.* Biocatalytic production of perillyl alcohol from limonene by using a novel Mycobacterium sp. cytochrome P450 alkane hydroxylase expressed in Pseudomonas putida. *Appl environ microbiol* **71,** 1737–1744 (2005).

94. Seifert, A., Antonovici, M., Hauer, B. & Pleiss, J. An Efficient Route to Selective Bio-oxidation Catalysts: an Iterative Approach Comprising Modeling, Diversification, and Screening, Based on CYP102A1. *ChemBioChem* **12,** 1346–1351 (2011).

95. *Protocol for Human 450 Metabolite Identification and Production* `www.sigmaaldrich.com/deepweb/assets/sigmaaldrich/product/documents/295/264/mtoxce1a2bul`. Sigma Aldrich, Oxford Biomedical Research. Accessed: 06.11.20.

96. Martinez, E., Das, S., Callewaert, D. & Subramanian, M. *A Novel, Robust Recombinant Human P450 Biocatalytic System* `www.sigmaaldrich.com/deepweb/assets/sigmaaldrich/marketing/global/documents/478/341/a-novel-robust-recombinant-human-p450-biocatalytic-system`. Oxford Biomedical Research. Accessed: 05.01.21.

97. Subramanian, M., Das, S., Martinez, E. & Callewaert, D. *Rapid identification and Production of Metabolites using CypExpress 2D6, 3A4 and 2C9* `www.sigmaaldrich.com/deepweb/assets/sigmaaldrich/marketing/global/documents/330/887/rapid-identification-and-production-of-metabolites-cypexpress`. Oxford Biomedical Research. Accessed: 15.03.22.

98. Poole, C. F. *Chapter 1 - General Concepts in Column Chromatography in The Essence of Chromatography.* 1–78. ISBN: 9780444501981 (Elsevier Science, 2003).

99. Mayer, S. & Schurig, V. Enantiomer Separation by Electrochromatography on Capillaries Coated with Chirasil-Dex. *J High Resolut Chromatogr* **15,** 129–131 (1992).

100. Trohjell, R. *Synthesis of 4-(2-(cyclopropylmethoxy)ethyl)phenol, a precursor for (S)-betaxolol* (Norwegian University of Science and Technology, 2021).

101. Anslyn, E. V., Dougherty, D. A. & Dougherty, E. V. *Modern Physical Organic Chemistry* ISBN: 9781891389313 (University Science Books, 2006).

102. Silverstein, R. M., Webster, F. X., Kiemle, D. J. & L, B. D. *Spectrometric Identification of Organic Compounds* 8th ed. ISBN: 9780470616376 (John Wiley and Sons, 2015).

103. Prosenko, A. E. *et al.* Interaction of functionally-substituted 4-alkyl-2,6-di-tert-butylphenols with hydrohalic acids. *Russ Chem Bull* **56,** 1119–1124 (2007).

104. Tennfjord, A. L. *Synthesis of enantiopure β-blocker (S)-esmolol* (Norwegian University of Science and Technology, 2021).

105. Lund, I. T., Bøckmann, P. L. & Jacobsen, E. E. Highly enantioselective CALB-catalyzed kinetic resolution of building blocks for β-blocker atenolol. *Tetrahedron* **72,** 7288–7292 (2016).

106. Hansen, M. B. *Improved understanding of reagents used in the syntheses of enantiopure precursors for (S)-atenolol and (S)- metoprolol* (Norwegian University of Science and Technology, 2019).

107. Reichardt, C. *Solvents and Solvent Effects in Organic Chemistry. Appendix A. Properties, Purification, and Use of Organic Solvents* ISBN: 9783527605675 (Wiley, 2006).

108. Khuong, H. International patent WO 87/03584 (1985).

109. Næss, S. B. *A study on the Cytochrome P450 catalyzed production of (S)-perillyl alcohol from (S)-limonene* (Norwegian University of Science and Technology, 2020).

110. Berg, E. *Biokatalytisk oksidasjon av limonen* (Norwegian University of Science and Technology, 2020).

111. Kadam, S. T. & Kim, S. S. Phosphomolybdic Acid: Mild and Efficient Catalyst for Acetylation of Alcohols, Phenols, and Amines under Solvent-Free Conditions. *Synthesis* **2008,** 267–271 (2008).

112. Gonçalves, J. A. & Gusevskaya, E. V. Palladium catalyzed oxidation of monoterpenes: multistep electron transfer catalytic systems $Pd(OAc)_2$/benzoquinone/$M(OAc)_2$ (M=Cu, Co or Mn) for the allylic oxidation of limonene with dioxygen. *Appl Catal A: Gen* **258,** 93–98 (2004).

113. Rumble, J. R. *"Physical Constants of Organic Compounds" in CRC Handbook of Chemistry and Physics,* 102nd ed. (CRC Press Taylor and Francis, 2021).

114. Parczewski, A. Essential oils of native plants from the family Umbelliferae. II. The essential oil of Sium latifolium fruits. *Dissertationes Pharmaceuticae* **12,** 223.

115. *"PhysProp" data were obtained from Syracuse Research Corporation of Syracuse, New York (US)* `https://scifinder-n.cas.org`. Accessed: 23.03.2022.

116. *Calculated using Advanced Chemistry Development Labs Software V11.02* `https://scifinder-n.cas.org`. Accessed: 23.03.2022.

117. Horrillo-Martínez, P., Virolleaud, M.-A. & Jaekel, C. Selective Palladium-Catalyzed Dehydrogenation of Limonene to Dimethylstyrene. *ChemCatChem* **2,** 175–181 (2010).

118. Lenz, R. W., Sutherland, J. E. & Westfelt, L. C. Cationic polymerization of p-substituted α-methylstyrenes, 2. Crystalline polymers from p-methyl- and p-isopropyl-α-methylstyrene. *Die Makromolekulare Chemie* **177,** 653–662 (1976).

119. Miyazawa, M., Shindo, M. & Shimada, T. Metabolism of (+)- and (-)-Limonenes to Respective Carveols and Perillyl Alcohols by CYP2C9 and CYP2C19 in Human Liver Microsomes. *Drug Metab Dispos* **30,** 602–607 (2002).

120. Fliszár-Nyúl, E., Mohos, V., Csepregi, R., Mladěnka, P. & Poór, M. Inhibitory effects of polyphenols and their colonic metabolites on CYP2D6 enzyme using two different substrates. *Biomed Pharmacother* **131,** 110732 (2020).

121. Martinez, E., Das, S., Callewaert, D. & Subramanian, M. *CypExpress 2C19 Catalyzed Conversion of Mephenytoin (MP) to 4-Hydroxymephenytoin (HMP)* `www.sigmaaldrich.com/deepweb/assets/sigmaaldrich/product/documents/992/114/mtoxce2c19pis`. Oxford Biomedical Research. Accessed: 05.11.21.

122. El-Dalatony, M. M., Saha, S., Govindwar, S. P., Abou-Shanab, R. A. I. & Jeon, B.-H. Biological Conversion of Amino Acids to Higher Alcohols. *TrendsBiotechnol* **37,** 855–869 (2019).

A Analysis of compounds in the pathway to (*S*)-betaxolol (10)

A.1 Characterization of 4-(2-(cyclopropylmethoxy)ethyl)phenol (2)

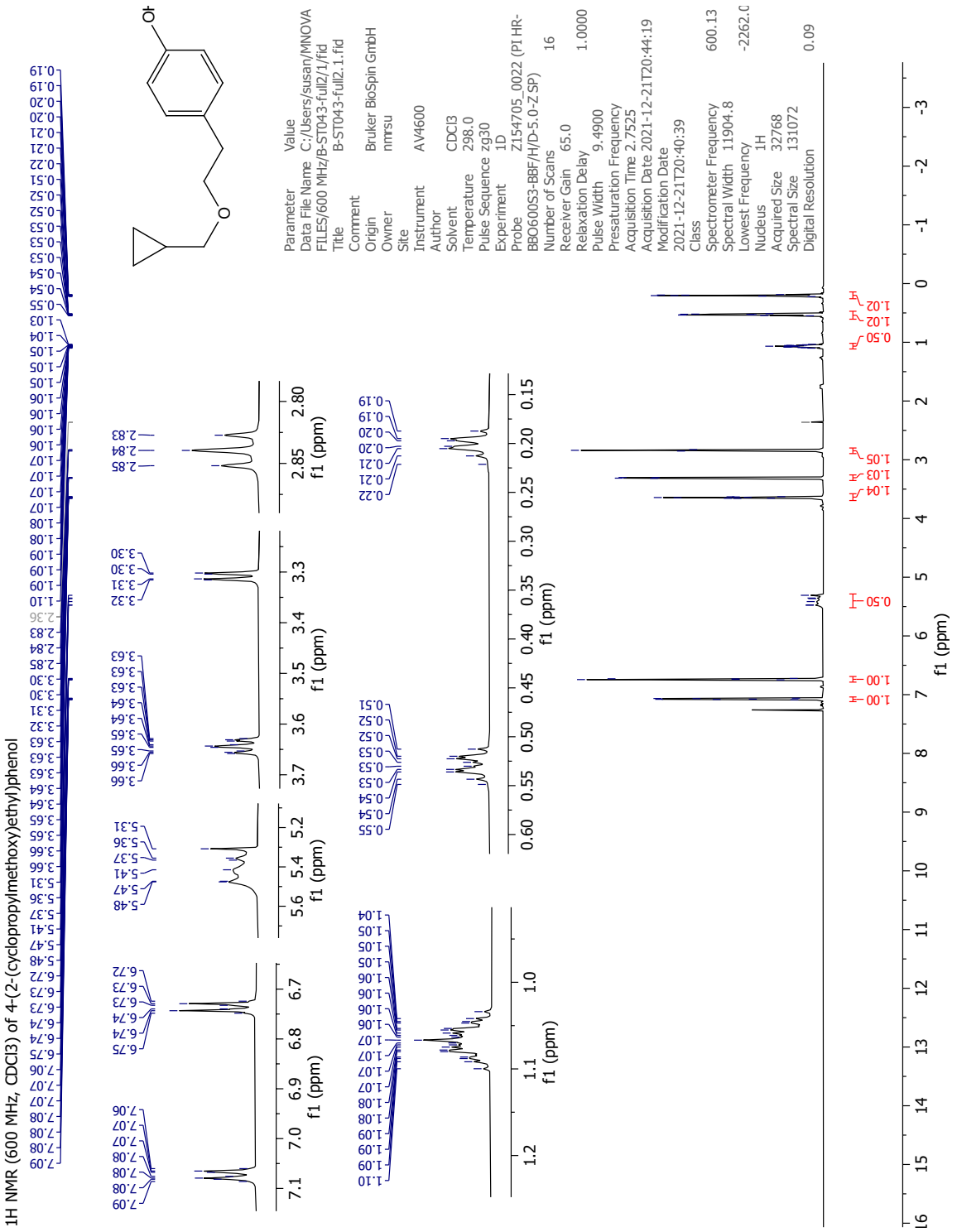

Figure A.1 ^{1}H NMR spectrum (600 MHz, $CDCl_3$) of 4-(2-(cyclopropylmethoxy)ethyl)phenol (**2**).

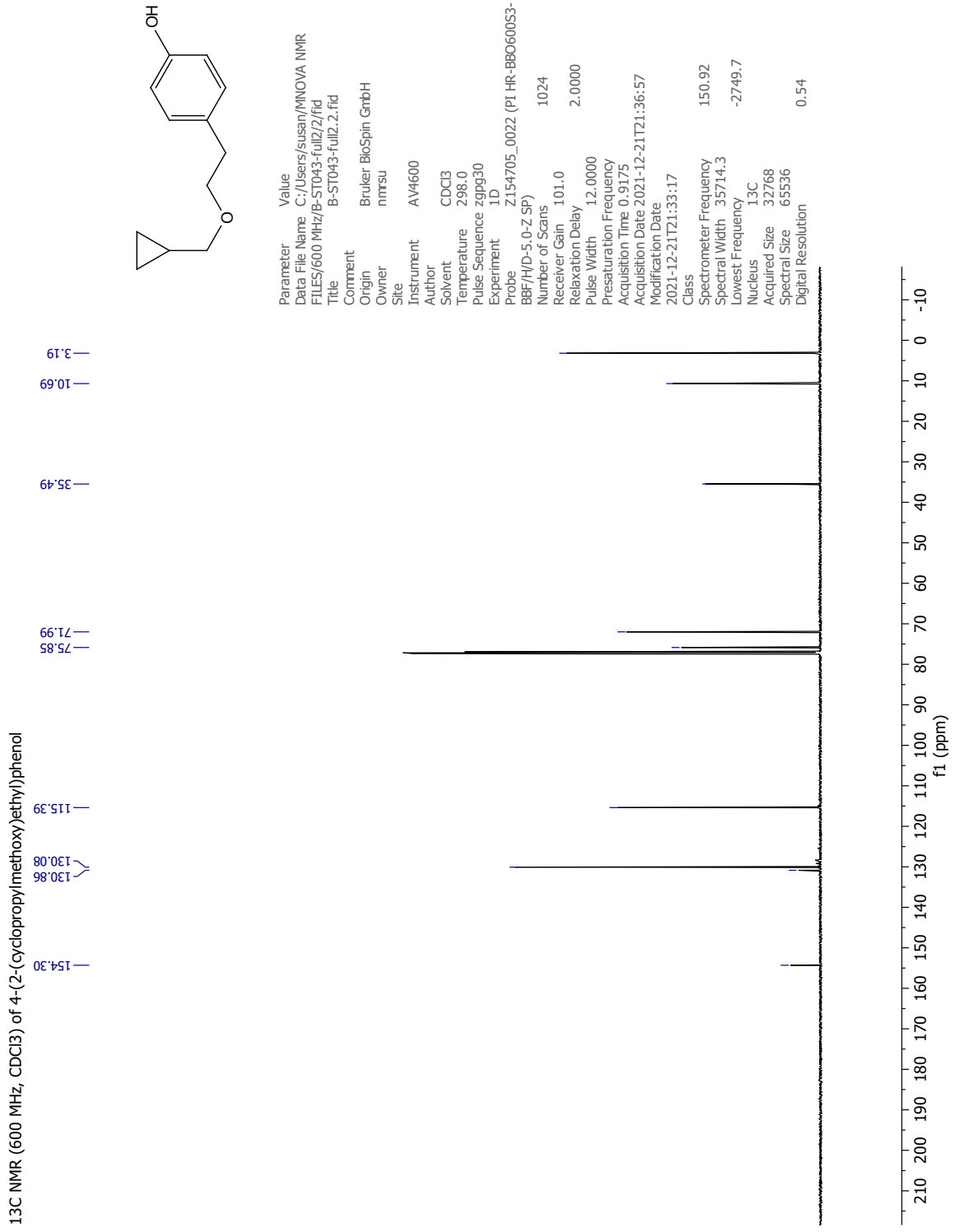

Figure A.2 ^{13}C NMR spectrum (150 MHz, $CDCl_3$) of 4-(2-(cyclopropylmethoxy)ethyl)phenol (**2**).

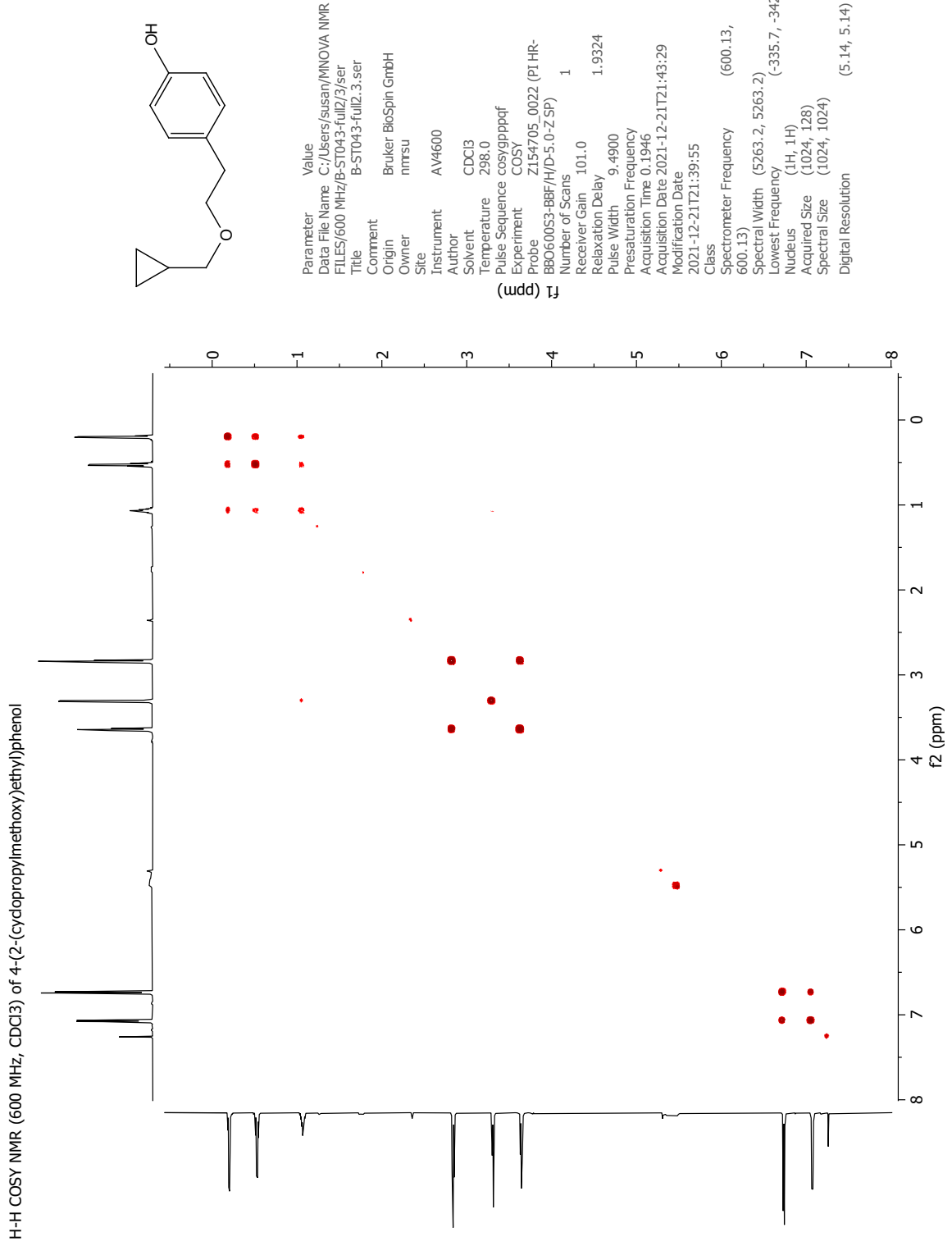

Figure A.3 COSY NMR spectrum (600 MHz, $CDCl_3$) of 4-(2-(cyclopropylmethoxy)ethyl)-phenol (**2**).

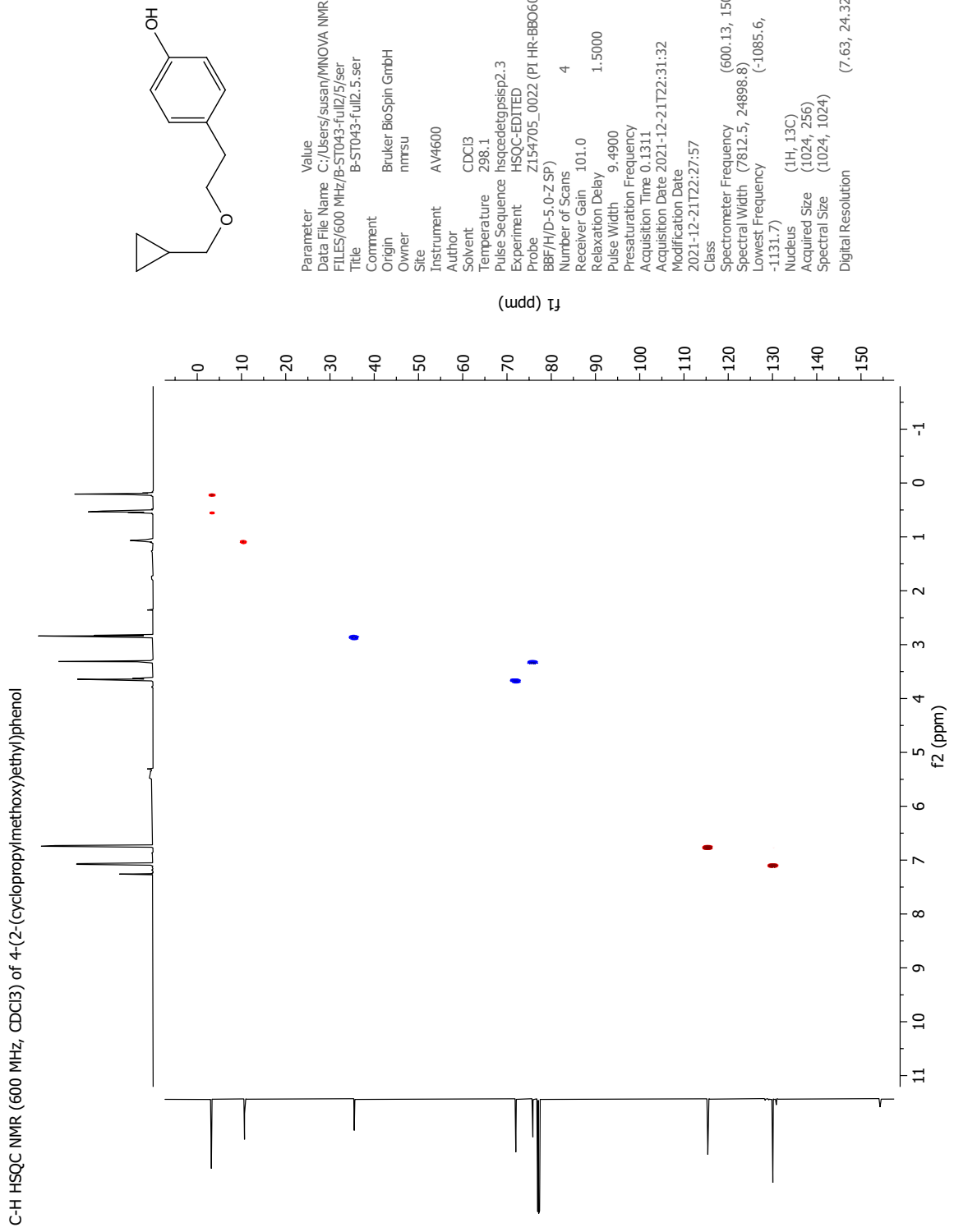

Figure A.4 HSQC NMR spectrum (600 MHz, $CDCl_3$) of 4-(2-(cyclopropylmethoxy)ethyl)-phenol (**2**).

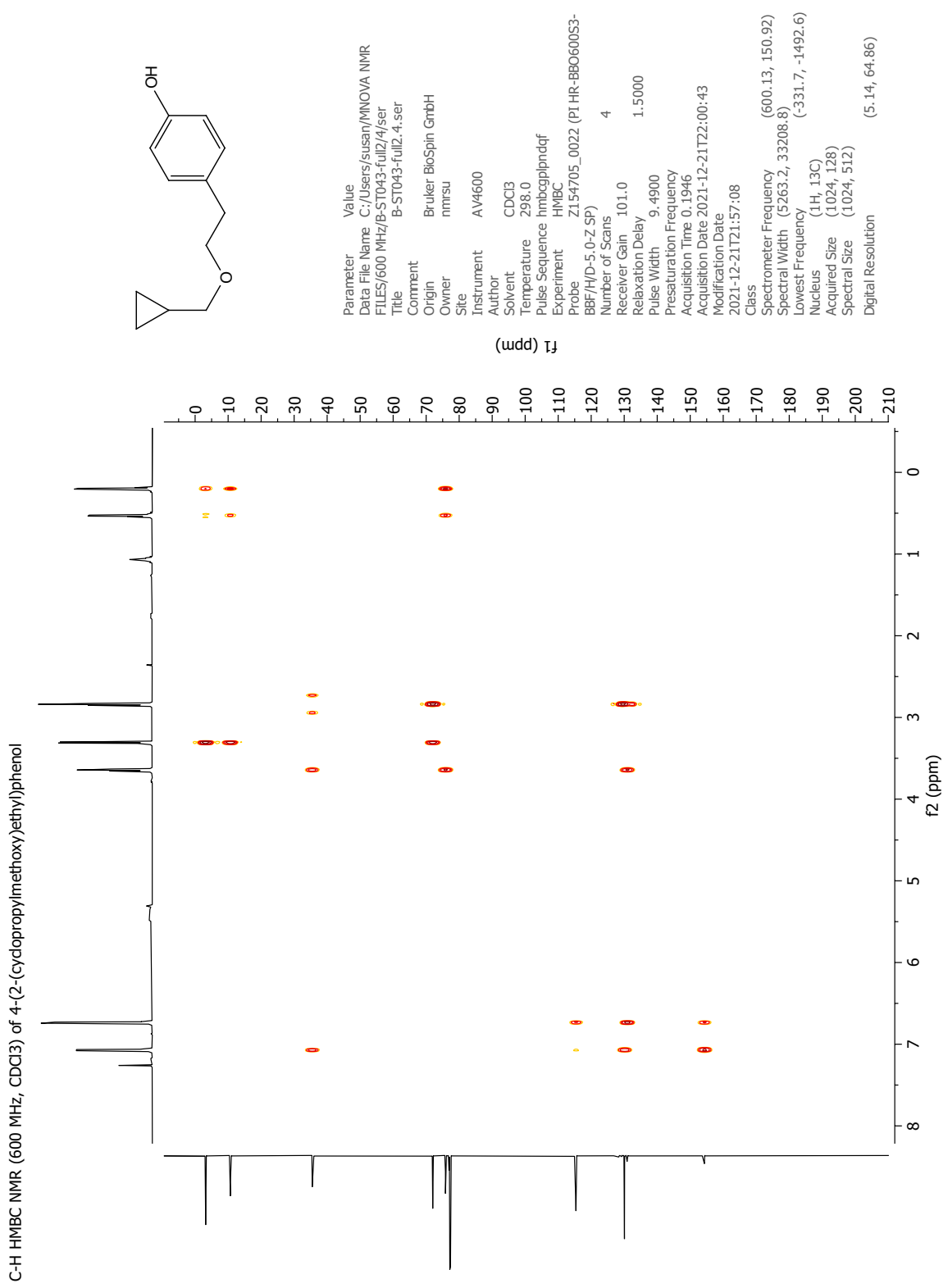

Figure A.5 HMBC NMR spectrum (600 MHz, $CDCl_3$) of 4-(2-(cyclopropylmethoxy)ethyl)-phenol (**2**).

A.2 Characterization of 2-(4-((perfluoropyridin-4-yl)oxy)phenyl)ethan-1-ol (3)

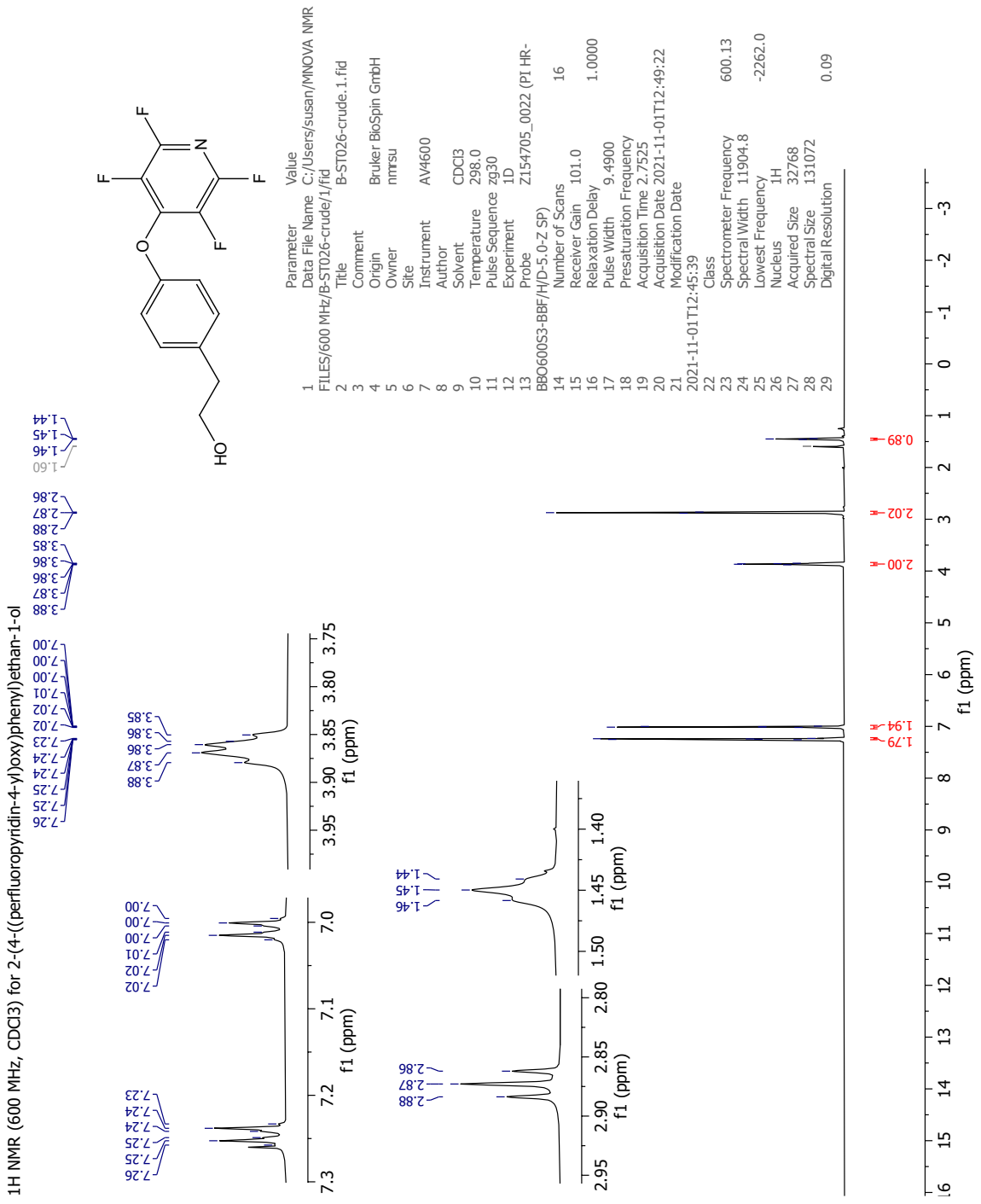

Figure A.6 ^{1}H NMR spectrum (600 MHz, $CDCl_3$) of 2-(4-((perfluoropyridin-4-yl)oxy)phenyl)ethan-1-ol (**3**). δ= 1.60 is water from the solvent.

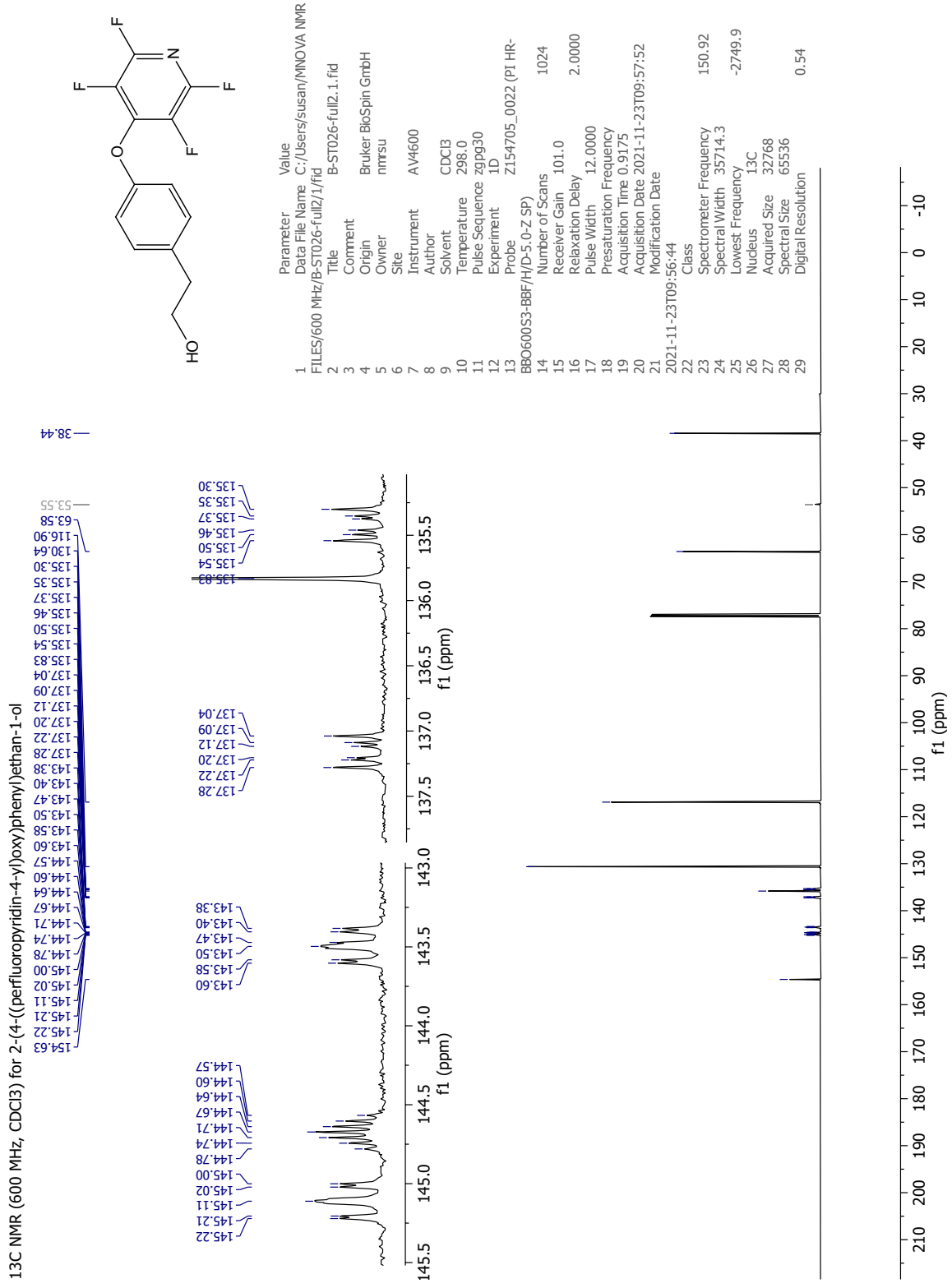

Figure A.7 ^{13}C NMR spectrum (150 MHz, $CDCl_3$) of 2-(4-((perfluoropyridin-4-yl)oxy)phenyl)ethan-1-ol (**3**). δ= 53.55 is resiudes of CH_2Cl_2.

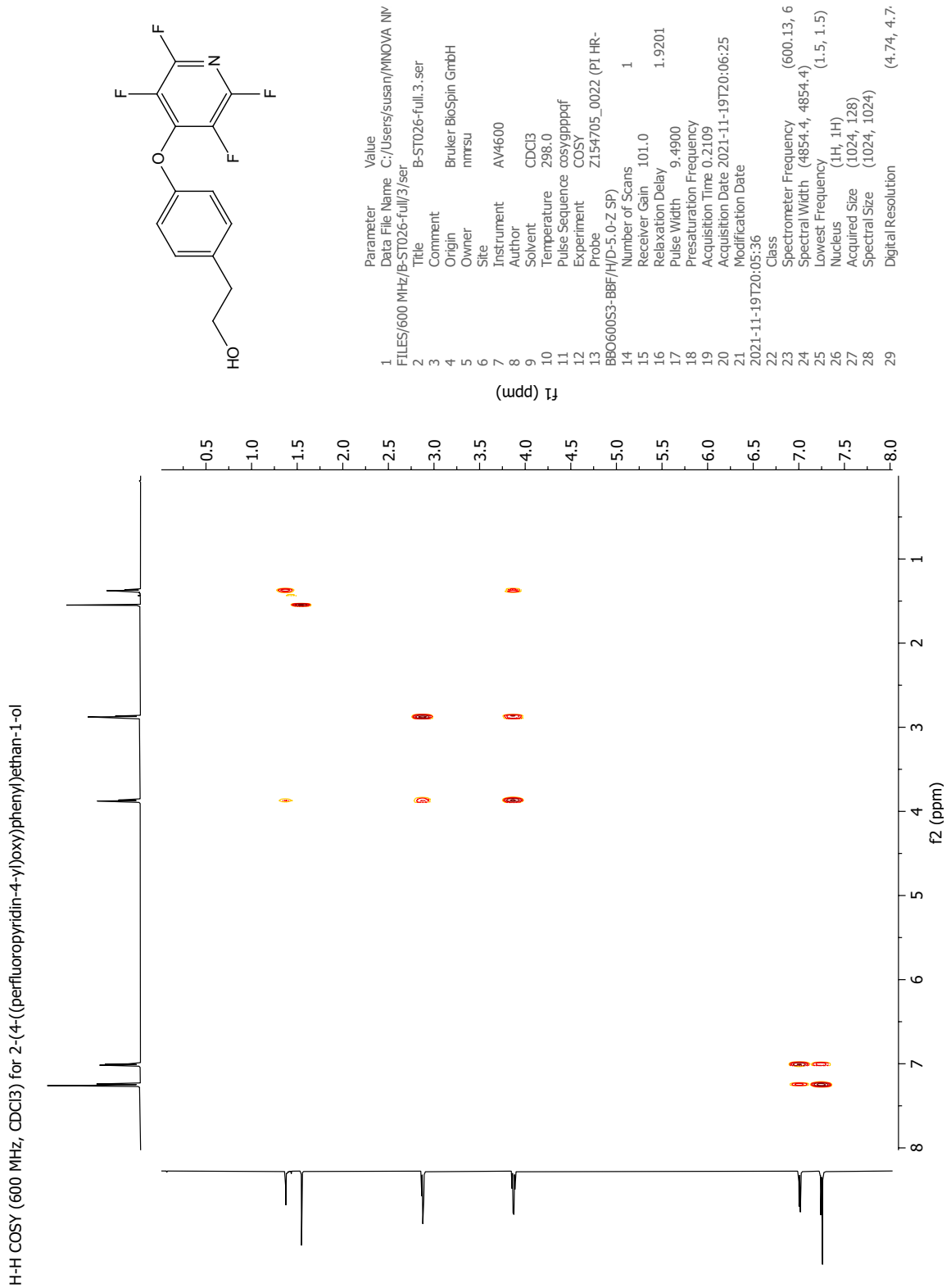

Figure A.8 COSY NMR spectrum (600 MHz, $CDCl_3$) of 2-(4-((perfluoropyridin-4-yl)oxy)phenyl)ethan-1-ol (**3**).

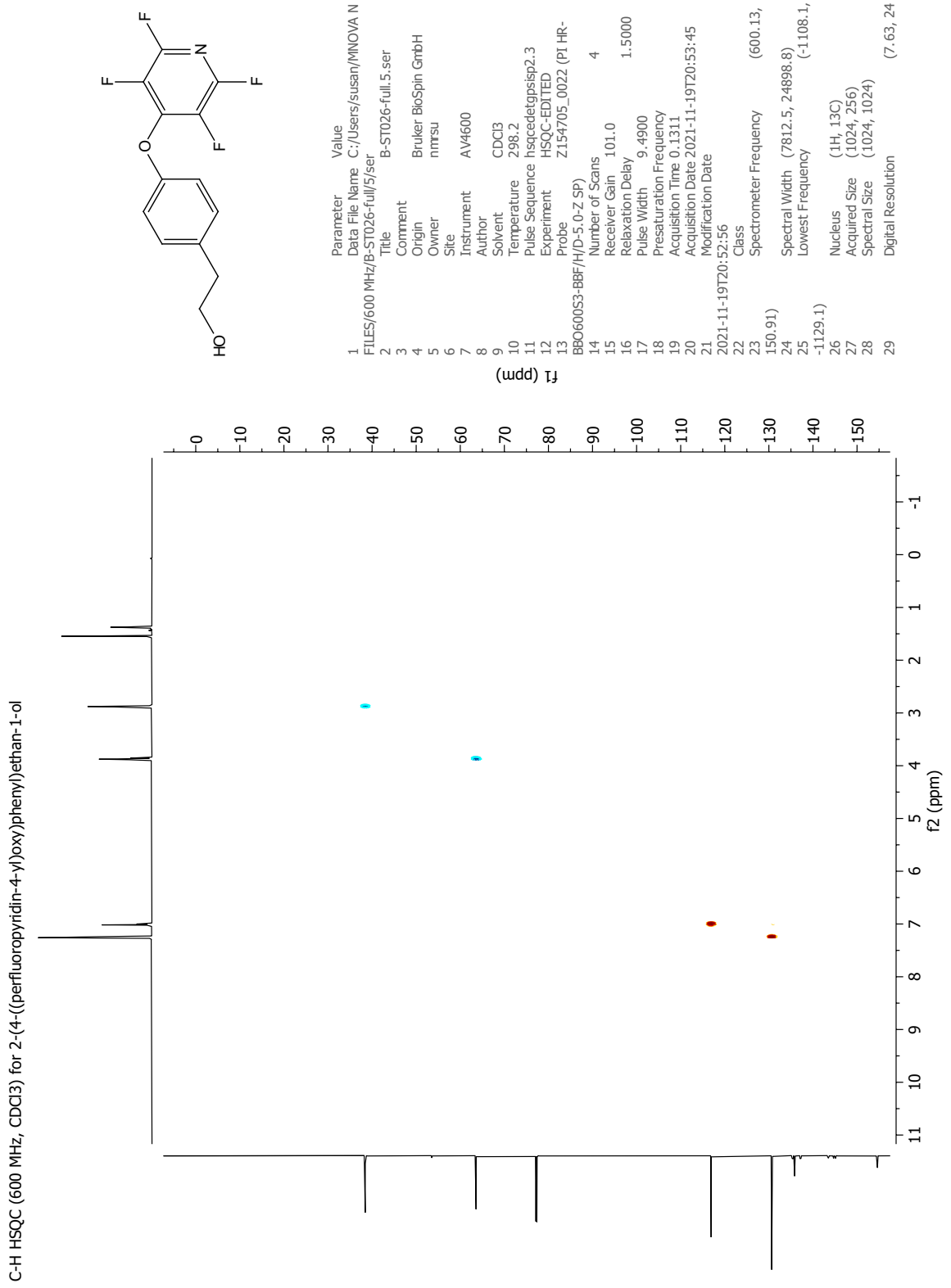

Figure A.9 HSQC NMR spectrum (600 MHz, $CDCl_3$) of 2-(4-((perfluoropyridin-4-yl)oxy)phenyl)ethan-1-ol (**3**).

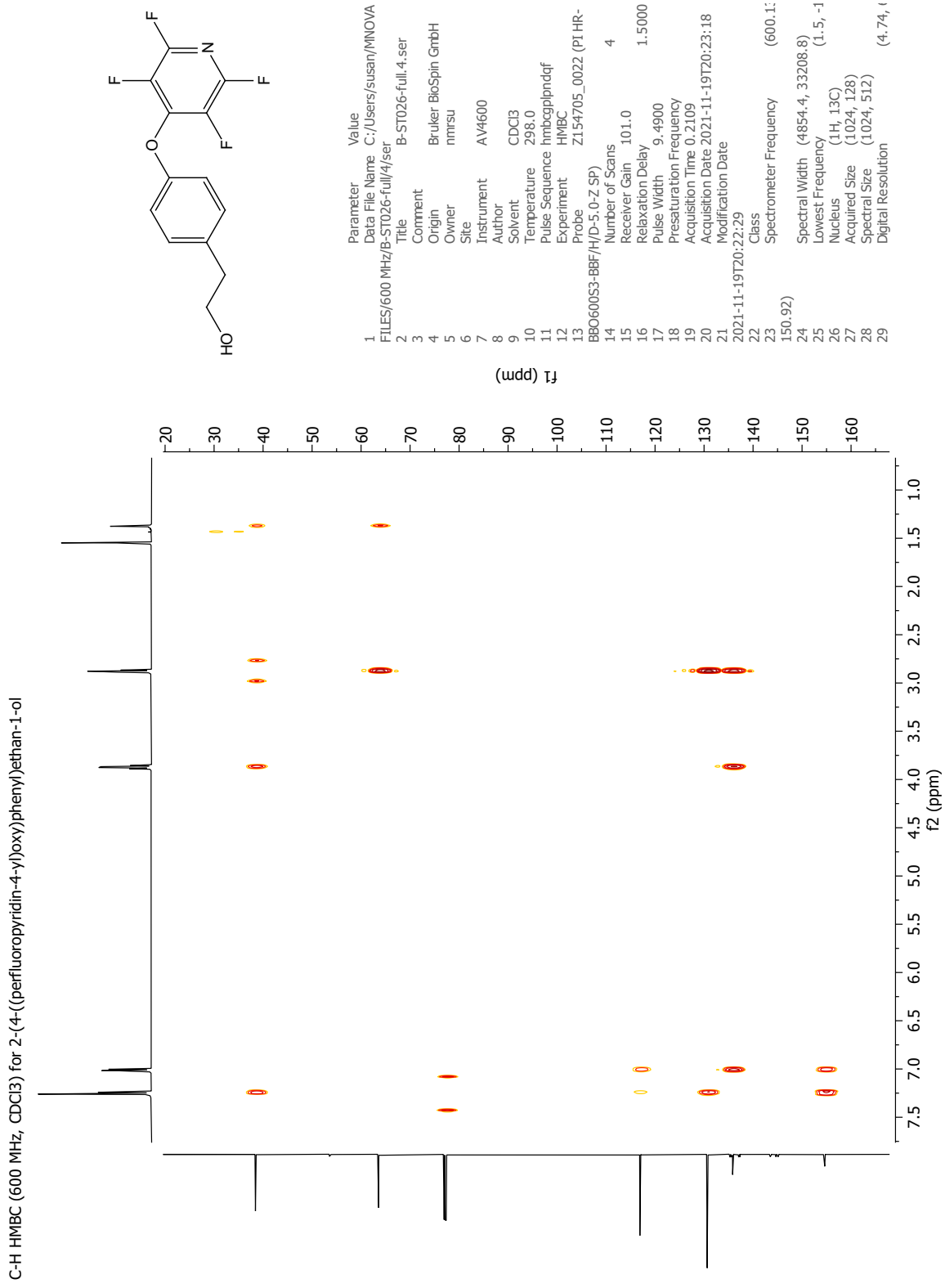

Figure A.10 HMBC NMR spectrum (600 MHz, $CDCl_3$) of 2-(4-((perfluoropyridin-4-yl)oxy)phe-nyl)ethan-1-ol (**3**).

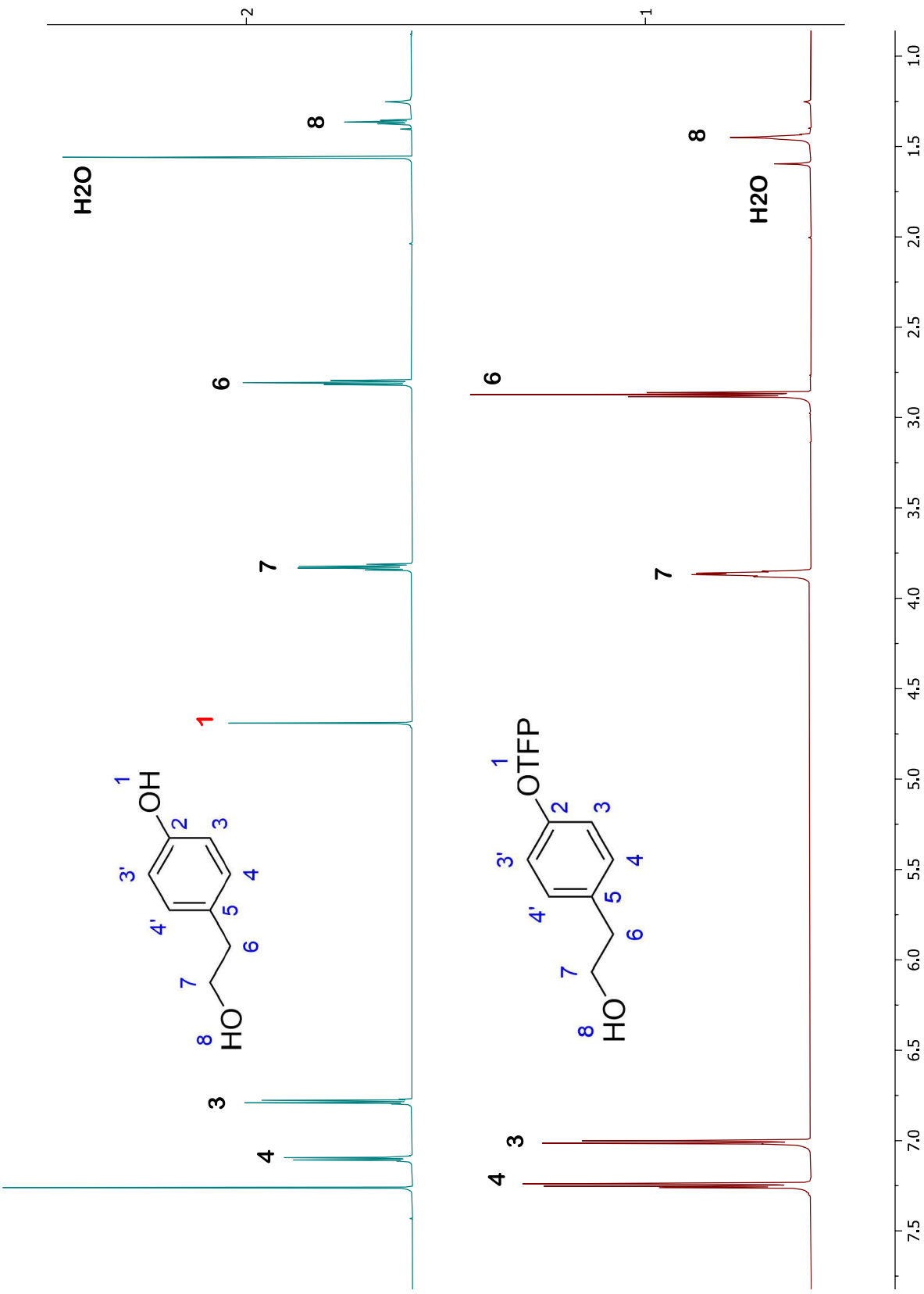

Figure A.11 Comparison of ^{1}H NMR spectra (600 MHz, $CDCl_3$) of 2-(4-((perfluoropyridin-4-yl)oxy)phe-nyl)ethan-1-ol (**3**) and the starting material (**1**). The starting material has a large water peak from storage.

A.3 Characterization of 4-(4-(2-chloroethyl)phenoxy)-2,3,5,6-tetrafluoropyridine (4)

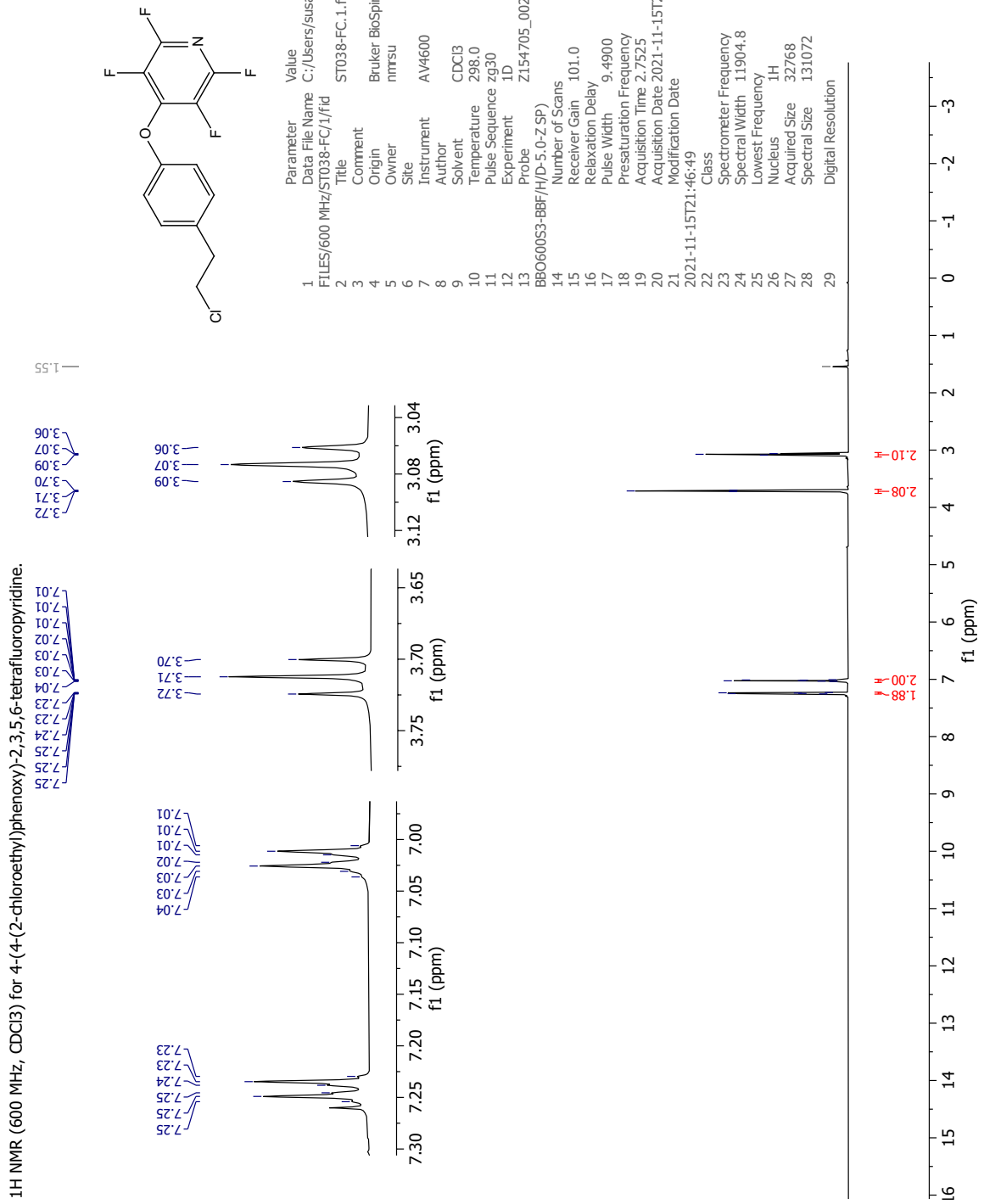

Figure A.12 ^{1}H NMR spectrum (600 MHz, $CDCl_3$) of 4-(4-(2-chloroethyl)phenoxy)-2,3,5,6-tetrafluoropyridine (**4**)

A.4 NMR analysis of attempted alkylations of 2-(4-((perfluoro-pyridin-4-yl)oxy)phenyl)ethan-1-ol (3)

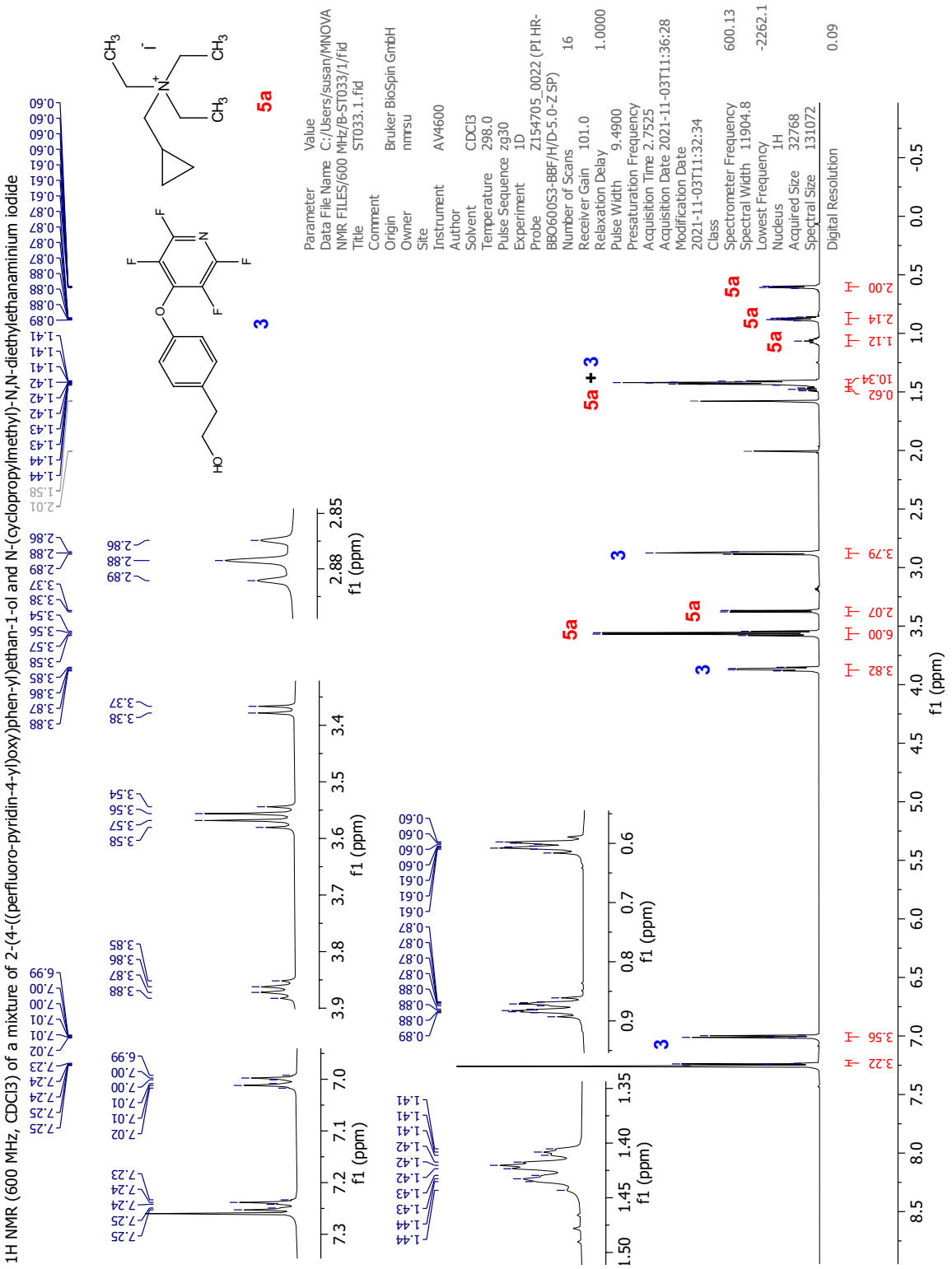

Figure A.13 ^{1}H NMR spectrum (600 MHz, $CDCl_3$) of a mixture of 2-(4-((perfluoro-pyridin-4-yl)oxy)phen-yl)ethan-1-ol (**3**) and *N*-(cyclopropylmethyl)-*N*,*N*-diethylethanaminium iodide (**5a**). δ = 2.01 is MeCN, and δ = 1.58 is water.

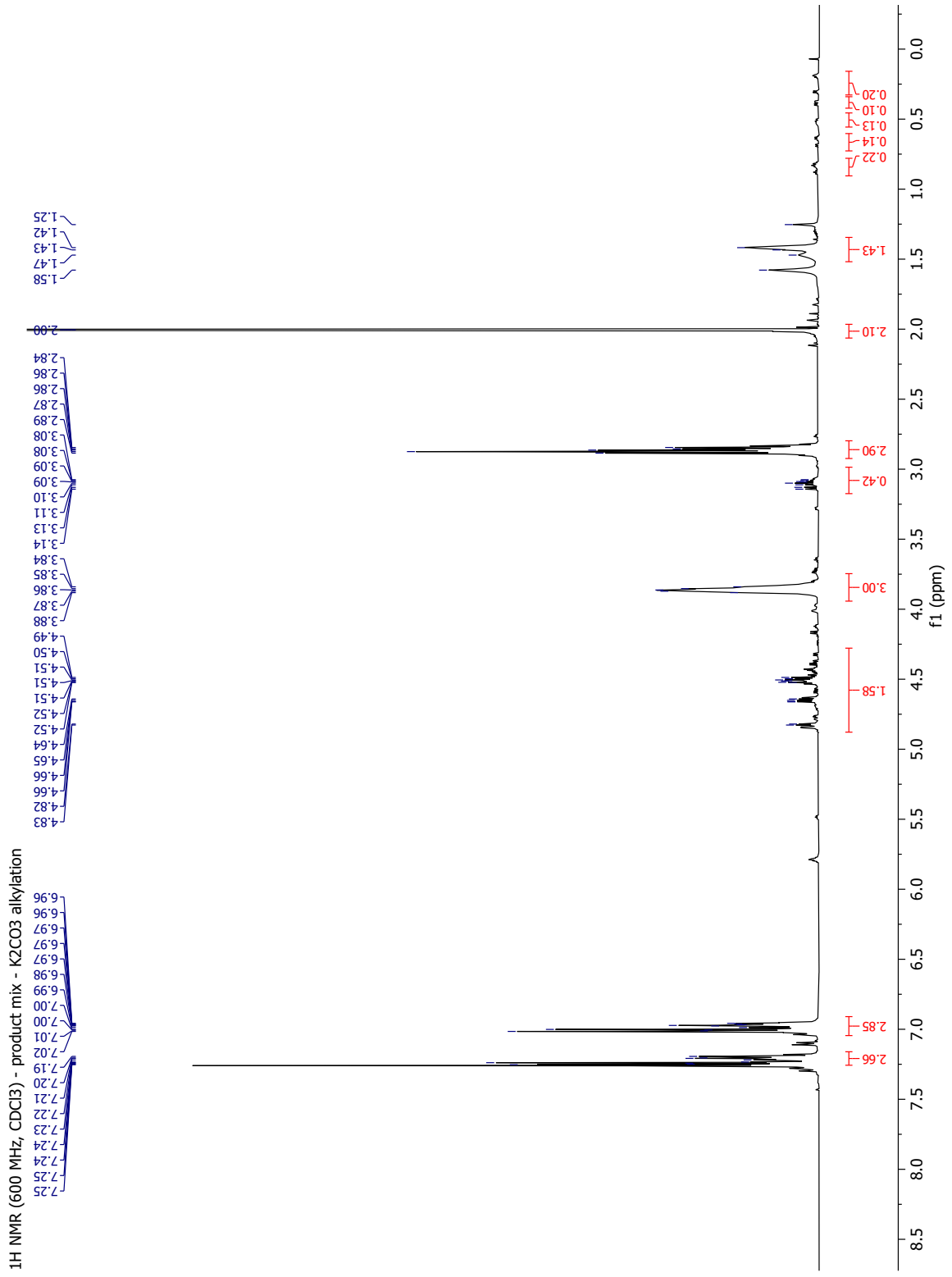

Figure A.14 ^{1}H NMR spectrum (600 MHz, $CDCl_3$) corresponding to entry 2 in Table 2.3.

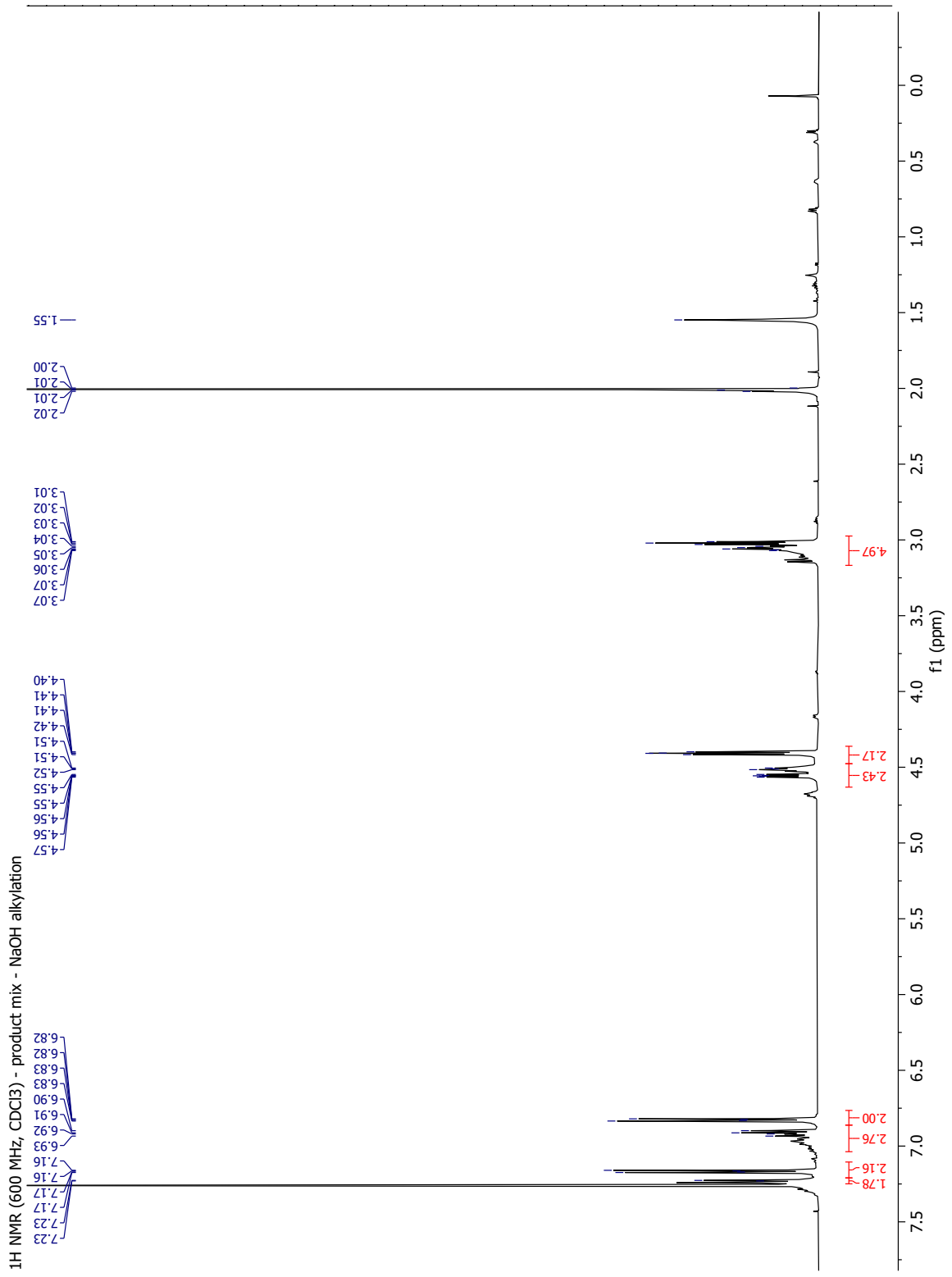

Figure A.15 ^{1}H NMR spectrum (600 MHz, $CDCl_3$) corresponding to entry 3 in Table 2.3.

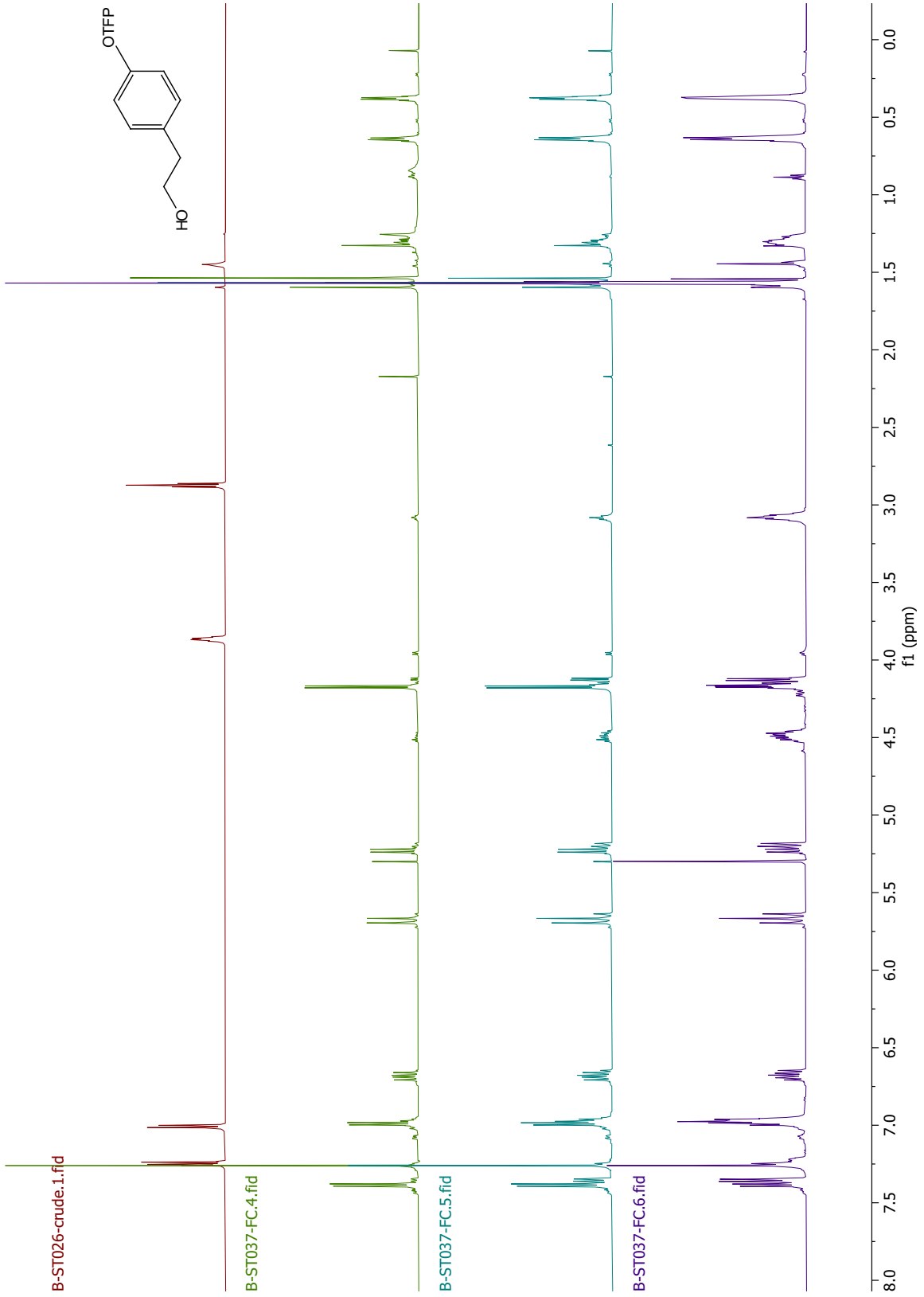

Figure A.16 ^{1}H NMR spectra (600 MHz, $CDCl_3$) corresponding to entry 4 in Table 2.3. Top spectrum: **3**. The rest are three fractions from flash chromatography.

A.5 Characterization of 2-((4-(2-(cyclopropylmethoxy)ethyl)phenoxy)methyl)oxirane (6)

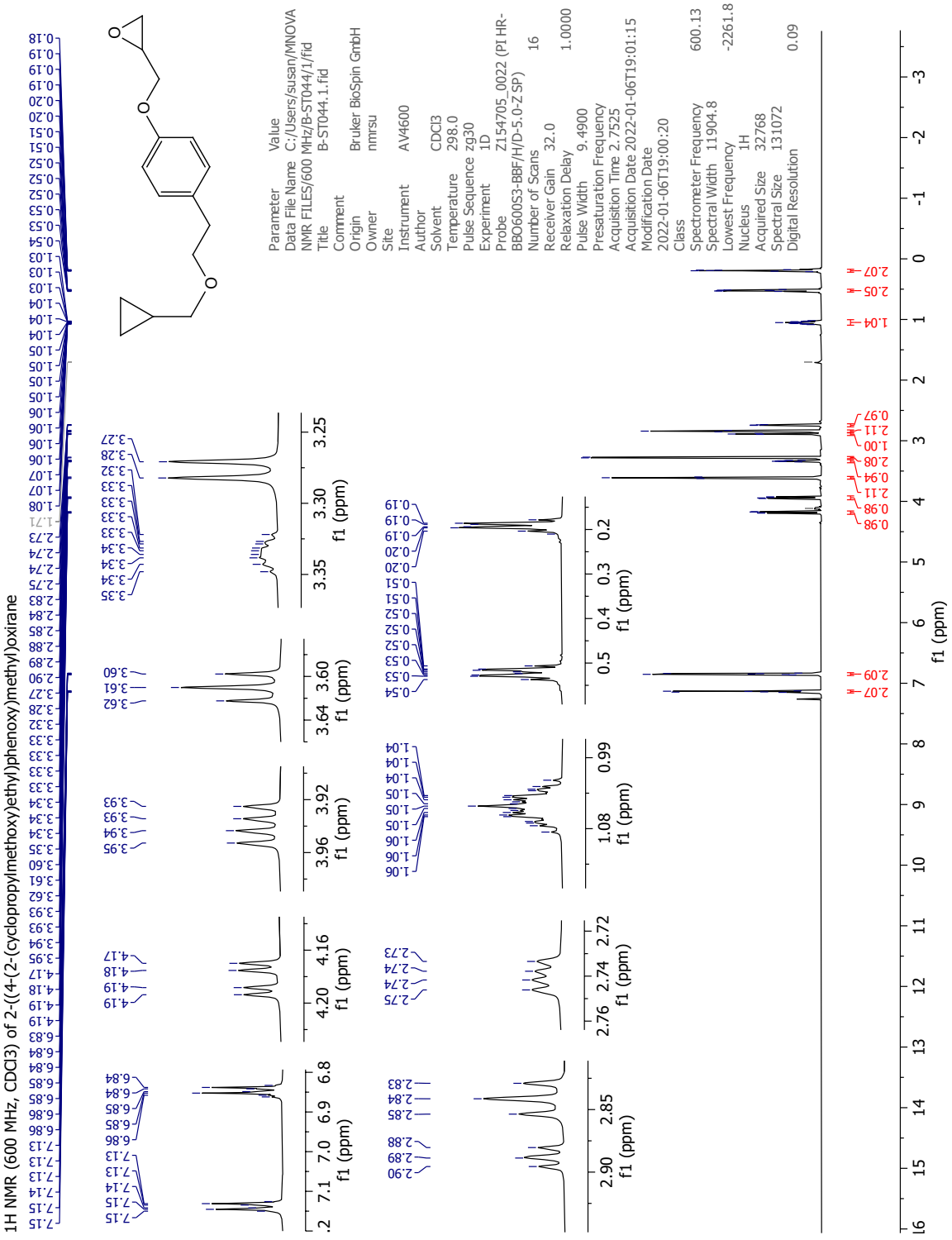

Figure A.17 ^{1}H NMR spectrum (600 MHz, $CDCl_3$) of 2-((4-(2-(cyclopropylmethoxy)ethyl)phenoxy)methyl)oxirane (**6**). δ= 1.71 is water from the solvent, and δ= 4.12 is trace EtOAc.

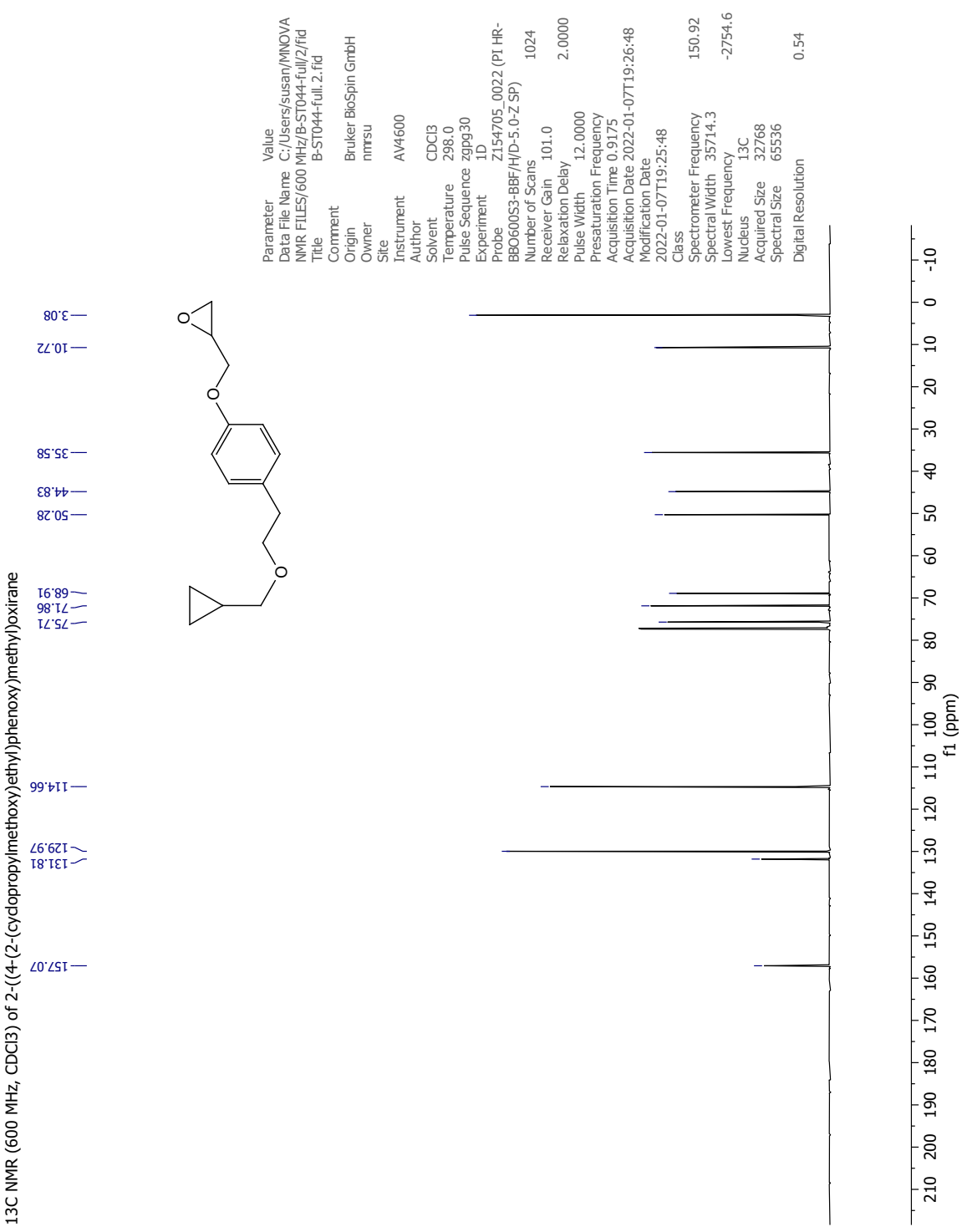

Figure A.18 ^{13}C NMR spectrum (150 MHz, $CDCl_3$) of 2-((4-(2-(cyclopropylmethoxy)-ethyl)phenoxy)methyl)oxirane (**6**).

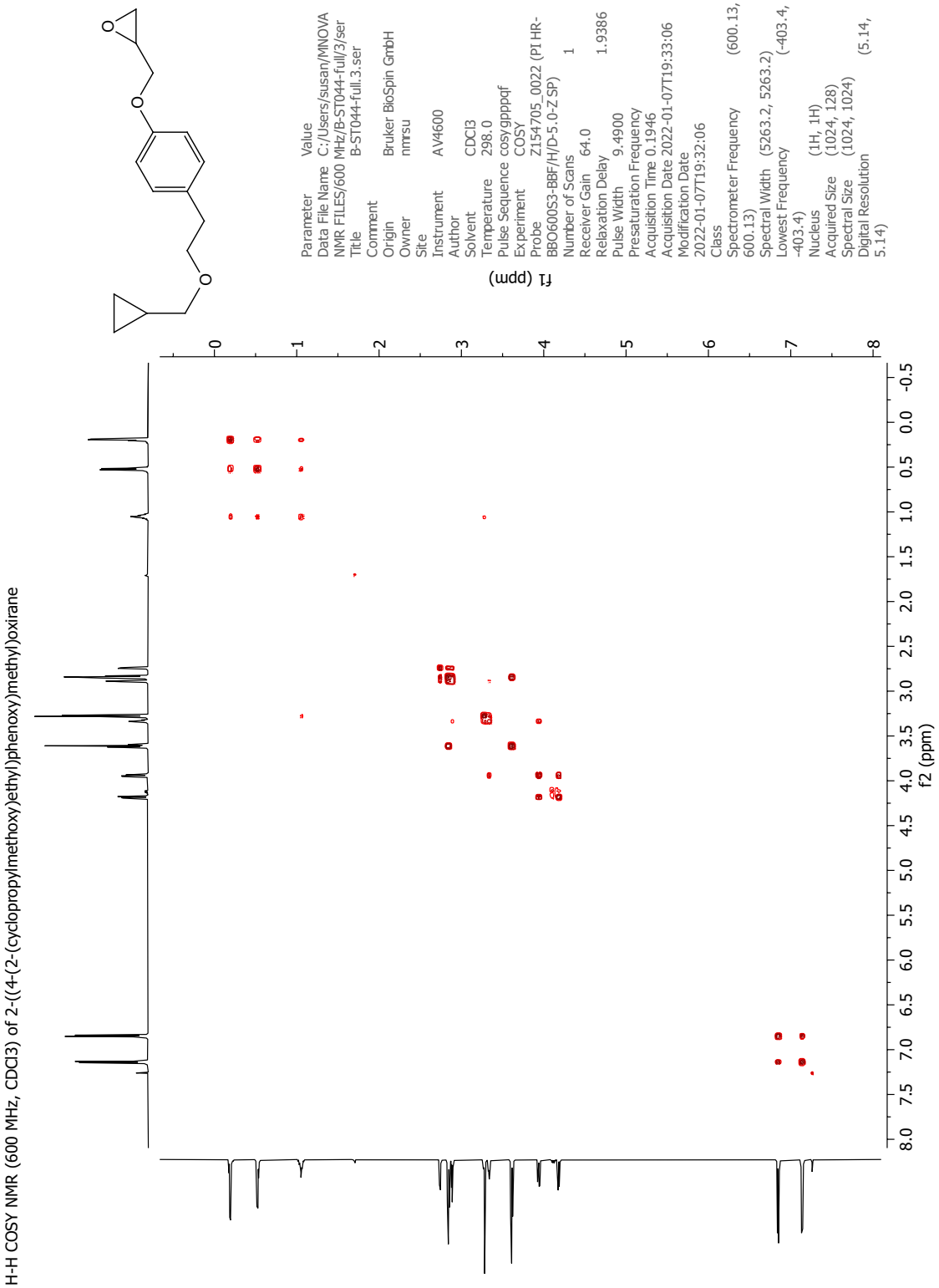

Figure A.19 COSY NMR spectrum (600 MHz, $CDCl_3$) of 2-((4-(2-(cyclopropylmethoxy)-ethyl)phenoxy)methyl)oxirane (**6**).

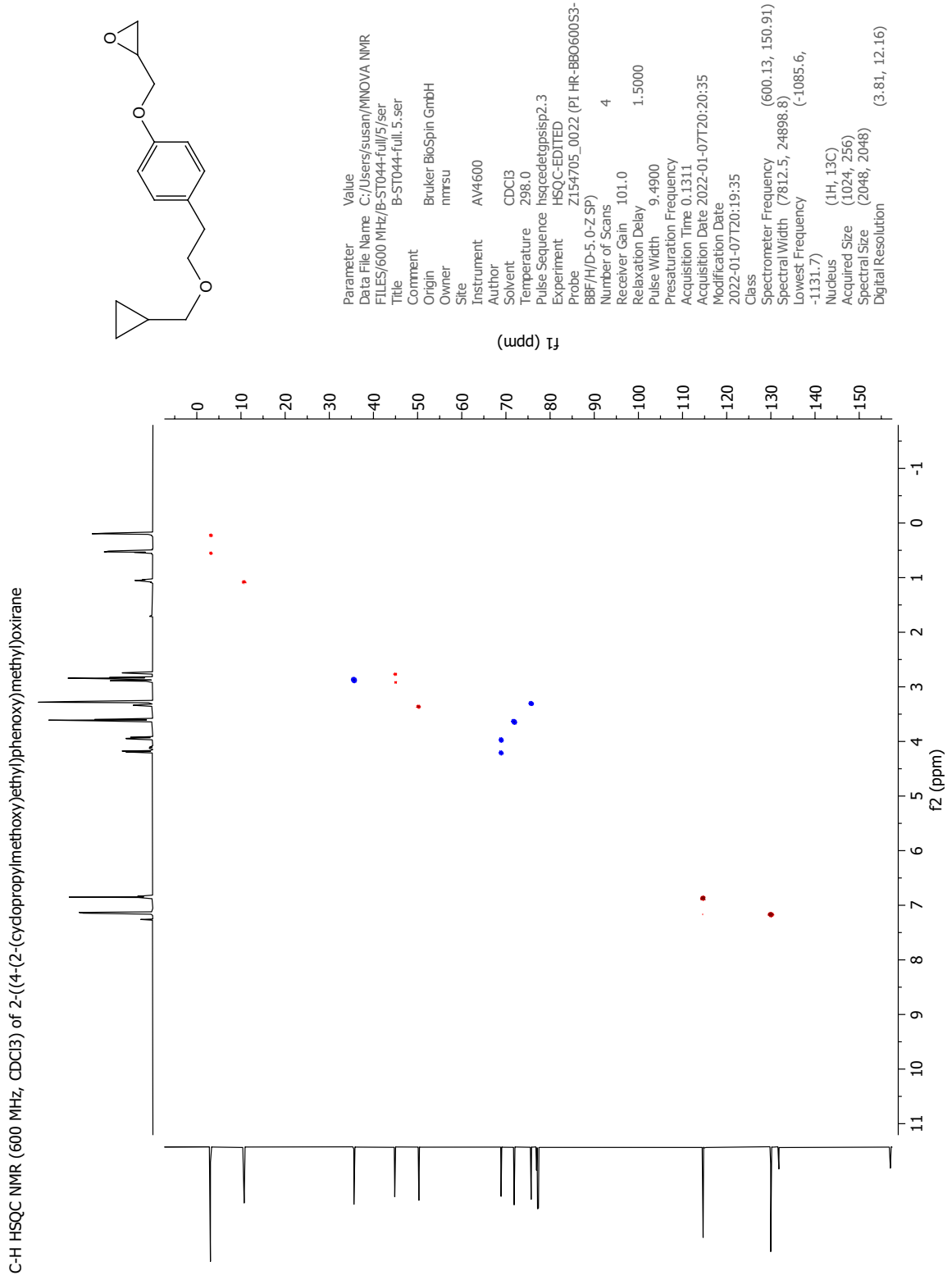

Figure A.20 HSQC NMR spectrum (600 MHz, $CDCl_3$) of 2-((4-(2-(cyclopropylmethoxy)-ethyl)phenoxy)methyl)oxirane (**6**).

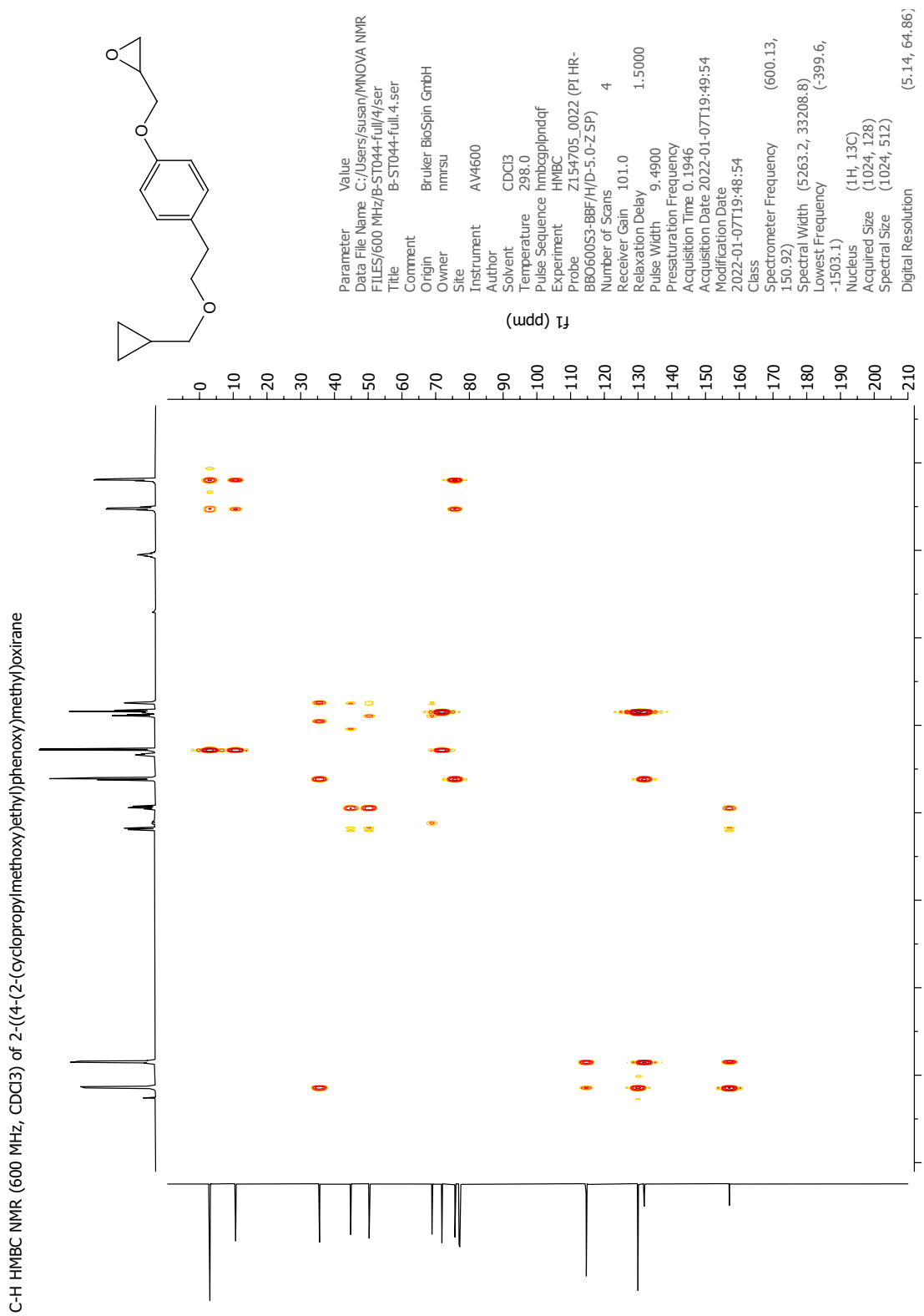

Figure A.21 HMBC NMR spectrum (600 MHz, $CDCl_3$) of 2-((4-(2-(cyclopropylmethoxy)-ethyl)phenoxy)methyl)oxirane (**6**).

A.6 Characterization of 2-(4-(oxiran-2-ylmethoxy)phenyl)ethan-1-ol (7)

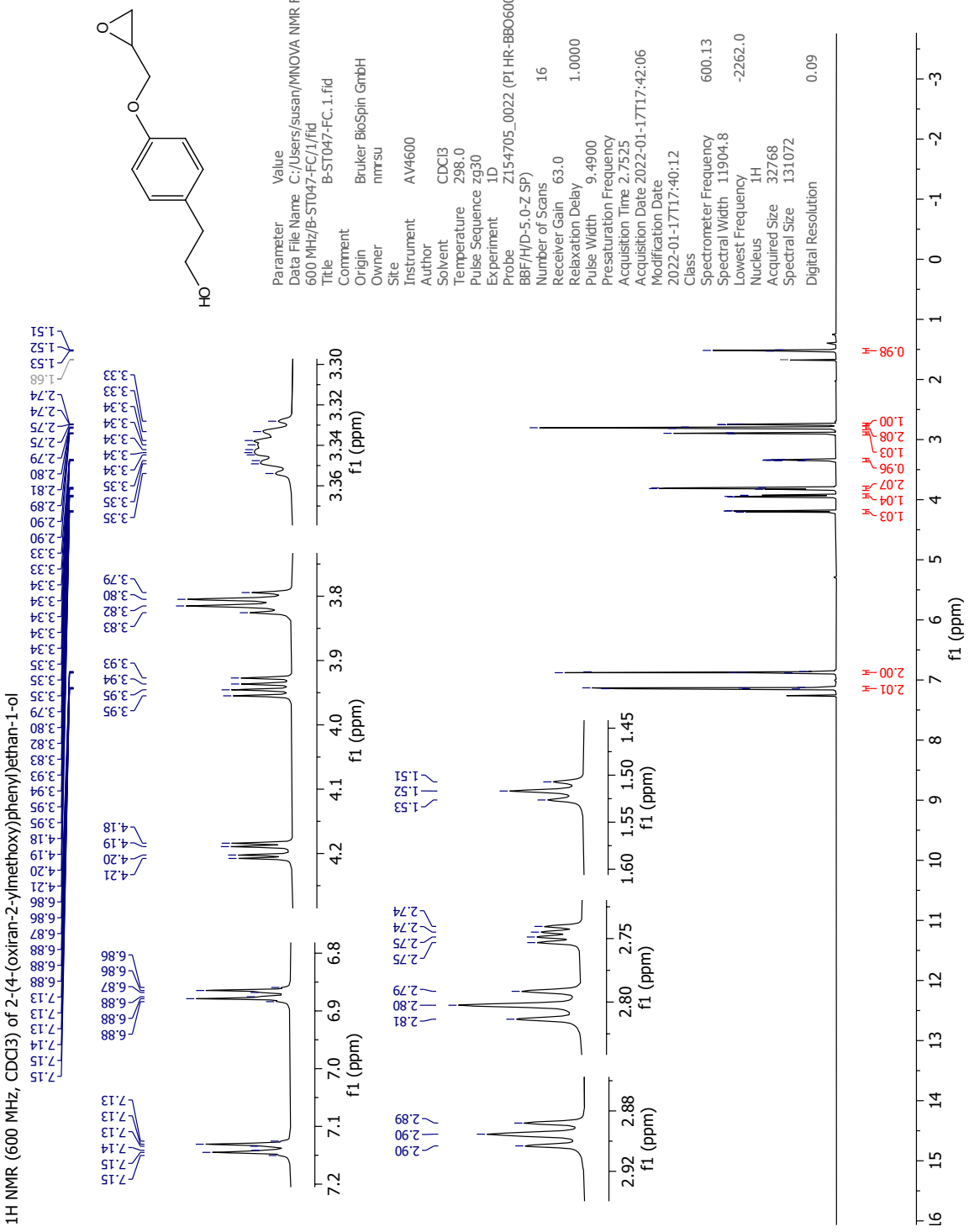

Figure A.22 ^{1}H NMR spectrum (600 MHz, $CDCl_3$) of 2-(4-(oxiran-2-ylmethoxy)phenyl)ethan-1-ol (**7**). δ= 1.68 is water from the solvent.

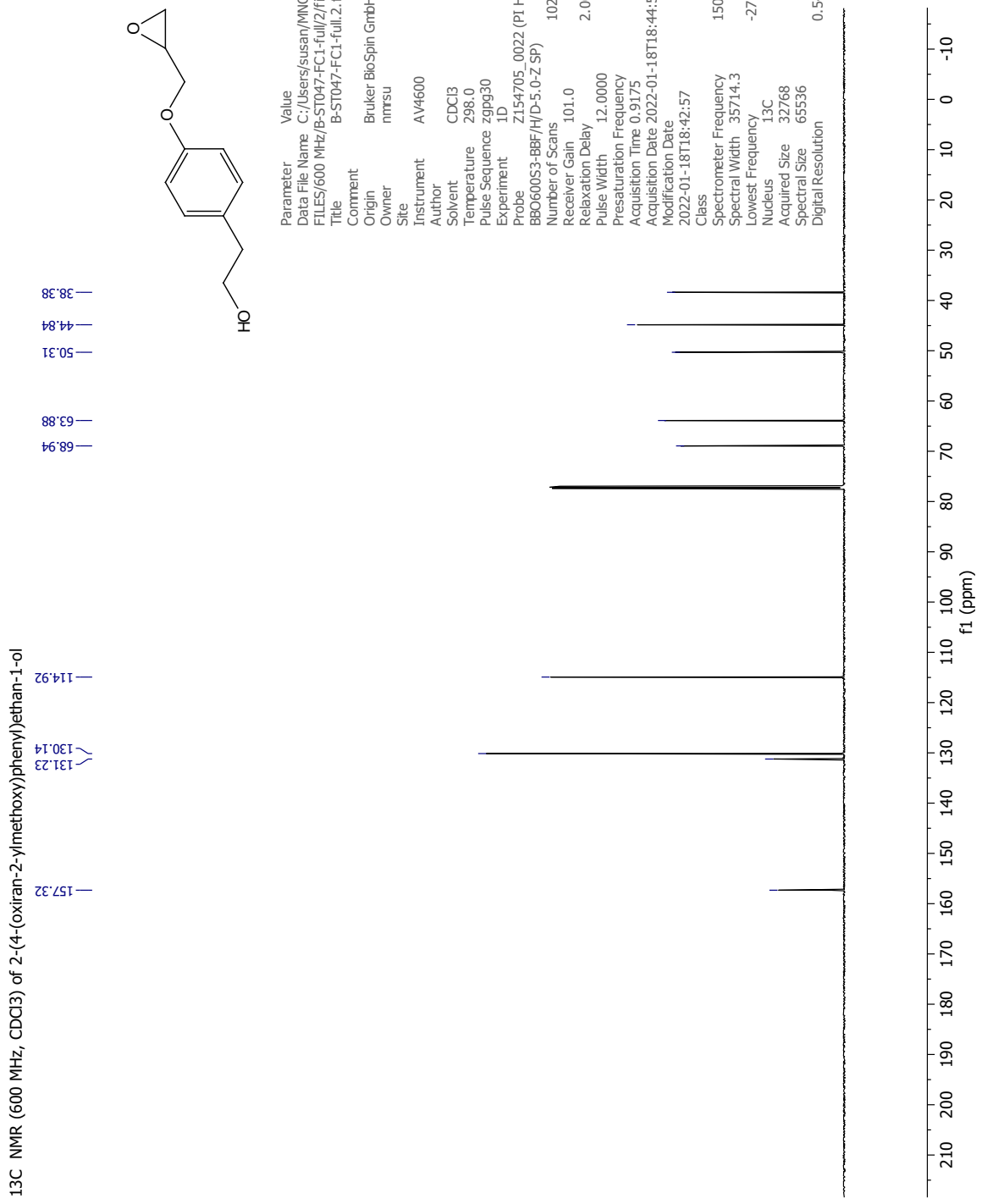

Figure A.23 ^{13}C NMR spectrum (150 MHz, $CDCl_3$) of 2-(4-(oxiran-2-ylmethoxy)phenyl)ethan-1-ol (**7**).

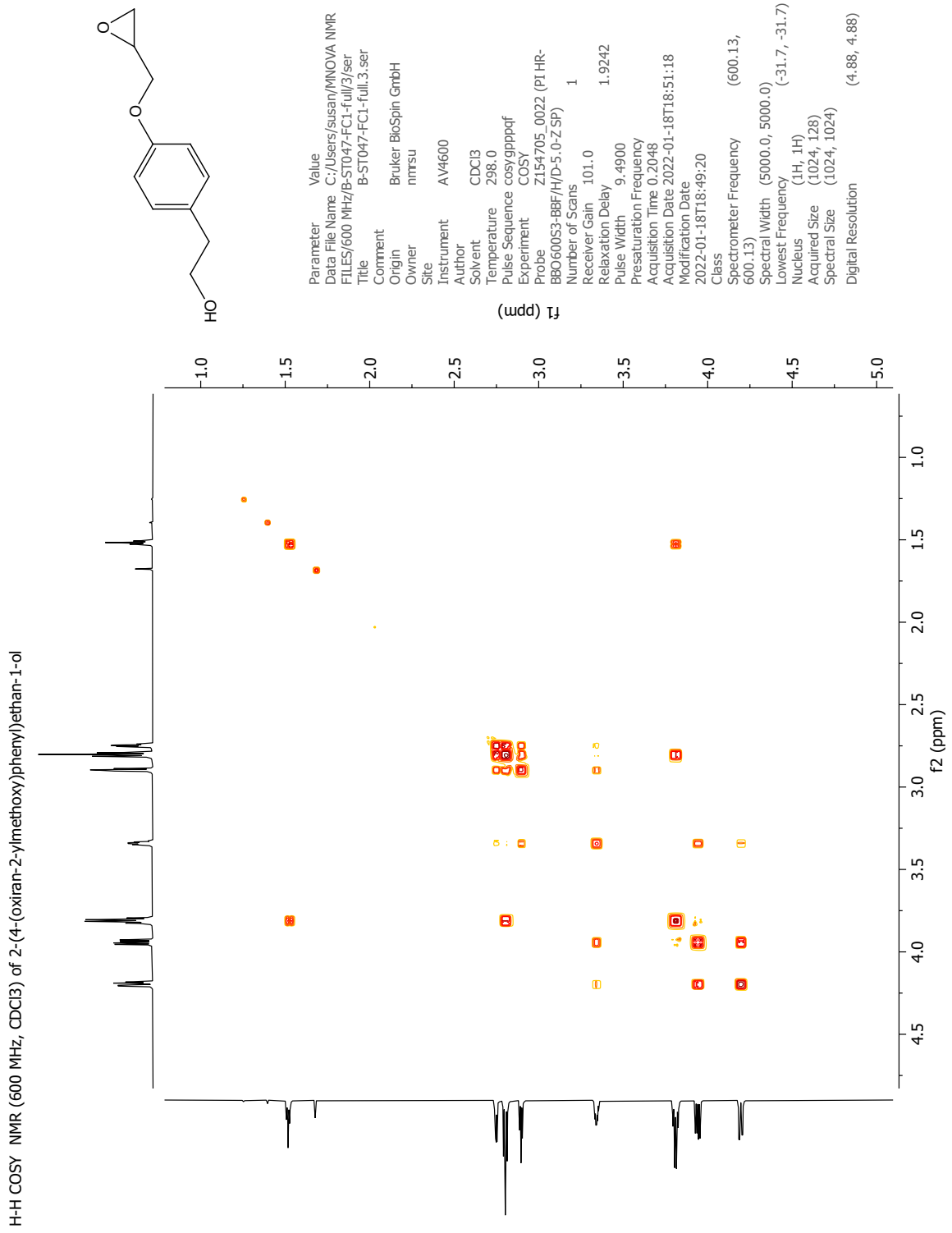

Figure A.24 COSY NMR spectrum (600 MHz, $CDCl_3$) of 2-(4-(oxiran-2-ylmethoxy)phenyl)ethan-1-ol (**7**).

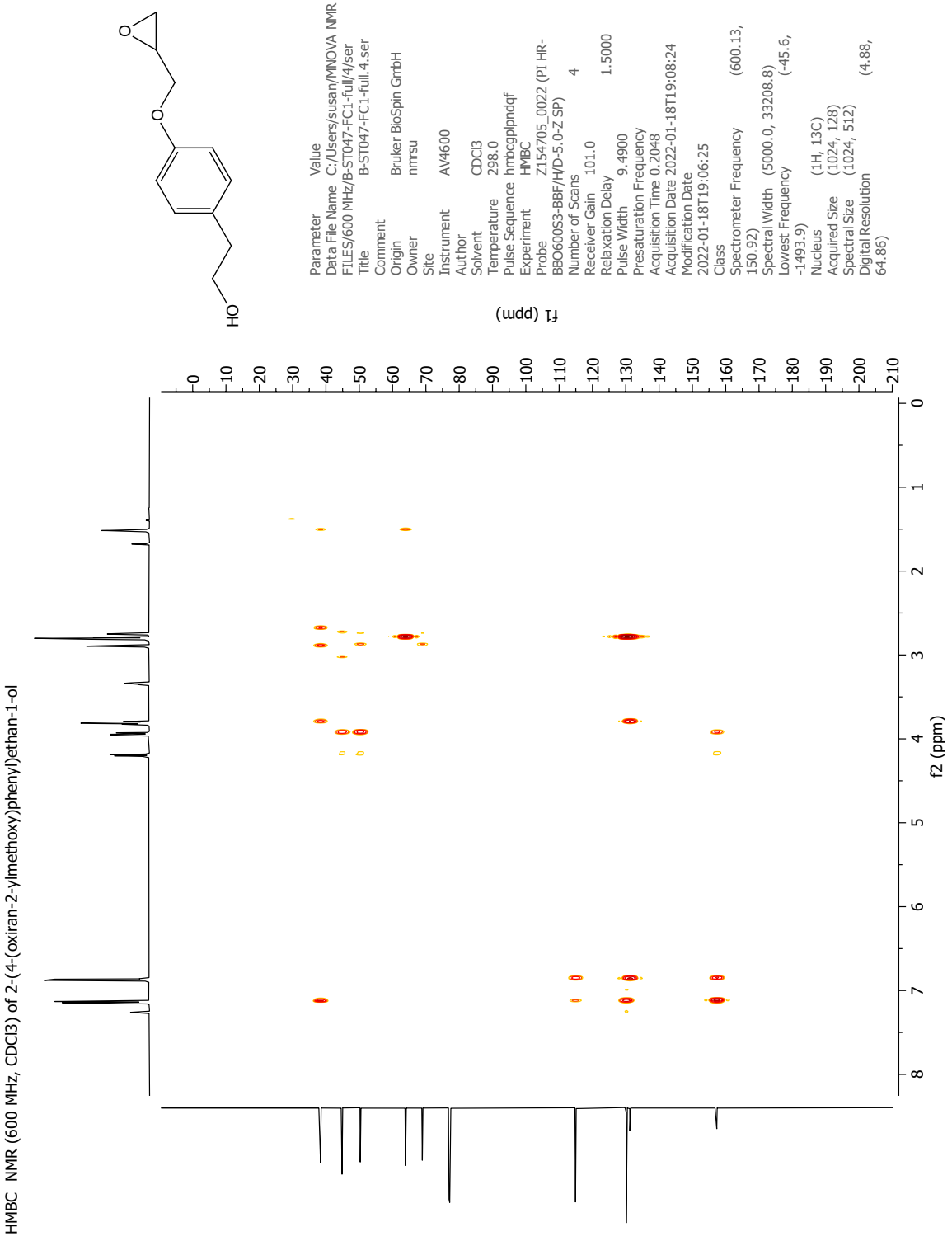

Figure A.25 HMBC NMR spectrum (600 MHz, $CDCl_3$) of 2-(4-(oxiran-2-ylmethoxy)phenyl)ethan-1-ol (**7**).

A.7 Characterization of 1-chloro-3-(4-(2-(cyclopropylmethoxy)-ethyl)phenoxy)propan-2-ol (8a)

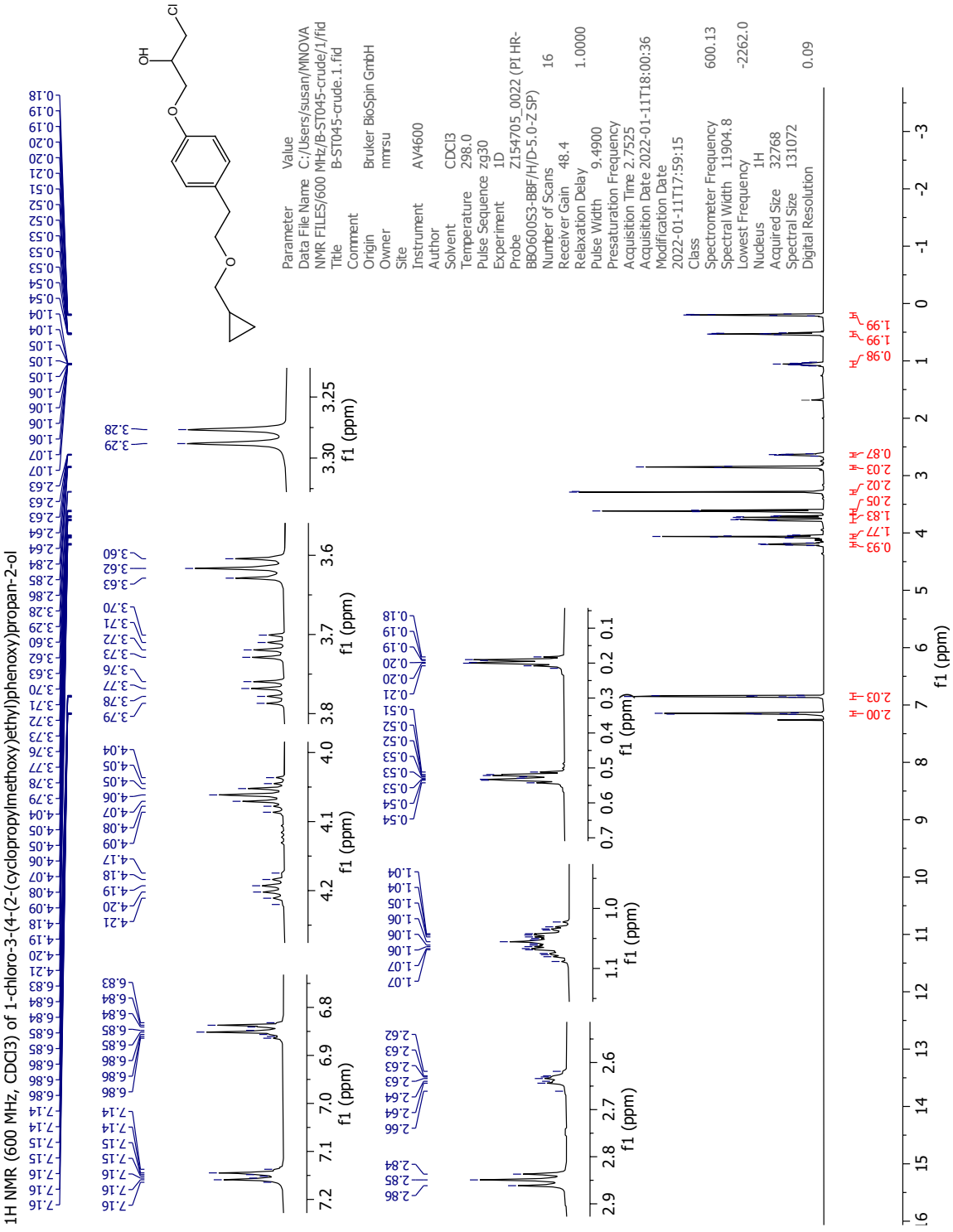

Figure A.26 ^{1}H NMR spectrum (600 MHz, $CDCl_3$) of 1-chloro-3-(4-(2-(cyclopropyl-methoxy)ethyl)phenoxy)propan-2-ol (**8a**). δ= 1.68 is water from the solvent.

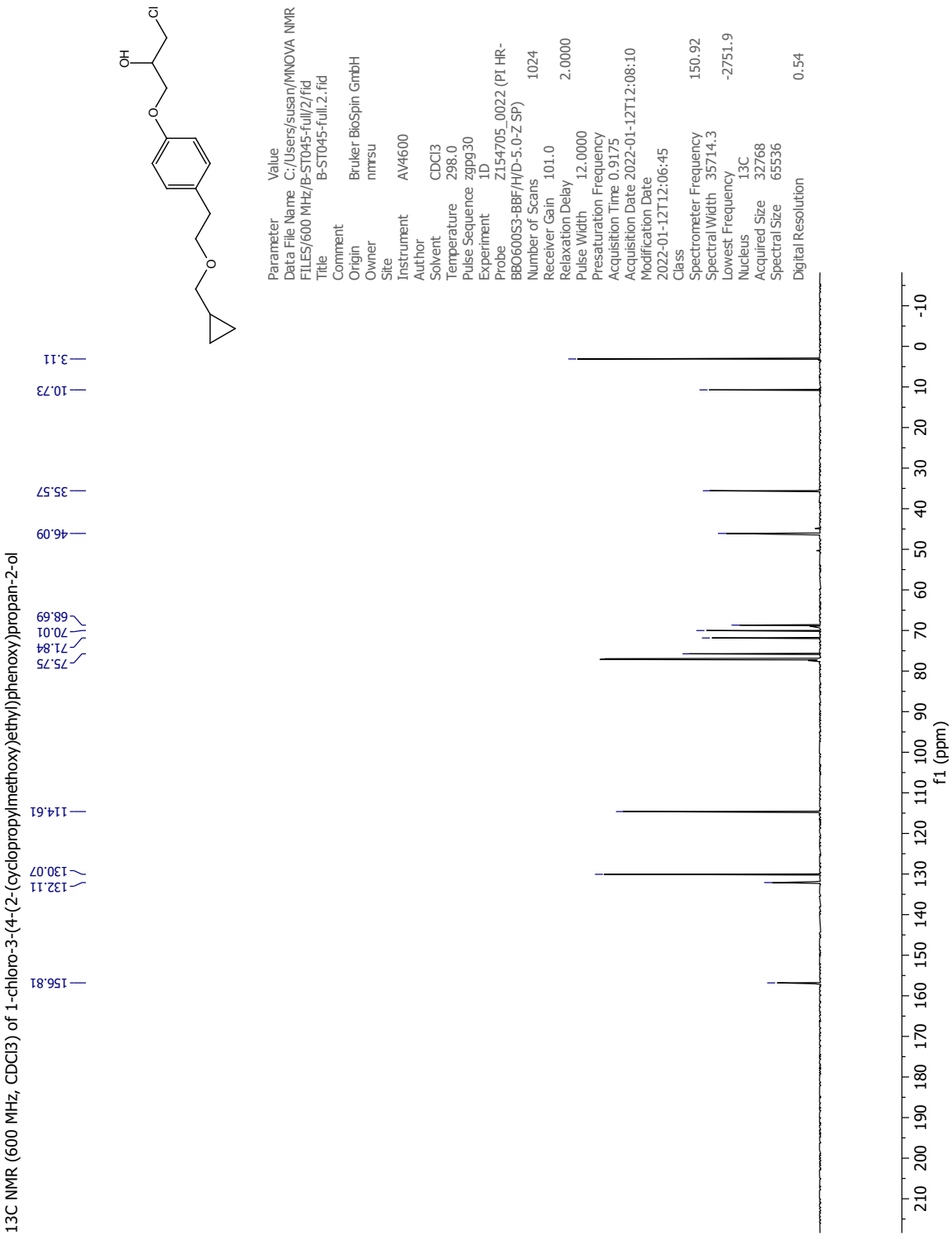

Figure A.27 ^{13}C NMR spectrum (150 MHz, $CDCl_3$) of 1-chloro-3-(4-(2-(cyclopropylmethoxy)ethyl)phenoxy)propan-2-ol (**8a**).

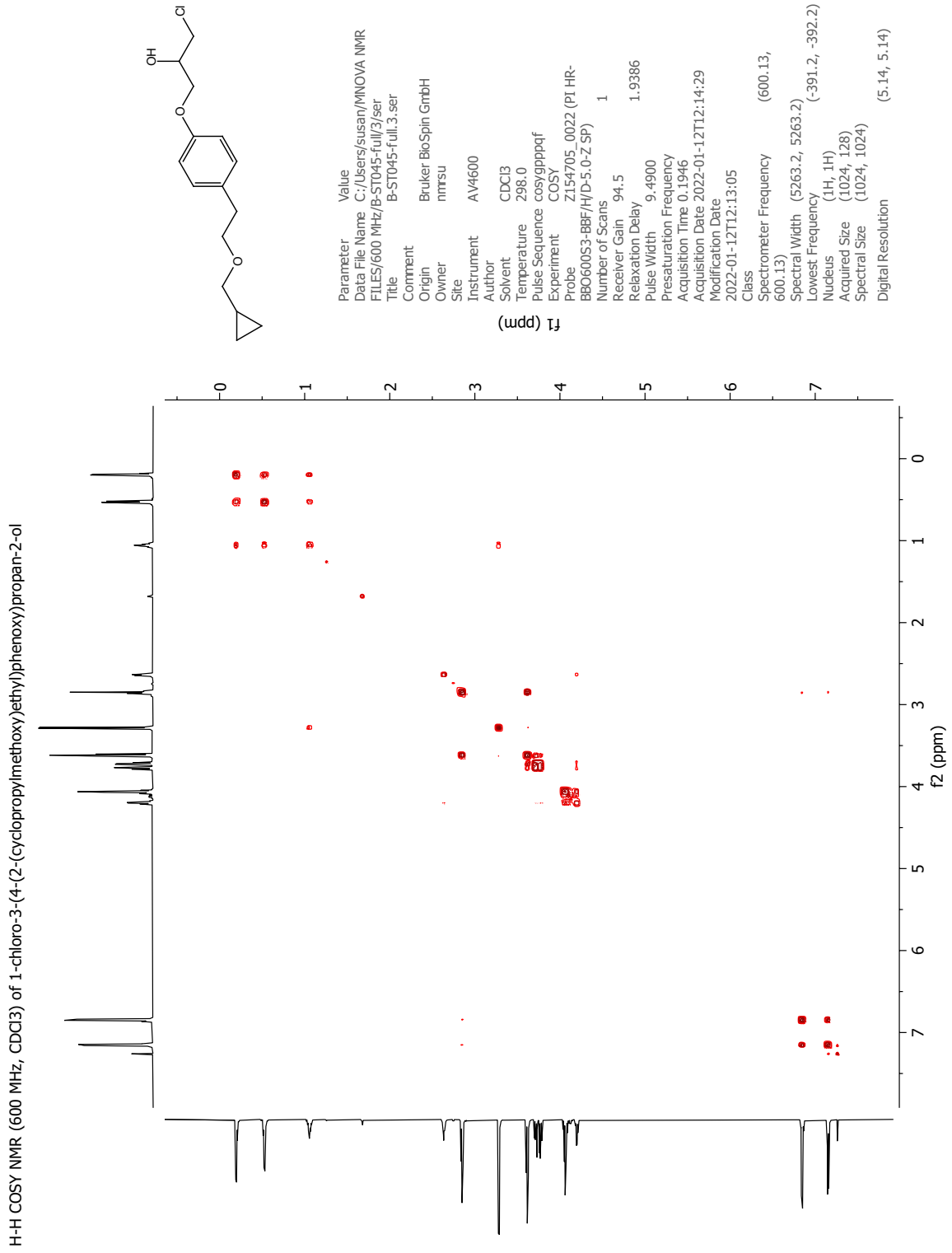

Figure A.28 COSY NMR spectrum (600 MHz, $CDCl_3$) of 1-chloro-3-(4-(2-(cyclopropylmethoxy)ethyl)phenoxy)propan-2-ol (**8a**).

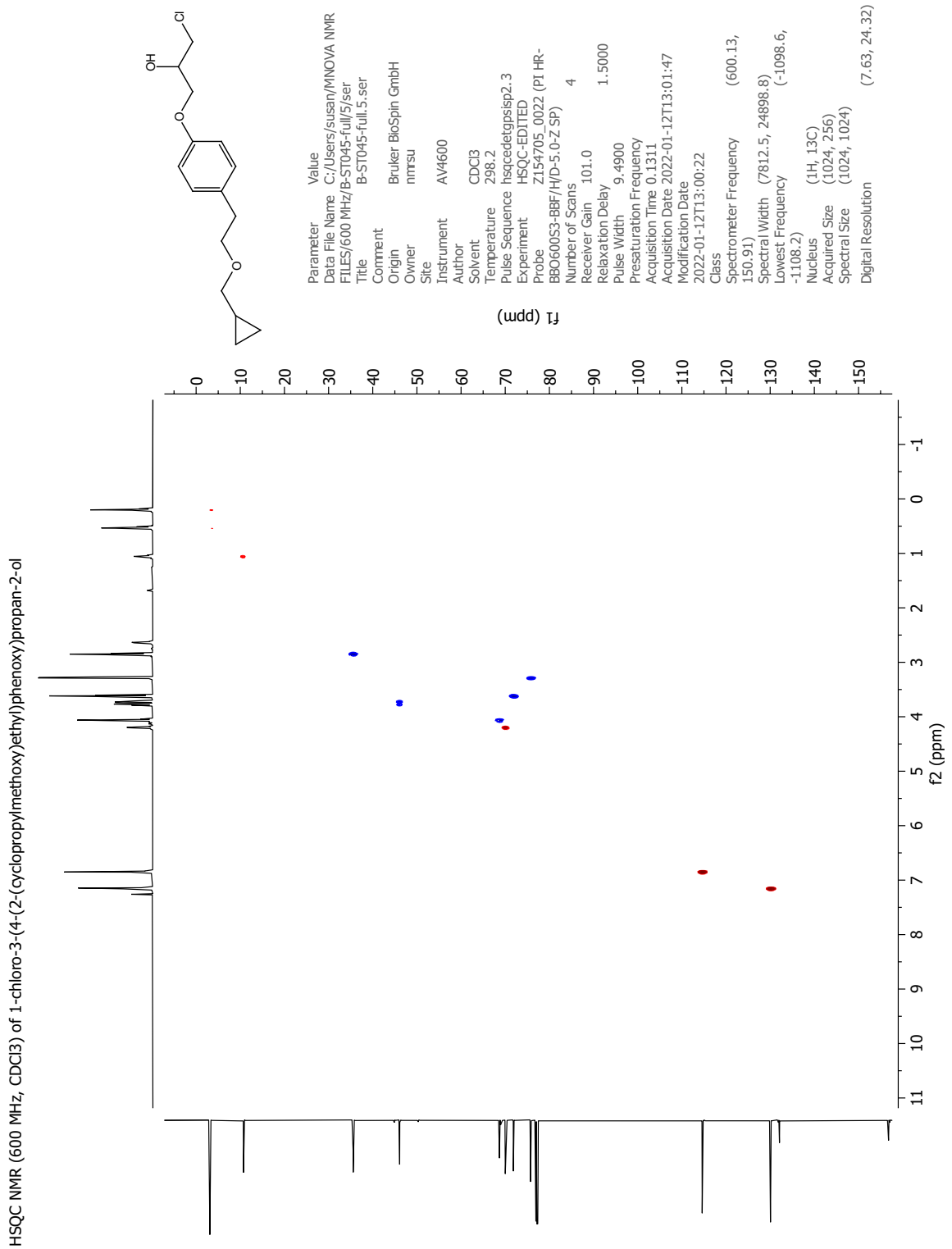

Figure A.29 HSQC NMR spectrum (600 MHz, $CDCl_3$) of 1-chloro-3-(4-(2-(cyclopropylmethoxy)ethyl)phenoxy)propan-2-ol (**8a**).

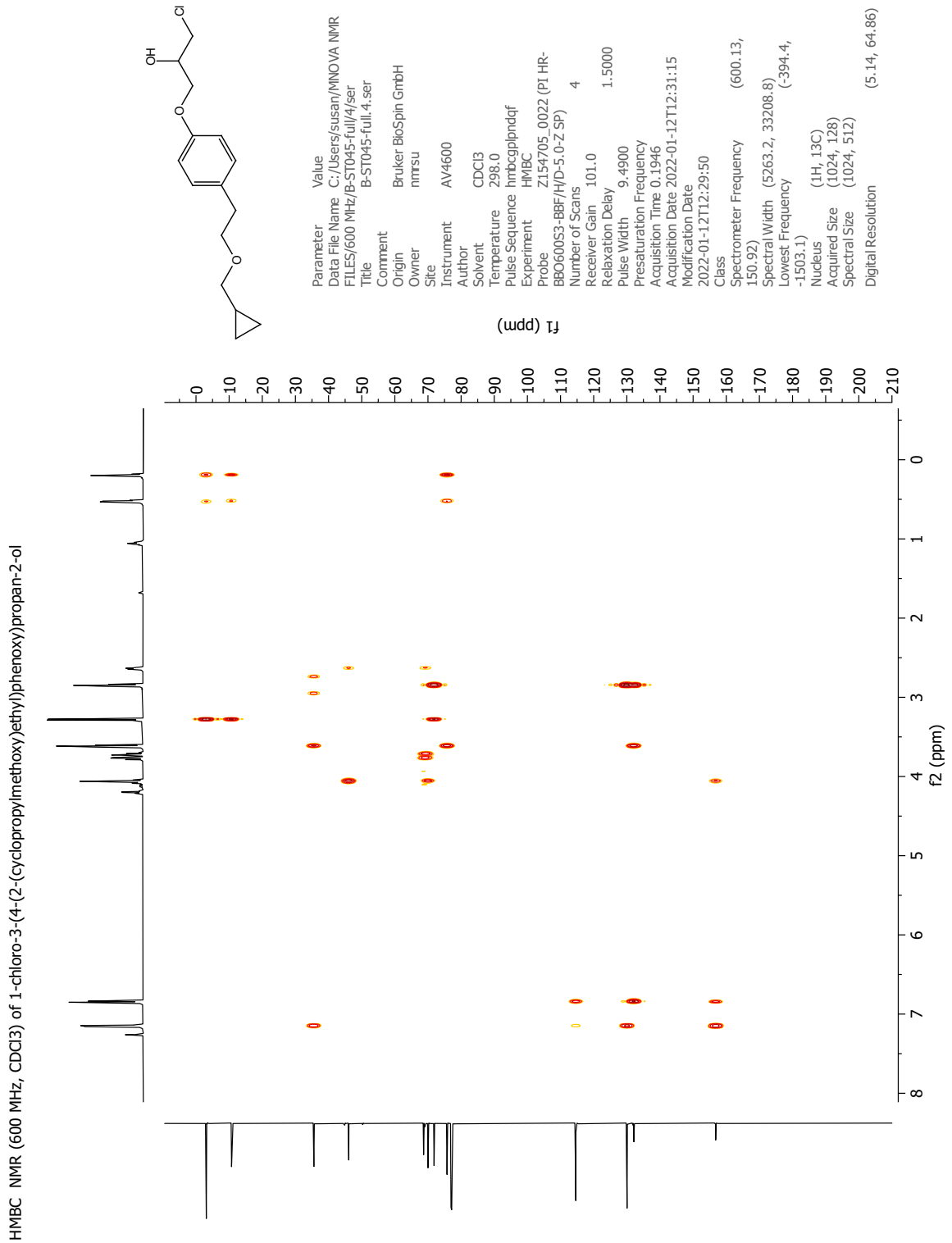

Figure A.30 HMBC NMR spectrum (600 MHz, $CDCl_3$) of 1-chloro-3-(4-(2-(cyclopropylmethoxy)ethyl)phenoxy)propan-2-ol (**8a**).

A.8 Characterization of 1-bromo-3-(4-(2-(cyclopropylmethoxy)-ethyl)phenoxy)propan-2-ol (8b)

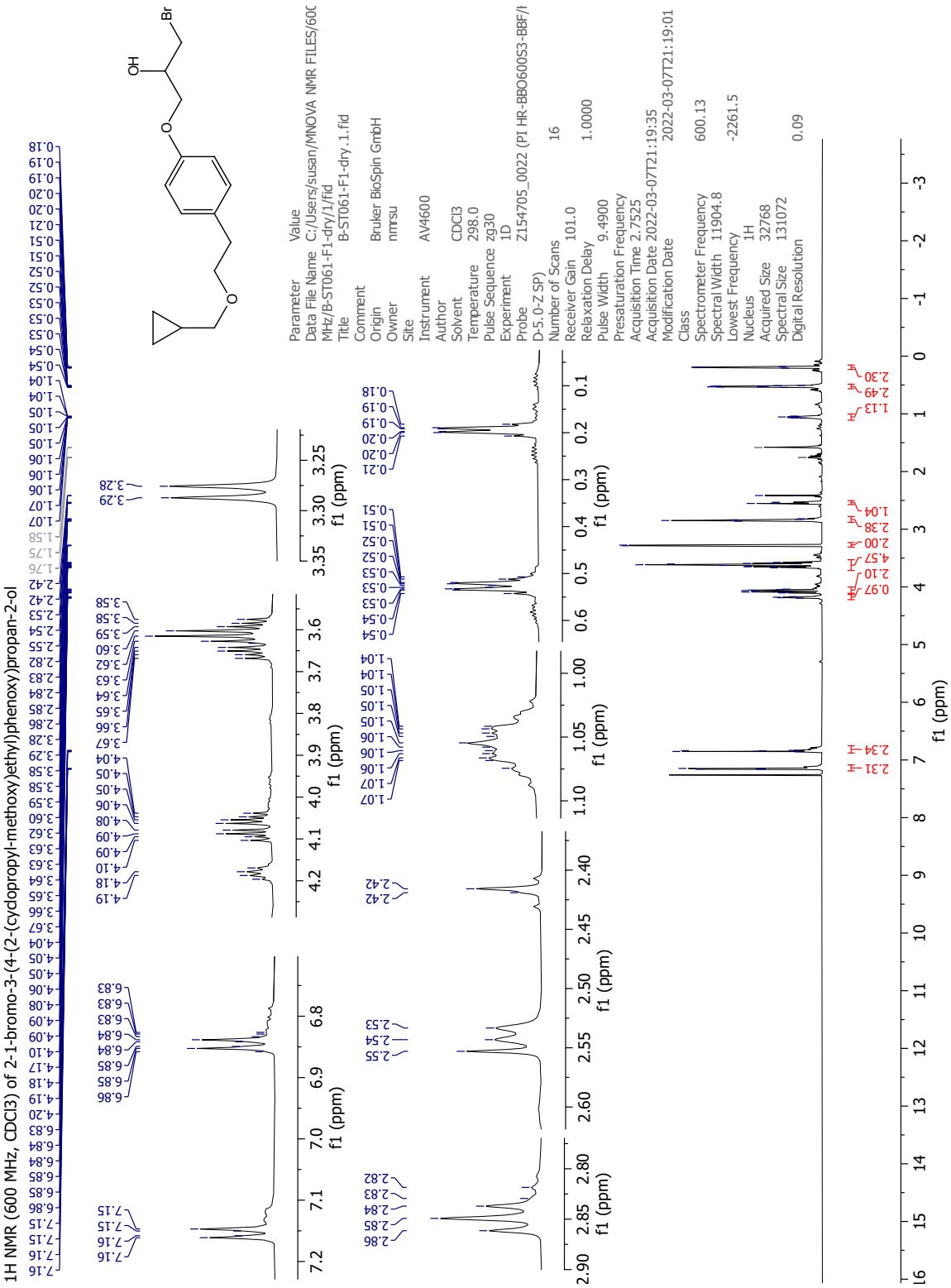

Figure A.31 ^{1}H NMR spectrum (600 MHz, $CDCl_3$) of 1-bromo-3-(4-(2-(cyclopropyl-methoxy)ethyl)phenoxy)propan-2-ol (**8b**). δ= 1.58 is water from the solvent. Other impurities are discussed in Section 2.1.6.

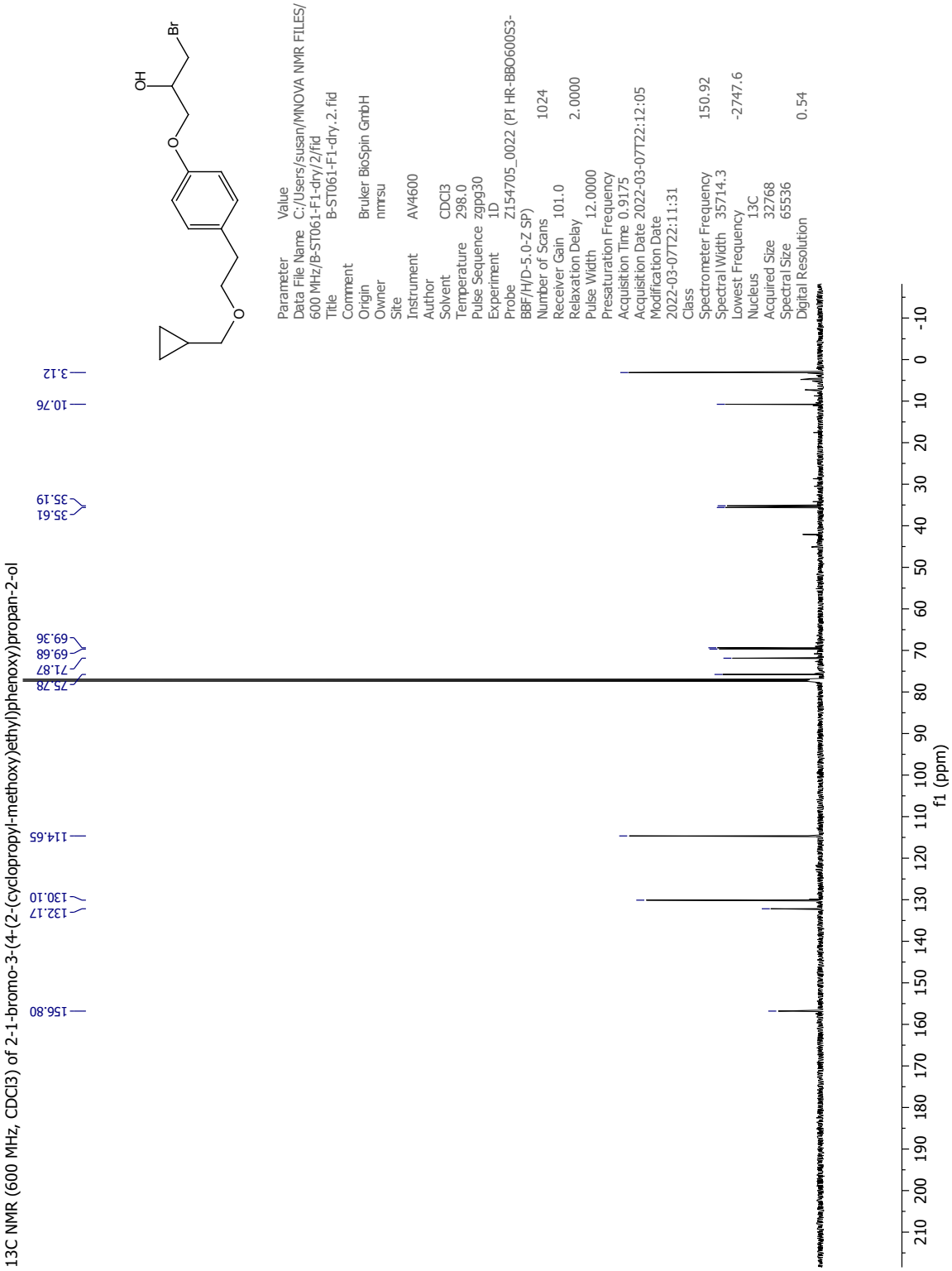

Figure A.32 ^{13}C NMR spectrum (150 MHz, $CDCl_3$) of 1-bromo-3-(4-(2-(cyclopropylmethoxy)ethyl)phenoxy)propan-2-ol (**8b**).

A.9 Analysis of a mixture of 8a and 8b

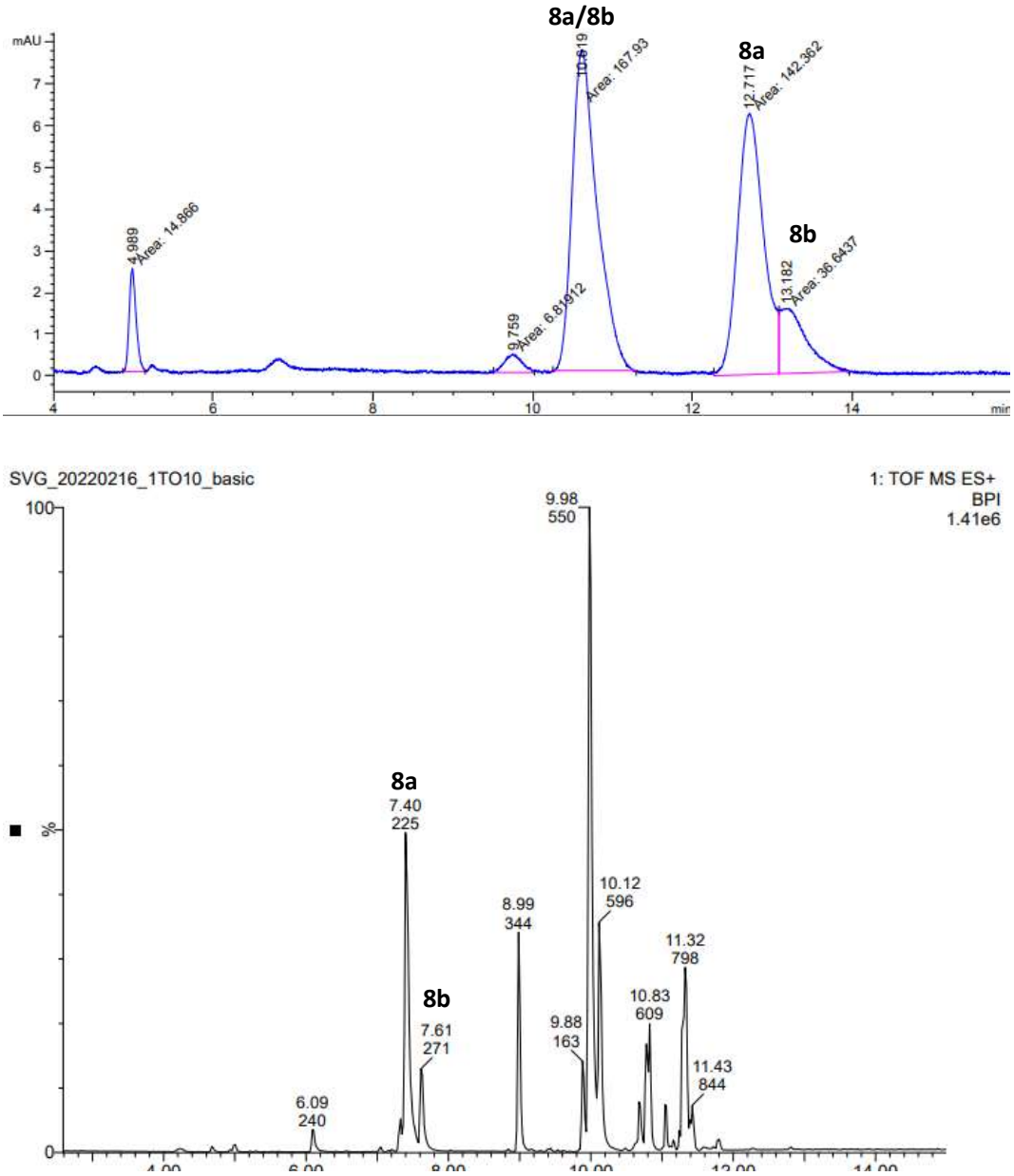

Figure A.33 Chiral HPLC chromatogram (top) and LC-MS chromatogram (bottom) of bromohydrin **8b** and chlorohydrin **8a**. HPLC measured on a Chiralcel OD-H column with mobile phase composition *n*-hexane:*i*-PrOH (90:10), and flow 1 mL min^{-1}. LC-MS performed on an ACQUITY UPLC HSS T3 Column.

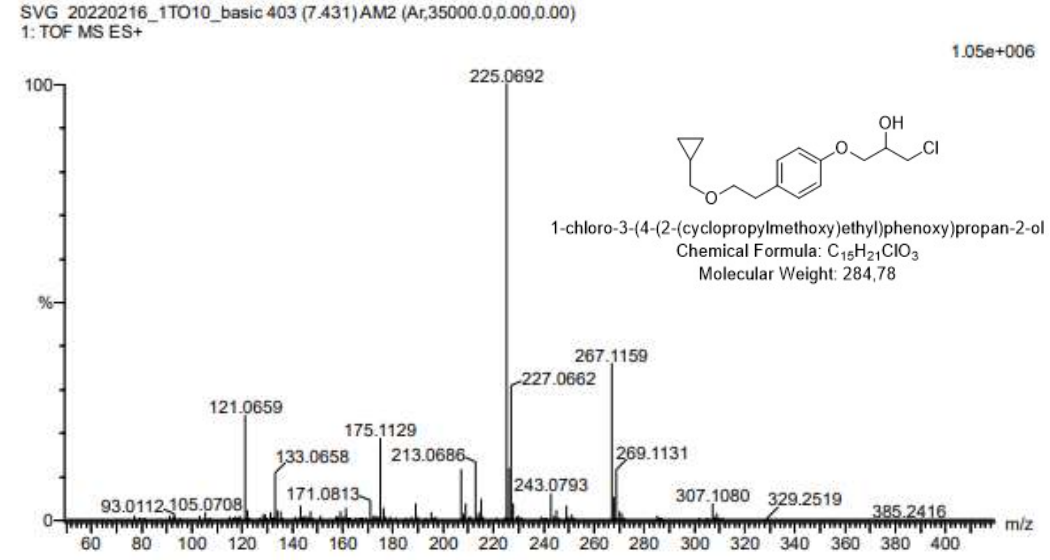

Minimum:				-1.5				
Maximum:		5.0	3.0	50.0				
Mass	Calc. Mass	mDa	PPM	DBE	i-FIT	Norm	Conf(%)	Formula
307.1080	307.1077	0.3	1.0	4.5	1033.7	0.361	69.66	C15 H21 O3 Na Cl
	307.1083	-0.3	-1.0	12.5	1053.3	19.927	0.00	C18 H15 N2 O3
	307.1074	0.6	2.0	8.5	1034.6	1.193	30.34	C13 H16 N6 O Cl

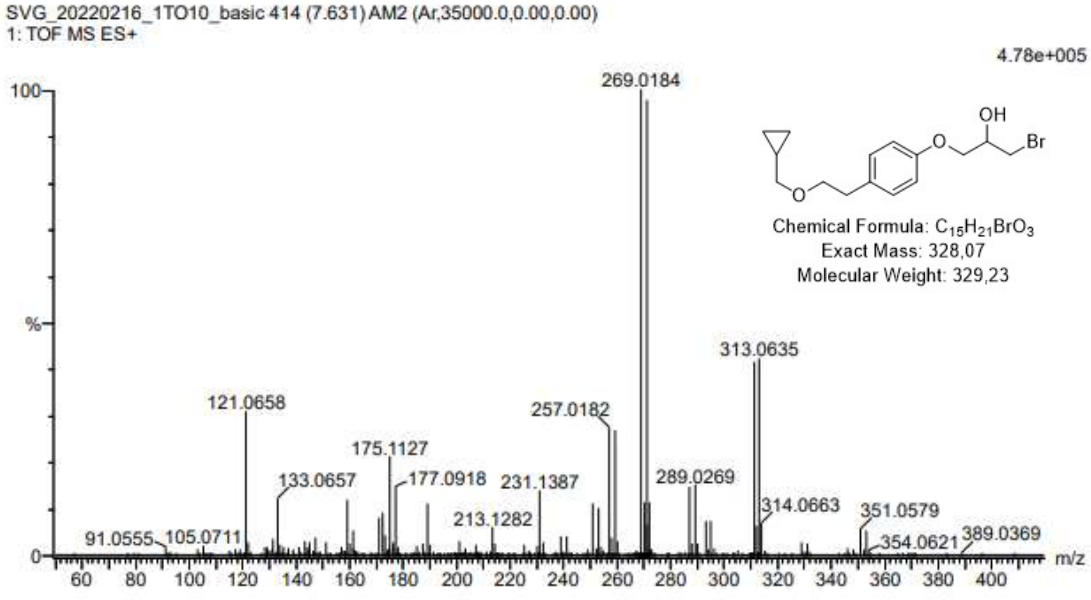

Minimum:				-1.5				
Maximum:		5.0	3.0	50.0				
Mass	Calc. Mass	mDa	PPM	DBE	i-FIT	Norm	Conf(%)	Formula
351.0579	351.0572	0.7	2.0	4.5	974.5	0.080	92.32	C15 H21 O3 Na Br
	351.0569	1.0	2.8	8.5	977.0	2.566	7.68	C13 H16 N6 O Br

Figure A.34 MS spectra recorded for chlorohydrin **8a** (top, $t_R = 7.40$ min) and bromohydrin **8b** (bottom, $t_R = 7.61$ min), corresponding to the chromatogram in Figure A.33.

A.10 Characterization of 1-chloro-3-(4-(2-(cyclopropylmethoxy)-ethyl)phenoxy)propan-2-yl butyrate (9)

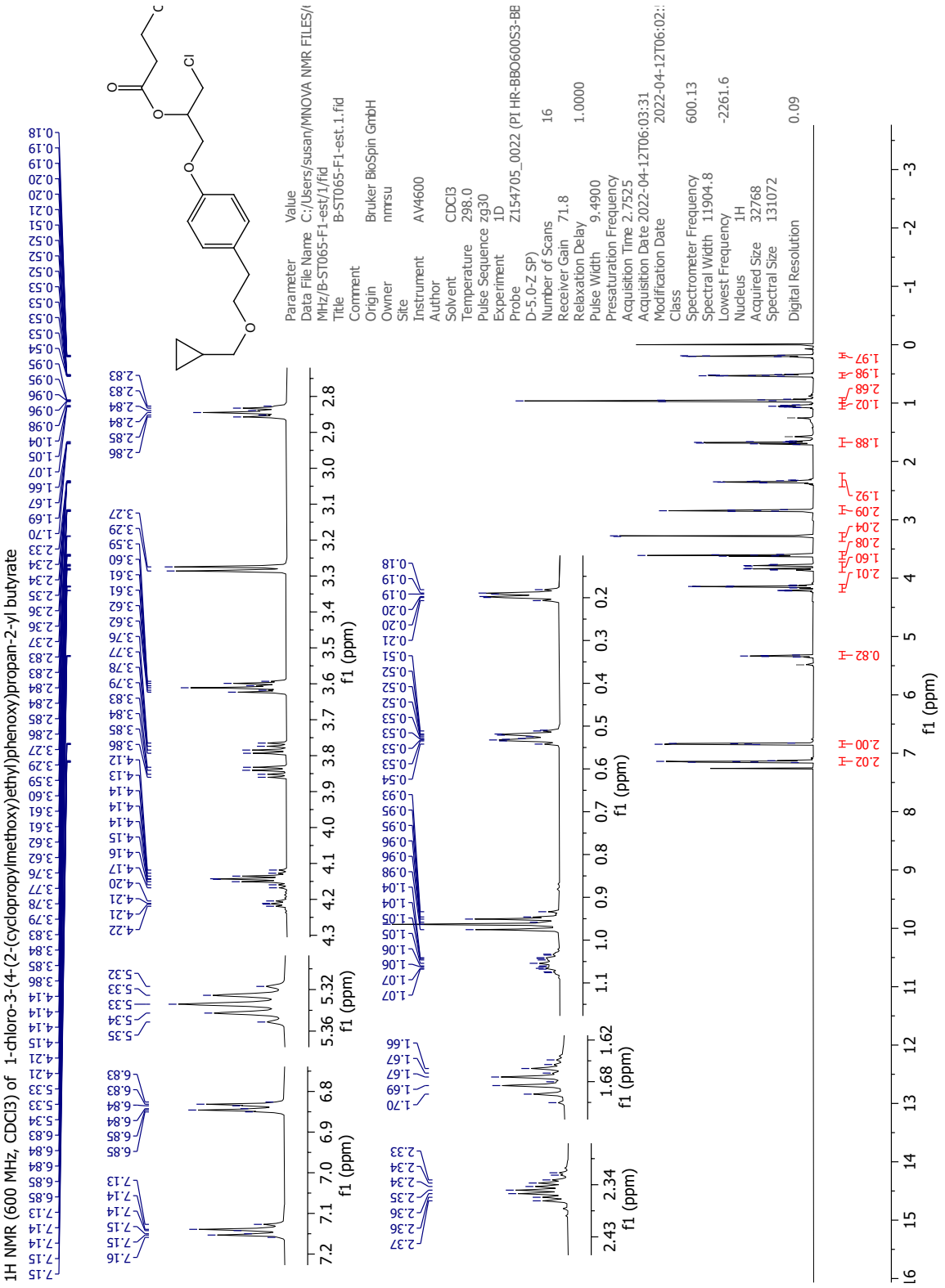

Figure A.35 ^{1}H NMR spectrum (600 MHz, $CDCl_3$) of 1-chloro-3-(4-(2-(cyclopropylmethoxy)ethyl)phenoxy)propan-2-yl butyrate (**9**).

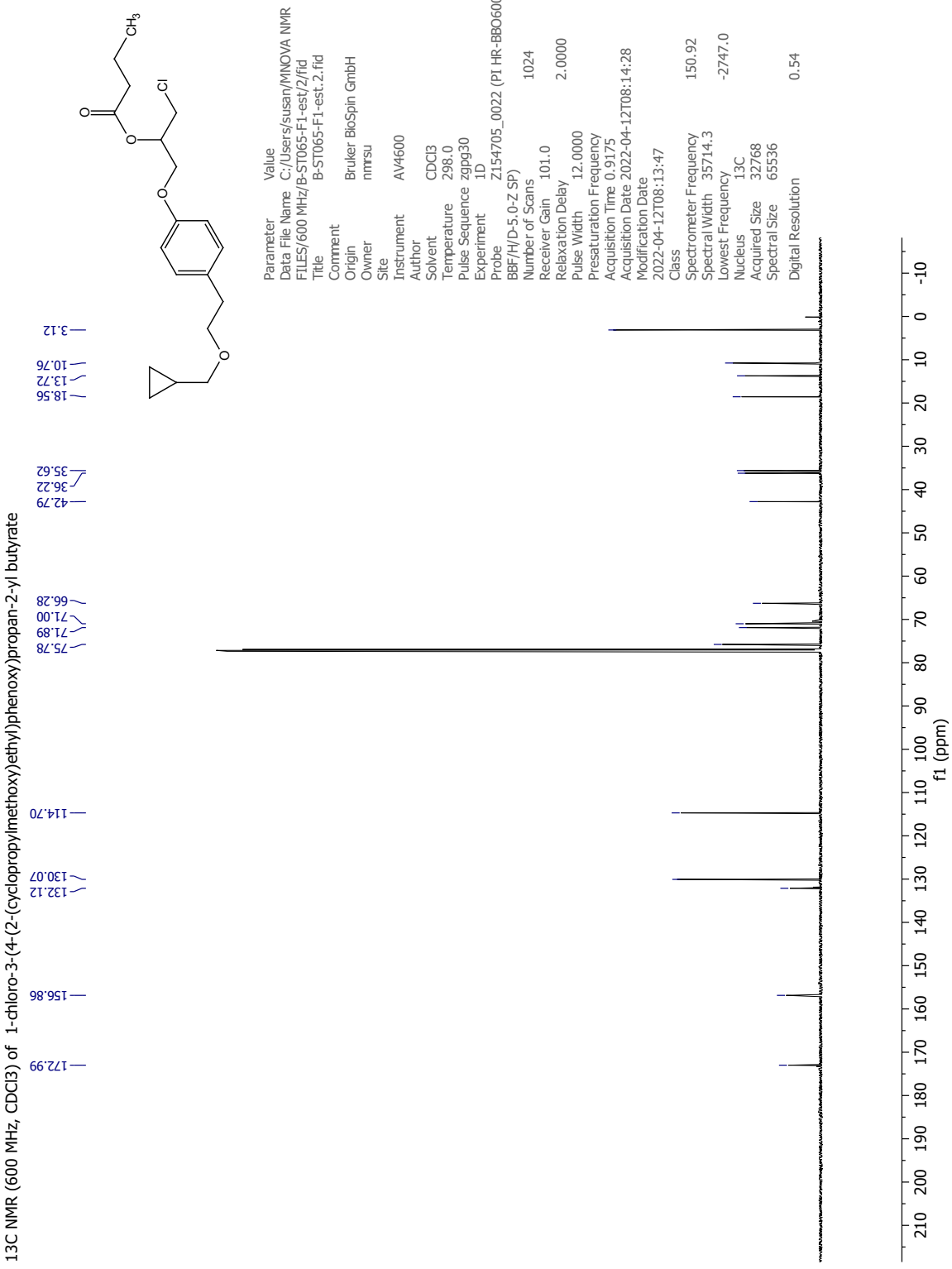

Figure A.36 ^{13}C NMR spectrum (150 MHz, $CDCl_3$) of 1-chloro-3-(4-(2-(cyclopropylmethoxy)ethyl)phenoxy)propan-2-yl butyrate (**9**).

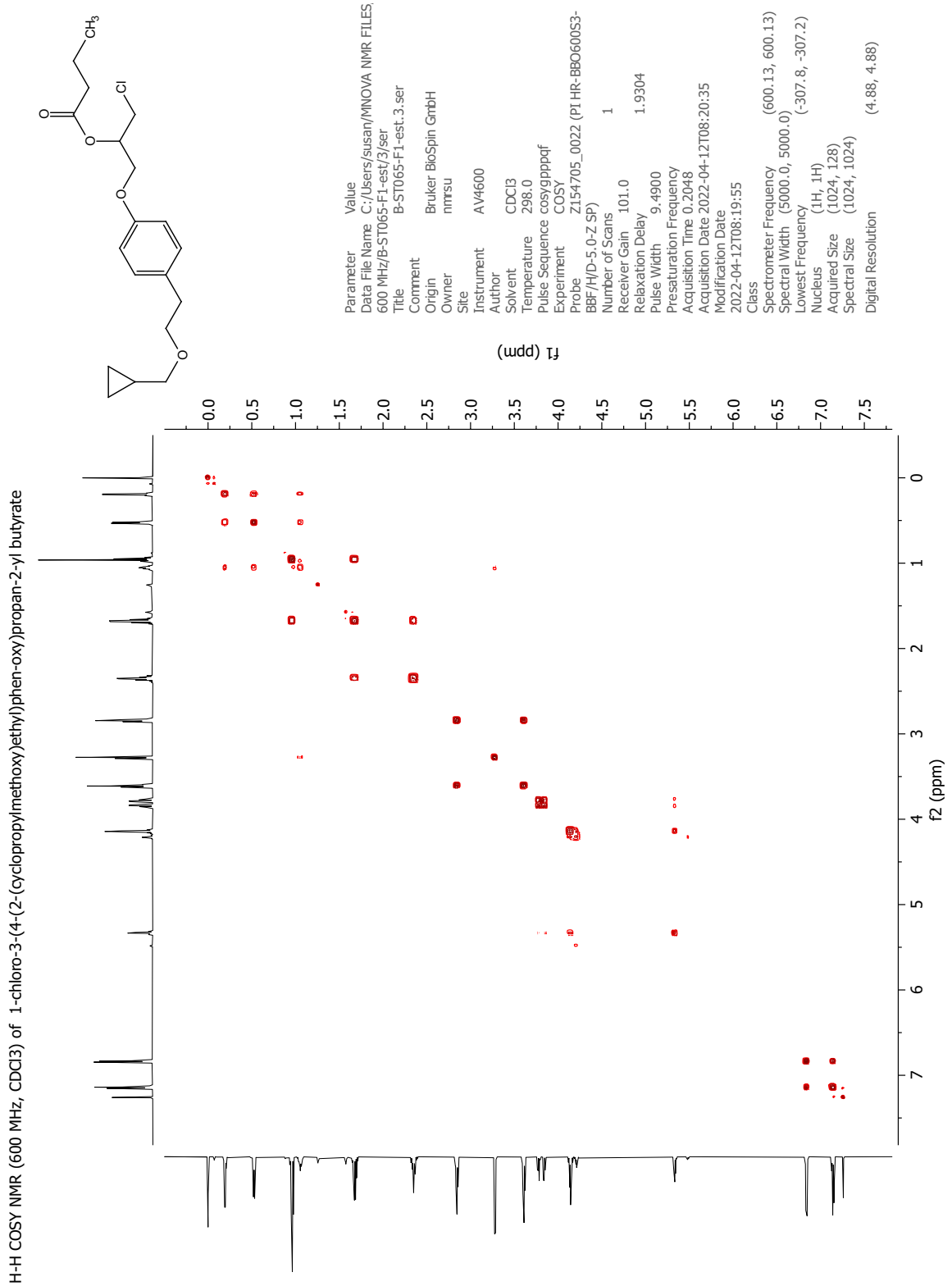

Figure A.37 COSY NMR spectrum (600 MHz, $CDCl_3$) of 1-chloro-3-(4-(2-(cyclopropylmethoxy)ethyl)phenoxy)propan-2-yl butyrate (**9**).

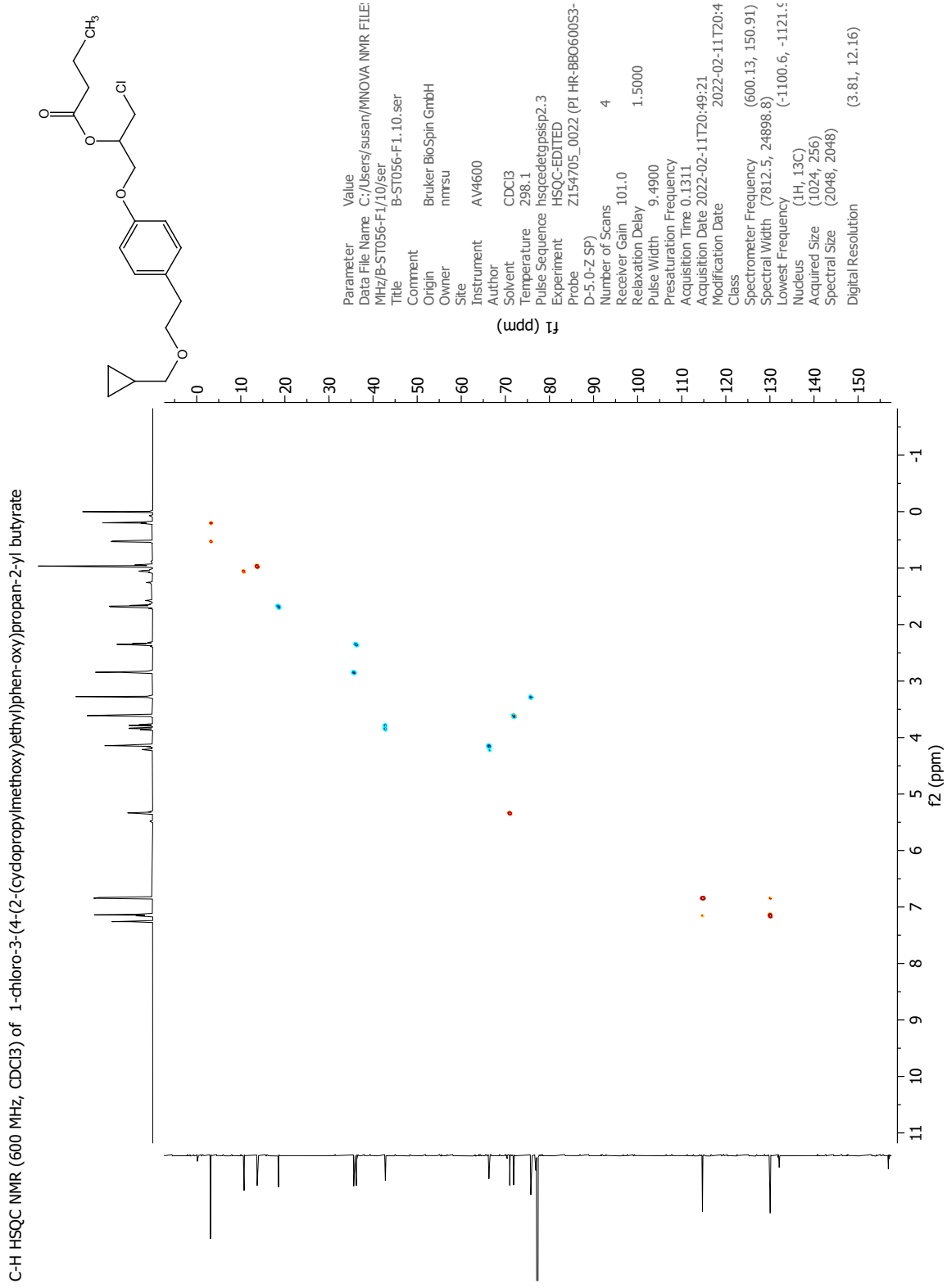

Figure A.38 HSQC NMR spectrum (600 MHz, $CDCl_3$) of 1-chloro-3-(4-(2-(cyclopropylmethoxy)ethyl)phenoxy)propan-2-yl butyrate (**9**).

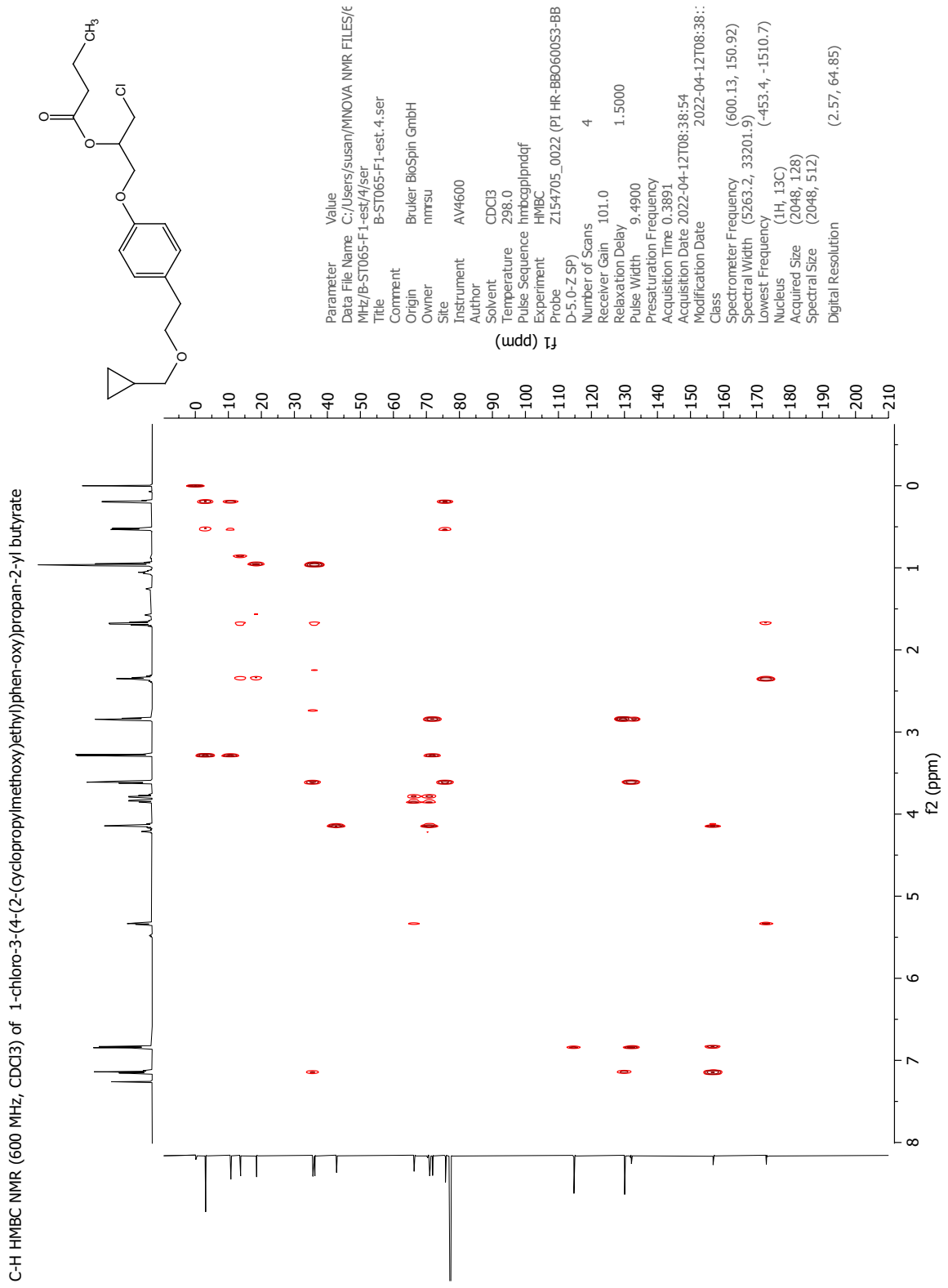

Figure A.39 HMBC NMR spectrum (600 MHz, $CDCl_3$) of 1-chloro-3-(4-(2-(cyclopropyl-methoxy)ethyl)phenoxy)propan-2-yl butyrate (**9**).

A.11 Characterization of betaxolol (10)

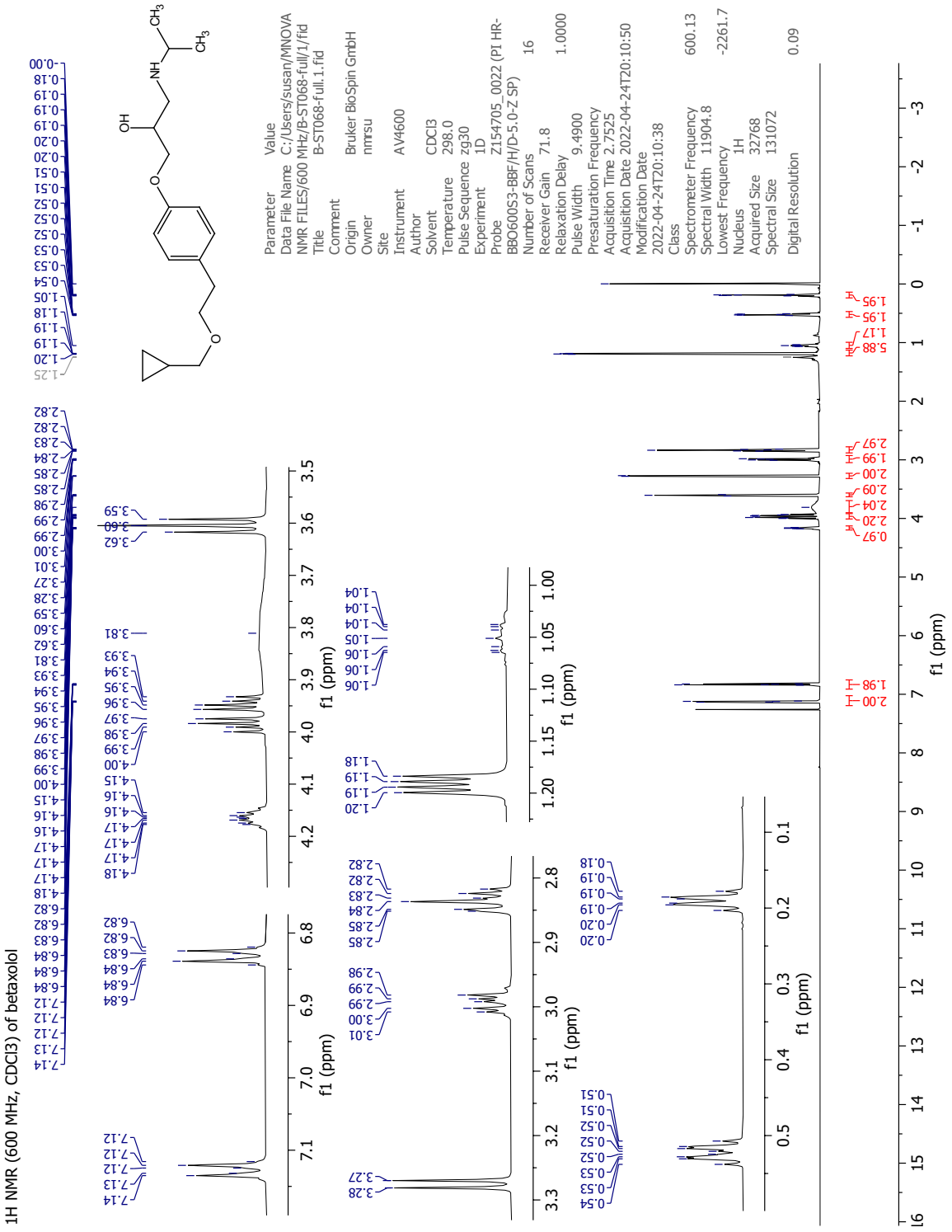

Figure A.40 ^{1}H NMR spectrum (600 MHz, $CDCl_3$) of betaxolol (**10**).

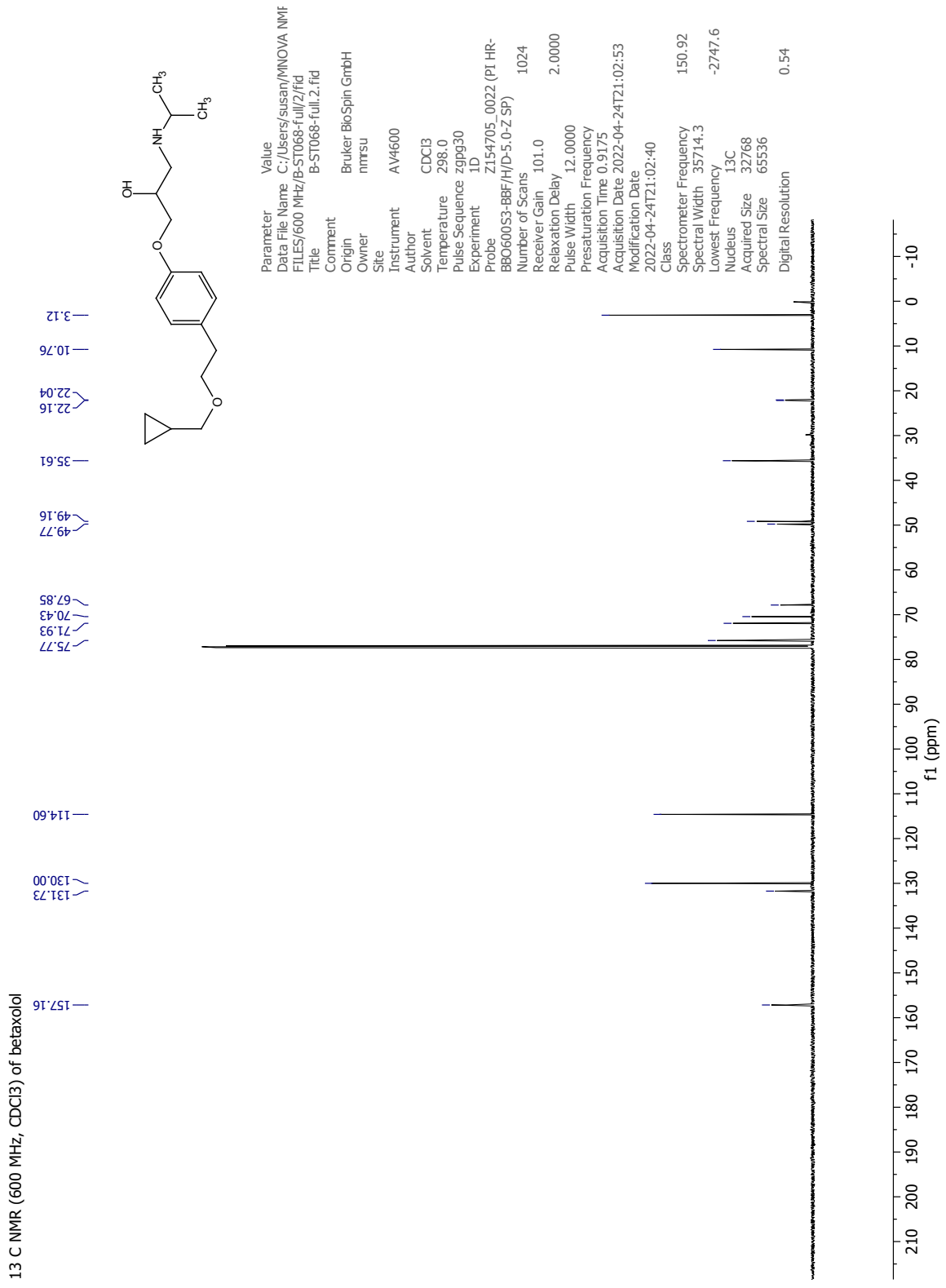

Figure A.41 ^{13}C NMR spectrum (150 MHz, $CDCl_3$) of betaxolol (**10**).

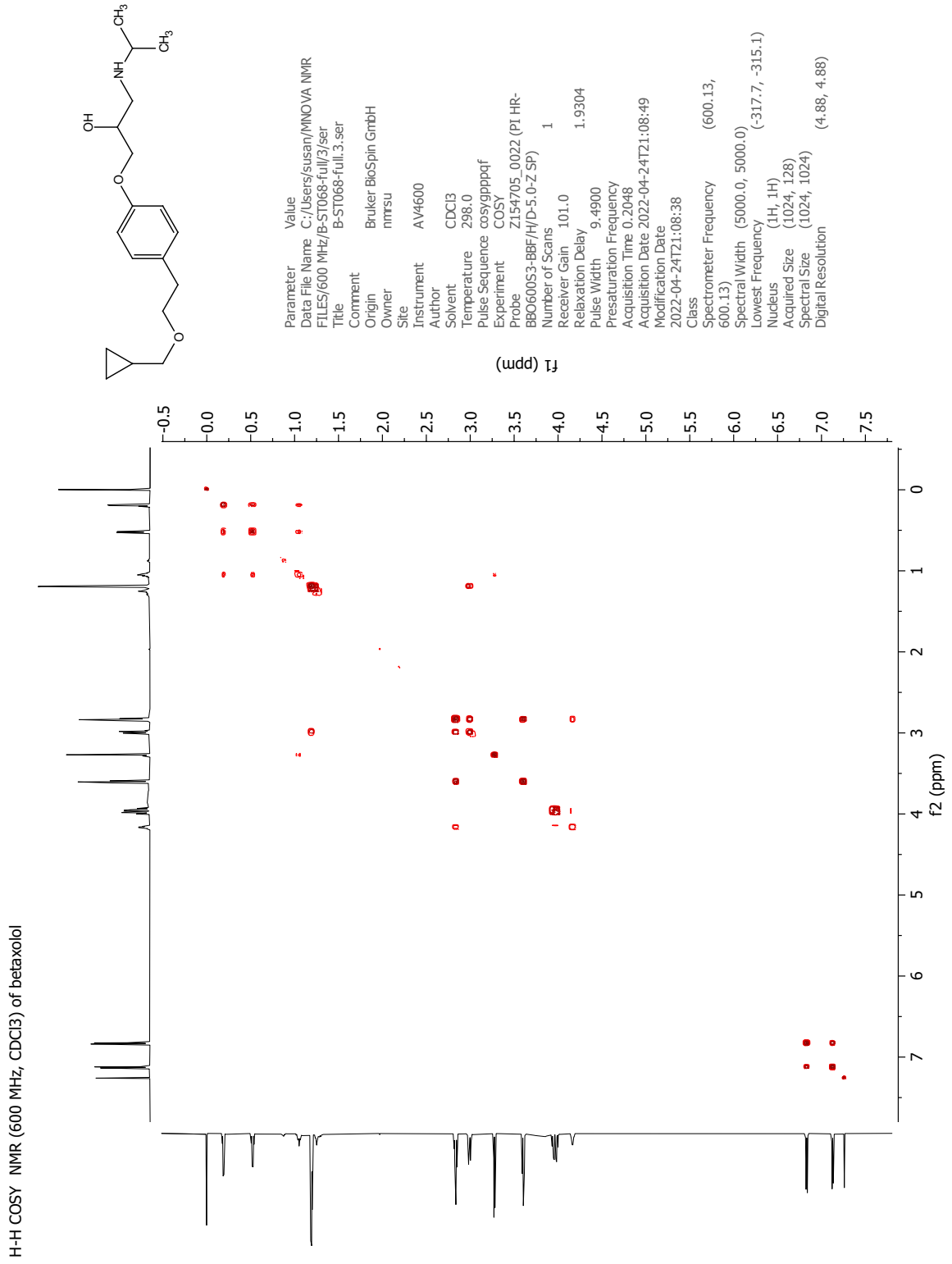

Figure A.42 COSY NMR spectrum (600 MHz, $CDCl_3$) of betaxolol (**10**).

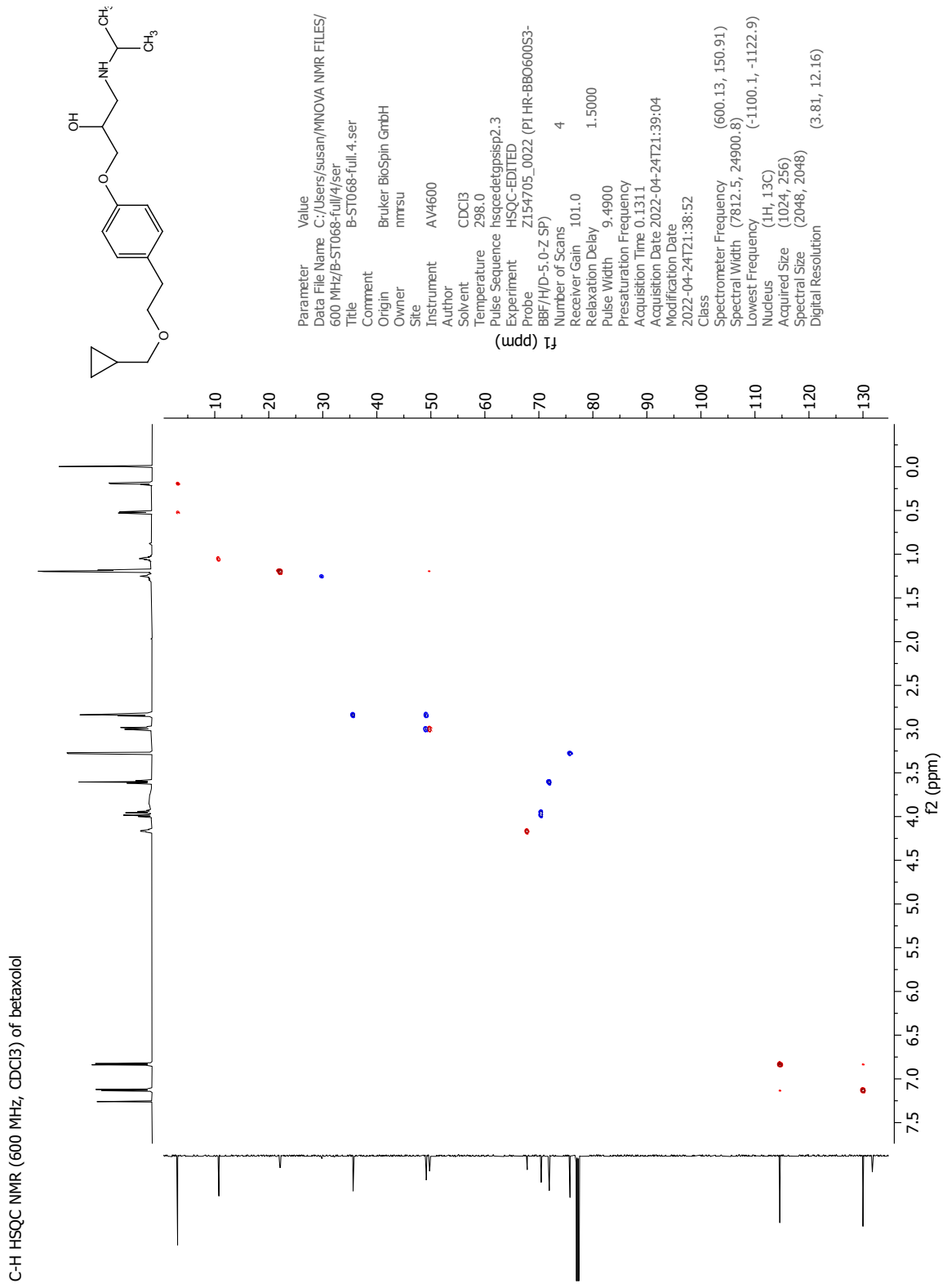

Figure A.43 HSQC NMR spectrum (600 MHz, $CDCl_3$) of betaxolol (**10**).

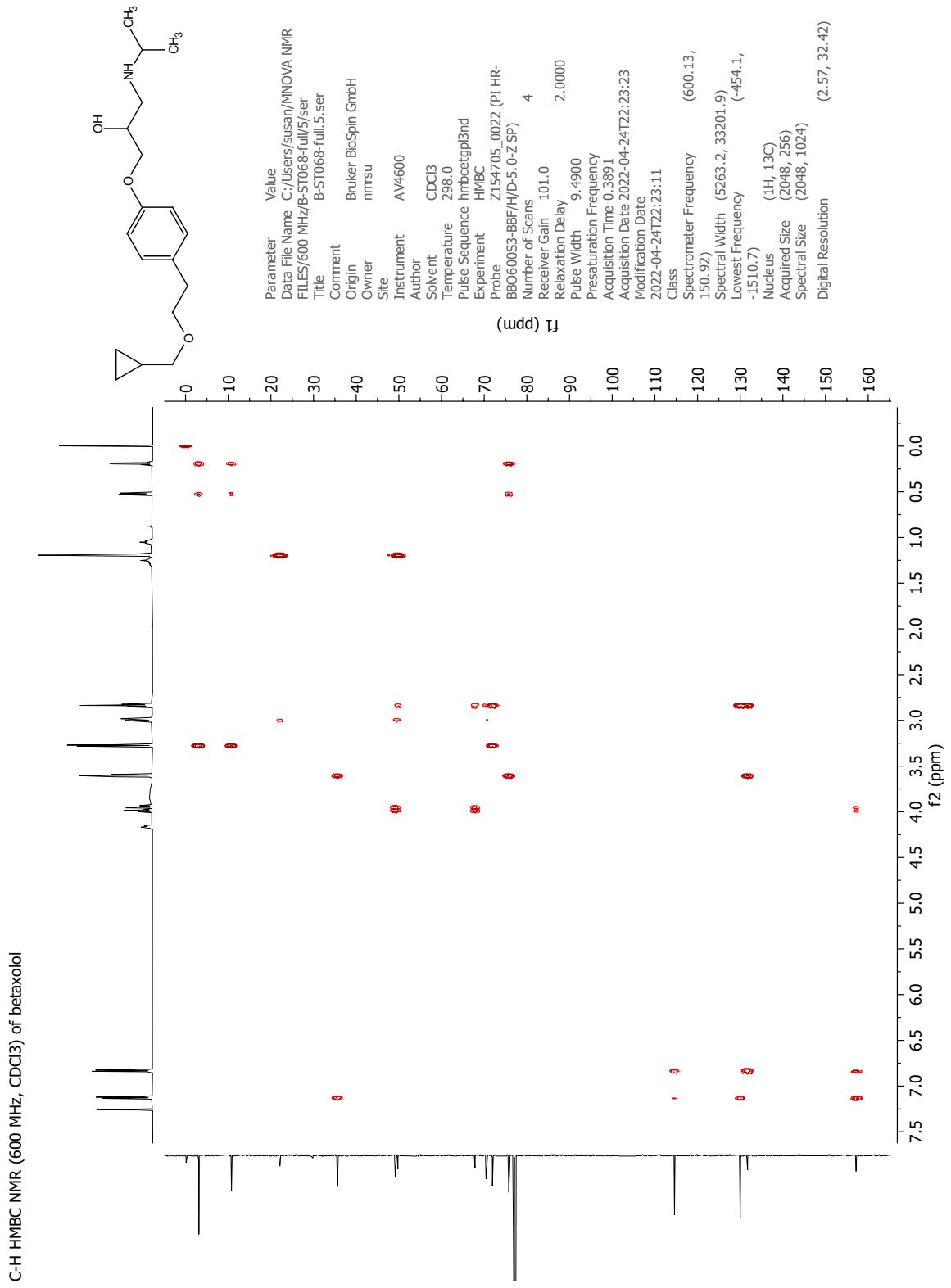

Figure A.44 HMBC NMR spectrum (600 MHz, $CDCl_3$) of betaxolol (**10**).

A.12 Characterization of by-products in the pathway to betaxolol

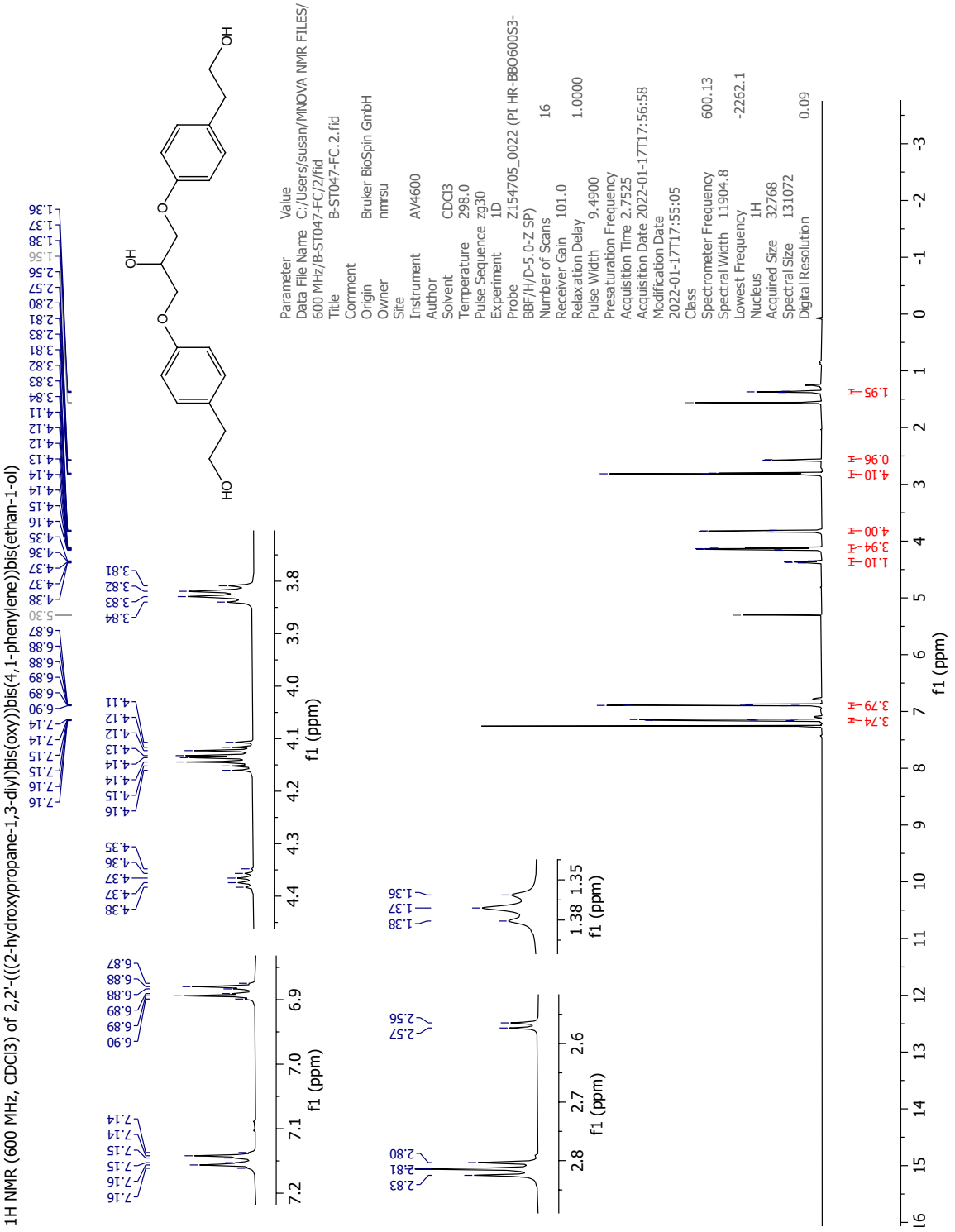

Figure A.45 ^{1}H NMR spectrum (600 MHz, $CDCl_3$) of 2,2'-(((2-hydroxypropane-1,3-diyl)bis(oxy))bis(4,1-phenylene))bis(ethan-1-ol) (**7b**). δ= 1.56 is water from the solvent, and δ= 5.30 is excess CH_2Cl_2.

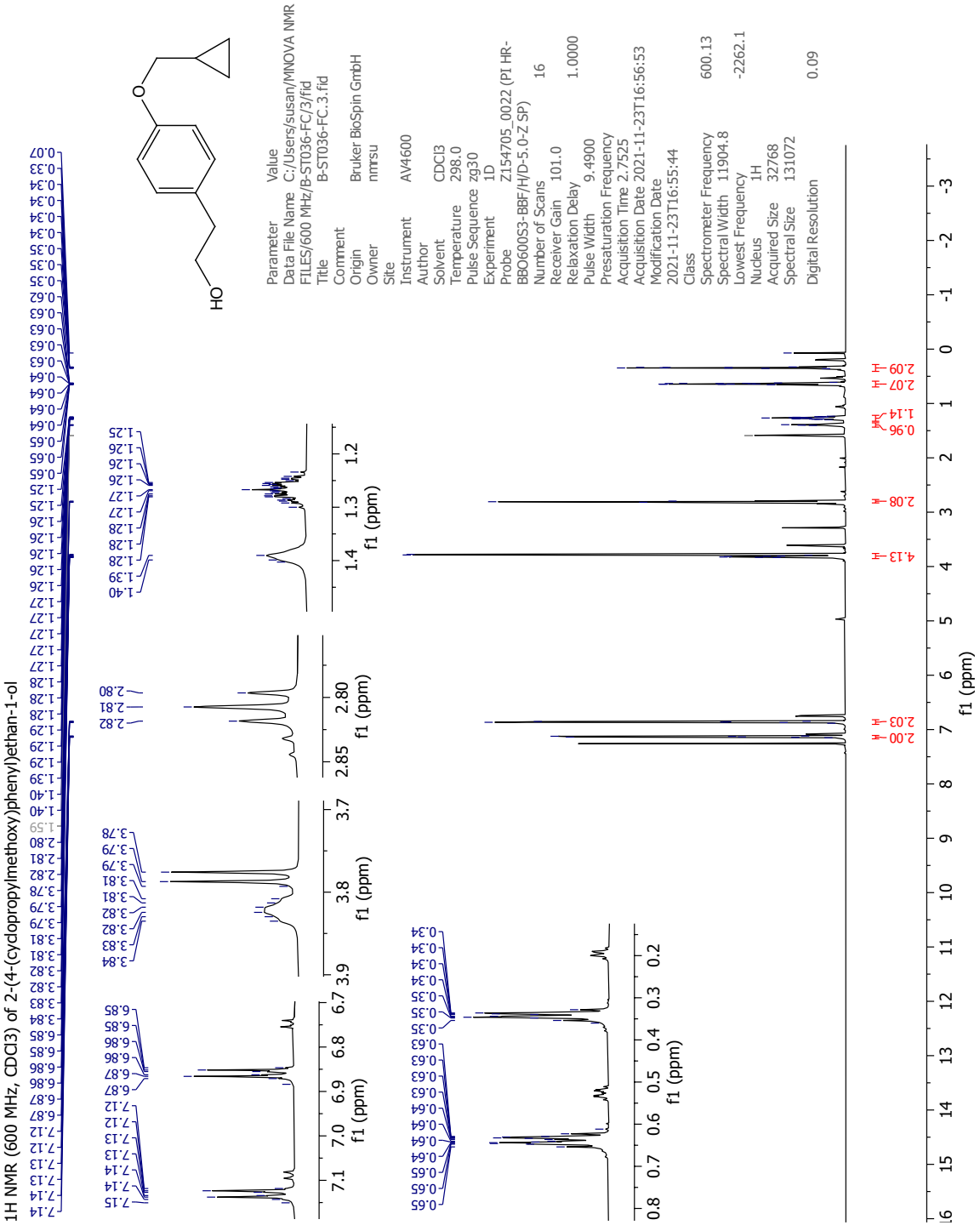

Figure A.46 ^{1}H NMR spectrum (600 MHz, $CDCl_3$) of 2-(4-(cyclopropylmethoxy)phenyl)ethan-1-ol (**2b**), with 87% purity.

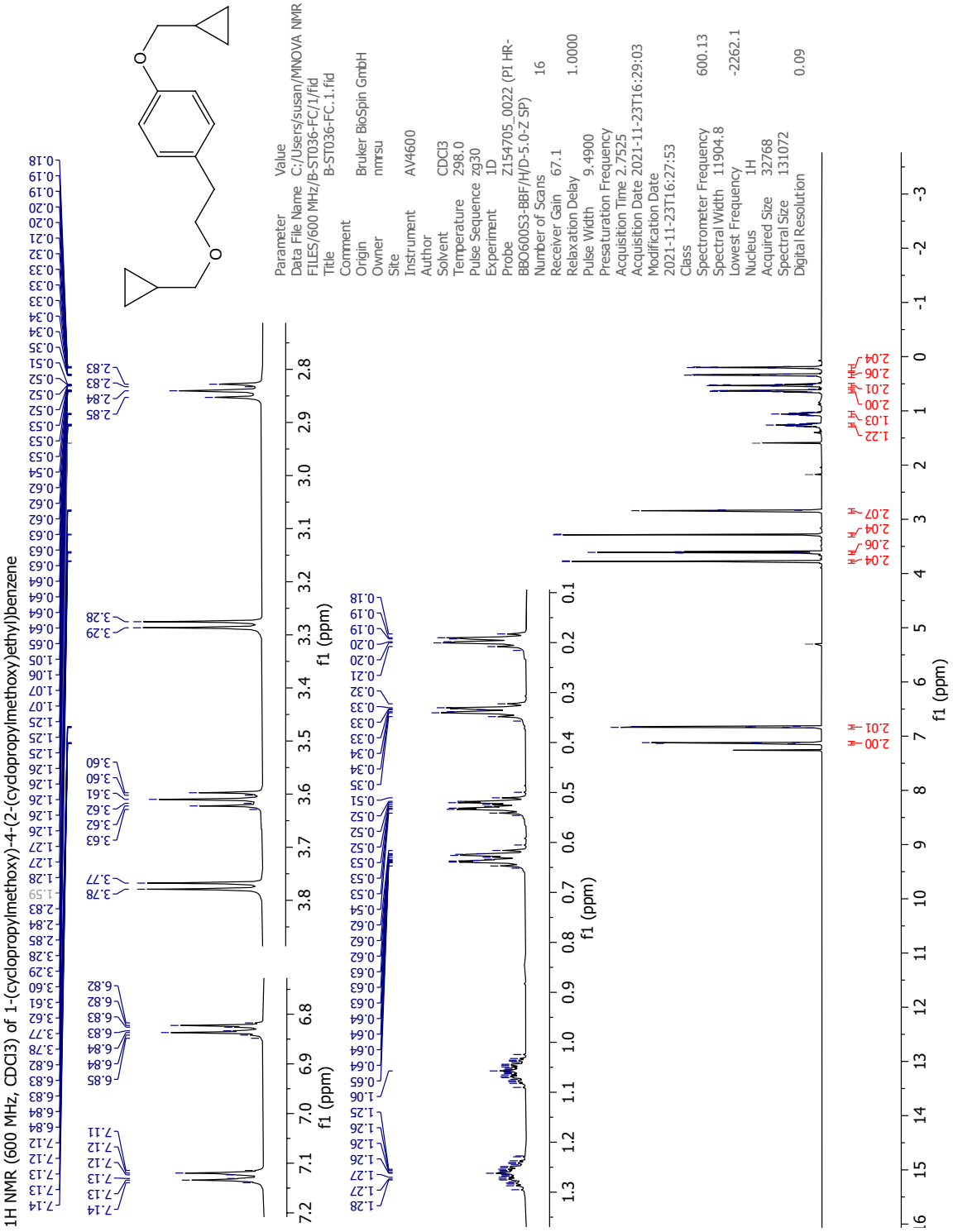

Figure A.47 ^{1}H NMR spectrum (600 MHz, $CDCl_3$) of 1-(cyclopropylmethoxy)-4-(2-(cyclopropylmethoxy)ethyl)benzene (**2c**), purity not determined.

A.13 HPLC blank analyses

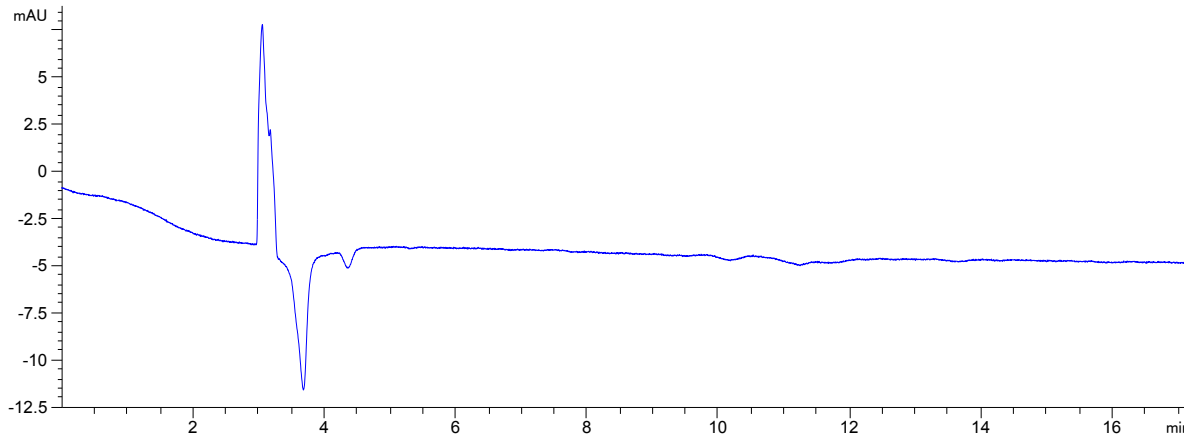

Figure A.48 Blank *i*-PrOH sample on Chiralcel OD-H column with mobile phase composition *n*-hexane:*i*-PrOH:diethylamine (90:19.8:0.2), and flow 1 mL min^{-1}.

B Analysis of compounds in the pathway to (*S*)-esmolol (15)

B.1 Characterization of methyl 3-(4-(oxiran-2-ylmethoxy)phenyl)propanoate (12)

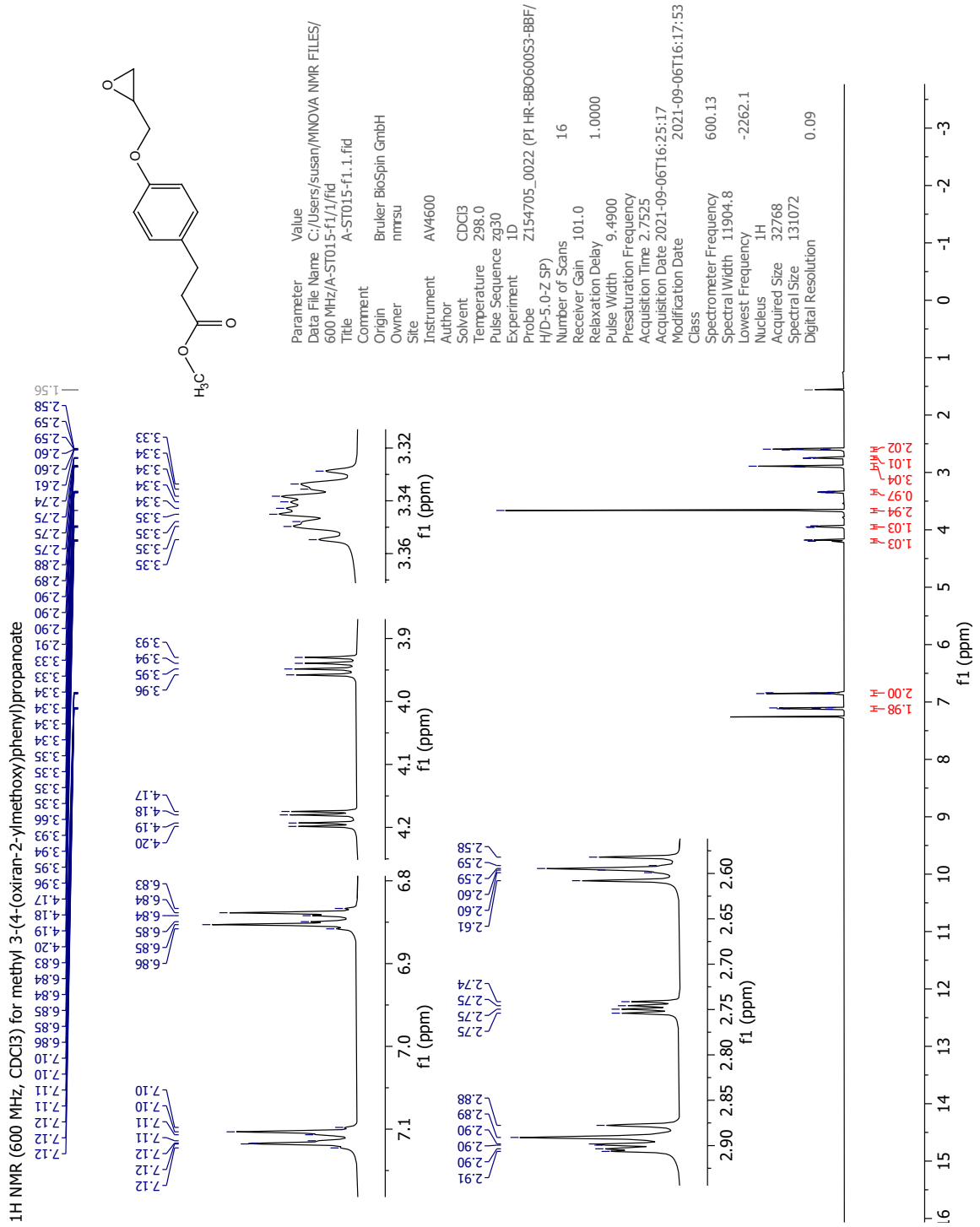

Figure B.1 ^{1}H NMR spectrum (600 MHz, $CDCl_3$) for methyl 3-(4-(oxiran-2-ylmethoxy)phenyl)propanoate (**12**). δ= 1.56 is water from the solvent.

B.2 Characterization of methyl 3-(4-(3-chloro-2-hydroxypropoxy)phenyl)propanoate (13)

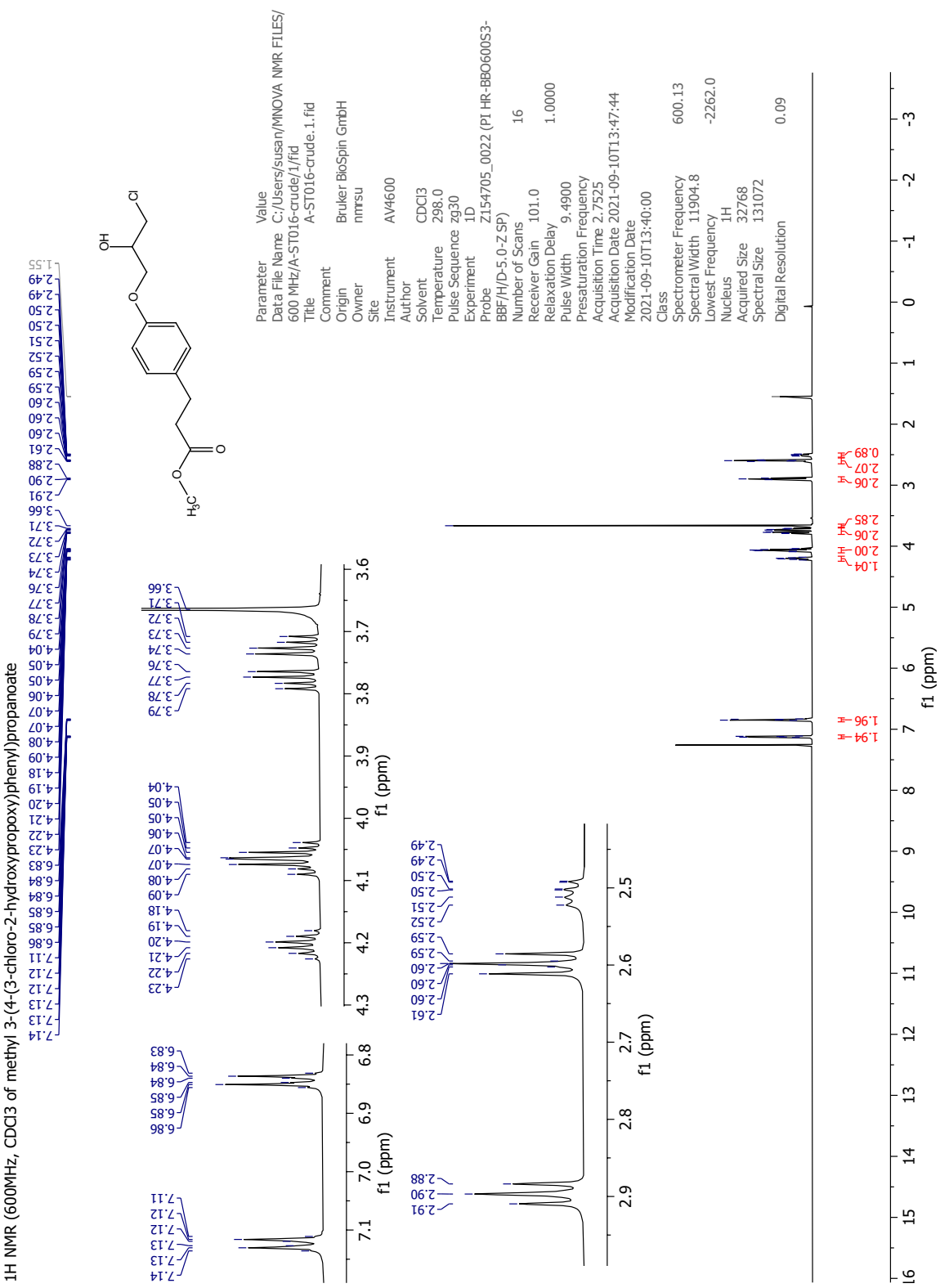

Figure B.2 ^{1}H NMR spectrum (600 MHz, $CDCl_3$) for methyl 3-(4-(3-chloro-2-hydroxypropoxy)phenyl)propanoate (**13**). δ= 1.55 is water from the solvent.

B.3 Characterization of 1-chloro-3-(4-(3-methoxy-3-oxopropyl)-phenoxy)propan-2-yl butyrate (14)

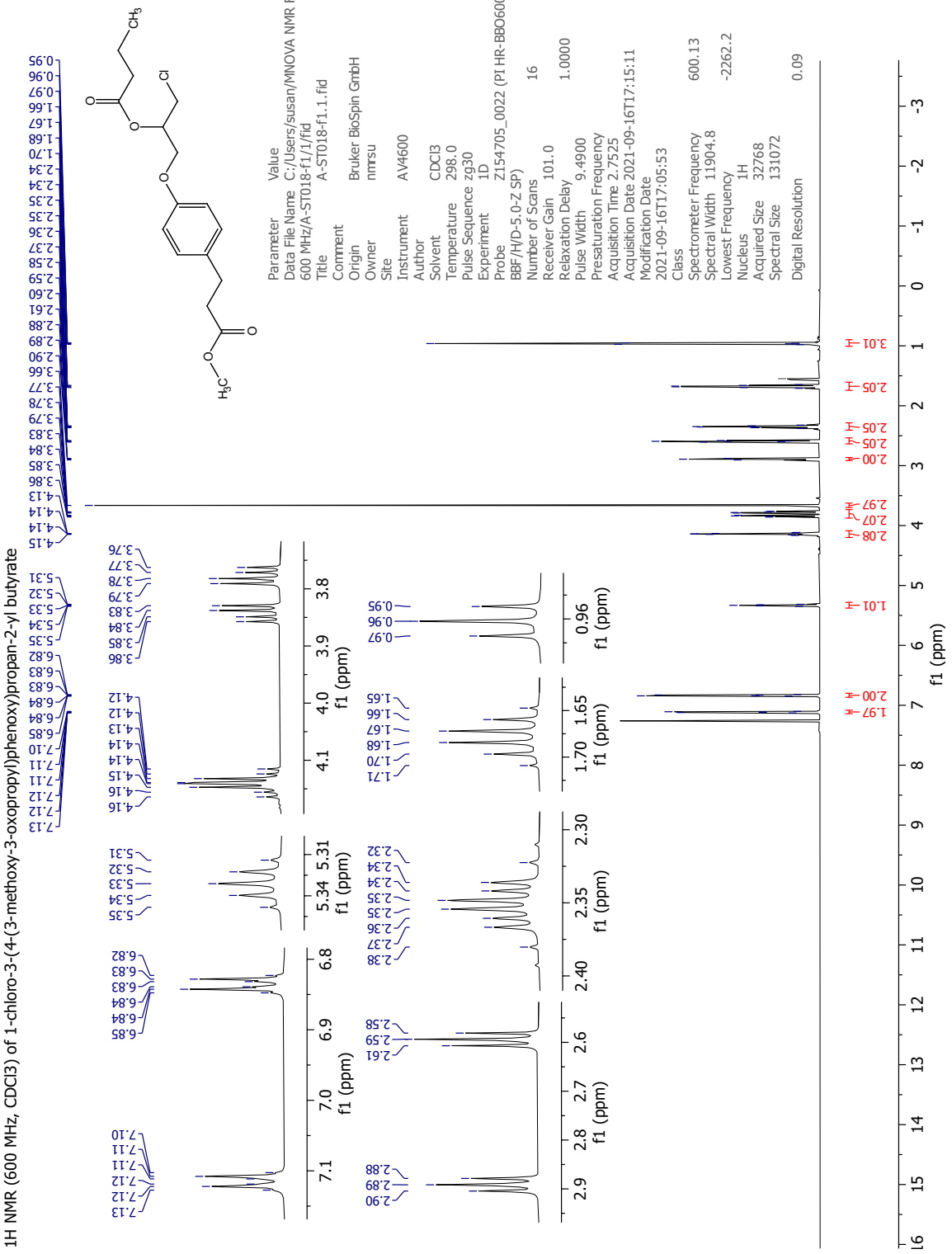

Figure B.3 ^{1}H NMR spectrum (600 MHz, $CDCl_3$) of 1-chloro-3-(4-(3-methoxy-3-oxopropyl)phenoxy)propan-2-yl butyrate (**14**). δ= 1.55 is water from the solvent.

B.4 Characterization of esmolol (15)

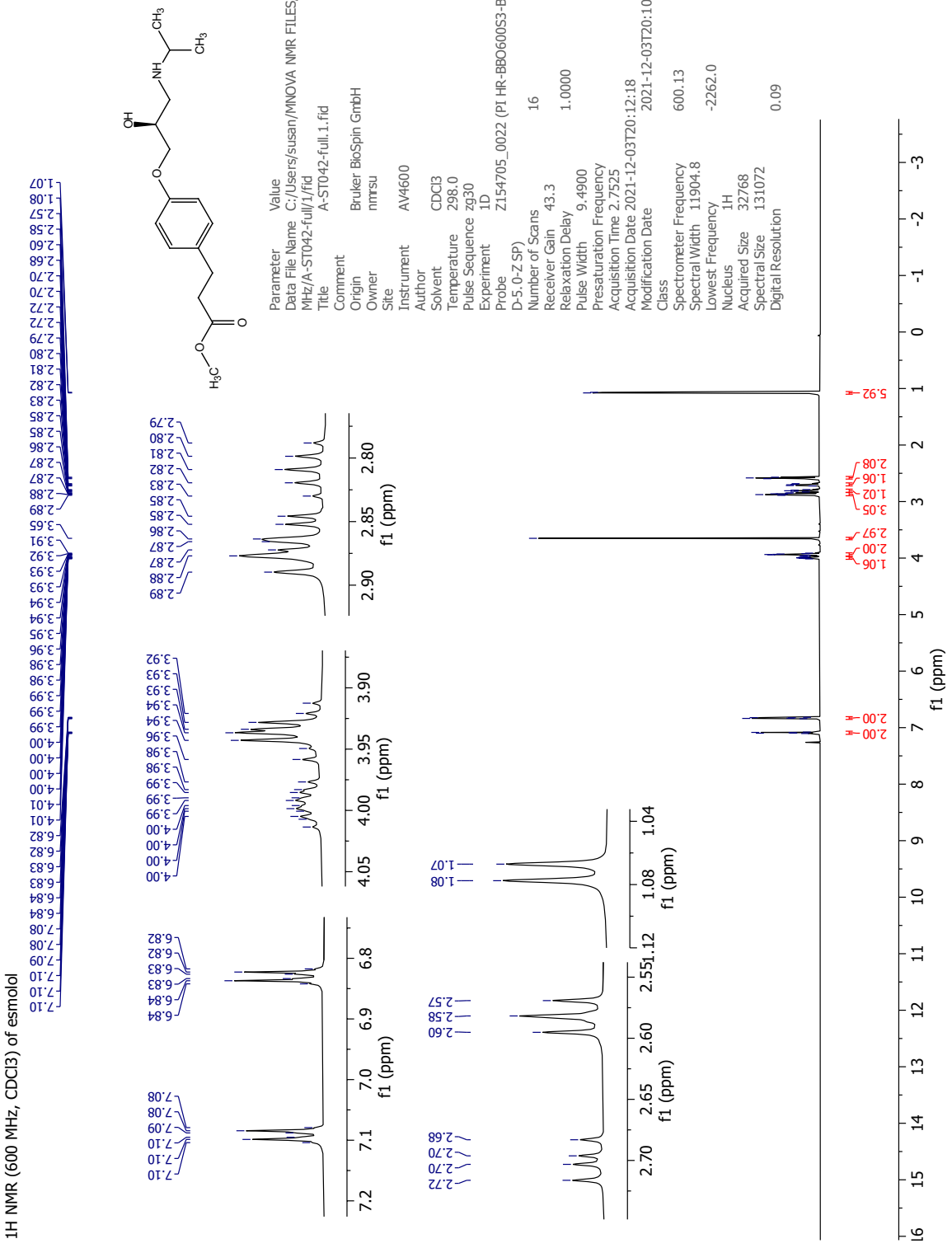

Figure B.4 ^{1}H NMR spectrum (600 MHz, $CDCl_3$) for esmolol (**15**).

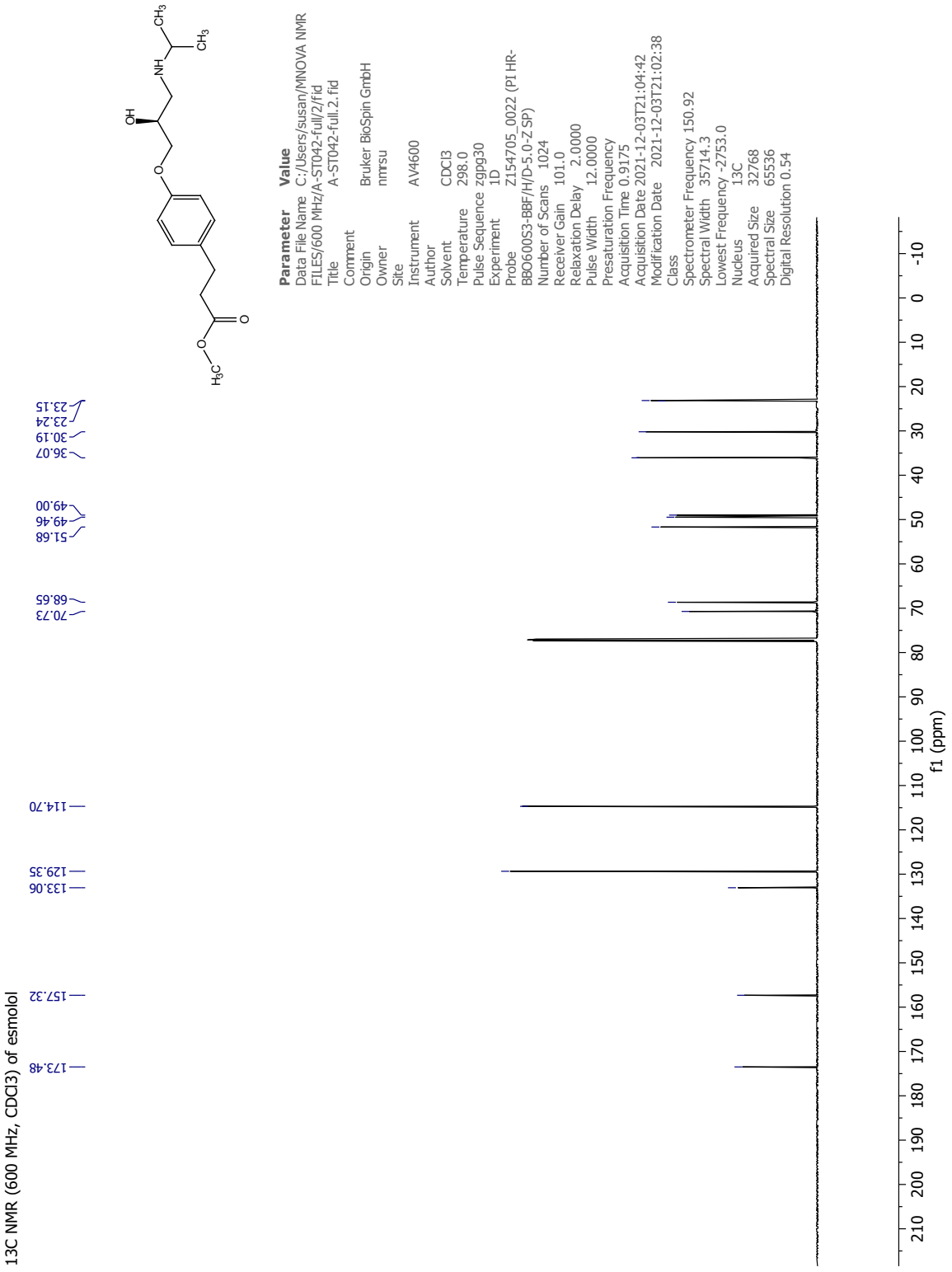

Figure B.5 ^{13}C NMR spectrum (150 MHz, $CDCl_3$) for esmolol (**15**).

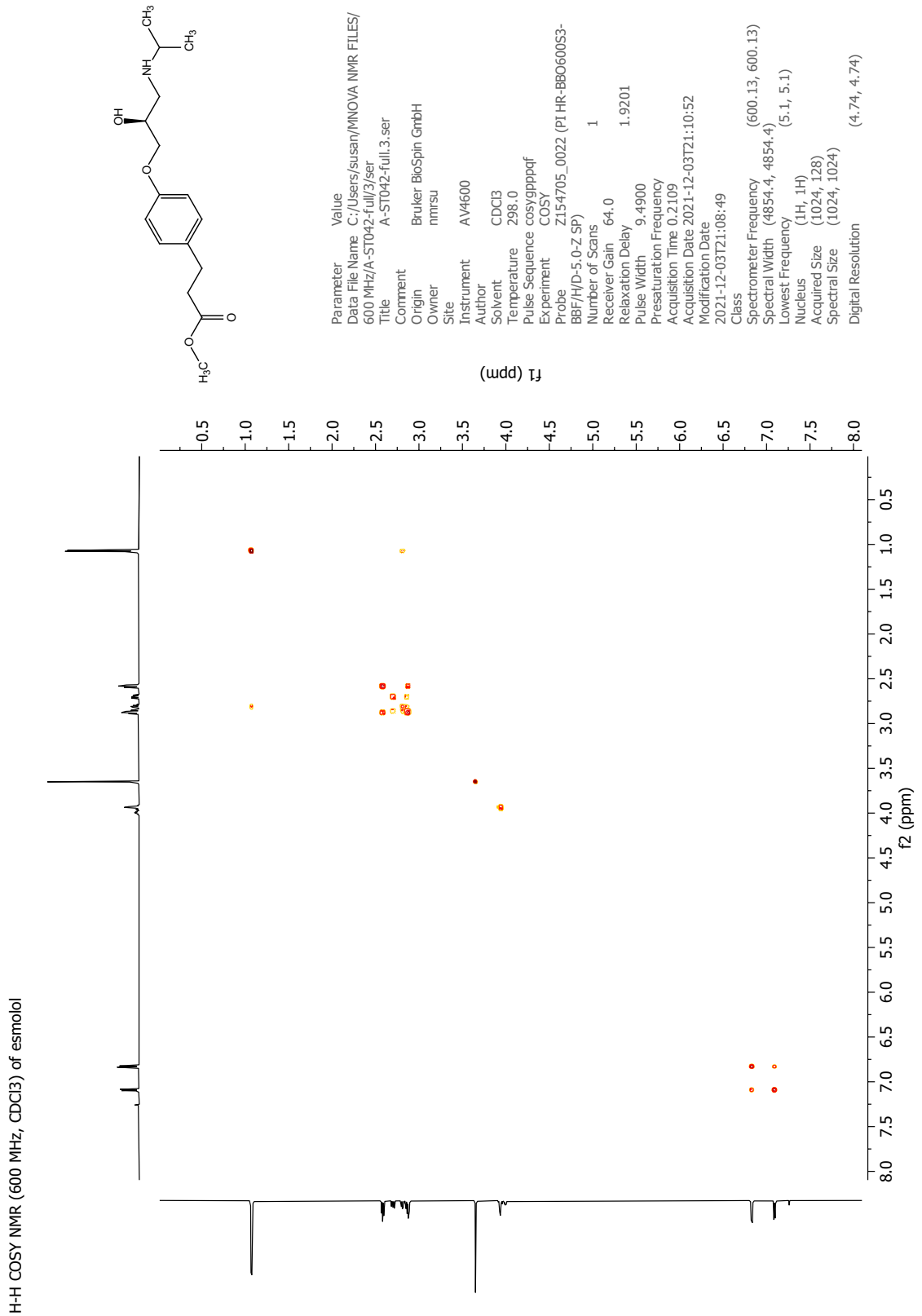

Figure B.6 COSY NMR spectrum (600 MHz, $CDCl_3$) for esmolol (**15**).

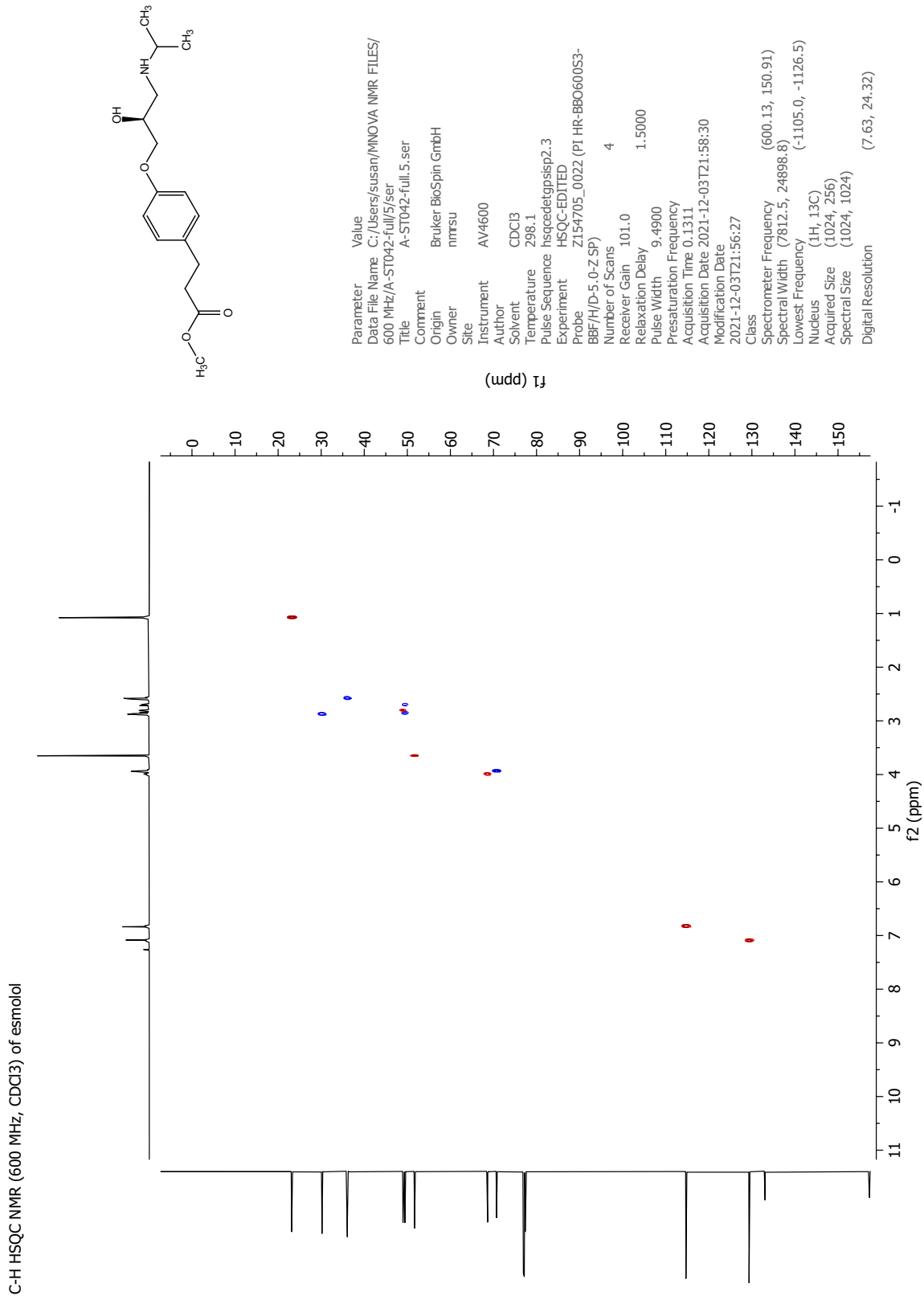

Figure B.7 HSQC NMR spectrum (600 MHz, $CDCl_3$) for esmolol (**15**).

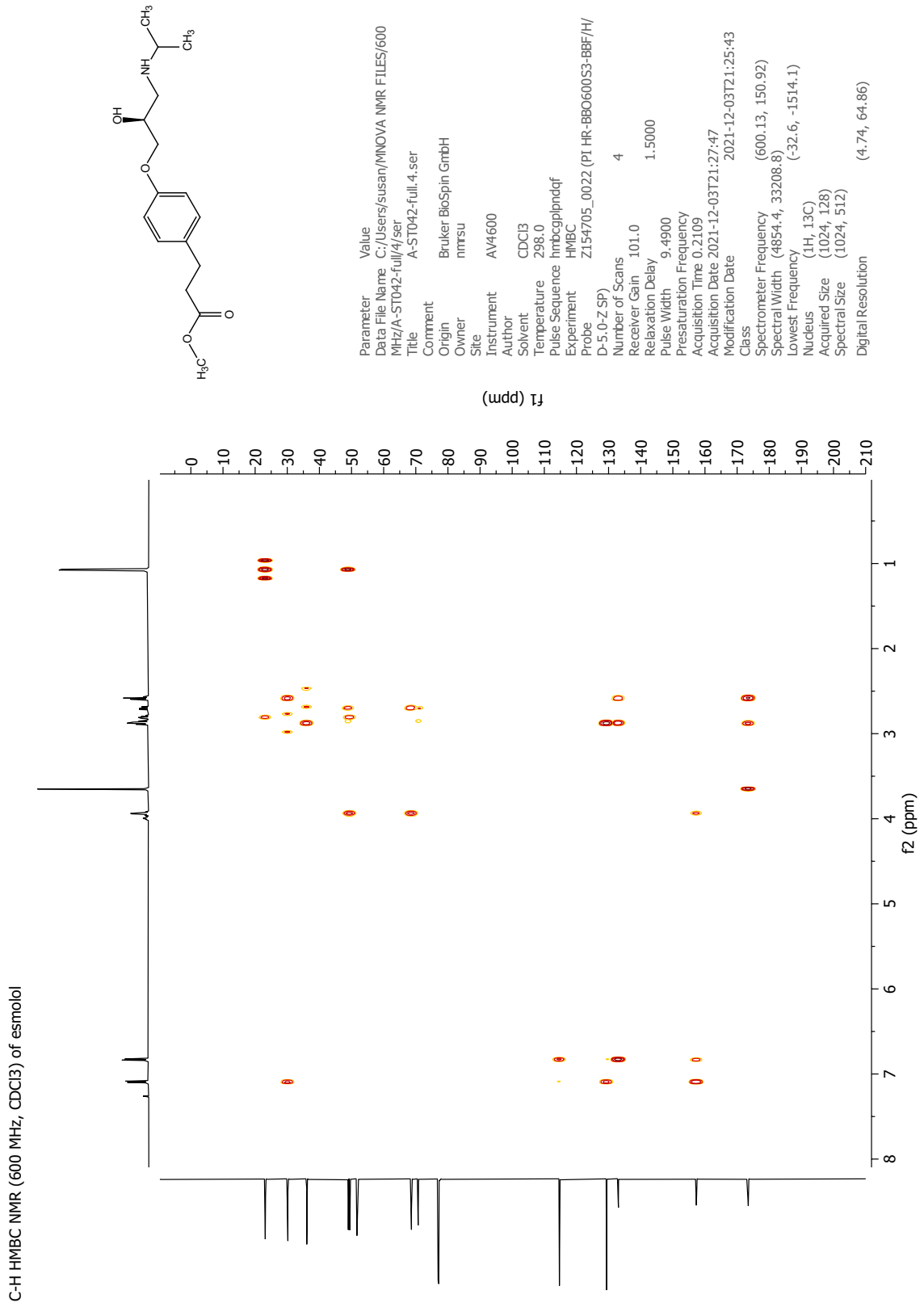

Figure B.8 HMBC NMR spectrum (600 MHz, $CDCl_3$) for esmolol (**15**).

C Analysis of compounds related to limonene

C.1 GC-MS analysis of perillyl acetate (18)

```
File       :D:\ikj\20210326SHT\20210326_ST003.D
Operator   : svg
Acquired   : 26 Mar 2021   9:41     using AcqMethod SHT_2021.M
Instrument :    GCMS2
Sample Name: ST003_DILUTED
Misc Info  :
Vial Number: 85
```

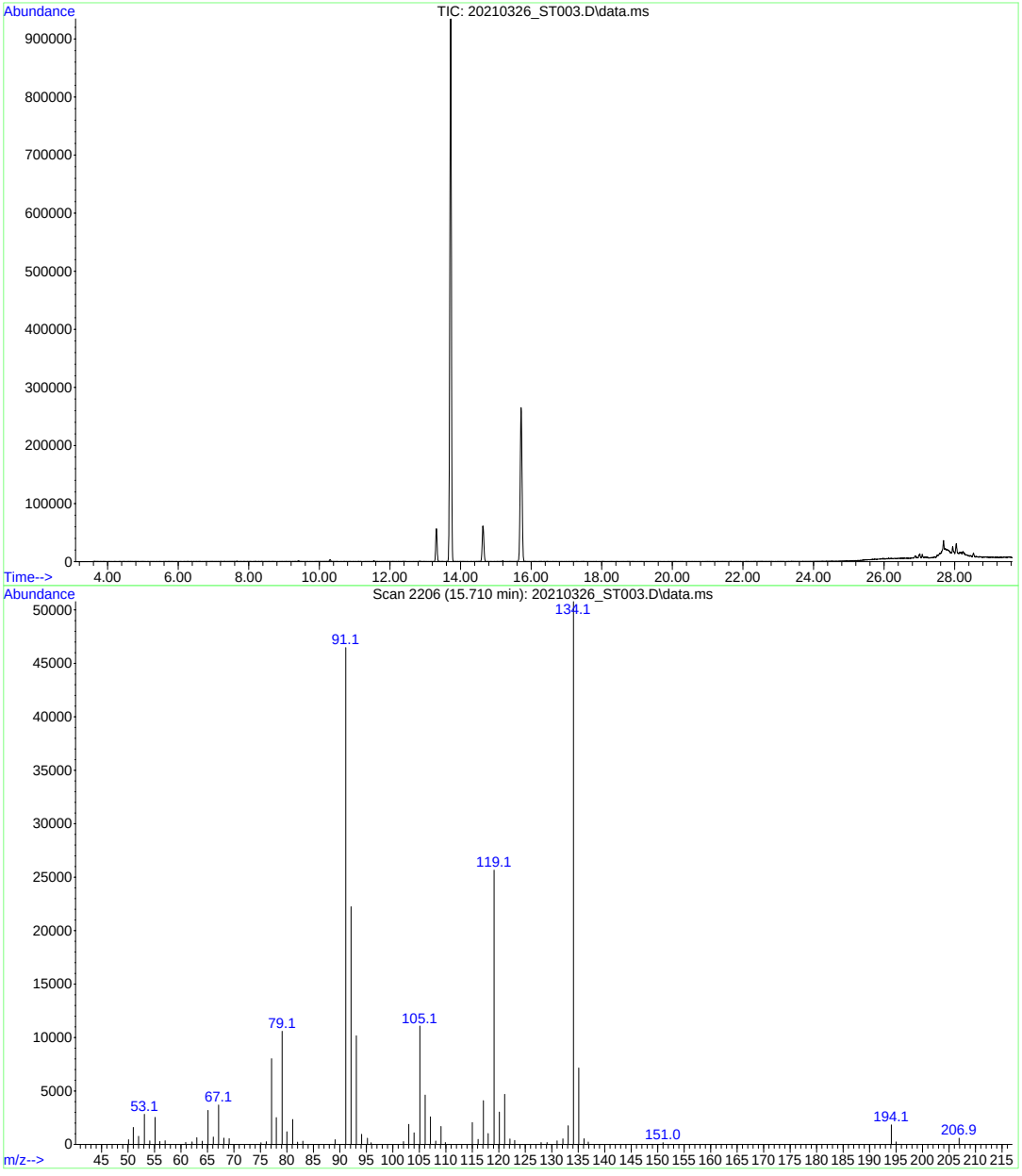

Figure C.1 GC-MS chromatogram (top) and MS spectrum (bottom) recorded for **18**.

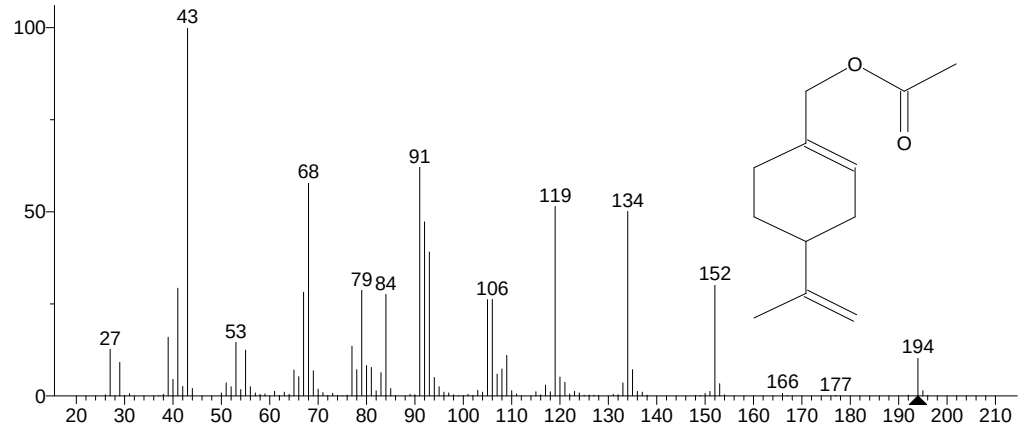

(mainlib) 1-Cyclohexene-1-methanol, 4-(1-methylethenyl)-, acetate

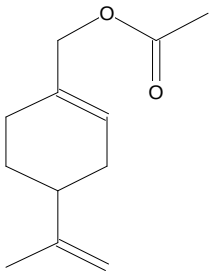

Name: 1-Cyclohexene-1-methanol, 4-(1-methylethenyl)-, acetate
Formula: $C_{12}H_{18}O_2$
MW: 194 CAS#: 15111-96-3 NIST#: 163741 ID#: 9051 DB: mainlib
Other DBs: TSCA, EINECS
Contributor: Chemical Concepts
10 largest peaks:

43 999 |	91 621 |	68 579 |	119 514 |	134 501 |	92 472 |	93 390 |	152 302 |	41 292 |	79 287 |

108 m/z Values and Intensities:

26	3 |	27	126 |	29	91 |	30	1 |	31	6 |	37	Tr |	38	4 |	39	159 |	40	45 |	41	292 |
42	26 |	43	999 |	44	20 |	50	8 |	51	35 |	52	25 |	53	146 |	54	17 |	55	124 |	56	25 |
57	8 |	58	4 |	59	5 |	61	12 |	62	1 |	63	10 |	64	4 |	65	70 |	66	52 |	67	281 |
68	579 |	69	68 |	70	18 |	71	9 |	72	Tr |	73	7 |	74	Tr |	75	Tr |	76	2 |	77	135 |
78	71 |	79	287 |	80	82 |	81	77 |	82	14 |	83	63 |	84	276 |	85	20 |	86	1 |	89	4 |
90	3 |	91	621 |	92	472 |	93	390 |	94	50 |	95	25 |	96	10 |	97	8 |	98	3 |	99	Tr |
100	Tr |	101	4 |	102	1 |	103	15 |	104	10 |	105	261 |	106	262 |	107	59 |	108	73 |	109	110 |
110	14 |	111	5 |	115	11 |	116	3 |	117	29 |	118	11 |	119	514 |	120	51 |	121	37 |	122	5 |

Figure C.2 NIST MS 2.0 library search results for the spectrum shown in Figure C.1.

C.2 Characterization of perillyl acetate (18)

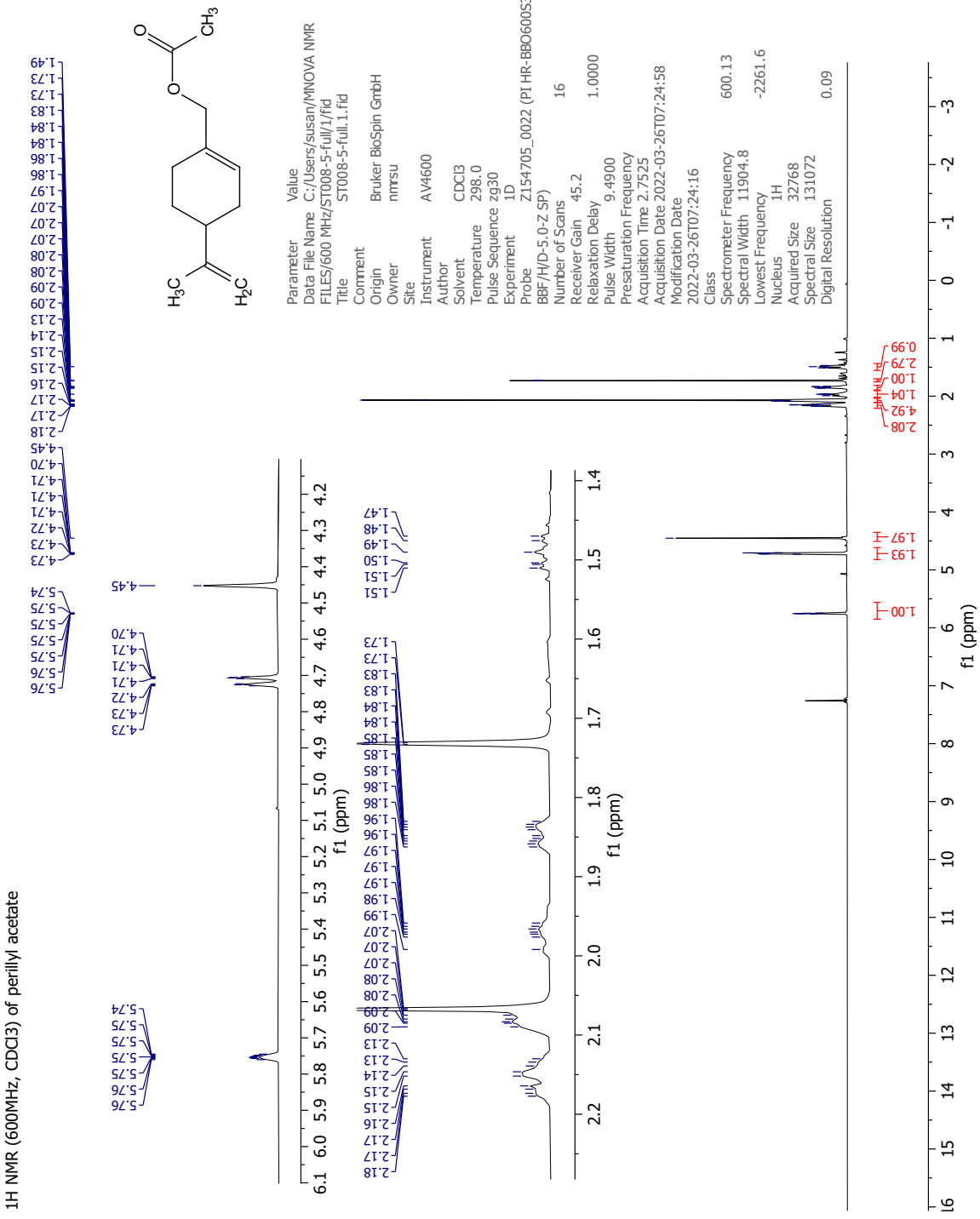

Figure C.3 ^{1}H NMR spectrum (600 MHz, $CDCl_3$) of perillyl acetate (**18**).

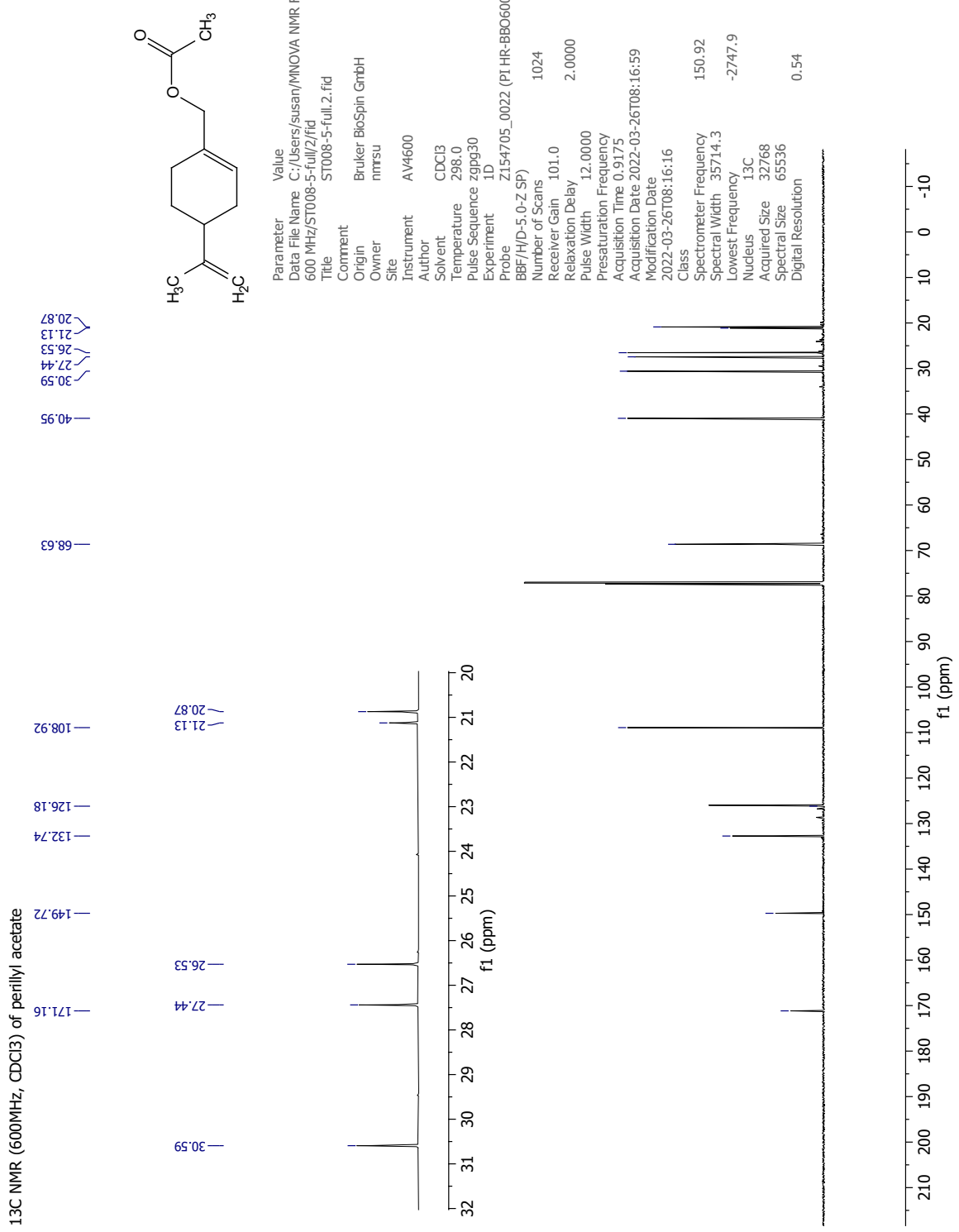

Figure C.4 ^{13}C NMR spectrum (150 MHz, $CDCl_3$) of perillyl acetate (**18**).

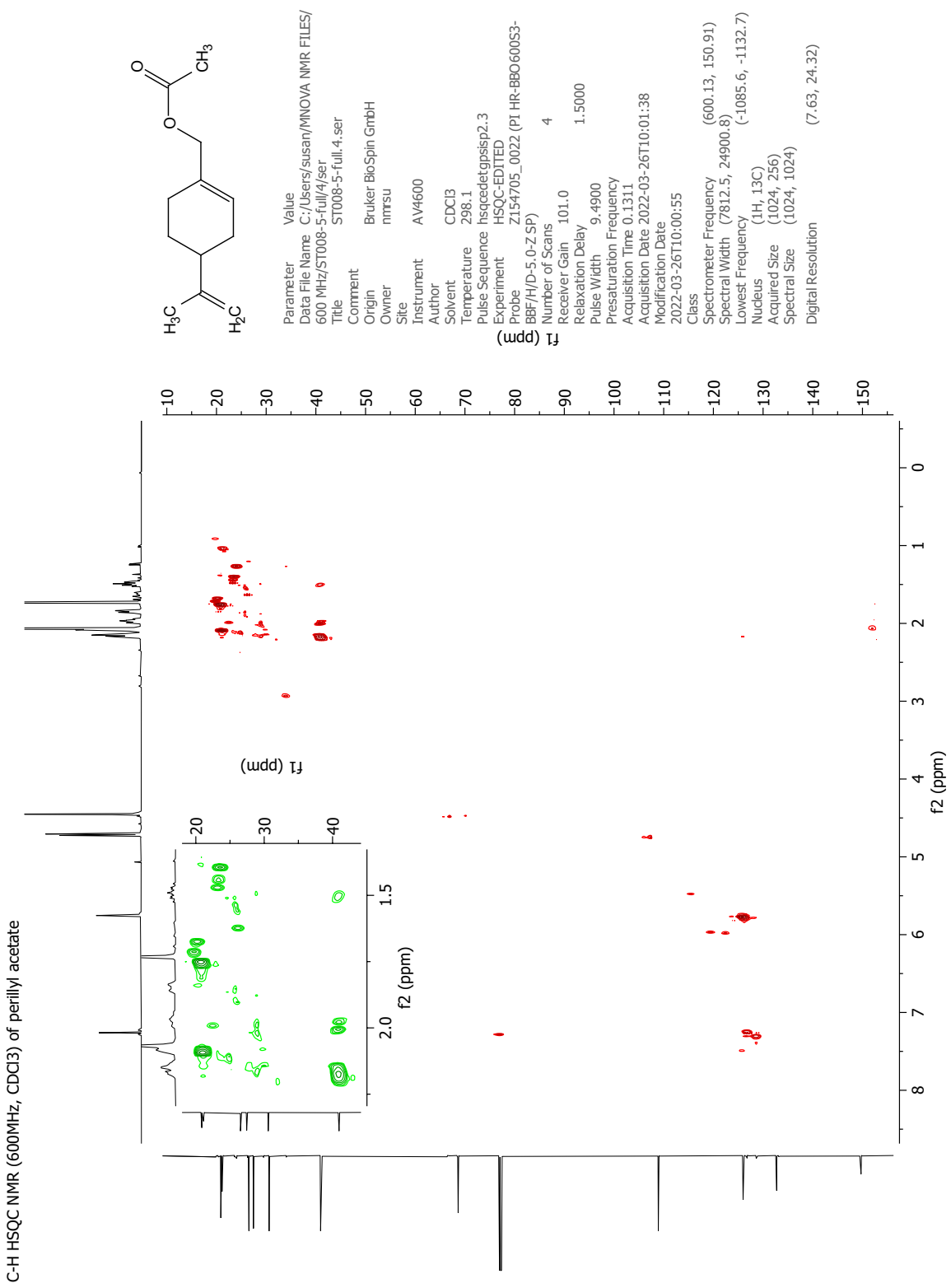

Figure C.5 HSQC NMR spectrum (600 MHz, $CDCl_3$) of perillyl acetate (**18**).

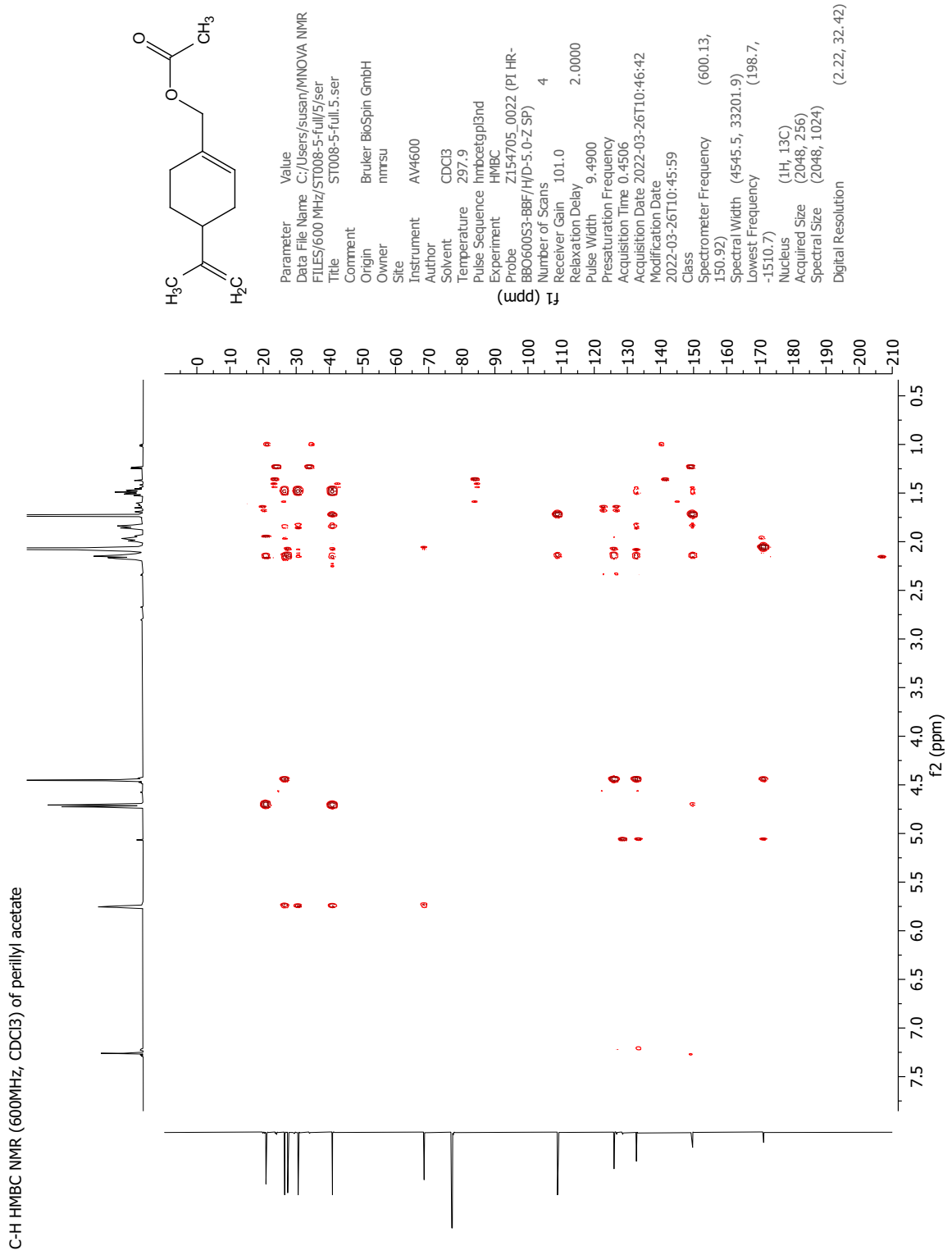

Figure C.6 HMBC NMR spectrum (600 MHz, $CDCl_3$) of perillyl acetate (**18**).

C.3 GC analysis of standard limonene derivatives

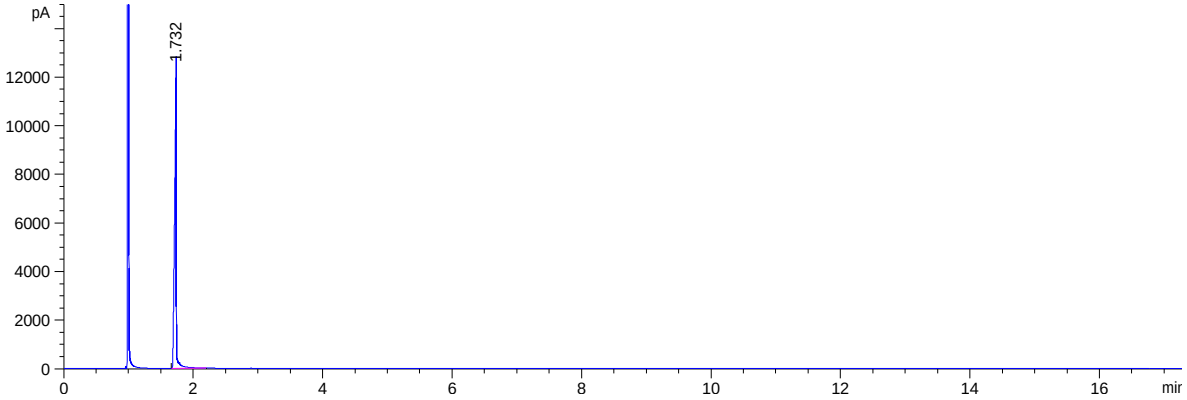

Figure C.7 GC chromatogram of limonene (**16**) in EtOAc recorded using GC method A.

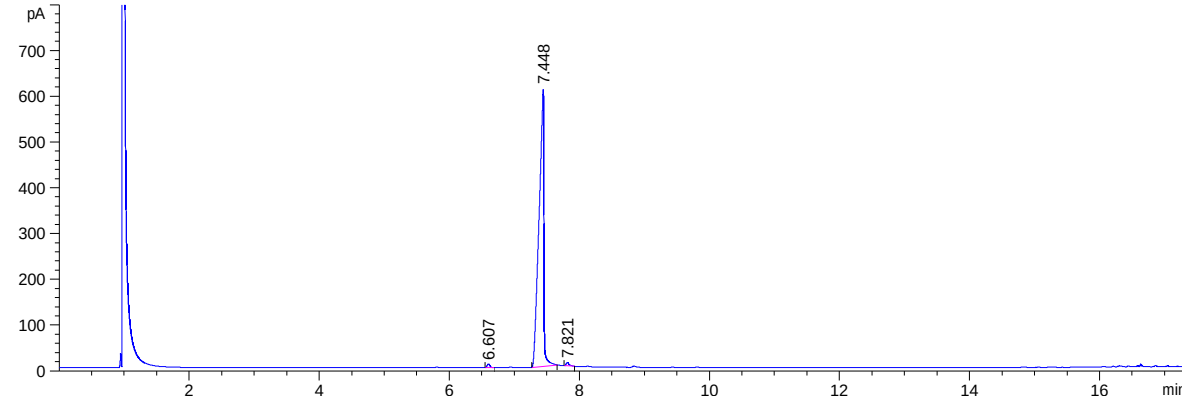

Figure C.8 GC chromatogram of perillyl alcohol (**17**) in EtOAc recorded using GC method A.

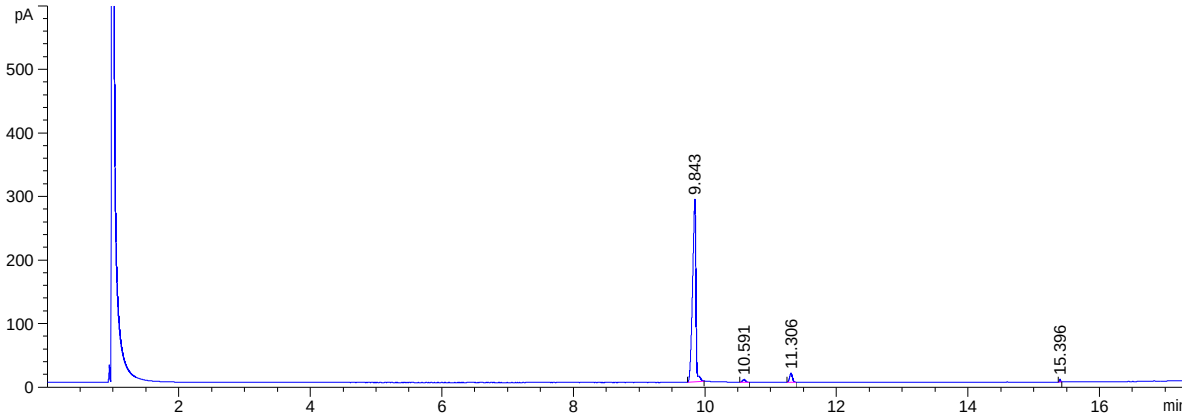

Figure C.9 GC chromatogram of perillyl acetate (**18**) in EtOAc recorded using GC method A.

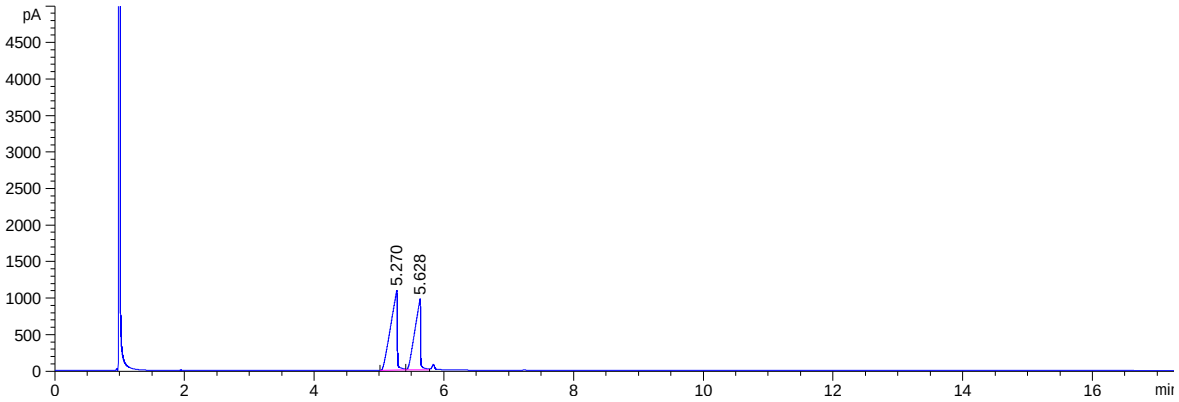

Figure C.10 GC chromatogram of *cis/trans*-carveol (**19**) in EtOAc recorded using GC method A.

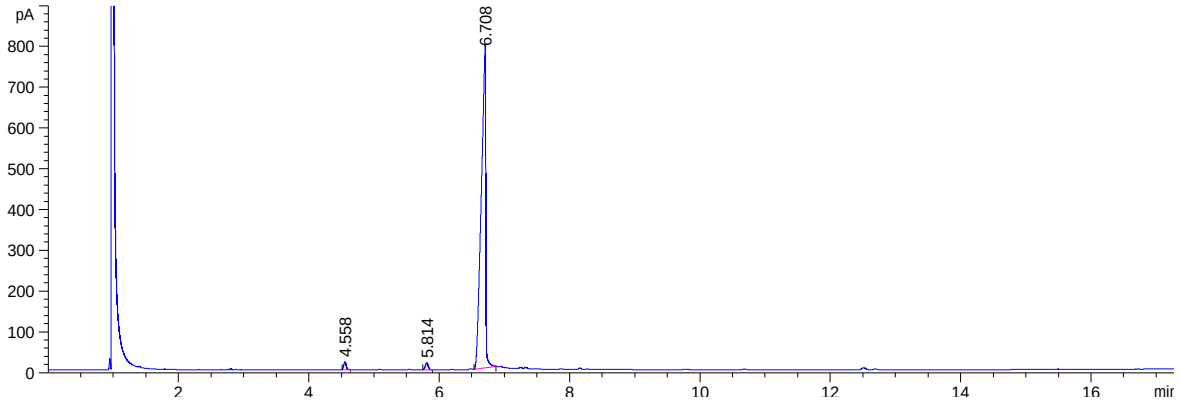

Figure C.11 GC chromatogram of perillaldehyde (**20**) in EtOAc recorded using GC method A.

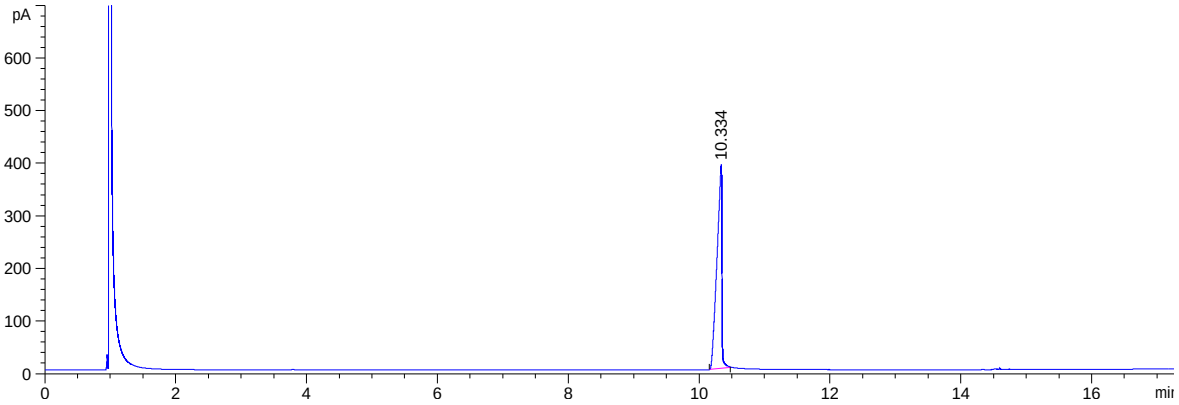

Figure C.12 GC chromatogram of limonene-1,2-diol (**21**) in EtOAc recorded using GC method A.

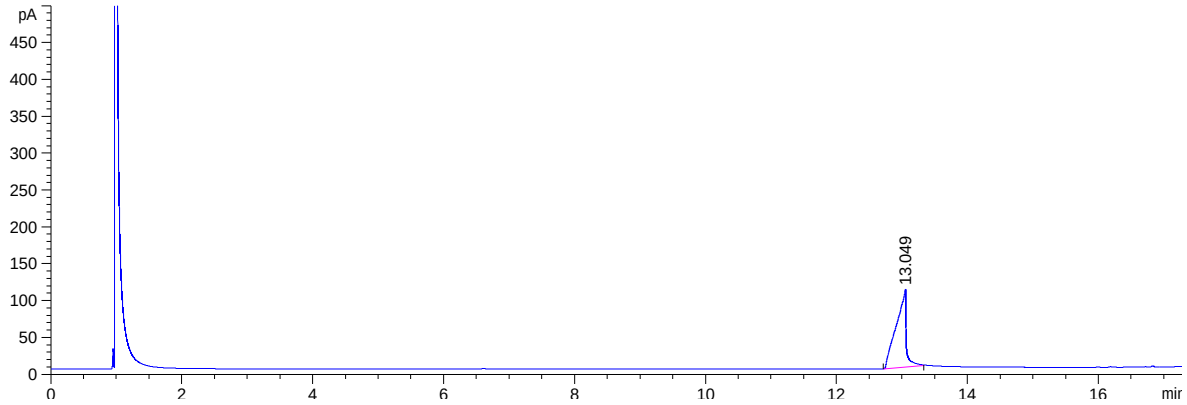

Figure C.13 GC chromatogram of perillic acid (**22**) in EtOAc recorded using GC method A.

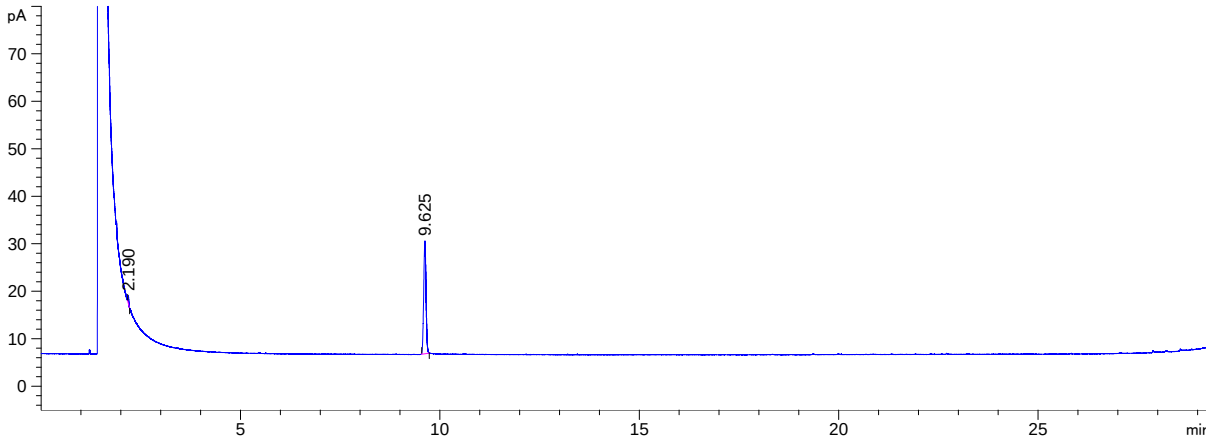

Figure C.14 GC chromatogram of limonene (**16**) in EtOAc recorded using GC method B. The sample was obtained by extraction of limonene from buffer/DMSO solution and washing with water (5 × 5 mL).

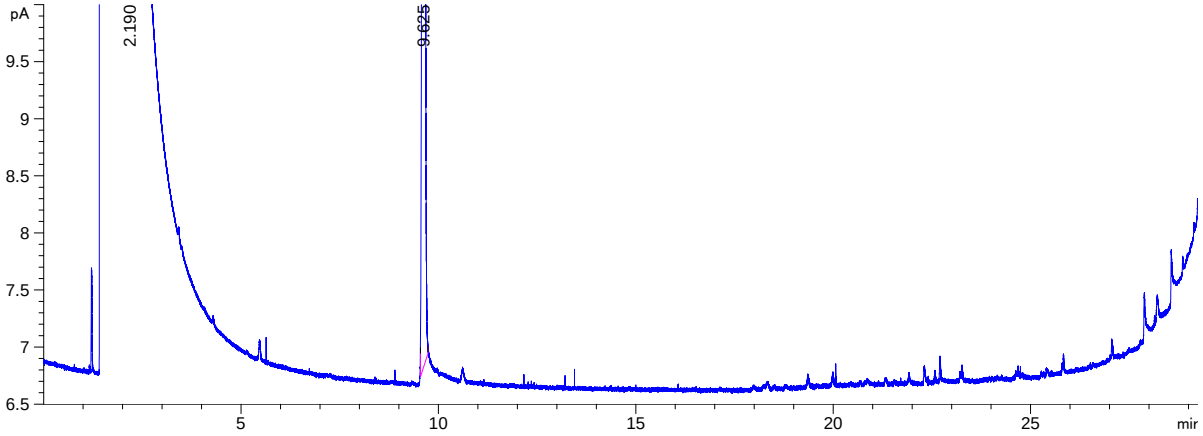

Figure C.15 Zoomed version of GC chromatogram shown in Figure C.14.

C.4 GC-MS analysis of 1-methyl-4-(prop-1-en-2-yl)benzene (16b)

```
File       :D:\ikj\SHT2021\20210422_SHT_DILUTED.D
Operator   : SVG
Acquired   : 22 Apr 2021  14:09     using AcqMethod SHT_2021.M
Instrument :    GCMS2
Sample Name: ST003 DILUTED
Misc Info  :
Vial Number: 86
```

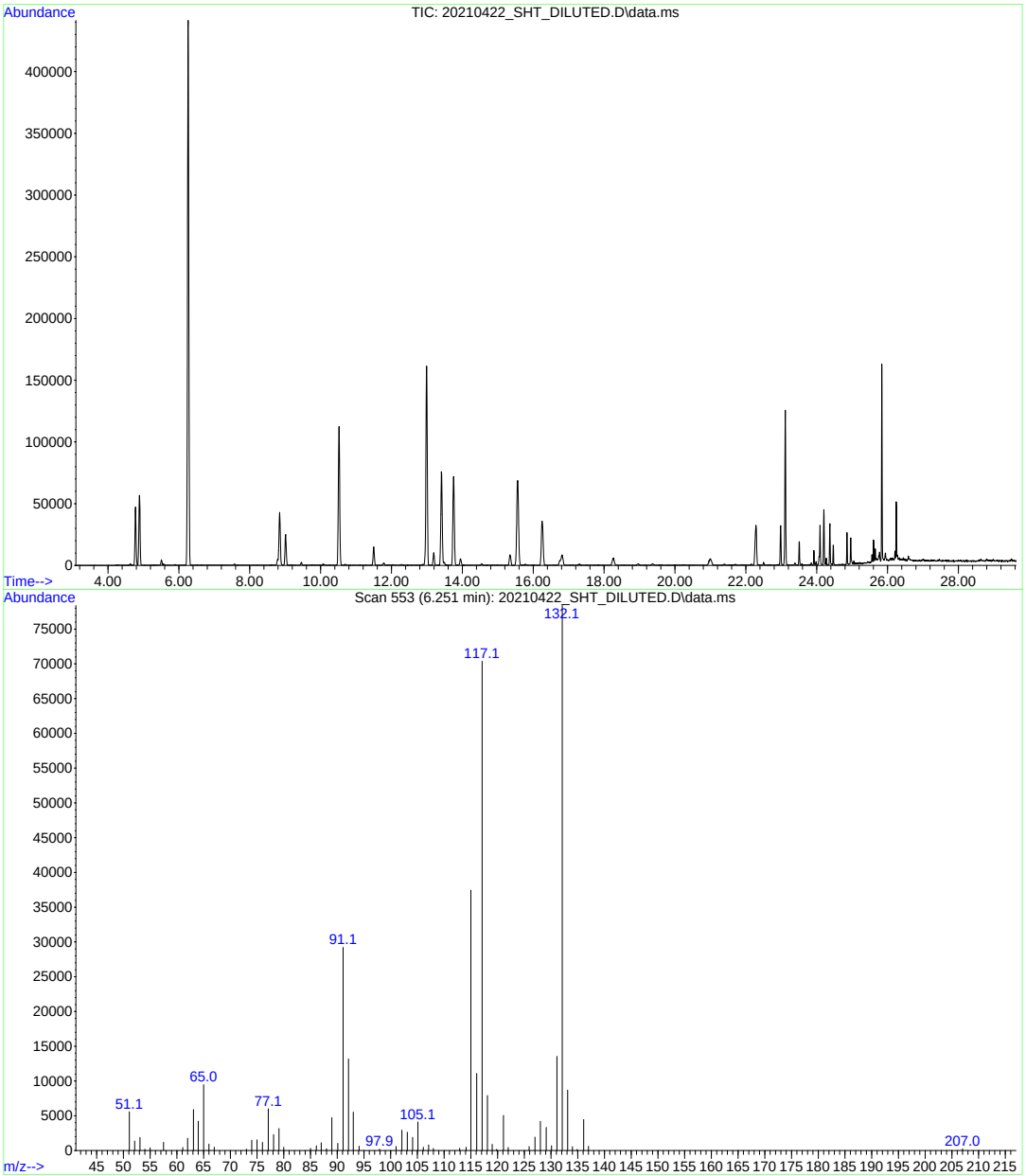

Figure C.16 GC-MS chromatogram (top) and MS spectrum (bottom) recorded for **16b**.

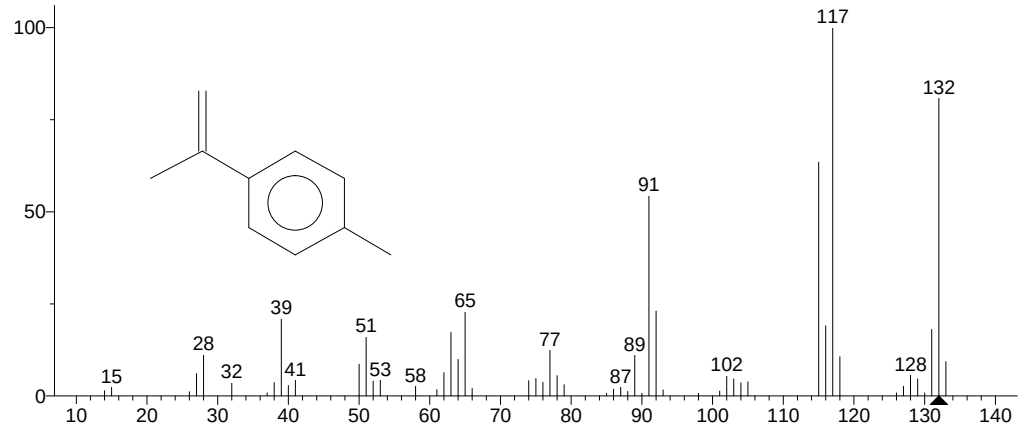

(mainlib) Benzene, 1-methyl-4-(1-methylethenyl)-

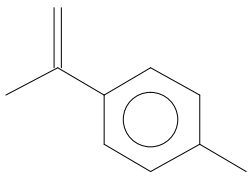

Name: Benzene, 1-methyl-4-(1-methylethenyl)-
Formula: $C_{10}H_{12}$
MW: 132 CAS#: 1195-32-0 NIST#: 113953 ID#: 70549 DB: mainlib
Other DBs: Fine, TSCA, HODOC, EINECS, IRDB
Contributor: NIST Mass Spectrometry Data Center, 1990.
10 largest peaks:

117 999	132 807	115 634	91 543	92 230	65 228	39 209	116 190	131 180	63 172

55 m/z Values and Intensities:

14	14	15	23	26	11	27	60	28	112	32	36	37	8	38	36	39	209	40	28
41	42	50	86	51	161	52	40	53	42	58	27	61	17	62	63	63	172	64	99
65	228	66	20	74	41	75	47	76	37	77	124	78	55	79	30	85	7	86	18
87	24	88	12	89	110	90	7	91	543	92	230	93	16	98	7	101	13	102	55
103	46	104	35	105	38	115	634	116	190	117	999	118	106	126	8	127	26	128	56
129	46	130	8	131	180	132	807	133	93										

Synonyms:
1.Styrene, p,.alpha.-dimethyl-

Figure C.17 NIST MS 2.0 library search results for the spectrum shown in Figure C.16.

C.5 GC-MS analysis of degradation products from CYP 2C19

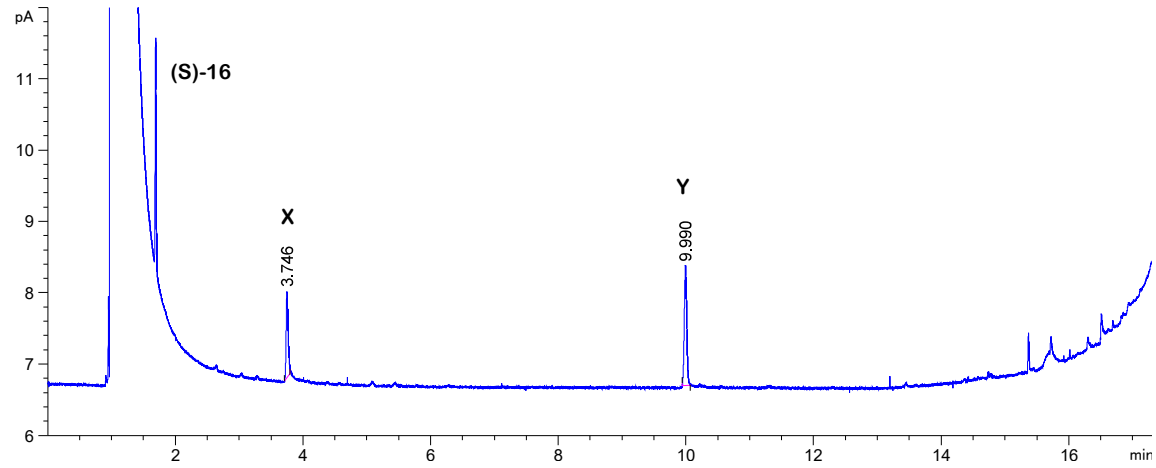

Figure C.18 GC chromatogram from CYP 2C19 oxidation of (*S*)-limonene ((*S*)-**16**) after 14 days reaction time, using GC method 1, with $t_R(\mathbf{X}) = 3.75$ min and $t_R(\mathbf{Y}) = 9.99$ min.

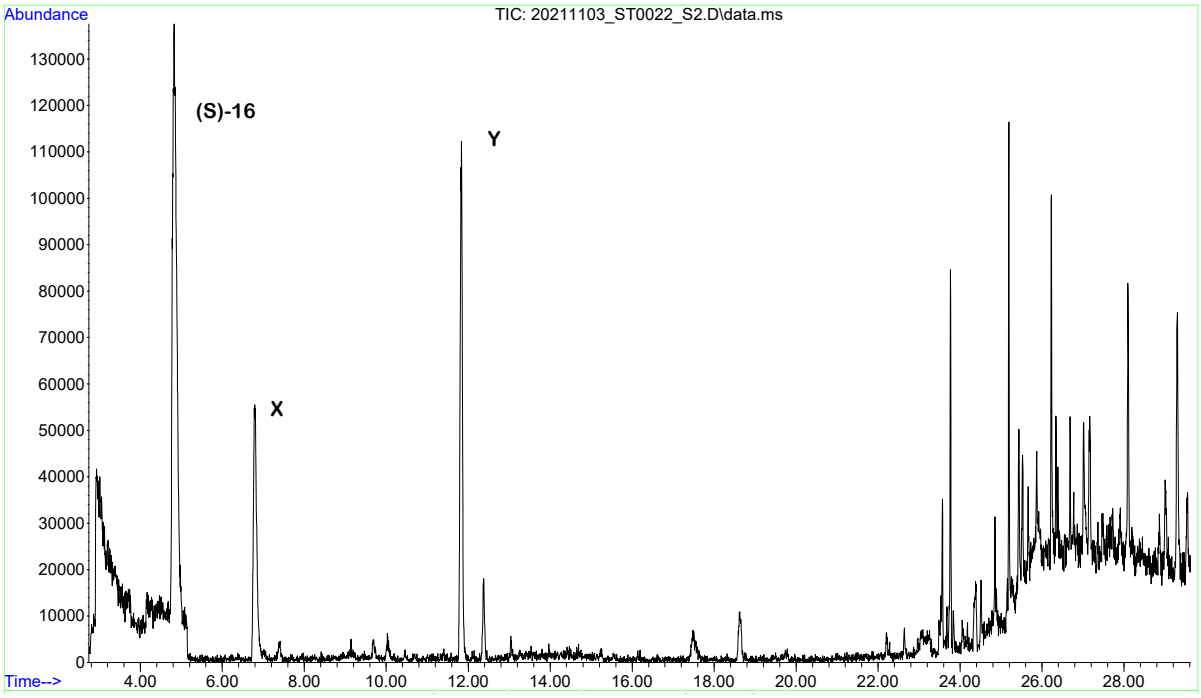

Figure C.19 GC-MS chromatogram recorded from CYP 2C19 oxidation of (*S*)-limonene ((*S*)-**16**) after 14 days reaction time.

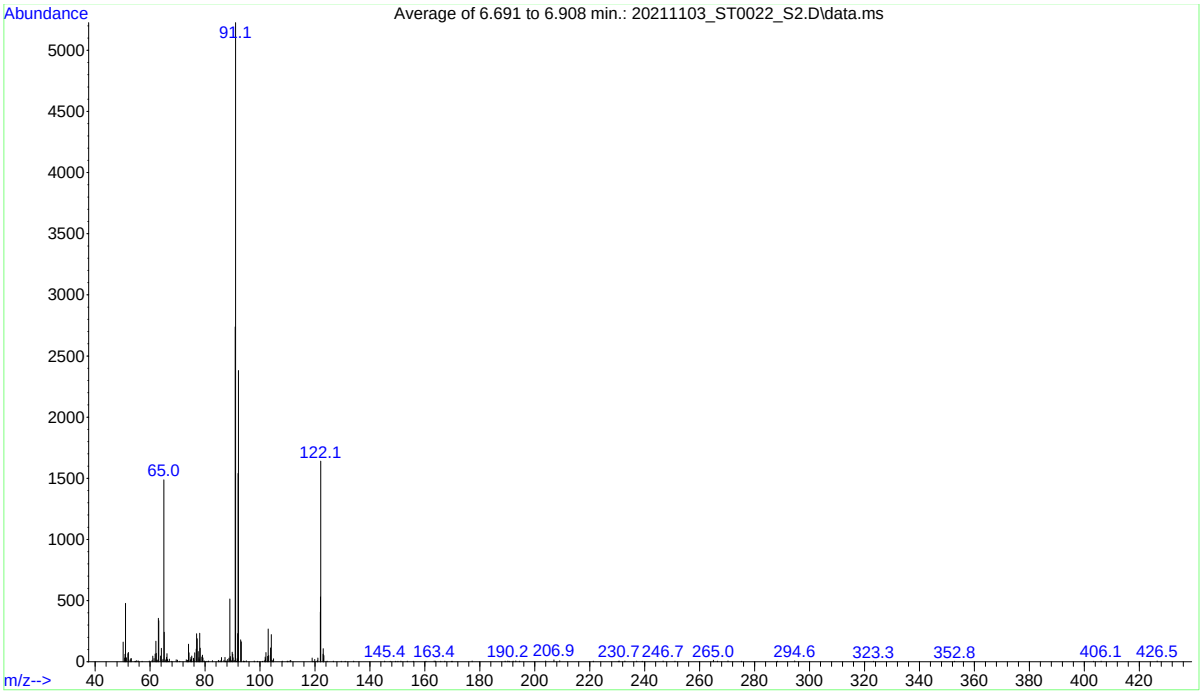

Figure C.20 MS spectrum recorded for **X** at $t_R(\mathbf{X}) = 6.8$ min in Figure C.19.

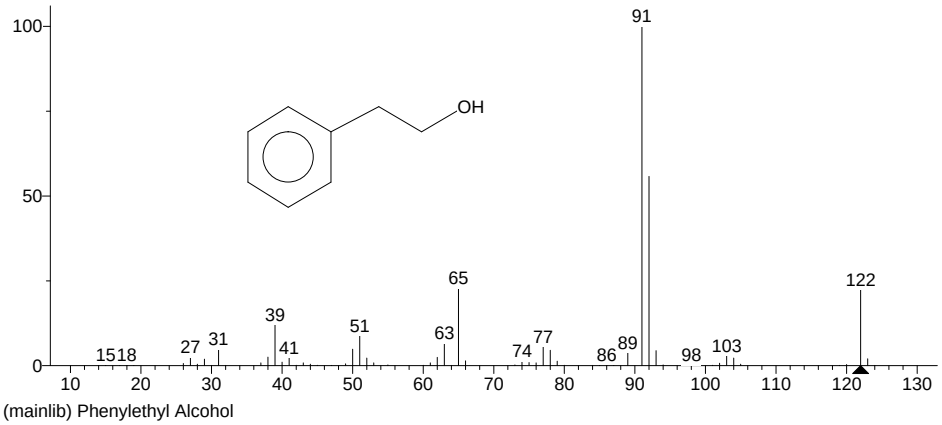

(mainlib) Phenylethyl Alcohol

Name: Phenylethyl Alcohol
Formula: $C_8H_{10}O$
MW: 122 CAS#: 60-12-8 NIST#: 229405 ID#: 11320 DB: replib
Other DBs: Fine, TSCA, RTECS, EPA, USP, HODOC, NIH, EINECS, IRDB
Contributor: Japan AIST/NIMC Database- Spectrum MS-NW- 710
10 largest peaks:

91	999	92	597	122	301	65	151	39	75	51	64	77	48	104	44	93	44	63	42

59 m/z Values and Intensities:

15	1	17	1	18	5	26	2	27	11	28	3	31	37	32	1	37	4	38	12
39	75	40	5	41	10	45	2	49	2	50	28	51	64	52	15	53	6	54	1
60	1	61	6	62	13	63	42	64	9	65	151	66	9	70	3	73	1	74	9
75	5	76	5	77	48	78	39	79	9	83	1	84	1	85	1	86	1	87	1
89	27	90	12	91	999	92	597	93	44	94	2	98	1	100	1	102	6	103	35
104	44	105	8	106	1	107	1	120	3	121	3	122	301	123	26	124	1		

Synonyms:

Figure C.21 NIST MS 2.0 library search results for the spectrum shown in Figure C.20.

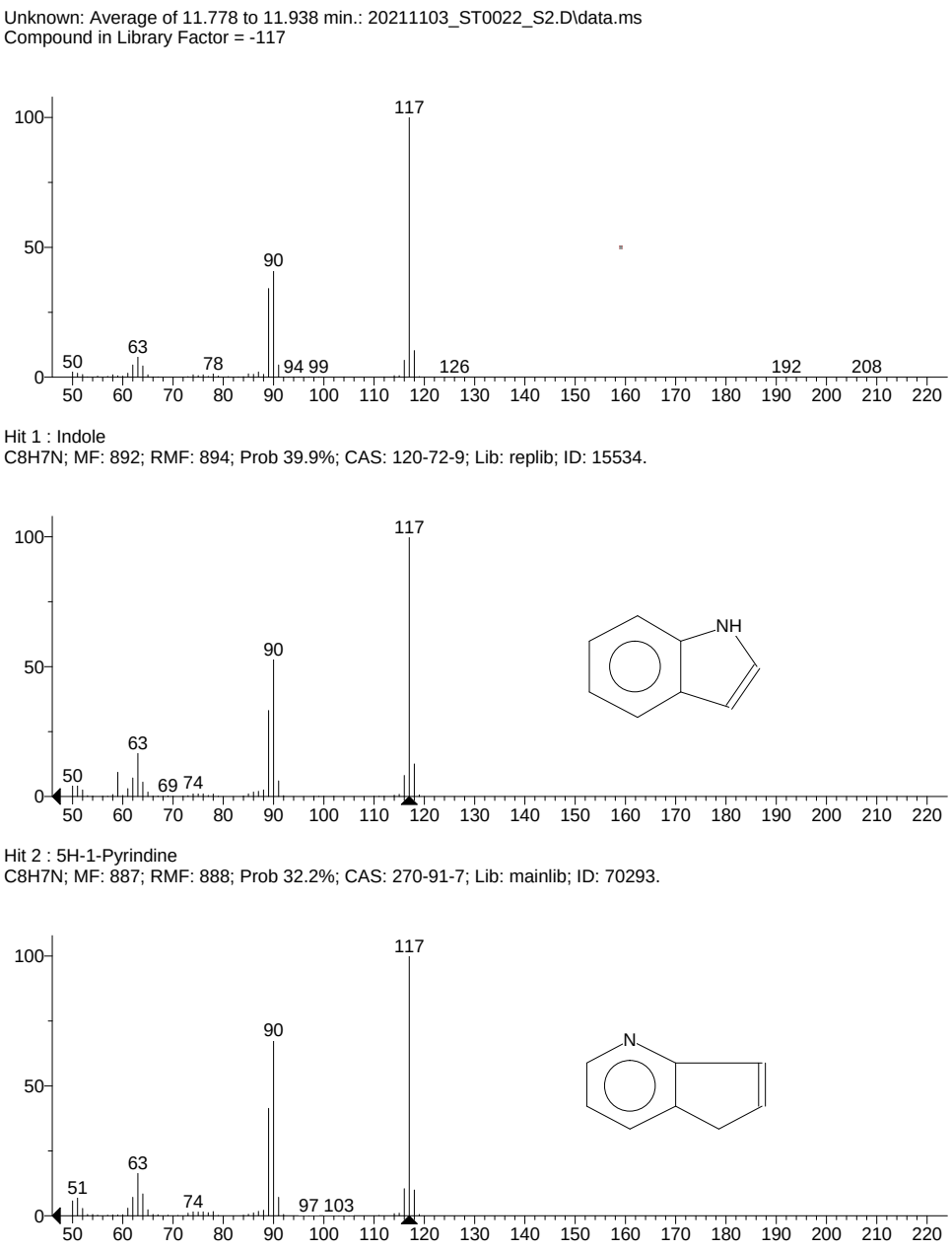

Figure C.22 MS spectrum recorded for $\mathbf{Y}$ at $t_R(\mathbf{Y}) = 11.8$ min in Figure C.19 (top) and two NIST MS 2.0 library search results for this spectrum (middle and bottom).

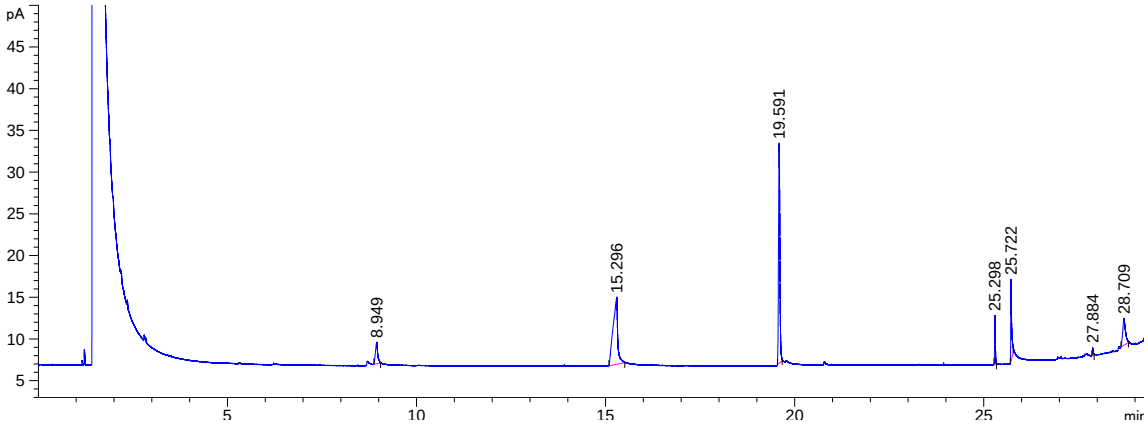

Figure C.23 GC chromatogram from CYP 2C19 blank batch without limonene, using GC method 2. Degradation products are observed.

C.6 GC analysis of attempted CYP 2C19 catalyzed oxidation of limonene (16)

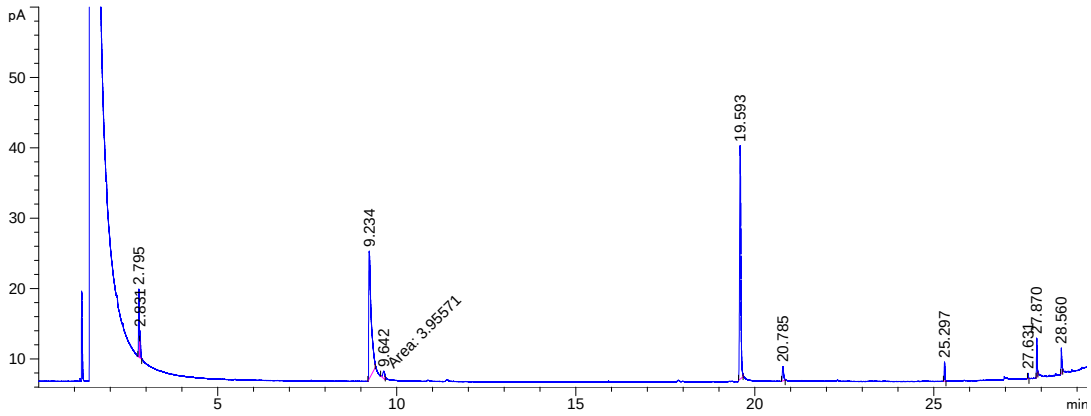

Figure C.24 GC chromatogram from CYP 2C19 oxidation of (*R*)-limonene ((*R*)-**16**) after 14 days reaction time, using GC method 2.

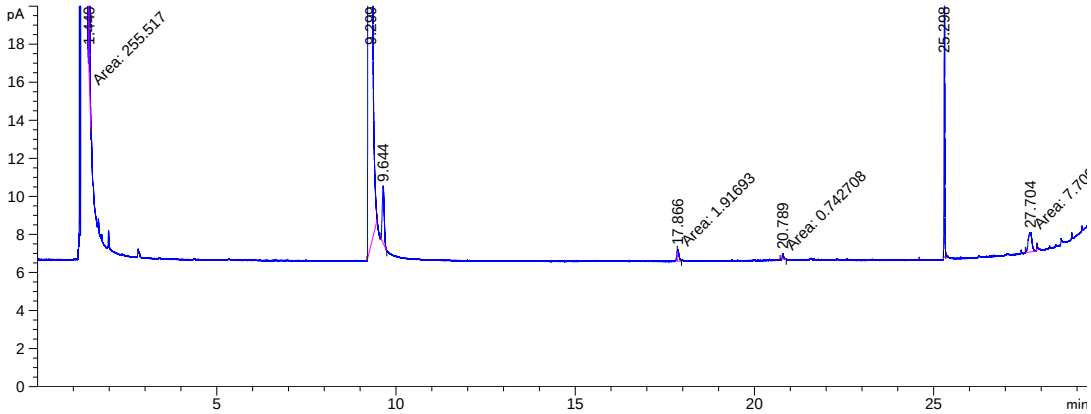

Figure C.25 GC chromatogram from CYP 2C19 oxidation of (*S*)-limonene ((*S*)-**16**) with 40 mg mL^{-1} enzyme concentration, after 9 days reaction time, using GC method 2. DMSO is not completely removed.

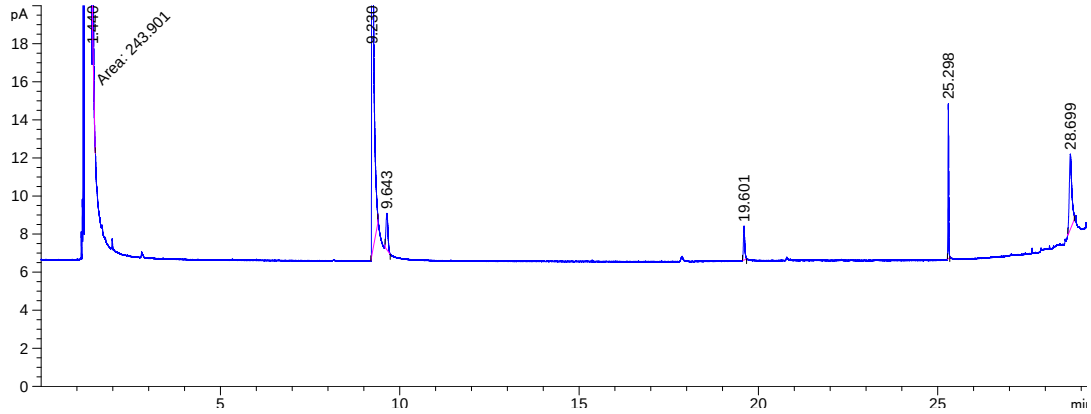

Figure C.26 GC chromatogram from CYP 2C19 oxidation of (*R*)-limonene ((*R*)-**16**) with 40 mg mL^{-1} enzyme concentration, after 9 days reaction time, using GC method 2. DMSO is not completely removed.

Susanne Hansen Troøyen

Synthesis of enantiopure β-blockers (S)-betaxolol and (S)-esmolol, and limonene valorization using biocatalysis

NTNU
Kunnskap for en bedre verden